Electronic Theses and Dissertations

2016

Reliability-based assessment on the performance of external dampers in controlling bridge stay cable vibrations

Seyed Ali Mohammadi
University of Windsor

Follow this and additional works at: http://scholar.uwindsor.ca/etd

Reliability-based assessment on the performance of external dampers in controlling bridge stay cable vibrations

By

Seyed Ali Mohammadi

A Dissertation
Submitted to the Faculty of Graduate Studies
through the Department of Civil and Environmental Engineering
in Partial Fulfillment of the Requirements for
the Degree of Doctor of Philosophy
at the University of Windsor

Windsor, Ontario, Canada

2016

Reliability-based assessment on the performance of external dampers in controlling bridge stay cable vibrations

By

Seyed Ali Mohammadi

APPROVED BY:

_____
H. J. Zhou, External Examiner
Civil Engineering, Shenzhen University, China

_____
J. Wu, Outside Reader
Electrical and Computer Engineering

_____
S. Das, Department Reader
Electrical and Computer Engineering

_____
A. El Ragaby, Department Reader
Civil and Environmental Engineering

_____
S. Cheng, Advisor
Civil and Environmental Engineering

_____
F. Ghrib, Co-Advisor
Civil and Environmental Engineering

August 18, 2016

DECLARATION OF CO-AUTHORSHIP AND PREVIOUS

PUBLICATION

I.   Co-Authorship Declaration

I hereby declare that this dissertation incorporates material that is the result of joint research undertaken with my Advisors, Dr. Shaohong Cheng and Dr. Faouzi Ghrib of the University of Windsor. In all cases, the key ideas, the primary contributions, and data analysis and interpretation were performed by the author of this dissertation. The contributions of the co-authors were primarily focused on the provision of the study and suggesting possible directions. Results related to this research are reported in Chapters 3 through Appendix B, inclusive.

I am aware of the University of Windsor's Senate Policy on Authorship and I certify that I have properly acknowledged the contributions of the other researchers to my dissertation, and I have obtained written permission from my co-authors to include the above materials in my dissertation.

I certify that, with the above qualification, this dissertation, and the research to which it refers to, is the product of my own work.

II. Declaration of Previous Publication

This dissertation includes contents of 3 papers that have been previously published/submitted for publication in conferences and peer reviewed journals, as follows:

Paper #	Dissertation Chapter	Publication title/full citation	Publication status
1	Chapter 3 & Chapter 4	Reliability assessment for damped bridge stay cables under dynamic excitation.	Published, Proc. of the 8th International Conf. on Structural Dynamics, (pp. 2993-2999), EURODYN Leuven, Belgium, 2011
2	Chapter 3 & Chapter 4	Assessment of dynamic behavior of an inclined sag cable with a transverse linear viscous damper using reliability-based approaches	Published, General Conference. Canadian Society of Civil Engineering (CSCE), (#336, pp. 1-9) Montreal, Canada, 2013
3	Chapter 4	Reliability-based design assessment on the performance of external dampers in controlling rain-wind induced bridge stay cable vibrations	Accepted for publication, International Journal of Structural Engineering

I certify that the above material describes work completed during my registration as graduate student at the University of Windsor.

I declare that, to the best of my knowledge, my dissertation does not infringe upon anyone's copyright nor violate any proprietary rights and that any ideas, techniques, quotations, or any other material from the work of other people included in my dissertation, published or otherwise, are fully acknowledged in accordance with the standard referencing practices. Furthermore, to the extent that I have included copyrighted material that surpasses the bounds of fair dealing within the meaning of the Canada Copyright Act, I certify that I have obtained a written permission from the copyright owners to include such materials in my dissertation.

I declare that this is a true copy of my dissertation, including any final revisions, as approved by my dissertation committee and the Graduate Studies office, and that this dissertation has not been submitted for a higher degree to any other University or Institution.

ABSTRACT

Inclined stay cables on cable-stayed bridges are prone to wind-induced vibrations due to their long flexible nature and low structural damping. Severe stay cable vibrations under either the combined effect of rain and wind or wind only have been observed in field and wind tunnel tests which caused great concerns to bridge designers. To suppress these vibrations, fluid dampers are often attached to the stay cables near the anchorages.

In order to facilitate effective and economical design of dampers for stay cable vibration mitigation, thorough understanding of both the vibration characteristics and the dynamics of the cable-damper system is necessary. Nevertheless, existing studies are limited to deterministic-based analysis of which the uncertainties of structural parameters (such as cable tension and damper capacity) and wind parameters (such as speed, direction, etc.) over the service life of a bridge are totally neglected. Thus, to provide complete information regarding the aerodynamic response of a damped cable, the problem should be more rationally studied from a probabilistic-based sense. This would offer bridge engineers a more reliable analytical tool for performance assessment of cable-damper systems.

The current study aims at improving the current practice of external damper design by proposing a time-variant reliability-based framework model of a damped stay cable subjected to wind load conditions. Two types of cable vibrations that are more probable, i.e. rain-wind-induced cable vibrations, and/or critical, i.e. dry-inclined cable galloping, than the others are investigated. The research outcomes are drawn to ensure reliability of design and enhance maintainability of external dampers for bridge stay cables. The flexible applications of the proposed time-variant reliability-based framework tool are demonstrated through some case study examples.

DEDICATION

I dedicate this work to my beloved parents for their incredible love and support.

ACKNOWLEDGEMENTS

TABLE OF CONTENTS

LIST OF TABLES

LIST OF FIGURES

LIST OF APPENDICES

CHAPTER 1

INTRODUCTION

1.1 BACKGROUND

The development of cable-stayed bridges as a structural choice for medium to long span bridges has been remarkable through the closing decades of the last century. Stay cables play an essential role in the dynamic behaviour of cable-stayed bridges. They are characterised by their low intrinsic damping and flexible nature, which makes them susceptible to wind-induced excitations (Fujino et al., 2014). Large amplitude vibrations of stay cables would result in structural damages in cables, bridge deck, and fatigue at cable anchorage, which would cause deep anxiety for the observing public. The vulnerability of stay cables has raised great concern in the bridge engineering community. Thus, it is imperative to take into account these issues in bridge design.

In the past years, numerous efforts have been made in order to understand the mechanisms of various types of wind-induced cable vibration phenomena and to find solutions for alleviating these unfavourable oscillations (e.g. Hikami and Shiraishi, 1988; Main and Jones, 2001; Cheng et al., 2003, 2008; Matsumoto et al., 2007).

It is learned from literature that some types of cable vibrations are more probable and/or critical than the others (Kumarasena et al., 2007). When cable is excited under the combined effect of wind and rain, the phenomenon is called rain-wind-induced cable vibration (RWIV). It is recognized as the most frequently observed wind-induced cable vibration on site of cable-stayed bridges (Hikami and Shiraishi, 1988; Yamaguchi, 1990; Zuo et al., 2008). In addition, dry-inclined cable galloping is the excitation solely induced

by wind, i.e. without the presence of precipitation. It was first observed in wind tunnel tests in Japan (Saito et al., 1994) and has subsequently been identified in a number of wind tunnel studies (e.g. Miyata et al., 1994; Cheng et al., 2003; Nikitas et al., 2009). The results suggested that the onset conditions of this violent motion are possible to be satisfied on site. It is shown that the phenomenon is related to the occurrence of negative aerodynamic damping induced by wind. If the negative aerodynamic damping is significant enough to overcome the positive structural damping, will result in negative effective damping of the body in the form of a divergent galloping type of response of bridge stay cables. This excitation is recognized as the most critical wind-induced cable vibration phenomenon for bridge stay cables due to its catastrophic consequences. Though at present, no field case has been formally confirmed as dry inclined cable galloping, the possibility of its occurrence on real bridges should not be disregarded.

To suppress excessive cable vibrations, external dampers are commonly installed near the cable-deck anchorage. The effectiveness of damper design in controlling wind-induced cable vibrations has been studied by many researchers, usually in terms of the structural modal damping level achieved by adding external damper (e.g. Yoneda and Maeda, 1989; Pacheco et al., 1993; Krenk, 2000; Tabatabaei and Mehrabi, 2000; Fujino et al., 2008; Cheng et al., 2010).

Due to the inherent uncertainties in loads, materials and manufacturing quality, variabilities in structural responses are unavoidable. To ensure the reliability of a structure, these uncertainties or variabilities must be considered in structural design. Accurate assessment of structural reliability would reduce costs and increase efficiency of design, maintenance and repair (Kulhawy and Phoon, 1996). In this regard, many investigators

2

have studied reliability of bridge structures with respect to established strength limit states, i.e. load versus resistance (e.g. Namini, 1992; Imai and Frangopol, 2001; Frangopol et al., 2007; Zhang et al., 2013). However, to the best knowledge of the author, none of the previous studies were focused on reliability-based design assessment of damped stay cables exposed to wind load conditions.

1.2 MOTIVATIONS

Stay cables play an important role in cable-stayed bridges which necessitates better understanding of their excitation mechanisms and also mitigation technique(s) to suppress their problematic vibrations. Even though much has been done to assess the performance of external dampers in suppressing cable vibrations, all of the existing works were based on deterministic assumptions of the system parameters; whereas in practical applications, the variability of system properties with respect to time needs to be taken into account. For example, tension in a stay cable may decrease during its life time because of cable slacking (Au and Si, 2012); thermal expansion or contraction of the fluid in a viscous damper may result in leakage which would affect the damper capacity and degrade its efficiency. In addition to the uncertainty of structural parameters, the uncertainty associated with the applied loads should also be considered. In the case of wind-induced cable vibrations, this requires the awareness of the probabilistic characteristic of design wind speeds (Holmes, 2007). Accordingly, the assumptions underlying deterministic approaches for the described damped stay cable models do not comply with the practical situations. Therefore, it would be beneficial to carry out a probabilistic analysis, of which the uncertainties in the structural and the wind parameters can be properly considered. This would offer bridge engineers a more reliable analytical tool for designing cable-damper systems.

The present study is perhaps the first attempt in bridge engineering to conduct a reliability-based analysis of external dampers in controlling bridge stay cable vibrations. This motivates the author to propose a reliability-based analysis model of which performance of a typical damped bridge stay cable subjected to wind load conditions could be assessed. Further, potential application of the proposed reliability-based framework model over service life of a typical cable-damper system needs to be explicated.

1.3 OBJECTIVES

This study aims at improving the current practice of external damper design for controlling bridge stay cable vibrations by taking into account the uncertainties existed in the structural and the load parameters of the system. The objectives of the current study are proposed to be:

- Develop a model to study wind-induced vibration problem of a typical cable-damper system in a probabilistic way. Thereof, a reliability-based design methodology for the assessment of a stay cable aerodynamic behavior will be proposed. The limit state function is established by defining the stability criterion in terms of the effective damping. Subsequently, trend of reliability-index as a function of time-varying wind and structural parameters will be quantified.

- Provide an assessment of the most admissible reliability method for evaluating the behavior of a cable-damper system under wind and rain-wind-induced vibrations. This would facilitate the reliability-based procedure of designing external dampers for stay cables. The Monte Carlo simulation (MCS) will be used as a reference reliability analysis method.

- Simplify the procedure of designing external dampers for stay cables in bridges by deriving a set of reliability-based damper design curves using non-dimensional form of system parameters. Resultantly, the probability of stay cable failure associated with rain-wind-induced vibration and/or dry inclined cable galloping would be predictable. This would provide structural engineers with a preliminary design tool to assess bridge stay cable performance over practical ranges of structural and wind parameters.

- Propose a service life reliability response diagram for an existing damped cable, of which the performance of a cable-damper system under wind conditions would be related to life time variation of system parameters. The offered service time reliability-based assessment curves would provide engineers with an estimation of the reliability response of the external damper corresponding to a desired return period of design wind speed after N years of service life. Besides, the sensitivity of influential parameters over the life time of a stay cable in triggering cable excitation such as RWIV/galloping would be predictable.

- Develop an efficient maintenance strategy for a cable-damper system over the service life of the bridge within defined maintenance period.

1.4 THESIS ORGANIZATION

The main body of this dissertation has five chapters. They are organized as follows:

- **Chapter 2**: Literature review for the current study is developed in this chapter by covering the essential components required to conduct reliability-based assessment on the performance of external dampers in controlling bridge stay cable vibrations. First, the existing studies on the excitation mechanisms of various wind-induced

cable vibrations are briefly summarized. Then, the suppression effect offered by external dampers to the vibrational response of stay cables is examined by reviewing the available research works of external damper design. It is shown that the studied cable-damper system needs to be more rationally investigated by including uncertainties associated with the structural and the loading parameters. Therefore, the reliability-based design approaches that are commonly applied to civil structures will be reviewed. Since the wind-excited response of structures depends on wind load conditions, which, in the current study, corresponds to the cable-damper system exposed to stochastic wind at a given bridge site, the review of the statistical-based methods on predicting uncertain characteristic of recorded wind speed data set will be presented. Finally, the existing application of reliability-based analysis methods to wind-induced response of bridge structures are reviewed.

- **Chapter 3**: The objective of this chapter is to explain the current state-of-the-art on the design of bridge stay cables equipped with external dampers. First, the analytical model for the free vibration problem of a horizontal non-flexural taut cable with an attached linear viscous damper is introduced. The solutions of the eigenfreqnecies and the equivalent structural modal damping ratios are obtained. Further, the analysis is extended to consider the influence of cable inclination, cable sag, and cable bending stiffness on the damping response. An alternative energy-based analysis method will be applied to facilitate the derivation of the damping design estimation curves. The information presented in this chapter will pave the road for the work presented in the subsequent chapters.

- **Chapter 4**: Reliability-based analysis of a damped stay cable under the risk of rain-wind-induced-vibration (RWIV) is conducted in this chapter. The objective is to develop a time-variant reliability-based framework model to assess how uncertainties in the structural parameters would influence the time specific reliability performance of an external damper designed according to the current deterministic-based practice. Various applications of the proposed time-variant reliability-based framework model, including the development of reliability-based damper design curves and long-term structural maintenance plan are addressed through some numerical examples.

- **Chapter 5**: This chapter extends the application of the proposed reliability-based design tool in Chapter 4 to the assessment of cable-damper systems performance prone to dry inclined cable galloping conditions. The limit state function is improved by adding uncertainties associated with the wind in the formulations. The wind parameters are derived by applying the statistical analysis methods to the recorded wind speed at a given bridge site. Some design cases show the application of the proposed time-variant reliability-based framework model in predicting aerodynamic stability of a damped stay cable when preliminary design or life time maintenance is needed.

- **Chapter 6**: Major conclusions obtained from the previous chapters are summarized and recommendations for future work are presented in this chapter.

CHAPTER 2

LITERATURE REVIEW

2.1 INTRODUCTION

The literature review is developed for the current study by covering the essential components required to conduct reliability-based assessment on the performance of external dampers in controlling wind-induced bridge stay cable vibrations. First, existing studies on the excitation mechanisms of various wind-induced cable vibrations are briefly summarized. The suppression effect offered by external dampers to the vibrational response of stay cables is then examined by reviewing the available research works. It is noticed that most existing studies and tools used for the design of external dampers are based on deterministic approaches. To better understand the dynamic behavior of a stay cable when attached with an external damper, the effects of potential deviation of certain system parameters such as the cable tension, the damper capacity, and the wind load over the life time of the damped stay cable system needs to be examined in a probabilistic point of view. In this matter, the reliability-based design approaches that are commonly applied to civil structures are reviewed. Since the reliable response of structures under wind excitation depends on the uncertainty of wind loading, thereof a summary of the statistical analysis methods for wind data are presented, of which the uncertain characteristics of wind speed data as well as the prediction of extreme design wind speed corresponding to a desired design return period are explained. Finally, the existing application of reliability-based analysis methods to wind-induced excitation of structures such as suspension and cable-stayed bridges are reviewed.

2.2 EXCITATION MECHANISMS OF VARIOUS WIND-INDUCED CABLE VIBRATIONS

Cables are sensitive to dynamic excitations by various sources because of their low intrinsic damping and flexible nature. Many unfavorable cable vibration incidences were observed or reported from bridge sites or wind tunnel experiments in recent years (e.g. Hikami and Shiraishi, 1988; Main and Jones, 2001; Cheng et al., 2003; Matsumoto et al., 2007; Kumarasena at al., 2007). Large amplitude vibrations of stay cables have been observed on site of cable-stayed bridges under the combined effects of rain and wind or wind only which caused great concerns to bridge designers. The identified phenomena include rain-wind-induced vibration, high-speed vortex excitation, and dry inclined cable galloping.

2.2.1 Rain-wind-induced cable vibration

Rain-wind-induced vibration (RWIV) has been reported as the most frequently observed cable vibration on bridge site (Kumarasena et al., 2007). It was first observed in 1986 on the Meiko-Nishi Bridge in Japan during the construction phase. Site report indicated that cables experienced large amplitude vibrations under certain wind conditions, i.e. in terms of velocity and direction, only when it was raining (Hikami and Shairaishi, 1988).

This phenomenon is found to be associated with the formation of water rivulet on cable surface and the subsequent alternation of the cross-sectional shape of the cable. Over the last three decades, besides an attempt to apply classical galloping theory to explain the mechanism (Yamaguchi, 1990; Geurts et al., 1998; 1999), the possible role of water rivulet thickness and its link with the rivulet motion speed (Flamand et al. 2001), as well as the

initial and instantaneous rivulet position (Gu and Lu, 2001) in exciting RWIV were investigated. The formation of water rivulet needs to be considered in the dynamic equilibrium equation in addition to gravity, capillary effect, and aerodynamic forces (Matsumoto et al., 2001). In another study, Verwiebe and Ruscheweyh (1998) pointed out that the circumferential oscillation of rivulets could be a primary cause of RWIV provided that the rivulets oscillate along the circumferential direction at the same frequency as that of the cable motion. Gu et al. (2009) carried out wind tunnel tests to obtain the aerodynamic forces acting on cable and upper rivulet and established a theoretical model in which the in-plane degree-of-freedom (DOF) of the cable and the tangential DOF of the rivulet were taken into account.

In parallel, various solutions have been developed to restrain occurrence of this type of vibration, which typically add supplementary devices such as external damper(s) and/or cable cross-ties (e.g. Xu et al., 1999; Bosch and Park, 2005; Sun et al., 2003) or modify cable surface condition by installing helical wires or making dimples on cable surface (Flamand, 1995; Miyata and Yamada, 1994; Matsumoto et al., 1989).

2.2.2 High-speed vortex excitation

In the absence of precipitation, however, similar response characteristics to that of RWIV of stay cables have been observed on site and in wind tunnels. The observation of such undesirable response was documented by Matsumoto et al. (1989) during a high-speed typhoon. Since the observed unstable cable response occurred at high reduced velocities comparing to the conventional Kármán-vortex induced vibration, it was referred to as high-speed vortex excitation. It is characterized by large but limited response amplitude and occurs within certain wind velocity region.

The mechanisms of this excitation has been studied in the last two decades through a series of wind tunnel tests. Matsumoto (1998) showed that high-speed vortex excitation was closely linked with the existence of an axial flow in the base region of an inclined cable. When wind is oblique to the cable, an axial component of flow also exists on the leeward side of the cable, which interacts with Kármán vortices along the cable length. The role of axial flow is to interrupt the interaction between the two separated shear layers in the wake of the cable and suppress Kármán vortex shedding. This increases the sensitivity of separated flow to external excitations like body motion and would result in a volatility of the cable (Matsumoto et al., 2001; 2007). Because of the three dimensional characteristics of vortex shedding, this excitation strongly depends on the end conditions and the yaw angle of the cable (Matsumoto et al., 2010). The study of Zuo and Jones (2010) showed that the associated mechanism might be a type of vortex excitation which occurs at lower frequencies close to the natural frequencies of the stay cables.

2.2.3 Dry-inclined cable galloping

It is indicated in a report (Kumarasena et al., 2007) by the US Federal Highway Administration (FHWA) Agency that the dry galloping excitation is the most critical wind-induced cable vibration phenomenon due to its probable onset conditions and catastrophic divergent nature. It is a type of divergent response which is observed in a number of wind tunnel studies such as Miyata et al. (1994), Saito et al. (1994), Cheng et al. (2003a), Ni et al. (2007), and Nikitas et al. (2009). Experimental results from a study in Japan by Saito et al. (1994) suggested that the onset conditions of this violent cable motion could be possible on site.

Nakamura and Hirata (1994) pointed out that the generation mechanism of dry inclined cable galloping was related to interruption of communication between the upper and lower separated flows. Because the communication between upper and lower separated flows can tend to cancel pressure difference on the upper and the lower surface of cable. Communication between the two separated flows can be interrupted due to: (1) a long downstream splitter plate attached to the cable; (2) vanishing effect of oscillation at low wind velocity related to low speed galloping; (3) geometry influence of the cylinder at high wind velocity which can produce a reattachment-type pressure distribution with high speed galloping (Schewe, 1983); (4) presence of axial flow on the leeward side of cable surface, which would act like a barrier and thus prohibit the interaction between the two separated shear layers (Matsumoto et al., 2007b).

Based on wind tunnel tests by Matsumoto and his research group on cross-flow cylinders, it was proposed that dry-state galloping of an inclined cable could be associated with the mitigation of regular Kármán vortex shedding (Matsumoto et al., 2007). It is important to mention that Kármán vortex shedding is produced by communication of upper and lower separated flows, or in another expression, Kármán vortex shedding would stimulate the communication between two separated flows. The interruption of this communication between two separated flows is identical to the interruption of Kármán vortex shedding. Thus, the mitigation or suppression of Kármán vortex shedding can excite galloping instability. As a consequence, self-excited vibrations would be promoted (Matsumoto et al., 2007; 2010). In addition, Cheng et al. (2005; 2008b) showed that the correlation of aerodynamic forces along the span of a stay cable could be another important factor responsible for this type of unstable response.

Divergent response of an oscillating body in wind is accompanied by the occurrence of negative aerodynamic damping. If the induced aerodynamic damping is negative and significant enough to overcome the positive structural damping, it will result in negative effective damping of the body. The response amplitude of the oscillating body will thus be drastically increased, leading to a divergent motion. Therefore, the stability of cables when exposed to various wind conditions can be assessed by evaluating the induced aerodynamic damping/forces. A pioneer study on this subject has been done by Virlogeux (1998) in which simple expressions of quasi-steady aerodynamic damping for cable vibrations in the directions parallel to and normal to wind were derived. Larose and Zan (2001) showed that for a cylinder free to vibrate, the changes in the relative velocity over a vibration cycle would cause corresponding changes in the aerodynamic forces. This normally gives positive aerodynamic damping for circular cylinders, but in the critical Reynolds number range, the force variations can be adverse. This could lead to negative aerodynamic damping and hence a galloping type instability, which is very similar to the classical Den Hartog galloping, with the exception that the changes in the flow region are due to variation of the relative direction of the flow, giving adverse changes in the lift coefficient (Macdonald, 2002). In parallel, the experimental study of Cheng et al. (2008b) on the wind-induced vibration of a dry inclined cable model verified the applicability of the Den Hartog criterion on the prediction of the critical onset condition(s) for the divergent galloping motion. Macdonald and Larose (2006) extended this classical approach and made it applicable to a cylindrical body vibrating in steady flow along any arbitrary direction normal to its axis. Most recently, Raeesi et al. (2013) presented a more realistic aerodynamic model by including the unsteady/turbulent characteristics of natural wind in

the cable aerodynamic response analysis. The effects of turbulence intensity and the role of each turbulence component in triggering aerodynamic instability of an inclined and/or yawed cable were investigated. It was shown that the existence of flow unsteadiness in natural wind would increase the risk of stay cables to experience galloping type of response.

2.3 DETERMINISTIC-BASED DESIGN OF EXTERNAL DAMPERS FOR CABLE VIBRATION CONTROL

Although the mechanisms associated with various wind-induced cable vibrations are still not fully understood, it has been demonstrated that to suppress these unfavorable cable vibrations or inhibit their onset, additional structural damping needs to be provided (Main and Jones, 2001). One possible solution is to attach external dampers to cables, which has been used in practice on many cable-stayed bridges (Watson and Stafford, 1988; Main and Jones, 2001; Fujino, 2002; Spencer and Nagarajaiah, 2003).

Over the last three decades, the effectiveness of damper design in controlling cable vibrations has been studied by many researchers to quantify the equivalent modal damping level achieved by damped cables by adding external dampers, which requires analyzing the full dynamic response of a cable-damper system (e.g. Yoneda and Maeda, 1989; Yamaguchi, 1995; Xu and Yu, 1999a; Tabatabai and Mehrabi, 2000; Krenk, 2000; Main and Jones, 2002a; 2002b; Sun et al., 2003; Fujino and Hoang, 2008; Cheng et al., 2010).

When a cable is subjected to end forces which are larger than the sum of transverse forces distributed along its length, its configuration is close to a straight line and the cable is called a taut cable. Typically, high level axial tension forces exist in stay cables and thus the assumption of taut cable is applicable. This simplification truly helped researchers in

the first step of cable-damper system studies to better investigate effects of external dampers utilized for suppressing stay cable vibrations.

Analysis of an elastic taut cable by Irvine and Caughey (1974) yielded a closed form solution for the linearized system. The symmetric and asymmetric in-plane motions of a cable and also the extensibility of a cable were explained by proposing a dimensionless inextensibility parameter, λ, which includes the effects of both cable geometry and elasticity. In the case of a horizontal taut cable, this parameter, which showed the relative significance of elastic stiffness to the catenary stiffness, was important and could be formulated as a function of the span length, the stretched length, the mass per unit length, the horizontal static tension and elastic stiffness of the cable. Study of Triantafyllou and Grinfogel (1983) was based on establishing an asymptotic analytical expression for the natural frequencies of a cable. The natural modes and the dynamic tension of a taut, elastic cable were derived for small ratios of cable weight to end forces.

Kovacs (1982) identified the existence of an optimal damping in a taut cable-damper system, which was confirmed by a number of other researchers (Yoneda and Maeda, 1989; Uno et al., 1991; Pacheco et al., 1993; Krenk, 2000). Yoneda and Maeda (1989) studied the effect of linear viscous dampers on increasing the structural damping of stay cables on cable-stayed bridges. The influence of damper installation on the damping characteristics of the cable was investigated by formulating a complex eigenvalue problem. Practical estimation formula for the optimal damper size was proposed on the basis of these analyses. The optimum damping coefficient associated with a specific damper location was evaluated using the complex eigenvalue analysis in this work. In particular, Pacheco et al. (1993) simplified the procedure of designing viscous dampers for stay cables by deriving

a universal damping estimation curve, which would relate the modal damping level of a damped taut cable directly to the mode number of cable vibration, the damper size, the damper location, the cable length, the mass per unit length of the cable, and the cable fundamental frequency. In obtaining the estimation curve in a universal form, it was assumed that only the first few modes of the cable were of interest, and that the distance of the damper from the cable anchorage was within several percentage of the cable length. The estimation curve was obtained from complex-eigenvalue analysis of a taut cable while grouping the above parameters into non-dimensional forms. With the universal damping estimation curve presented in this study, the preliminary design of a linear viscous damper, including predicting the additional amount of damping offered by the damper for the first few cable modes, became very convenient.

Krenk (2000) presented an analytical solution to the problem of a taut cable equipped with a concentrated linear viscous damper. By formulating the system equation as a complex eigenvalue problem, an asymptotic formula for the modal damping of a cable was derived and effort was made to keep it compact, accurate and thus suitable for practical design. This formula allowed explicit determination of the optimal damper size depending on its damping parameter. The damping parameter was introduced to represent the equivalent modal damping ratio of a damped stay cable. It was defined in terms of the damping coefficient, the damper location, the cable mass per unit length, and the cable tension.

Approximation of a stay cable as a taut string neglects the bending stiffness, the axial extensibility and the sagged equilibrium profile of a cable under its self-weight. Mehrabi and Tabatabai (1998), and Krenk and Nielsen (2002) presented a refined solution

to a typical cable-damper system by including the influence of cable sag and cable bending stiffness in the formulation. Further, Tabatabai and Mehrabi (2000) attempted to propose a recommendation for the design of mechanical linear viscous dampers for stay cables. The governing differential equation for vibration of a flat-sag cable attached transversely to a linear viscous damper was first derived as a complex eigenvalue problem similar to that by Krenk (2000). It was then converted to a dimensionless form by introducing non-dimensional cable and damper parameters. A parametric study was conducted for a wide range of non-dimensional cable parameters based on a bridge stay cable database (Tabatabai et al., 1998). Finally, simplified non-dimensional relationships associated with external viscous dampers were proposed for determining damper-induced changes in the cable first modal damping ratio. The discretized non-dimensional form of this equation greatly facilitated parametric studies for a vast range of non-dimensional parameters of stay cable and damper. Based on the developed relationships, simple form design equations were proposed for determining the location and size of a linear viscous damper that would most effectively suppress stay cable vibrations.

The accurate asymptotic formula of the structural modal damping ratio of a general cable-damper system was analytically derived by Fujino and Hoang (2008) in the form of a transcendental equation. The study resulted in an explicit evaluation of reductions in the damper effectiveness due to influential parameters such as the sag and the bending stiffness of a cable and the stiffness of a damper support. This could significantly simplify the damper design procedure for stay cables. The analytical results were also extended to high-damping rubber (HDR) damper. Resultantly, empirical formulae relevant to the design of both types of damper (viscous damper and HDR damper) were found from this study.

Alternatively, other researchers tried to develop different approaches to simplify the solution procedure and verify the analytical results of a cable-damper system derived from complex eigenvalue analysis. Using the time variation of the kinetic energy of a damped cable as an index, Cheng et al. (2010) studied the damping property of a stay cable equipped with a transverse linear viscous damper. A numerical approach was developed for a practical scenario where both the cable bending stiffness and sagging effect were considered. Besides, the existing analytical limitation on the location of damper were eliminated. A set of damping estimation curves were developed for practical parameter ranges of bridge stay cables. These curves can be utilized to relate a specific damper design to the corresponding equivalent structural modal damping of a damped stay cable. These tools were particularly useful in the preliminary stage of a damper design. Recently, a novel passive control approach to suppress vibration of horizontal cables with damped flexible end restraints consisting of a viscous damper and an elastic spring has been studied by Jiang et al. (2013). The dynamic equation of the cable-damper system has been established using the D'Alembert's principle in conjunction with a solution based on the Galerkin method.

In addition to the analytical and numerical approaches, experimental studies were also conducted, which played an important role in developing the scope of knowledge in this field. Ko et al. (2002) conducted an experimental study on cable vibration control using nonlinear hysteretic dampers. Modal testing on a single cable without damper was first performed to identify the natural frequencies and mode shapes of the cable under three different tension levels. The magnitude of the tension level was selected to be high enough, to ensure the cable was a taut one. A series of dynamic tests were conducted for a cable-

damper system by exciting the cable transversely at a point near the anchorage. Results were collected in the form of some nonlinear frequency-response curves of which the resonant frequencies and the equivalent viscous damping ratio of a damped cable under different excitation levels were identified.

A full-scale experiment on vibration mitigation of a damped stay cable system was performed by Sun et al. (2003) to estimate its optimal damping. Seven types of mechanical dampers, including oil damper, viscous damper and magneto-rheological (MR) damper, were used in the tests. Results showed that the mechanical dampers installed near the cable anchorage were effective in mitigating cable vibrations. It was found that if more than one damper were attached to the cable, the total amount of additional damping contributed to the cable did not equal to the summation of the additional damping offered by each individual damper. Subsequently, the efficiency factor between the analytical designated damper and the tested damper was determined.

Christenson et al. (2006) experimentally verified a smart damping control strategy by employing H_2 linear quadratic Gaussian (LQG) clipped optimal control based on using only the force and displacement measurements at the damper location for two stay cable models representing respectively, taut and sagged design cases. A shear mode MR fluid damper was attached to an inclined cable to reduce cable vibration. The cable response was found to be substantially reduced by the smart damper.

Experimental evaluation of a self-powered smart damping system in reducing vibrations of a full-scale stay cable was conducted by Kim et al. (2010). In this study, the effectiveness of a self-powered smart damping system consisting of a MR damper and an electro-magnetic induction (EMI) device in reducing cable vibrations was investigated.

The focus of their study was to construct a prototype smart damping system, particularly designed for cable vibration control applications, and experimentally evaluate its effectiveness in reducing excessive vibrations of stay cable. In the experiment, a full-scale inclined cable with high tension force was used. A series of free vibration tests were conducted in four different testing cases, i.e. the uncontrolled, the passively controlled, the EMI only, and the self-powered smart damping. Based on the results of this study, the self-powered smart damping system was found to outperform the passively controlled one in reducing vibration amplitude of the cable and also the EMI could operate the smart damping system as a power source, demonstrating the feasibility of the self-powering capability of the system.

Another experimental study of cable vibration mitigation using external viscous damper was carried out by Huang (2011) to select an optimum damper size for a specific cable with designed damper location. A linear viscous oil damper with six adjustable damper sizes was designed and fabricated. The study mainly focused on evaluating the equivalent structural damping ratio of a cable-damper system using forced vibration tests. Results are presented in the form of general damper design curves noting that the damper stiffness effect has been considered. It was found that the impact of damper stiffness on cable damping behavior is highly dependent on the damper location. Besides, an approximately linear relationship was shown to exist between the damper stiffness and the damping ratio. Thus, as stiffness of the damper increases, the equivalent modal damping ratio of the system will decrease.

Fournier and Cheng (2014) investigated the individual and the combined effects of damper stiffness and damper support stiffness on the performance of a linear viscous

damper. The study showed that higher damper stiffness and/or lower damper support stiffness would have an adverse impact on damper performance. Increasing the stiffness of a damper and/or its support would result in a larger optimum damper size. However, the maximum attainable damping ratio would decrease with larger damper stiffness but increase if the support is more rigid. To facilitate practical design, a set of asymptotic relationships has been proposed, of which the optimum damper size and the maximum achievable damping ratio were expressed concisely as functions of nondimensional damper properties in terms of its location, stiffness, and support stiffness.

Similarly, a series of laboratory experiments were also conducted by Jiang et al. (2013) which resulted in a comprehensive parametric study on a prototype cable by investigating the influence of various parameters, particularly the damper coefficient and the spring stiffness, on the suppression of cable vibrations.

2.4 RELIABILITY-BASED STRUCTURAL ANALYSIS

To ensure design of a structure would satisfy its intended performance with a desired level of confidence, the uncertainties contained in the structure itself and the external excitation should be taken into account. The traditional way of dealing with uncertainties is to introduce safety factors in the framework of deterministic design. However, design based on a deterministic approach is often sensitive to variations of system and operating parameters, and therefore of limited value for the solution of practical problems (Frangopol and Maute, 2003). Deterministic design enhanced by reliability assessment and formulated within a probabilistic framework is called reliability-based design (RBD). It has been under development recently and are gaining momentum (Benjamin, 1970; Kulhawy and Phoon, 1996).

Reliability is attained when a system can properly perform its function over a specified period of time and under specified service conditions (Ellingwood, 1980; Choi et al., 2007). In RBD, the response is considered satisfactory when the design requirements imposed on the structural behavior are met within an acceptable degree of certainty, whereas deterministic design discards uncertainty of the data. The purpose of RBD is to interpret how the stochastic nature of a random structural resistance R and a random loading S can be integrated in evaluation of a system performance within a probabilistic-based context (Simoes and Negrao, 2005). Probabilistic design explicitly incorporates the effect of the system parameters uncertainties into the design. Once the probability is determined, the next step is to choose design alternatives.

The definition of several probabilistic terms will be reviewed to facilitate the presentation.

- Statistical tolerancing

   The determination or selection of the distribution functions of random variables depends on the nature of the problem, the assumption associated with the distribution as well as the convenience and simplicity obtained by the distribution in subsequent computations. The associated process is called statistical tolerancing.

- Normal (Gaussian) distribution

   In probability theory, the normal distribution is a continuous probability distribution which has a bell-shape. It is also referred to as Gaussian distribution. A normal distribution is often used as the first approximation to describe real random variables that cluster around a single mean value. It arises as the outcome of the central limit theorem, which states that the sum of many arbitrarily distributed random variables asymptotically converge to a normal distribution

when the sample size becomes large. A normal random variable with zero mean and unity variance is called the standard normal distribution or the unit normal distribution.

- Limit-state function (LSF)

The LSF of a structure is an indicator for the margin of safety between its resistance and load. This function is used to determine the failure region, the failure surface and the region of safety for the studied structure. In the case of a bar subjected to a tensile force, LSF can be defined as the difference between the tensile stress induced by the load and the resistance that is available in the bar. The LSF will be positive when the resistance is greater than the loading effect, which suggests that the design is safe. On the other hand, a region of negative LSF represents the failure region of the bar.

- Safety index (reliability index)

Safety index for the case of a normal LSF is defined as the ratio between the mean and the standard deviation of LSF. It is defined as the shortest distance from the mean of LSF to the surface of LSF. This distance is then normalized by the uncertainty scale parameter, i.e. the standard deviation.

Reliability analysis evaluates the probability of structural failure by determining whether the limit state functions are exceeded. Consider an example of a stay cable with an attached damper subjected to wind load force. The cable tension in stay cable may decrease during its life time because of cable slacking. Thus, the cable tension should be defined as a random variable. Consequently, the problem should be treated in a non-deterministic sense, of which the reliability of the system should be related to the life time

variation of the tension force. Another condition of the example that requires reliability

analysis of the damped cable performance could be that the damper capacity degrades due

to leakage caused by thermal expansion or contraction of the fluid in the viscous damper.

Thereof, variation of damping coefficient should be investigated in a probabilistic-based

sense and the problem, again, should be treated as a non-deterministic case.

As mentioned earlier, the probability of failure P_f is defined by the limit state which

is a function of resistance R and loading effect S. The original concept of limit state design

refers to a design philosophy that entails the following three basic requirements: (1)

identify all potential failure modes called limit states, (2) apply separate checks to each

limit state, and (3) determine the design condition(s) in which the failure occurs (Kulhawy

and Phoon, 1996). In other words, the reliability of a structural system can only be correctly

assessed by considering the full structural system as a single entity and can be accurately

computed only if all its failure modes are taken into account (Frangopol and Moses, 1994).

Therefore, using probabilistic methods to assess the structural response and safety requires

the evaluation of the response function or LSF with respect to the random variables. Thus,

the probability of failure in structural reliability analysis can be considered as the

probability of violation of a limit state at any stage during the life of a structure and the

reliability is defined as the complement of the probability of failure. Therefore, the

structure is considered unreliable if the failure probability of the structure exceeds the

allowable safety level imposed by law, standard, specification, contract or custom to which

a structure must conform.

Due to the dimensionality in the LSF and complexity of the probability-of-failure

calculations, numerous methods are used to simplify the calculation process of the

reliability analysis. The reliability analysis methods are normally established by approximating the LSF using different numerical techniques. Among them, the Monte Carlo simulation (MCS) and the reliability surface method (RSM) are widely used to evaluate the reliability of structures (Frangopol et al., 2007). The RSM includes the first-order-second-moment (FORM) method and the second-order-second-moment (SORM) method. The selection of a reliability method among the others is a key task which depends on the uncertain characteristic(s) of input variable(s), the degree of nonlinearity of LSF, and the analysis processing time associated with each reliability method.

2.4.1 Monte Carlo simulation (MCS)

Monte Carlo simulation (MCS) is a reliability analysis method for structures with implicit and/or highly non-linear limit state functions with respect to the uncertain parameters. The method uses randomly generated samples of the input variables for each deterministic analysis, evaluate the occurrence of failure events, and estimates the probability of failure after numerous repetitions of deterministic analysis. This method is robust, simple and easy to use because it relies on the process of explicitly representing uncertainties by specifying inputs as probability distribution. Therefore, the method is often used to validate other analysis techniques (Cheng et al., 2005).

In the Monte Carlo simulation, the entire system is simulated a large number of times. Each simulation is equally referred to as a realization of the system. All of the uncertain parameters are sampled. For each realization, a single random value is selected from the specified distribution describing each parameter and the system is then simulated through time, given the particular set of input parameters such that the performance of the system can be computed. The results of the independent system realizations are assembled

into probability distributions of possible outcomes. Thus, the outputs are not single values, but probability distributions of the response. The simulation process can be divided into the following steps: (1) simulation of random variable distribution functions and sampling of these variables; (2) solution of the deterministic problem for a large number of realizations; and (3) statistical analysis of the results (Elishakoff, 1999).

A common reason for using Monte Carlo simulation is its formulation simplicity and the ease with which problems having complex LSFs can be handled. A major disadvantage of this method becomes evident when it requires to estimate the sensitivity of failure probability to the statistical parameters (e.g. mean, standard deviation or higher moments describing the probability distributions of the system variables), especially when the reliability level is high (Schneider, 2006).

2.4.2 Reliability surface methods (RSM)

The RSMs are frequently used because of their relative high computational efficiency (compared to MCS), their adaptability to complex problems, and their simplicity of calculation in comparison to analytical methods (Li et al. 2007). RSMs are adapted by applying a Taylor series expansion to approximate the LSF, knowing that random variables are characterized by their first (mean), second (variance), and higher moments. The method requires a search for the most probable point (MPP) on the failure surface with the lowest level of safety index. The task of structural reliability analysis is normally a nonlinear constrained optimization problem, mainly solved by optimization algorithms or iterative schemes (Elishakoff, 1999).

If the response surface is approached by a first-order Taylor expansion approximation at the MPP, the method is called the first-order reliability method (FORM);

26

if the response surface is approached by a second order Taylor expansion approximation at the MPP, the method is called the second-order reliability method (SORM) (Choi et al. 2007).

FORM

FORM is primarily known by the Mean Value First Order Second Moment method (MVFOSM), since it is a point expansion method at the mean point and the second moment is the highest-order statistical result used in this analysis. Here, inputs and outputs are expressed in terms of mean and standard deviation. Higher moments, which might describe skew and flatness of the distribution, are ignored.

The MVFOSM method changes the original complex probability problem into a simple form by using an approximate linear LSF. Accordingly, the value of mean and standard deviation of the approximate LSF can be calculated. The reliability index is then computed as a ratio between the mean and the standard deviation.

Although it is possible to directly establish the relationship between the reliability index and the basic parameters by means of the MVFOSM method (mean and standard deviation of the random variables), there are two serious drawbacks: 1) Evaluation of reliability by linearizing the LSF about the mean values leads to erroneous estimates for performance functions with high nonlinearity, or for variables with large coefficients of variation; 2) The MVFOSM method fails to be invariant with different mathematically equivalent formulations of the same problem. This is an issue in finding true reliable response of a system (Choi et al., 2007).

The improvement of the MVFOSM method can be obtained by changing the expansion point from the mean value point to the MPP. In this regard, the numerical

technique has been proposed by Hasofer and Lind (1974) which relies on a linear mapping of the basic variables into a set of normalized and independent variables. Subsequently, the original failure surface is mapped into the corresponding failure surface in a standard normalized space. It was shown that due to the rotational symmetry of the second-moment representation of standard normal variable, the geometrical distance from the origin in the standard normalized space to any point on the transformed limit state failure surface is simply the magnitude of standard deviations from the mean value point in original space to the corresponding point on limit state surface. Therefore, the distance to the failure surface can be measured by the safety index function. Of particular interest, the safety index was defined by the shortest distance from the origin to the failure surface.

The Hasofer-Lind (HL) reliability index can be interpreted as a first-order-second-moment (FOSM) reliability index. The value of HL reliability index is the same for the true failure surface as well as for the approximate tangent hyperplane at the design point. The ambiguity in the value of the first-order reliability index is thus resolved when the design point is taken as the linearization point. The resultant reliability index is a sensible measure for the distance to the failure surface.

The main steps of the HL iteration method are summarized as follow:

1) Define the appropriate LSF; 2) Set the mean value point as an initial design point; 3) Compute the initial reliability index using the MVFOSM method; 4) Compute a new design point; 5) Compute the HL safety-index; 6) Repeat steps 4 to 6 until the estimate of reliability index converges; 7) Compute the coordinates of the design point or MPP.

Even though the HL method usually provides better results than the MVFOSM method for nonlinear problems, there is no guarantee that the HL algorithm converges in

all design situations. The convergence of the iteration scheme depends greatly on a proper starting point that is not easy to obtain in complex scenarios. Furthermore, the HL method only considers normally distributed random variables, so it cannot be used for reliability problems with non-Gaussian random variables (Choi et al., 2007).

To overcome these limitations, the LSF should be approximated by other reliability analysis methods, such as the Two-point Adaptive Nonlinear Approximations (TANA) method. This new class of approximation is constructed by using the Taylor series expansion in terms of new type of variables called "adaptive variable". Here, adaptability refers to the capability to automatically match the nonlinearity of various functions by defining a nonlinear index term. The nonlinearity of the adaptive approximations is changed by using the function values and gradients at the known points generated during the iteration process. The corresponding reliability method is called FORM with adaptive approximation (Wang and Grandhi, 1995).

Usually, the adaptive safety index algorithm is computationally better than the HL method, because the nonlinear index is determined by comparing linear approximations in each iteration run and minimizing the difference between the exact and the approximate LSF. Here, computation of the exact performance function is not required; therefore, computer time is greatly reduced for problems involving complex and implicit performance functions, particularly with a sophisticated finite element models for structural response simulation.

Furthermore, the superiority of the FORM with adaptive approximation method lies in the fact that it is able to include different types of uncertainty for the input variables; whereas the HL method is limited to variables with normal distribution (Wang et al., 1995).

Although the implementation of FOSM reliability methods is simple, it has been shown that the accuracy is not acceptable for low probability of failure or for highly nonlinear responses (Arora, 2004). Thus, if the linear approximation approach is used to describe the LSF, the reliability assessment results could be inaccurate and misleading. In addition, the selection of the initial trial point for the iteration will also affect the convergence rate especially for a design point associated with a large curvature of LSF. This is due to the fact that the calculated nonlinear index would remain the same for the rest of the iteration process, which would affect the efficiency of calculations.

SORM

FORM usually works well when the limit-state function is nearly linear in the neighborhood of the design point and the limit state surface has only one MPP on the failure surface. However, if the failure surface has large curvature due to high nonlinearity, the failure probability estimated by FORM using the safety index may give unreasonable and inaccurate results (Melchers, 1987). To address this problem, the second-order Taylor series (or other polynomials) should be employed. The SORM features an improved accuracy by using a quadratic approximation. Thereof, the second-order approximation of the response surface where LSF equals to zero is given by the second-order Taylor series expansion at the MPP.

The SORMs have been developed in previous studies (e.g. Hohenbichler and Rackwitz, 1981; Breitung, 1984; Tvedt, 1984, 1990; Koyluoglu and Nielsen, 1994) by using the second order approximation for the original LSF at each design point. Further, Der Kiureghian et al. (1987) and Wang and Grandhi (1995) simplified the calculation procedure of the second-order failure probabilities by replacing the original limit state

surface curvature with an adaptive function by using a constant nonlinear index over the design process. The proposed reliability method is called SORM with adaptive approximation.

2.4.3 Sensitivity analysis

If a reliability based structural design method is employed in an environment where frequent estimate of reliability indices are required, analysis can be updated by repeatedly applying the approximation at each design point. However, the repeated application may result in a high computational cost, and may also suffer from the risk of non-convergence at the studied design point (Haukaas and Der Kiureghian, 2005).

Assume a structure is subjected to a varying load condition. The structural parameters (e.g. stiffness, damping, and strength) and the characteristics of excitation source (e.g. intensity and frequency) are identified. Then, reliability analysis is applied to determine response of the system, normally in terms of an index known by reliability-index. Usually, in many practical problems, the uncertainties due to the randomness of the effective parameters are not of equal importance. In these cases, the reliability analysis methods should be combined with random process and random vibration methods. The integrated technique would help to compute failure probabilities as well as sensitivity factors in a more efficient way. Noteworthy, sensitivity factors quantifies the importance of the parameters that mainly contribute to the reliable performance of the structure. Thus, applying the sensitivity analysis is useful in reducing the size of problems with large number of random variables. This is due to the fact that in general only a few variables would have a significant effect on the structural reliability response(s). Consequently, sensitivity of the failure probability or the safety index to small changes in the random

variables would provide information useful in studying the statistical variation of the response. Therefore, the reliability analysis method needs to be modified to obtain sensitivity derivatives at each design point. These derivatives are later used to study the effect of parametric modifications (Li et al., 2007).

2.4.4 Reliability-based design optimization (RBDO)

In most of the reliability studies, an optimized solution is considered for the problem of structural sensitivity analysis (e.g. Madsen and Tvedt, 1990; Simoes and Negaro, 2005; Li and Lence, 2007). Deterministic optimization enhanced by reliability evaluation and formulated within the probabilistic framework is called reliability-based design optimization (RBDO). RBDO methods can be viewed as the optimization algorithms that utilize reliability methods to evaluate the probabilistic constraints and/or the objective functions used to describe reliability (Chiralaksanakul and Mahadevan, 2005).

In structural optimization, the objectives and constraints are generally functions of the structural response which in turn is a function of the optimization variables. RBDO methods have been applied to a broad range of structural design and maintenance problems in civil engineering. Weight, stiffness, displacements, stress, Eigen frequencies, buckling load, and geometrical properties are included in typical structural reliability-based design optimization problems.

Mori and Ellingwood (1993; 1994) conducted the reliability-based service-life assessment analysis of aging concrete structures by applying a RBDO method. Maintaining reliability of concrete structures was treated as a role of inspection or repair in their findings by including the uncertainties in loading conditions, structural strength, and strength

degradation due to aggressive environmental stressors. Enright and Frangopol (1998) evaluated the effects of load redistribution on the concrete bridges over their life-time by applying different RBDO methods.

2.5 STATISTICAL WIND SPEED ANALYSIS

In order to assess the reliable performance of a damped stay cable when subjected to wind load, effect of uncertainty associated with wind should be considered in a way which can be handled in a probabilistic approach. In this matter, the establishment of appropriate design wind speeds is a critical first step towards the calculation of design wind loads for structures, as they enable the random variables involved such as wind speed and wind direction to be modelled mathematically. Since these variables are random processes, i.e. they have time-varying characteristics, the probabilistic analysis of historical data on recorded wind speed is required. In this regard, some statistical-based methods for the identification of wind properties and prediction of extreme design wind speed are developed (Holmes, 2007).

The approaches to probabilistic analysis of wind speed database can be divided into those based on the parent distribution analysis methods, and those based on the extreme value wind distribution analysis methods. The underlying assumptions behind these two approaches are different. This arises from the fact that the stochastic nature of the wind would result in an independent relationship between the parent population of regular everyday winds and the annual extreme winds.

The parent wind probability analysis describes the distribution of the magnitude or amplitude of the recorded wind data without any regard to the time axis. Here, mathematical modelling of wind random variables including wind speed and wind

direction is conducted by statistical analysis. Frequency distribution of complete population of wind speed database at a site will be fitted with some of the most common wind engineering probability distributions including Weibull, Rayleigh and Gamma probability distributions. Then, the goodness of the fitted probability distributions will be compared by means of numerical techniques. Resultantly, the best-fitted probability distribution will be recognized. The adapted distribution could be applied to estimate the probability of occurrence of a certain wind speed or to predict the extreme design wind speed corresponding to a selected structural design return period.

Alternatively, since in wind engineering, we are often concerned with the attainable largest value of random variables (e.g. wind speed) rather than the bulk of the population, thus in practice, it has been found useful to start with a reference annual extreme wind speed based on the statistical analysis of wind speed records obtained at meteorological stations. For a very wide class of parent distributions including the daily wind records, the cumulative distribution function of the extreme values which has taken from the large random samples tends to converge to certain limiting forms of the asymptotic extreme-value distributions. In this regard, the theory of the generalized extreme value analysis of wind speed was proposed by Fisher and Tippette (1928), based on the application of one or more of the three asymptotic extreme value distributions to annual extreme wind speed database, including the Gumbel (Type I), the Frechet (Type II), and the Weibull (Type III) distribution models. In order to make predictions, the asymptotic extreme value distributions are used as empirical fits to the existing extreme wind speed data at a studied site and the goodness-of-fit of the distribution models will be compared, which depends on the form of the tail of the underlying parent distribution. Finally, by performing an inverse

analysis of the results of the corresponding cumulative distribution function, the value of extreme wind speed can be calculated for the expected structural design return period at the studied site.

2.5.1 Parent probability distribution analysis

Knowing that the reliable wind-excited response of a structure depends on the uncertainty of wind imposed by wind speed variation and frequency at a given site, it is helpful to characterize the wind speed data in the form of a known PDF. The solution simplifies presentation of the real wind speed data at a given design site by fitting them into an approximate PDF. This is attainable by using mathematical fitting techniques which yielded parameters of the corresponding probability distribution function.

Over the past few decades, a number of studies have been conducted around the world to statistically analyze the wind speed data at different design sites by using the parent probability distribution analysis methods (e.g. Hennesessey, 1977; Torres et al., 1999; Waewsak et al., 2011). In these studies different probability distributions such as Weibull, Rayleigh, Gamma, Lognormal, Exponential, and Gaussian distribution are implemented from which the uncertainty of wind can be modeled in a quantitative sense. Among these methods, the Rayleigh and the Weibull functions are the widely accepted and extensively used statistical models for wind speed data analysis and energy applications (Akpinar and Akpinar, 2004; Ohunakin, 2011).

The Rayleigh distribution function is suitable to describe wind speed independent of wind direction (Olaofe and Folly, 2012). The Weibull distribution is capable of including wind directional effect. The assigned function would be expressed by calculating the scale,

the shape, and the location parameters. These parameters represent nature of the wind (variability or stability of the wind) for an investigated wind speed and directional angle.

A number of methods have been developed to estimate the Weibull parameters (Seguro and Lambert, 2000; Costa Rocha et al., 2012; Saleh et al., 2012). The maximum likelihood, graphic, moment, Chi-square, and regression methods are commonly used in fitting wind speed frequency distribution using a Weibull function (Palutikoff, 1999). Besides, several tests are adopted to validate accuracy of the estimated wind distributions from the above statistical functions, which indicate if the accuracy of the fitted distribution function is satisfied or not.

2.5.2 The Generalized Extreme Value distribution (GEV) analysis

It has been shown by Fisher and Tippett (1928) that if a sample of *n* cases is chosen from a parent distribution, and the maximum of each sample is selected, then the distribution of the maxima approaches one of the three limiting forms: the Gumbel (Type I), the Frechet (Type II), and the Weibull (Type III) distribution models, as the size of the samples increases. Thus, the Fisher-Tippett distributions could be fitted to the set of annual maxima of wind speed database resulting in the form of the asymptotic extreme value distributions. The objective of implementing extreme value distribution analysis method is to define the form of the limiting distributions and estimate the parameters, so that values of extreme wind speed can be calculated.

The generalized extreme value distribution was introduced by Jenkinson (1955) by combining the three extreme value distributions into a single mathematical form which has been widely applied in wind engineering as follows:

$$F(U) = \exp\left\{-\left[1 - k\frac{(U-u)}{\alpha}\right]^{\frac{1}{k}}\right\}$$

(2-1)

where $F(U)$ is the cumulative probability distribution function of the random wind speed variable U. The parameters α, u and k are the scale factor, the location factor and the shape factor, respectively. In the case of $k = 0$, Eq. (2-1) will become the Type I extreme value distribution (Gumbel distribution). In addition, $k > 0$ and $k < 0$, represent the cases of the Type II extreme value distribution (Frechet distribution), and the Type III extreme value distribution (Weibull distribution), respectively.

The Type I extreme value distribution method (Gumbel method) is applied to wind speed database as a primary method due to its simplicity in formulation among other methods. The Type II extreme value distribution method (Frechet method) does not seem to have received enough interest in the statistical wind speed analysis due to the fact that the atmosphere would produce a limited value for the maxima of wind speed and the Frechet method entails an unbounded value for its higher end. Therefore, it lacks capability to be fitted for the annual extreme wind speed data set. However, it has been adopted as a useful method for modeling and analyzing several extreme events such as the accelerated life testing, earthquake, flood, rainfall, and sea current probability density function (Harlow, 2002; Nadarajah and Kotz, 2008; Abbas and Tang, 2013).

Since it is expected that there is an upper limit to the wind speed that the atmosphere can produce, the Type III distribution (Weibull distribution) may be more appropriate for statistical wind speed analysis. Accordingly, the Type III extreme distribution methods including the three-parameter Weibull model (Weibull 3P) and the two-parameter Weibull model (Weibull 2P) can be applied to estimate the values of the extreme wind speed.

2.5.3 Prediction of extreme wind speed corresponding to a desired design return period

It is of interest to predict the value of extreme wind speed attainable at a design site. Substituting for the cumulative distribution function (CDF) of wind speed data from the results of the fitted distribution models, the extreme wind speed corresponding to a selected return period R can be calculated, $U_{ext}(R)$.

Due to stochastic nature of wind, there is an independent relationship between occurrences of each wind speed within service life of structure. Assume a structure exposed to wind load at service time of N-years, this implies that N-discrete independent records of annual extreme wind speed would be expected. Besides, the structure should be designed in regard to a definite return period. For instance, consider a return period of R-years in design of a structure under wind load, the extreme wind speed $U_{ext}(R)$ should be predicted. Further details on the required calculations will be illustrated in Appendix B.

2.6 APPLICATION OF RELIABILITY ANALYSIS METHODS TO WIND-INDUCED EXCITATION OF BRIDGE STRUCTURES

In recent decades, numerous reliability-based studies have been conducted on wind-sensitive structures. As a point of interest, some of them were devoted to reliability assessment of bridge structures including suspension bridges and cable-stayed bridges of which the flutter and/or fatigue reliable response induced by wind loading conditions were determined. In these studies, the life time performance of bridge structures was evaluated through applying numerical-based reliability software's such as FERUM or OpenSees accompanied by a sensitivity-based reliability analysis (Haukaas and Der Kiureghian, 2007; Bourinet et al., 2010).

The pioneer study on bridge flutter reliability analysis is done by Namini et al. (1992) who proposed a probabilistic approach to computational finite element-based flutter analysis of cable-suspended bridges. The defined method allowed determination of the critical wind velocity that initiated damping-or stiffness-driven flutter in this type of bridge. Later, application of a series of probability calculation approaches to a reliability-based flutter model of a cable-stayed bridge under extreme winds was presented by Ge et al. (2000). In this study, a LSF has been established as a function of the resistance given by the critical flutter speed and the load variable which is the extreme wind speed corresponding to a given return period at the bridge site. Similarly, Cheng et al. (2005) carried out a reliability analysis on the flutter sensitivity of suspension bridges with respect to the mean values and the standard deviations of the variables of interest. Also, Cheng and Xiao (2005) proposed a stochastic finite-element-based algorithm for the probabilistic flutter analyses of suspension bridges through combination of the advantages of the response surface method, finite element method and Monte Carlo simulation.

Further, Kusano et al. (2015) applied two of the most commonly used RBDO approaches including reliability index approach (RIA) and the performance measure approach (PMA), to cables and bridge deck of long-span suspension bridges under flutter constraint. The probabilistic flutter design optimization method were conducted for a real bridge example by including girder thickness and main cable area as design variables, while extreme wind speeds and flutter derivatives were also considered as random variables. Ultimately, bridge collapse due to flutter was framed in a risk analysis approach by Argentini et al. (2014) and later by Mannini and Bartoli (2015) in which the uncertainty propagation from flutter derivatives to critical wind speed was examined. The statistical

properties of experimental flutter derivatives as well as the probability distribution of the flutter critical wind speed was included in the MCS-based analysis to solve the problem in several case studies.

The probabilistic-based lifetime assessment of bridge structures due to the detrimental effect induced by fatigue is also investigated in some of the previous studies. For instance, performance of long span suspension bridge hangers due to fatigue effect induced by wind action and train transit was estimated by Petrini and Bontempi (2011). Resultantly, general formulations of the design of suspension bridges were presented in a reliability context. The study can be applied as a typical framework for a preliminary bridge design or for a feasibility analysis for a proposed structural scheme as a base in the performance-based design of an extreme long-span suspension bridge. Likewise, Zhang et al. (2013) showed that during a bridge's life cycle, the stresses from multiple dynamic loads such as wind and traffic might be superposed and progressive fatigue damage might accumulate and induce serious fatigue damage issues. They proposed a reliability method in accordance to fatigue damage increments (associated with the number of stress cycles at different stress range levels) as obtained using the fatigue damage accumulation rule. The probability of failure from the fatigue damage at the end of each block of stress cycles and the cumulative probability of failure were calculated. Hence, the reliable fatigue life response for a given structure was assessable. Pourzeynali and Datta (2005) combined overall concepts of bridge aerodynamics, fatigue analysis and reliability analysis to present a probabilistic model of suspension bridges against fatigue failure due to the wind gust. Thereof, the fluctuating response of bridge deck was obtained for buffeting force using finite element method and spectral analysis in the frequency domain. It was concluded that

the value of probability of fatigue failure in suspension bridges was significantly influenced by the exponential decay coefficient of the spatial correlation of the gustiness of the wind velocity, duration and number of storms in a year, mean wind distribution parameters, and the assumed design life of the bridge.

The idea of applying reliability methods to lifetime assessment of bridge structures has been extended in several studies via computational reliability techniques integrated with finite element analysis. Imai and Frangopol (2001) conducted finite-element analysis of suspension bridges using reliability-based approach with the consideration of geometric nonlinearity. Noteworthy, is the capability of their model to assess the effects of failure of various elements on the reliability of undamaged elements and on the reliability of the overall bridge. Cheng and Li (2009) presented an efficient method for reliability assessment of long-span steel arch bridges against wind-induced stability failure by proposing a generalized first-order reliability algorithm via a MATLAB software tool called FERUM. Notable is the work of Haukaas and Der Kiureghian (2007) in which the reliability and response sensitivity algorithms were implemented in a general-purpose finite-element-based software (OpenSees). They adapted an object-oriented programming approach to achieve a sustainable software with focus on maintainability and lifetime extensibility of bridge structures. Yan and Chang (2009) assessed the vulnerability of cable-stayed bridges through a stochastic finite-element analysis using the first-order second-moment reliability method via an event tree approach. The proposed assessment methods were illustrated using a hypothetical single-tower cable-stayed bridge to provide a quantitative tool for analyzing the vulnerability performance of cable-stayed bridges. In parallel, the response surface Monte Carlo method (RSMCM) was proposed by Su et al.

(2010) for reliability analysis of aerostatic response and aerostatic stability of different types of long-span bridges, in which the nonlinear effects due to geometric nonlinearity and deformation-dependent aerostatic loads were taken into consideration.

Practical implementation of probabilistic-based design and assessment methods for bridges was presented by Enevoldsen (2011). It was attempted to achieve higher wind load tolerance rate from a bridge structure (i.e. higher load carrying endurance) while comparing that with a traditional deterministic-based design. In parallel, a case study was analyzed by Leon et al. (2015) to determine the bridge structural reliability against wind loading. The inherent variabilities of the random wind force and of the mechanical properties of steel were included and it was shown that they contribute to the probability of failure of the steel girder. The structural reliability-based response for different life-cycles were presented for a risk-aversive design.

CHAPTER 3

DETERMINISTIC-BASED DESIGN ANALYSIS OF BRIDGE STAY CABLES EQUIPPED WITH EXTERNAL DAMPERS

This chapter is developed based on the current state-of-the-art on the dynamic analysis of cable-damper systems. The presented materials aim to provide ample understanding on the pertinent deterministic-based design approaches on evaluation/assessment of the structural damping ratio of stay cables equipped with external dampers.

3.1 INTRODUCTION

3.1.1 Backgrounds

Steel cables used in cable-stayed bridges and suspension bridges are flexible and have low inherent damping, resulting in high susceptibility to vibrations either induced by direct loads on the cable from wind or a combination of wind and rain, or via motion of the supported structure (Yamaguchi and Fujino, 1998). These vibrations can result in premature cable or connection failure and/or breakdown of the cable corrosion protection systems, reducing the life of the cable structure (Watson and Stafford, 1988). Moreover, cable vibrations can have a detrimental effect on public confidence in the safety of cable structures (Kumarasena et al., 2007).

A number of controlling methods such as tying cables together, aerodynamic cable surface modification, passive and active axial and transverse cable dampening have been applied to mitigate cable vibrations (Main and Jones, 2001). For aesthetic and practical reasons, external dampers are most commonly used in field. The potential for widespread

application of dampers to suppress cable vibrations necessitates a thorough understanding of the resulting dynamic system.

The performance of a damper in controlling large-amplitude vibration of a stay cable is often evaluated in terms of the equivalent structural modal damping level (ratio) achieved after the damper is added. Carne (1981) was among the first to investigate the vibrations of a taut cable with an attached damper by focusing on determination of first-mode damping ratios when damper locations are near the end of the cable. Carne developed an approximate analytical solution by proposing a transcendental equation for the complex eigenvalues. As a result, an accurate approximation for the first mode damping ratio as a function of the damper coefficient and location was found. Similarly, Kovacs (1982) developed approximation solutions for the maximum attainable damping ratio in agreement with Carne. The research showed that an optimal damper size exists and the optimal damping coefficients for the transverse passive viscous damper control strategy of a taut cable have been developed. Later, Yoneda and Maeda (1989) and Uno et al. (1991) have conducted numerical studies on the optimum damper size and presented that the maximum attainable modal damping is directly proportional to the damper distance from the cable anchorage and is independent of the vibration mode number.

Several investigators have worked to develop modal damping estimation curves of general applicability (e.g. Yoneda and Maeda, 1989; Pacheco et al., 1993). Notable is the work of Pacheco et al. (1993) toward simplifying the procedure of designing viscous dampers for stay cables, by properly grouping the relevant parameters into dimensionless forms, which can be applicable in many practical design situations. The results have been displayed in the form of a "universal estimation curve", relating the modal damping ratio

to the damper size (damping coefficient). Krenk (2000) derived an analytical formula for Pacheco's damping "universal estimation curve" by utilizing a small perturbation on well-known solutions of the cable without a damper, based on which, an asymptotic solution to the free vibration of a horizontal taut cable-damper system was developed.

Although, assumption of a taut string would simplify the analysis process, in this way, effects of some of the actual parameters affecting the dynamic behavior of cables are ignored. The most important of these cable parameters are the sag and the bending stiffness. In this regard, Mehrabi and Tabatabai (1998) presented a refined solution to a cable-damper system by considering the cable sag and the cable bending stiffness in the formulations, based on using a finite difference method. It was shown that influence of the cable sag is not significant for most real cables, but the cable bending stiffness parameter plays a more important role. Similarly, effect of these two parameters on the dynamic behavior of cable-damper system was addressed by Krenk and Nielsen (2002) and Hoang and Fujino (2007).

Subsequently, several attempts on finding a more general expression for the damping property of a typical cable-damper system were directed. Tabatabai and Mehrabi (2000) introduced a set of non-dimensional parameters to include effects of the cable (inclination, sag, and bending) and the damper parameters on the structural frequency and the damping response over the practical ranges of the cable and the damper parameters. Analytical study performed by Fujino and Hoang (2008) has been resulted in an accurate asymptotic formula of the equivalent structural modal damping ratio of a general cable-damper system. The damping response was derived in an explicit form by taking into account reductions in the damper effectiveness due to influential parameters such as the cable sag, the cable bending stiffness, and the damper support stiffness.

In a different approach, Cheng et al. (2010) proposed an energy-based method, relying on the kinetic energy decay ratio as a key index, to evaluate the mitigation effect of a damper on the damping property of a cable. The solution of the dynamic equation of the system was obtained by conducting a series of finite element analysis. The model was enhanced to taken into account the flexural rigidity and the sagging effect of the cable. Noteworthy, for the development of the solution, the restriction on the damper location which has been existed in the previous studies was eliminated. This is resulted in a more general design tool on the structural damping evaluation of bridge stay cables.

3.1.2 Organization of the chapter

The contents of this chapter are organized in the following order: First, a typical model of a horizontal non-flexural taut cable with an attached linear viscous damper is introduced. The analytical formulation of the free-vibration problem is developed from which a transcendental equation for the complex eigenvalues is derived. Then, the solution of the equivalent structural modal damping ratios are extracted from the imaginary parts of the eigenfrequencies. The problem is further extended by considering influence of the cable sag, the cable bending stiffness, and the cable inclination in the analysis formulations.

In the remaining of the study, an energy-based method is applied to evaluate the damping property of a typical cable-damper system. A finite element based model of the representative cable-damper system is developed by using the numerical software, ABAQUS, of which the structural modal damping ratio is determined. It is shown that by implementing the energy method in the analysis process, the effects of cable and damper parameters (such as cable inclination, cable bending stiffness, cable flexural rigidity, damper capacity, and damper location parameter) on the damping response of a cable-

damper system could be evaluated promptly. Subsequently, damping estimation curves are presented by considering the practical ranges of structural parameters for the studied cable-damper system. The results would be employed to simplify the preliminary design of linear viscous dampers assigned to the stay cables due to different structural design configurations. Besides, the magnitude of the maximum attainable damping ratio corresponding to an optimum damper size would be determined.

The information presented in this chapter will pave the roads for the work presented in the subsequent chapters, with consideration of uncertainties associated with structural and load parameters in the problem using a probabilistic-based sense.

3.2 FREE VIBRATION OF A HORIZONTAL TAUT CABLE-DAMPER SYSTEM

In this section, the analytical method on formulation of the free vibration problem of a cable-damper system is reviewed. First, a basic model of a horizontal taut cable with an externally attached damper is introduced. The equation of motion of the studied cable-damper system is derived of which the frequency equation to determine complex eigen frequencies are presented. Subsequently, solution to this complex eigenvalue problem is presented in the form of an attainable structural modal damping ratio for a given damper location.

The principal advantage of having an analytical model is that the influence of the important system parameters on the system behavior can be studied in depth. In addition, the derived formulations will provide a base to assess the reliability of system performance in the subsequent chapters.

3.2.1 Description of the system

The studied cable-damper system consists of a horizontally laid cable with length L and mass per unit length of m. The pretention of the cable is T. An external viscous damper with damping coefficient c is transversely attached to the cable at a distance L_d from one cable end. A coordinate system is defined with the X-axis along the cable chord and the Y-axis in the perpendicular direction, as shown in Figure 3.1. For the convenience of derivation and discussion, two local coordinate systems X_1 and X_2 are also defined and shown in the figure.
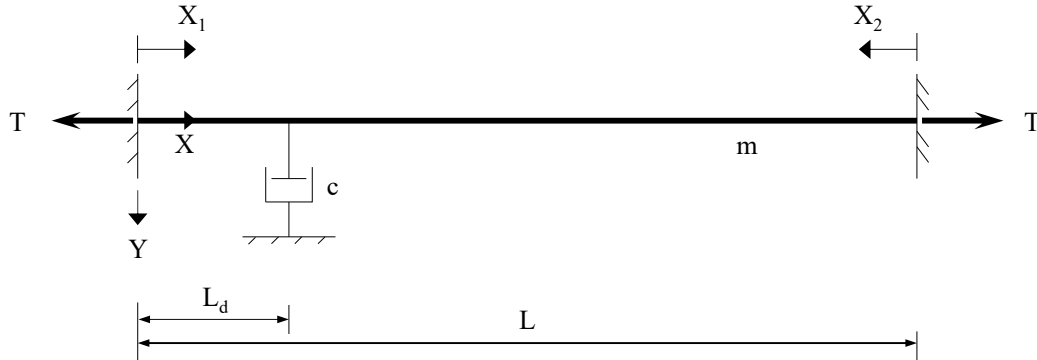
Figure 3.1: Basic taut cable model with an external linear viscous damper

3.2.2 Assumptions

The assumptions made for the taut cable-damper system of interest are listed as follows:

Assumptions for the cable:

1. Only consider the in-plane motion of the cable.

2. The magnitude of the cable tension is high enough to ensure a taut cable profile.

3. The small axial strain in the cable due to tensile force can be neglected.

4. The bending stiffness is neglected.

48

5. The cable material is assumed to behave elastically, so Hooke's law is valid.

6. The structural damping of the cable itself is neglected.

Assumptions for the damper:

1. The damper is attached transversely to the cable.

2. The damper is of an idealized linear viscous type.

3. The stiffness of the damper itself and its support are neglected.

3.2.3 Equation of motion

In this section, the free body diagram of a typical infinitesimal small element of the cable in Figure 3.1 will be presented first, based on which, the partial differentiation equation describing the motion of a damped taut cable will be derived.

Considering a typical infinitesimal small cable element in Figure 3.1, the free body diagram of such an element is depicted in Figure 3.2.
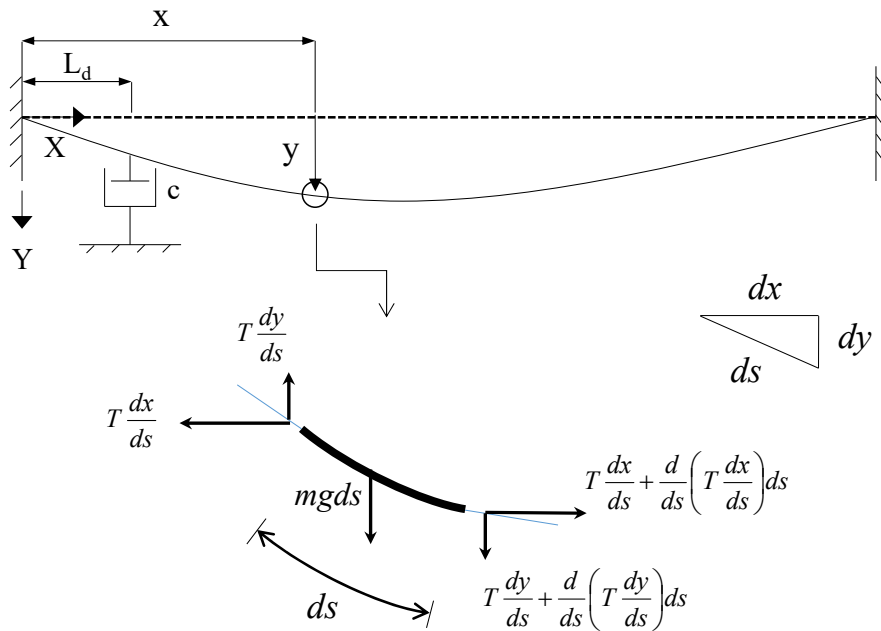
Figure 3.2: Free body diagram of an infinitesimal small cable element

The equilibrium equations in the vertical and horizontal directions are:

Horizontal direction:
$$T\frac{dx}{ds} = T\frac{dx}{ds} + d\left(T\frac{dx}{ds}\right) \rightarrow d\left(T\frac{dx}{ds}\right) = 0 \tag{3-1}$$

Vertical direction:
$$T\frac{dy}{ds} + d\left(T\frac{dy}{ds}\right) = T\frac{dy}{ds} + mgds \rightarrow d\left(T\frac{dy}{ds}\right) = mgds \tag{3-2}$$

where T is the tension in the cable, m is the unit mass of the cable, ds is the length of the infinitesimal element.

Assume that the intensity of the transverse load per unit span is a constant; the resulting profile of the cable thus has a parabolic shape. Since the cable element is very small, it gives $ds = \sqrt{(dx)^2 + (dy)^2}$. Considering the equilibrium in the vertical direction, by dividing both sides of Eq. (3-2) by ds, yields

$$\frac{d}{ds}\left(T\frac{dy}{ds}\right) = mg \tag{3-3}$$

or
$$T\frac{d^2y}{ds^2} = mg \tag{3-4}$$

$$Td^2y = mgds^2 \tag{3-5}$$

$$T\frac{d^2y}{dx^2} = mg\frac{d^2s}{dx^2} \tag{3-6}$$

$$T\frac{d^2y}{dx^2}\frac{dx}{ds} = mg\frac{ds}{dx} \tag{3-7}$$

$$\left(T\frac{dx}{ds}\right)\frac{d^2y}{dx^2} = mg\frac{ds}{dx} \tag{3-8}$$

$$T \frac{dx}{ds} \frac{d^2 y}{dx^2} = mg \frac{\sqrt{dx^2 + dy^2}}{dx} \qquad (3\text{-}9)$$

The governing static equilibrium equation of a cable in the vertical direction is thus derived to be

$$T \frac{dx}{ds} y'' = mg \sqrt{1 + [y'(x)]^2} \qquad (3\text{-}10)$$

where $y' = \dfrac{dy}{dx}$ and $y'' = \dfrac{d^2 y}{dx^2}$. For simplicity, the horizontal force component $T\,(dx/ds)$ is denoted as H.

When the cable is vibrating, both cable tension and its displacement vary with time. The dynamic equilibrium equation of the cable in the transverse direction at any arbitrary time instant t can be derived by replacing the horizontal component H of the static cable tension and the static cable deflection y in Eq. (3-2) with the dynamic cable tension $H(t) = H + h(t)$ and the dynamic displacement $y(x, t) = y(x) + \eta(x, t)$, respectively, where $h(t)$ and $\eta(x, t)$ are the additional cable tension and vertical deflection due to cable vibration, respectively.

By substituting the new variables into Eq. (3-10), and also considering the inertia force, the equation of motion describing the vertical in-plane vibration of a taut cable is

$$[H + h(t)] \cdot [y''(x) + \eta''(x,t)] = [mg - m\ddot{\eta}(x,t)] \sqrt{1 + [y'(x) + \eta'(x)]^2} \qquad (3\text{-}11)$$

Based on Eq. (3-10), the two static terms in Eq. (3-11), i.e. $mg \sqrt{1 + [y'(x) + \eta'(x)]^2}$ and Hy'', could be cancelled out. In addition, for a taut cable, $|y'(x)| \ll 1$, which means $[y'(x)]^2 \approx 0$. Consequently, the reduced form of Eq. (3-11) will be

51

$$m\ddot{\eta}(x,t)+[H+h(t)]\cdot\eta''(x,t)+h(t)y''(x)=0 \tag{3-12}$$

Eq. (3-12) is a second order nonlinear differential equation. Assume that the additional cable tension "$h(t)$" due to vibration is small compared to the pretension T, the second order terms $h(t)\cdot\eta''(x,t)$ and $h(t)y''(x)$ can be neglected and Eq. (3-12) will become a linear differential equation, i.e.

$$m\ddot{\eta}(x,t)+H\eta''(x,t)=0 \tag{3-13}$$

Damper force, boundary condition, continuity and equilibrium condition at damper location

The equation of motion of a taut cable-damper system can be obtained by adding the effect of the linear viscous damper into Eq. (3-13). The damper force is expressed as $F_d=c[d\eta(L_d,t)/dt]$, where $\eta(L_d,t)$ denotes the transverse displacement of the cable at the damper location at time t, which has a distance L_d from the cable end and F_d is the damper force. For convenience, the damper force could be described by using the Dirac delta function, i.e.

$$F_d=c\,\dot{\eta}(x,t)\,\delta(x-L_d) \tag{3-14}$$

The equation of motion describing the free vibration of a taut cable-damper system in the vertical plane can thus be expressed as

$$m\ddot{\eta}(x,t)+H\eta''(x,t)=c\dot{\eta}(x,t)\delta(x-L_d) \tag{3-15}$$

The partial differential equation, Eq. (3-15), is to be solved with the boundary conditions specifying the fixed ends, i.e. $\eta(0,t)=\eta(L,t)=0$.

By attaching the damper, the cable is divided into two segments. At the damper location, the continuity of displacement and equilibrium of forces must be satisfied as depicted in Figure 3.3.
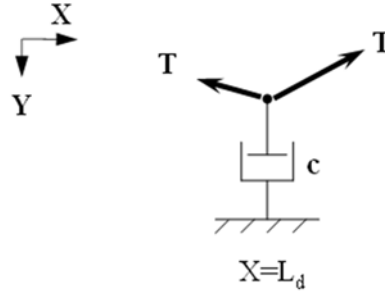
Figure 3.3: Equilibrium and compatibility conditions at cable-damper attaching point

The summation of the vertical component of the cable tension in the left and right segments with respect to the damper location should balance the force in the damper, so the vertical equilibrium equation at the damper location can be written as:

$$T\left(\frac{\partial \eta}{\partial x}\bigg|_{L_{d^+}} - \frac{\partial \eta}{\partial x}\bigg|_{L_{d^-}}\right) = F_d \tag{3-16}$$

where η is the dynamic vertical displacement in the Y direction. Eq. (3-16) implies relation between the space and time derivatives of the cable displacement at $x=L_d$. Coupling of spatial and time variables will lead to complex mode shapes and frequencies for free vibration of the system.

Frequency equation

By using the separation of variables technique, the free vibration response of each cable segment is assumed to have the form of

$$\eta_k(x_k,\tau) = \upsilon_k(x_k)\, e^{\lambda \tau} \qquad k=1,\, 2 \tag{3-17}$$

where $\tau = \omega_{01}t$ is a non-dimensional time variable as introduced by Pacheco et al. (1993), ω_{01} is the complex eigen frequency defined as $\omega_{01} = (\pi/L)\sqrt{H/m}$, λ represents a non-dimensional eigenvalue that is complex in general, and $v_k(x_k)$ is the corresponding complex mode shape at distance x_k for cable segment k (k=1,2).

The complex mode shape $v_k(x_k)$ satisfies the ordinary differential equation (Main 2002):

$$\frac{d^2 v_k(x)}{dx^2} + \omega_{01}{}^2 v_k(x) = 0 \tag{3-18}$$

The solution to Eq. (3-18) could be expressed in the following form:

$$\text{For } k\text{=1,} \quad v_1(x) = v_1(L_d)\sin(\omega_{01}x_1)$$
$$\text{For } k\text{=2,} \quad v_2(x) = v_2(L - L_d)\sin(\omega_{01}x_2) \tag{3-19}$$

The boundary conditions of zero vertical displacement at the cable ends can be expressed as $v_1(0,t)$=0, $v_2(0,t)$=0. Considering the continuity of displacement at the damper-cable attaching point which is $v_1(L_d) = v_2(L-L_d)$, and applying it to Eq. (3-19), gives

$$v_k(x_k) = v_1(L_d)\frac{\sinh(\omega_{01}x_k)}{\sinh(\omega_{01}L_d)} \tag{3-20}$$

where $v_1(L_d)$ is the deflection at the damper location.

Substitute the mode shape representation, Eq. (3-20), into the force balance relation, Eq. (3-16), while considering the assumption of Eq. (3-17), yields an equation for the determination of the complex eigen frequencies which is

$$\coth(\omega_{01}L_d) + \coth[\omega_{01}(L - L_d)] + \frac{c}{\sqrt{Hm}} = 0 \tag{3-21}$$

54

Eq. (3-21) is called the "frequency equation" by Krenk (2000). Its roots are the eigenvalues of the system, each corresponding to a distinct mode of vibration. This form of frequency equation can be solved in an asymptotic form or numerically by iterations.

3.2.4 Solution to the complex eigenvalue problem

For specific values of $c/\sqrt{Hm}$ and L_d/L, Eq. (3-21) can be directly solved numerically to obtain the damping ratios in as many modes as desired. Each eigenvalue can be written explicitly in terms of real and imaginary parts. The eigenvalue associated with the ith mode is

$$\phi_i = \frac{\omega_i}{\omega_{01}}\left(\sqrt{1-\zeta_i^2} + i\zeta_i\right) \tag{3-22}$$

where ζ_i is the damping ratio and ω_i is the modulus of the dimensional eigenvalues of the ith mode, which is termed as pseudo-undamped natural frequency by Krenk (2000).

The structural damping ratio ζ_i can then be calculated from the real and the imaginary parts of Eq. (3-22) as

$$\zeta_i = \frac{-\operatorname{Im}(\phi_i)}{\omega_i/\omega_{01}} = \left\{\left[\frac{\operatorname{Re}(\phi_i)}{\operatorname{Im}(\phi_i)}\right]^2 + 1\right\}^{-0.5} \tag{3-23}$$

Eq. (3-23) will provide the damping property of the studied cable-damper system in terms of the equivalent modal damping ratio of the ith mode.

Alternatively, Eq. (3-21) can be solved asymptotically. Introducing the asymptotic representation of the wave number $\omega_{0n}=n\pi/L$ in the nth mode and also considering $L_d/L<<1$ in Eq. (3-21), leads to an asymptotic approximation of the damping ratio in Eq. (3-23). It is simplified in Eq. (3-24) as

$$\frac{\zeta_n}{L_d/L} \approx \frac{\left(\dfrac{c}{\sqrt{Hm}}\, n\pi L_d/L\right)}{1+\left(\dfrac{c}{\sqrt{Hm}}\, n\pi L_d/L\right)^2} \qquad (3\text{-}24)$$

The relation in this form expresses the modal damping ratio of the cable as a simple function of the cable-damper parameters which are combined as $cn\pi L_d/(\sqrt{Hm}L)$ and the non-dimensional damper location parameter, L_d/L. This form of the frequency equation can be solved either in asymptotic form or numerically by applying an iteration technique.

The asymptotic relation of Eq. (3-24) is shown in Figure 3.4. As depicted in this figure, for $c=0$, the addition of damper has no effect on the dynamic behavior of the cable, i.e. modal damping ratio remains zero. Then, the modal damping increases with the increase of external damper size c. It reaches the maximum and decreases upon further increase of c. This is due to the fact that, for higher damping parameters, the damper acts more like a rigid support. Thus, the effective length of the cable is reduced. Therefore, the frequency of the first mode of vibration will be increased. This frequency is approximately equal to the frequency of a cable that is shortened by a support at the damper location. In other words, when $c=\infty$, the cable has been divided and the equivalent modal damping ratio is obtained for a modified cable with length of $(L_d\text{-}L)$.

Estimation of the maximum attainable damping for a given damper location L_d can be derived from the condition of

$$\left.\frac{\partial \zeta_n}{\partial\left(\dfrac{c}{\sqrt{Hm}}\right)}\right|_{L_d} = 0 \qquad (3\text{-}25)$$
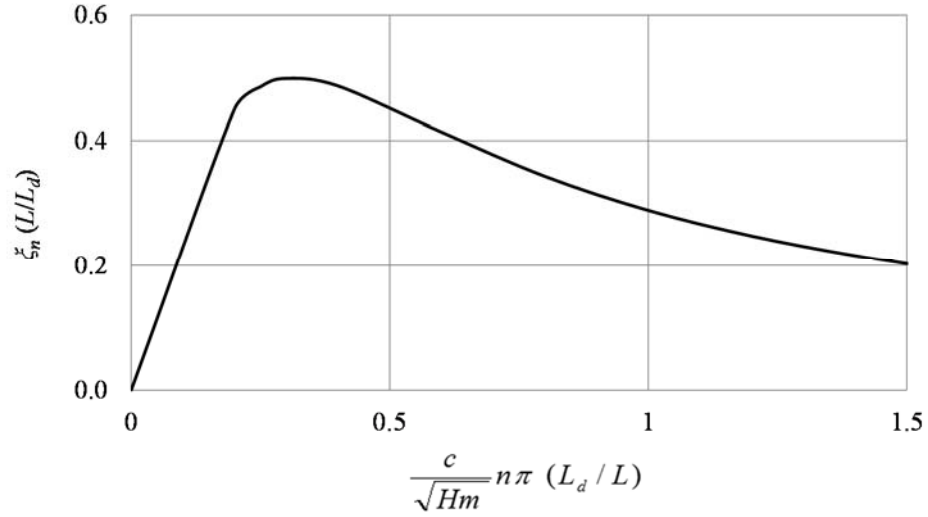
Figure 3.4: The asymptotic approximation of modal damping ratio scaled by the damper location

Thus a good approximation of the optimal value of the parameter $cn\pi L_d/(\sqrt{HmL})$ can be determined by the numerical solution of Eq. (3-25) using an iterative technique suggested by Krenk (2000). The relation between the two non-dimensional parameters, i.e. $\zeta_n/(L_d/L)$ and $cn\pi L_d/(\sqrt{HmL})$, when L_d=0.06L are shown for the first five modes in Figure 3.5. This figure represents the numerical solution of modal damping ratio of a typical horizontal taut cable-damper in terms of non-dimensional parameters. The input parameters, H, c, m, L, and L_d are combined to be the non-dimensional parameter $cn\pi L_d/(\sqrt{HmL})$. The solution of the system damping ratio has been also normalized by a non-dimensional damper location parameter as presented along the vertical axis.

Figure 3.5 highlights the existence of an optimal modal damping point in each mode. Even though, the calculated optimal design points obtained are different, the deviation is negligible. The deviation corresponds to a value of the external damping parameter $c/(Hm)^{0.5}$ slightly larger than $(\pi nL_d/L)^{-1}$.
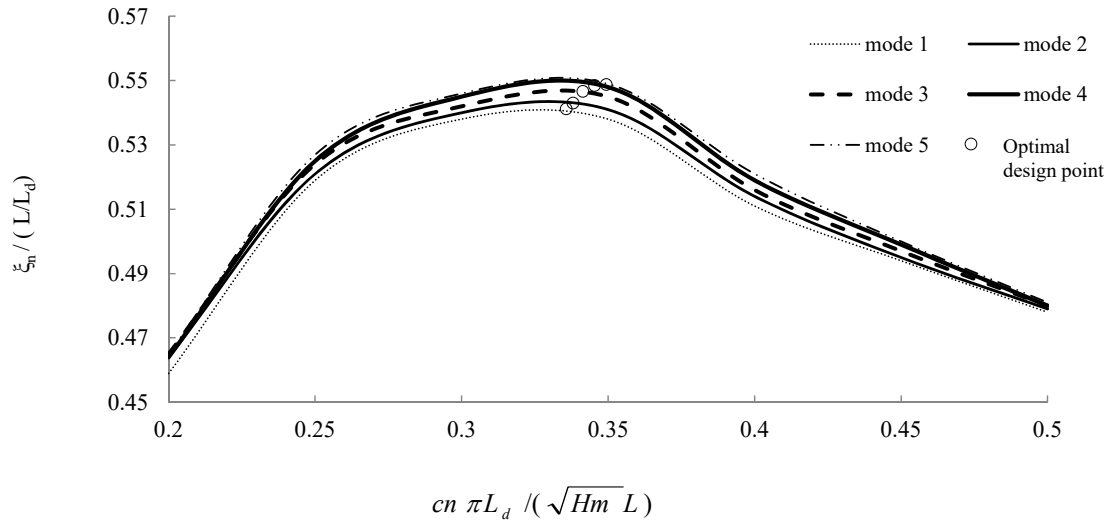
Figure 3.5: Equivalent structural modal damping ratio when L_d/L=0.06

By continuing the calculations of the equivalent structural modal damping ratio over an extended range of non-dimensional damping parameter (up to $cn\pi L_d /(\sqrt{HmL}) \approx 1.5$), it is noticeable that a single curve can accurately represent the modal damping ratio for the first few modes when small values of L_d/L are considered. This implies that a universal curve can be used to represent the damping estimation curve by grouping of structural parameters into nondimensional factors as recommended by study of Pacheco et al. (1993).

3.3 INFLUENCE OF CABLE INCLINATION, CABLE SAG, AND CABLE BENDING STIFFNESS

A schematic model of an inclined sagged cable with a transverse linear viscous damper is shown in Figure 3.6. The coordinate system is defined such that the X-axis is along the cable chord and the Y-axis is in the perpendicular direction.

58
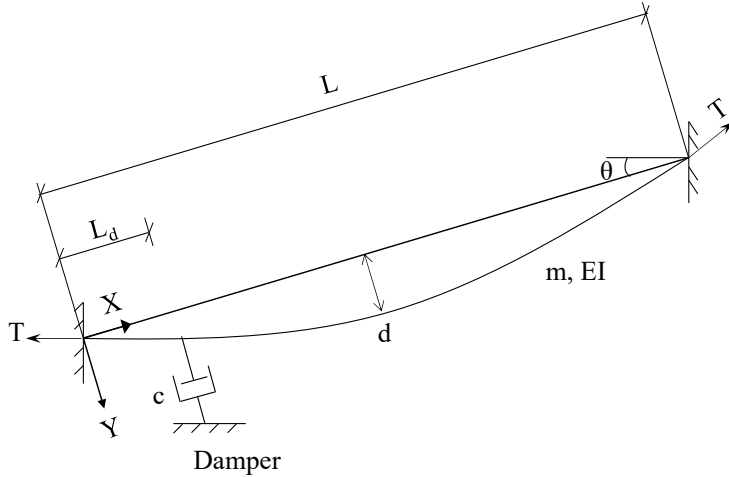
Cable with elastic material

L: length
m: mass per unit length
EI: finite flexural rigidity
θ: inclination angle
d: sag at mid-span
T: tension force

Damper

c: damping coefficient of the
     damper
L_d: damper installation location
     from the lower end support
     of cable

Figure 3.6: A model of an inclined sag cable with a transverse linear viscous damper

For a uniform cable suspended between two supports, when the cable tension is large (as in the case of bridge stay cables), its static profile can be expressed as $y=4d\cdot(x/L)\cdot(1-x/L)$, where L is the cable length, $d=mgL^2\cos\theta/(8H)$ is the cable sag at mid-span, m is the mass per unit length, g is the gravitational constant, and H is the cable tension component along its chord direction. A non-dimensional sag parameter is defined by Irvine and Caughey (1974) as $\lambda^2=(mgL\cos\theta/H)^2\cdot(EAL/HL_e)$, where A is the cross-sectional area of the cable, and $L_e=L[1+8(d/L)^2]$ is the static length of the cable. The non-dimensional sag parameter λ^2 does not only include the effect of cable sag, but also that of the cable axial stiffness and inclination. For simplicity, it is assumed that variation of λ^2 represents variation in the level of sag. For example, $\lambda^2=0$ physically represents the case of a taut cable. Stay cables on cable-stayed bridges typically have λ^2 values in the order of 10 or smaller. This is the range that will be used in the current study. Besides, a non-dimensional flexural rigidity parameter $\varepsilon=EI/(HL^2)$ is also introduced .

The in-plane transverse vibration of the cable-damper system in Figure 3.6 can be described by adding the bending stiffness contribution to Eq. (3-12):

$$H\frac{\partial^2 \eta(x,t)}{\partial X^2} - m\frac{\partial^2 \eta(x,t)}{\partial t^2} + h\frac{d^2 y}{dx^2} - EI\frac{\partial^4 \eta(x,t)}{\partial x^4} = c\,\dot{\eta}(x,t)\delta(x-L_d) \tag{3-26}$$

By introducing two dimensionless parameters, an asymptotic solution to Eq. (3.26) was derived by Fujino and Hoang (2008) in terms of the modal damping ratio of a damped cable. These two parameters are the wave number $\beta=\omega\cdot(m/H)^{1/2}$ and the flexural rigidity parameter $\varepsilon=EI/(HL^2)$. Thus, the equivalent n^{th} modal damping ratio, ζ_n, of a damped cable is represented in an explicit form by:

$$\frac{\zeta_n}{L_d/L} = R_f R_{sn} \frac{\eta_f \eta_{sn} \eta_n}{1+(\eta_f \eta_{sn} \eta_n)^2} \tag{3-27}$$

where ζ_n is the equivalent n^{th} modal damping ratio of the system, R_f and R_{sn} are respectively the reduction factors of the maximum modal damping ratio due to cable flexural rigidity and sag as defined by Krenk and Nielsen (2002), $\eta_n=\pi nc\cdot(L_d/L)/(Hm)^{1/2}$ is the dimensionless damper coefficient parameter of mode n of a corresponding horizontal non-flexural taut cable-damper system (Krenk, 2000), and η_f and η_{sn} are the modification factors for η_n due to the influence of cable flexural rigidity and sag, respectively. The simplified form of ζ_n can be obtained when the effect of sag or flexural rigidity is neglected. By taking $R_{sn}= \eta_{sn}= R_f= \eta_f=1$, Eq. (3-27) can be reduced to $\zeta_n=\eta_n/(1+\eta_n^2)\cdot(L_d/L)$, for a taut non-flexural cable.

Figure 3.7(a) shows the effect of cable sag on the first modal damping ratio ζ_1 of a horizontal cable attached with a transverse linear viscous damper ($c=102$ kN·s/m), at 6%L. The cable is assumed to be a non-flexural one, i.e. the flexural rigidity parameter $\varepsilon=0$ for

all the cases. Results show that the presence of sag would decrease the equivalent modal damping ratio of a damped cable. Further, the peak points in these curves, which represent the damper size associated with the maximum achievable damping level at the studied damper position, or known as the optimal design points, are found to correspond to the same value of η_n. This suggests that the optimal damper size is not affected by the cable sag. The combined effects of cable sag and flexural rigidity on the equivalent modal damping ratio of the studied cable-damper system is shown in Figure 3.7(b). As a reference base for comparison, the results of an ideal taut, non-flexural cable ($\lambda^2=0$, $\varepsilon=0$) is also plotted in the figure. Comparison between Figures 3.7(a) and (b) reveals that the influence of cable flexural rigidity on the cable modal damping ratio is negligible. However, the reduction of cable modal damping ratio due to its sagging effect is considerable. For example, when cable sag reaches the level of $\lambda^2=10$, the equivalent 1st modal damping ratio of the damped cable reduces by almost 65% from 2.88% to 1.04%.

3.4 NUMERICAL SIMULATION USING ENERGY-BASED APPROACH

3.4.1 A review on energy-based approach

In this section, a general energy balance approach for a vibrating cable is discussed when the response can be obtained by using Hamilton's energy principle. The value of the Hamiltonian or the energy function is the total energy of the system. For a vibrating cable, it is the sum of the potential energy due to pretension and gravitational effect as well as the kinetic energy due to oscillation. For an un-damped system, Hamiltonian will be a constant, whereas with the presence of external damper, the total energy will not be conserved over time.
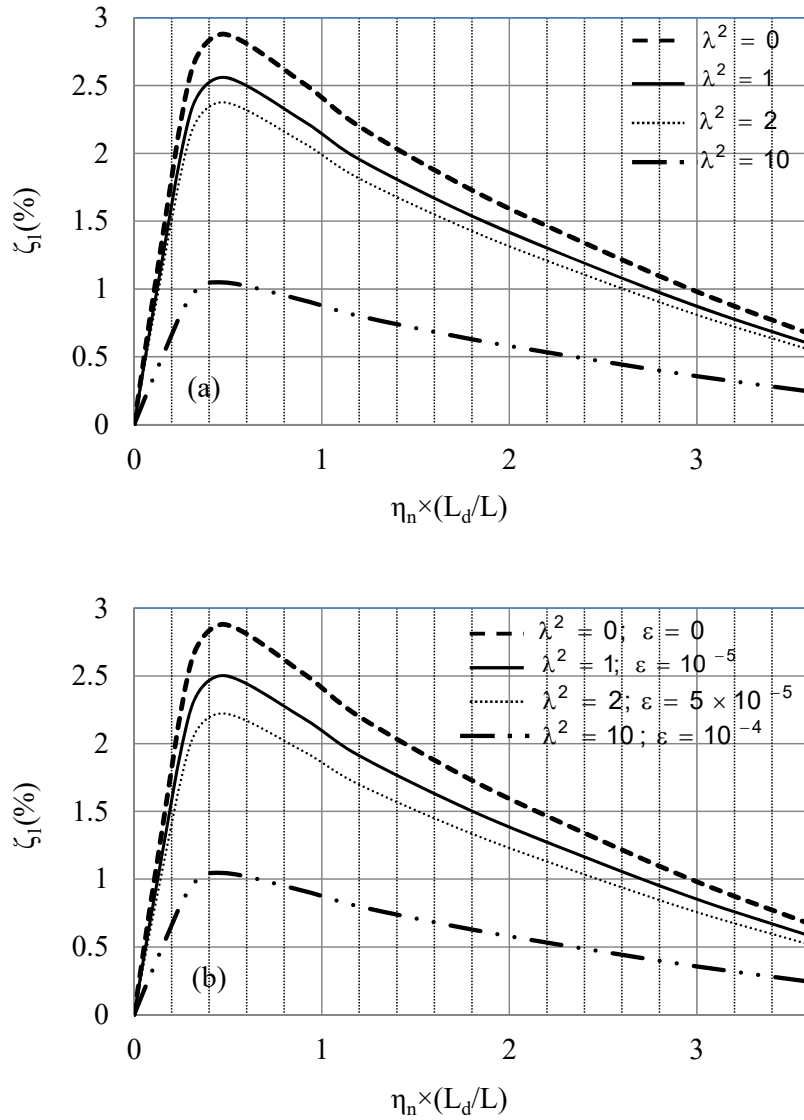
Figure 3.7: Effect of (a) sag; (b) combined effects of cable sag and flexural rigidity; on the equivalent first modal damping ratio of a horizontal cable-damper system (damper location=6%L)

The energy method reviewed in this section is based on the time variation of the maximum kinetic energy in a cable-damper system to derive the amount of existing damping when the cable is excited, the vibration generally contains a few different modes. The response of the mode of interest, for example, mode *n*, is extracted and the associated

modal damping ratio can be determined based on the decreasing rate of the maximum modal kinetic energy of the system. This ratio, known as the "n^{th} modal kinetic energy decay ratio d_n", is defined by (Cheng et al., 2010)

$$d_n = \frac{1}{j} \sum_{i=1}^{j} \frac{\left(E_{ki,n}\right)_{max} - \left(E_{k(i+1),n}\right)_{max}}{\left(E_{ki,n}\right)_{max}} \qquad (3\text{-}26)$$

where $\left(E_{ki,n}\right)_{max}$ and $\left(E_{k(i+1),n}\right)_{max}$ are the maximum kinetic energy in the ith and $(i+1)^{th}$ cycle of the modal vibration for the nth mode and j is the number of vibration cycles considered in the calculation. The kinetic energy decay ratio for a given linear system can be related to the modal damping ratio as

$$d_n = 1 - e^{-2\zeta_n \omega_n T_{dn}} \qquad (3\text{-}27)$$

where ω_n is the nth modal circular frequency, T_{dn} is the damped period of the nth mode, and d_n for a linear cable-damper system is a constant. Hence, the nth modal kinetic energy decay ratio is a function of the frequency, period, and damping ratio of the nth mode.

Finally, the simplified expression for the nth modal damping ratio considering the fact that $\omega_n T_{dn} \approx 2\pi$, can be expressed as

$$\zeta_n = -\ln(1 - d_n)/(4\pi) \qquad (3\text{-}28)$$

In the next section, the kinetic energy time history of a cable-damper system will be calculated by the finite element simulation using ABAQUS. The equivalent structural damping ratio of a damped cable will be computed.

3.4.2 Description of the finite element model

The analytical solution to a taut cable-damper system, involves the calculation of complex eigenvalue and eigenvectors and a large amount of computational effort. Therefore, the effectiveness of a transversely attached damper in suppressing cable vibrations will be investigated by numerical simulations which were carried out in ABAQUS. Since modal damping ratio provides a useful means of determining the effectiveness of linear viscous damper, the energy-based method discussed in the previous section will be used to calculate the values of the modal kinetic energy decay ratio, from which, the modal damping ratio can be determined using Eq. (3-28). Results of this simulation will be used to verify the analytical results obtained from complex eigenvalue analysis.

For simulating the behavior of the cable, the element type B21 in ABAQUS was used. Each node of this beam element has three degrees-of-freedom, i.e. two translational and one rotational. The pretension force in the cable was defined as the initial axial stress of the beam element. Both ends of the cable model were assumed to be fixed. The linear viscous damper was modeled by using DASHPOT1 element. The damper capacity was assigned in the transverse direction to the cable axis. The damper was located at certain nodes of the cable model in the numerical model. Its position varied between 2-15% of the cable length in the simulation. The properties of the cable-damper model used for simulation are listed in Table 3.1.

To determine the optimum mesh size of the studied cable-damper numerical model, sensitivity analysis was conducted. The relation between the first modal frequency and the mesh size is plotted in Figure 3.8. This step is done to determine the minimum number of

Table 3.1: Cable-damper model properties

Length, L (m)	13.695
Diameter of circular section, D (m)	0.027
Pretension, H (N)	2.1×10^7
Density (kg/m^3)	7850
Mass/Length, m (kg/m)	90.43
Damping coefficient, c (N m s^{-1})	2646
Elasticity, E (kN/m^2)	8.2×10^9
Damper location, L_d (m)	0.548

required cable elements, and thus the least amount of simulation time, to have sufficient of the fundamental frequency of the system. As can be seen from Figure 3.8, for the studied cable, the optimum number of cable element is 58, which gives the fundamental frequency of the model as 6.861Hz.
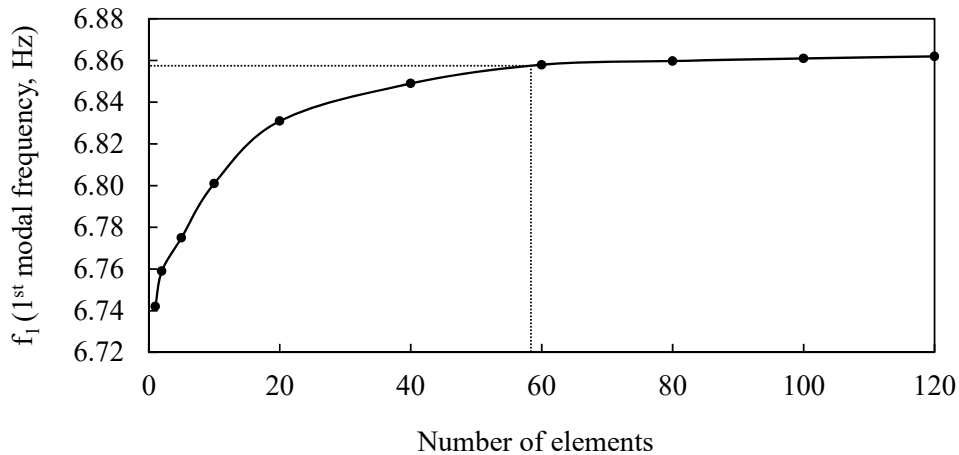
Figure 3.8: Results of sensitivity analysis

3.4.3 Practical ranges of system parameters

Though the number of factors that could potentially influence the behavior of a horizontal taut cable-damper system could be a lot, the key parameters identified to be

associated with the cable are its span length, unit mass and pretension; and those associated with the damper are its location and damper capacity (Tabatabai et al., 2000).

To evaluate the effect of system parameters, these important properties of cable and damper were combined into non-dimensional form to conduct a comprehensive parametric study. Converting the dimensional parameters (H, c, L_d) to the non-dimensional forms will simplify monitoring the structural inputs and provide results in a general fashion. Moreover, results of this study could be compared with those from other studies simply by unifying inputs through the non-dimensional form. The defined non-dimensional parameters in this study are the damper location parameter, the bending stiffness parameter of the cable and the damper damping parameter. They are defined as

- Damper location parameter: $\Gamma_d = L_d/L$

- Cable bending stiffness parameter: $\xi = L\sqrt{H/EI}$

- Damper damping parameter: $\psi = (\pi c)/(mL\omega_{01})$, where $\omega_{01} = (\pi/L)\sqrt{H/m}$ is the fundamental modal frequency of a taut string equivalent to the cable

The damper location parameter was selected to be 2%, 4%, 6%, 10% and 15%. At each damper position, analyses were performed using different values of ψ and ξ. According to the cable database developed by Tabatabai et al. (1998), which was prepared based on over 1400 stay cables from 16 different cable-stayed bridges, the range of $\sqrt{Hm}$ values are between 3 and 43 kN·s/m. Assuming a range of 0 to 200 kN·s/m for the damping factor c, ψ value varies between 0 to 60. ξ should be large enough to establish a taut cable condition, the value of which varies between 50 and 400 in the current study.

3.4.4 Results

Results of a taut cable attached to a transverse linear viscous damper have been obtained by numerical simulation in ABAQUS. This section is organized to present damping estimation curves of the investigated cable-damper system. Subsequently, optimum damper size corresponding to different damper locations, damper capacities and cable properties, was obtained based on finding the peak point on the corresponding damping estimation curve. The maximum attainable damping ratio of a given damper when installed at a specific location was determined by considering three non-dimensional parameters within the practical ranges of system parameters defined in the previous section.

Damping estimation curves

In this section, the free vibration response of a cable-damper system, obtained from numerical simulation, was combined with the energy-based approach to develop the damping estimation curves for the system to suppress cable vibrations. With these curves, the preliminary design of linear viscous dampers, including the estimation of expected additional damping in the nth mode of the cable, becomes very convenient.

It is necessary to mention that, the intrinsic damping of the cable itself was ignored in these analyses as stated in the assumptions made for the cable. Therefore, the damping ratio obtained from the analysis was fully contributed by the damper.

As an example, Figure 3.9 illustrates the equivalent first modal damping ratio of such a taut cable-damper system. The horizontal axis shows the variation of damper capacity c in terms of the non-dimensional damper damping parameter ψ. Each curve corresponds to a specific level of pretension in the cable with the damper installed at a certain location, which, in the case of Figure 3.9, is 6%*L*.
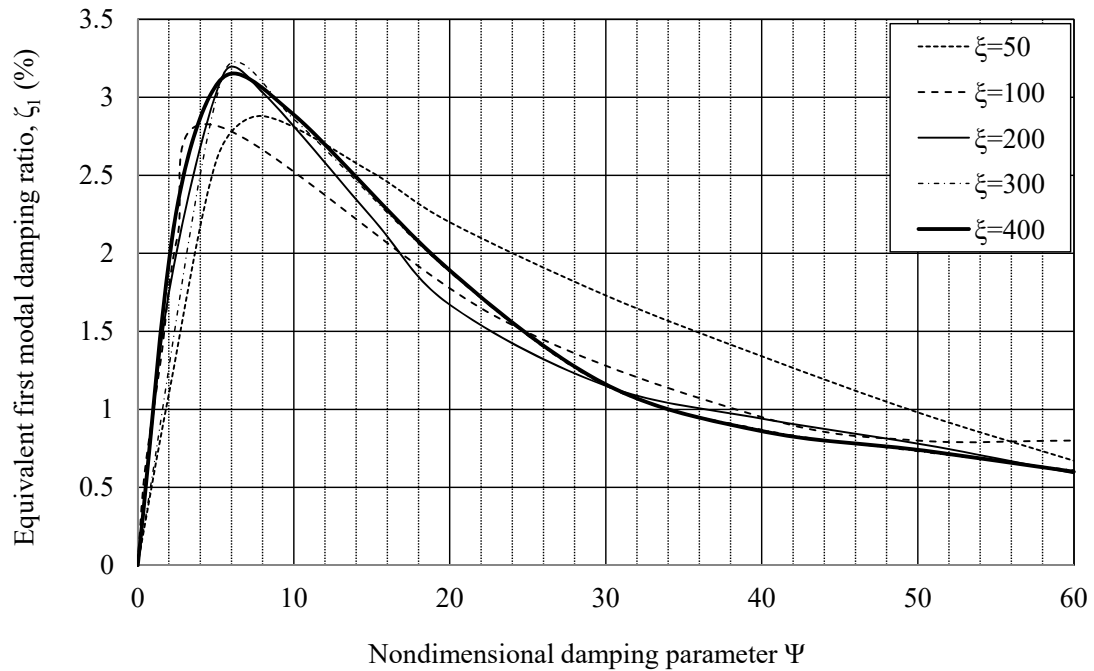
Figure 3.9: Equivalent first modal damping ratio of a damped cable with a transverse viscous damper attached at 0.06L

As can be seen in Figure 3.9, in general, the damping ratio increases with the increase of non-dimensional damping parameter (ψ) up to an optimum level. After reaching its optimum efficiency, further increase in the damping parameter result in reduction of the cable damping ratio. It should be pointed out that overdesign of external dampers may be counterproductive. Beyond the optimum point, the damper will act more as a rigid support and the damping contribution will decrease.

Different damper locations (0.02-0.15L) will absolutely affect response of a cable-damper system. A non-dimensional damper location parameter Γ_d was introduced to define the damper location in the analysis. Following the same procedures described above, damping estimation curves, similar as those given in Figure 3.9, but for different damper

locations, were obtained. Linear interpolation can be used to determine the damper size

and the corresponding equivalent modal damping ratio based on the developed curves.

Optimum damper size and maximum attainable damping ratio

The optimum damper size is "an upper-bound to show that within the practical

range of real stay cables, what would be the maximum achievable suppression effect at a

specific damper location" (Cheng et al., 2010).

Refer to Figure 3.9, for a non-dimensional cable bending stiffness of 200 and

damper located at 0.06L, the optimal damper design point exists at ψ=6.2, which

corresponds to a damper coefficient c=8.2 kN·s/m. The associated maximum equivalent

first modal damping ratio is thus 3.21%. It means that if a stay cable has a non-dimensional

bending stiffness of 200 and the damper is installed at 0.06L from cable end, a linear

viscous damper with size of c=8.2 kN·s/m will be most effective in suppressing cable

vibration in its first mode, and the maximum attainable first modal damping ratio of the

damped cable is 3.21%.

Table 3.2 presents both numerical and analytical results of the cable tension T and

the damper coefficient c corresponding to the optimum damper design points at damper

location 6%L when the non-dimensional cable bending stiffness is taken as 50, 100, 200,

300 and 400, respectively. A good agreement can be observed between the analytical

results and the numerical ones. Similar approach can be taken to obtain the equivalent first

modal damping ratio of the cable-damper system at different damper locations.

The simplicity of the analytical formulation of the studied cable-damper model and

also the accuracy of the obtained results, which were confirmed by numerical simulations

in ABAQUS, leads to the decision to develop a reliability assessment model for the studied

cable-damper system in next chapters based on the current non-deterministic analytical model.

Table 3.2: Cable tension and damper coefficient corresponding to the optimum damper design at damper location 6%L

c (kN·m/s)	T (kN)	ξ	ψ_{opt}		$\zeta_{1,max}$ (%)	
			FEA	Analytical	FEA	Analytical
3.3	30.3	50	8.60	8.80	2.88	3.05
4.0	121.5	100	6.05	6.15	3.02	3.1
8.2	485.9	200	6.20	6.35	3.21	3.18
14.0	1092.9	300	7.06	7.00	3.28	3.15
15.0	1942.9	400	5.67	5.80	3.14	3.2

3.5 SUMMARY

In this chapter, in-plane free vibration of a taut cable attached with a transverse linear viscous damper was examined. In the first part, an extensive review on the existing studies in this field was conducted. This review included literatures which were categorized as analytical, numerical and experimental studies on a cable-damper system.

In the case of a linear viscous damper, the cable-damper system was described and assumptions for the cable and damper were introduced for analysis of the free vibrations of a taut cable-damper system. The supplemental modal damping ratios provided by the damper were determined.

Equation of motion for a taut cable-damper model was developed and solution to the complex eigenvalue problems was derived. From this eigenvalue equation, an equivalent modal damping ratio of the system was obtained while considering the damper capacity, the damper location and the cable pretension as the most important parameters of the system. The optimum value of the equivalent modal damping ratio corresponding to a specific damper location was identified.

Numerical simulation of a taut cable-damper system was conducted to determine its kinetic energy time history during free vibration. An energy-based approach proposed in an existing study (Cheng et al., 2010) was used to calculate the amount of damping provided by the damper to the cable. A finite element model was developed and analysis was conducted for the practical ranges of system parameters.

Finally, the results from numerical simulation using ABAQUS were presented to obtain damping estimation curves, from which the optimum damper size and the maximum attainable damping ratio for a specific damper location could be found.

The numerical results were then compared with the analytical ones obtained from the complex eigenvalue analysis. The two sets of results were found to agree with each other.

As a conclusion for this chapter, the deterministic analytical model of a taut string-linear viscous damper system derived here will be used as a base to develop a non-deterministic model in the following chapters to assess the reliability of such a structural system over its life time.

CHAPTER 4

RELIABILITY-BASED DESIGN ASSESSMENT ON THE PERFORMANCE OF EXTERNAL DAMPERS IN CONTROLLING RAIN-WIND INDUCED BRIDGE STAY CABLE VIBRATIONS

Dampers are widely used to control excessive cable vibrations. Their effectiveness was addressed in many studies using deterministic approaches. However, the mechanical and/or physical properties of cables and dampers could not only deviate from their nominal design values at a given design point, but also vary considerably during the lifetime of a cable-stayed bridge and thus affect damper efficiency. The objective of this chapter is to present a time-variant reliability-based framework model to assess how uncertainties in the structural parameters of a cable-damper system would influence the time specific reliability performance of damped stay cables yielded from the current design practice when they are prone to the rain-wind-induced vibration.

4.1 INTRODUCTION

4.1.1 Background

Stay cables on cable-stayed bridges are sensitive to dynamic excitations induced by various sources due to their low intrinsic damping and long flexible nature. In particular, a study by the US Federal Highway Administration (Kumarasena et al., 2007) indicates that majority of the large amplitude cable vibration field incidents are associated with rain-wind-induced vibrations (RWIV). As revealed from numerous site reports and wind tunnel studies (e.g. Hikami and Shiraishi, 1988; Matsumoto, 1998; Matsumoto et al., 2003; Chen et al., 2004), for cables satisfying certain orientation and location conditions, when mild

72

wind is combined with moderate rain, water rivulet could form on cable surface as a result of a sensitive equilibrium between gravity, capillary and aerodynamic forces. Existing studies show that the presence of upper water rivulet would not only alter the geometric shape and aerodynamic feature of the cable cross-section, but its circumferential oscillation could be aerodynamically coupled with flexural oscillation of the cable and lead to negative aerodynamic damping (Yamaguchi, 1990). Over the last two decades or so, besides an attempt to apply classical galloping theory to explain the mechanism (Yamaguchi, 1990; Geurts et al., 1998; 1999), the possible role of water rivulet thickness and its link with the rivulet motion speed (Flamand, 2001), as well as the initial and instantaneous rivulet position (Gu and Lu, 2001) in exciting RWIV were investigated. Gu et al. (2009) carried out wind tunnel tests to obtain aerodynamic forces acting on the cable and upper rivulet and developed a theoretical model by considering the cable in-plane motion and rivulet tangential motion in the analysis. Further, Xu et al. (2008) tried to develop a statistical-based framework for estimating the occurrence probability of rain-wind induced cable vibration in order to make a rational decision on whether anti-vibration measures (such as cable surface treatment, cross ties, and external dampers) should be taken or not. Although encouraging progress has been made to better understand the phenomenon, current knowledge is still inadequate to fully explain the underlying physics associated with its excitation mechanism.

A practical criterion proposed by Irwin (1997) suggests that RWIV can be suppressed to a harmless level if the Scruton number is greater than 10, i.e.

$$S_c = \frac{m\zeta}{\rho D^2} \geq 10 \qquad\qquad (4\text{-}1)$$

where m is the cable mass per unit length, ζ is the damping ratio of the cable, ρ is the air density, and D is the cable diameter. Consider an example of a typical bridge stay cable having $D = 20$ cm and $m = 100$ kg/m, this is equivalent to a structural damping requirement of approximately 0.5%. The criterion is not only supported by experience in Japan (Saito et al., 1994; Yamada, 1997) and France (Virlogeux, 1998), but also confirmed by recent field monitoring program in China (Chen et al., 2004). In addition, when revising design guideline of bridge stay cables, this criterion is recommended by the Post-Tensioning Institute (PTI publication, 2001) to be used in practical design to predicate the required damping in a stay cable to mitigate RWIV.

Besides modifying the cable surface configuration and adding cross-ties, external dampers are commonly used to suppress unfavorable cable vibrations on site. The effectiveness of a damper design in controlling cable vibrations has been studied by many researchers in terms of the structural modal damping level achieved by a stay cable when attached with an external damper. Kovacs (1982) identified the existence of an optimal damping in a taut cable-damper system, which was confirmed by a number of researchers (Yoneda and Maeda, 1989; Uno et al., 1991; Pacheco et al., 1993; Krenk, 2000). In particular, Pacheco et al. (1993) simplified the procedure of designing viscous dampers of stay cables by deriving a universal damping estimation curve, which allowed relating the modal damping level of a damped taut cable directly to the size and the location of a damper. By solving the same problem using complex mode shapes, Krenk (2000) developed an analytical form of this universal curve. Further, Mehrabi and Tabatabai (1998), as well as Krenk and Nielsen (2002) presented a refined solution to a typical cable-damper system by including the influence of cable sag and cable bending stiffness in the

formulation. The accurate asymptotic formula of the structural modal damping ratio of a general cable-damper system was analytically derived by Fujino and Hoang (2008). The study resulted in an explicit evaluation of reductions in the damper effectiveness due to influential parameters such as the sag and the bending stiffness of a cable and the stiffness of a damper support. Recently, Cheng et al. (2010) proposed an energy-based method to evaluate the dynamic behavior of a cable-damper system. A set of damping estimation curves were developed for the practical parameter ranges of bridge stay cables. These curves can be utilized to relate a specific damper design to the corresponding equivalent structural modal damping of a damped stay cable.

At present, when an external damper is used to control RWIV of a stay cable, upon considering the limitations of its installation location, the size of the damper is typically selected using either the damper design curve or the design formula proposed in the above mentioned studies so that the resulted equivalent structural damping ratio of the damped cable would satisfy the damping requirement for suppressing RWIV proposed by Irwin (1997). However, it is worth noting that most existing studies are based on the assumption that the parameters of a cable-damper system are deterministic; whereas in practice, it is expected that the system properties could not only deviate from their respective nominal design values at a given design point, but also vary over time due to changes in ambient conditions. For example, tension in a stay cable may increase or decrease during its lifetime because of creep and shrinkage in concrete deck and/or pylon and cable slacking (Au and Si, 2012). Thermal expansion or contraction of the fluid in a viscous damper may result in excessive internal pressure in a damper or the formation of a vacuum inside the damper, which would change the fluid properties or even cause leakage and thus affect the damper

capacity and degrade its efficiency. Therefore, the assumption underlying deterministic approaches does not comply with the most common practical situations. For a rational assessment of the life-long performance of a cable-damper system and for a better understanding of the impact of the system parameter uncertainties on the vibration control efficiency of an external damper designed according to the current practice, it is crucial to carry out a time-dependent probabilistic analysis to consider these uncertainties. This can be achieved by combining the existing time-invariant reliability analysis methods with the time varying characteristics of system parameters. In the present chapter, we propose to formulate the reliability of cable-damper systems as a time-dependent up-crossing problem. The time dependency appears in the form of a propagation kinetics of structural properties decaying. Because only degradation mechanisms are considered, the solution of the time-variant reliability problem can be treated as a series of time specific reliability problem and solved using classical time invariant reliability tools (Pagnini, 2010).

A number of time-invariant reliability analysis approaches are available in the literature for the assessment of structural performance. These include the Monte Carlo simulation (MCS) technique, the first and the second order reliability methods. Although there might be many reasons for choosing one method over another, Monte Carlo simulation is generally selected for its simplicity in formulation and its capability to handle problems with complex limit state functions. However, the computational cost of this approach is deemed very high when being used for parametric studies (Frangopol and Maute, 2003). Mohammadi et al. (2011) studied the time specific performance of external dampers in suppressing rain-wind-induced vibrations of bridge stay cables. The Monte Carlo simulation was conducted by treating the cable tension and the damper capacity as

two random variables at a given design point. The limit state function of a horizontal taut cable-damper system was expressed explicitly in terms of an equivalent system modal damping ratio to restrain the occurrence of rain-wind-induced cable vibrations. The high computational cost associated with MCS motivated the author to propose an alternative solution. In a subsequent study, Mohammadi et al. (2013) proposed the use of the Two-point Adaptive Nonlinear Approximations (TANA) method, which is a first-order-second-moment (FOSM) method, to assess the time specific performance of an inclined sag cable equipped with a linear viscous damper in resisting rain-wind-induced cable vibrations.

4.1.2 Organization of the chapter

In Section 4.2, a time-variant reliability-based framework model will be proposed to include the time-varying characteristics of system properties in the performance assessment of a cable-damper system. The influence of structural parameter uncertainties in a cable-damper system on the current deterministic-based damper design practice will be investigated. The cable tension and the damper capacity will be treated as two independent time-varying random variables. The problem will be formulated as a limit state up-crossing scenario to determine the time-dependent reliability of a typical cable-damper system under rain-wind-induced cable vibrations. In Section 4.3, different reliability analysis methods will be introduced to evaluate the LSF. Application of the reliability methods will be illustrated by a numerical example in Section 4.4. As a result, the most admissible reliability method will be selected to solve this probabilistic problem. Besides, the impact of structural parameter uncertainty at a given design point will be investigated. In Section 4.5, the application of the proposed time-variant framework model for analyzing the reliable performance of a cable-damper system in resisting RWIV will be

illustrated through three numerical examples. A set of sample reliability-based damper design curves are proposed using a non-dimensional form of system parameters. The relation between the time specific system reliability-index and various cable-damper system parameter uncertainties is described. In addition, the potential application of the proposed time-variant reliability-based framework model and results to the development of maintenance strategy of a cable-damper system over its lifetime will be demonstrated.

4.2 FORMULATION OF TIME-VARIANT RELIABILITY-BASED PERFORMANCE ASSESSMENT METHOD

4.2.1 Control parameters of a cable-damper system

A schematic model of a typical inclined sag cable attached transversely with a linear viscous damper is depicted in Figure 4.1. The coordinate system is defined such that the X-axis is along the cable chord and the Y-axis is the perpendicular direction. The cable has a length L, a mass per unit length m, a finite flexural rigidity EI, an inclination angle θ, and carries a tension T. The cable attachment at both sides are assumed to be fixed which represents clamped-clamped end condition. A damper is attached to the cable at a distance L_d from the lower end support. The damping coefficient is denoted by c.

The sagging effect in a real cable due to its self-weight is usually considered in terms of a sag d at the cable mid-span. The sag is given by $d=mgL^2\cos\theta/(8H)$, where H is the cable tension component along its chord direction, and g is the gravitational acceleration. A non-dimensional sag parameter is defined by Irvine and Caughey (1974) as:

$$\lambda^2 = \left(\frac{8d}{L}\right)^2 \frac{L}{\left[HL_e/(EA)\right]} \tag{4-2}$$

78

where *EA* is the axial rigidity of the cable, and $L_e=L[1+8(d/L)^2]$ is the static (stretched) length of the cable. It should be noted that, as indicated by Eq. (4-2), the non-dimensional sag parameter λ^2 does not only include the effect of cable sag, but also that of the cable axial stiffness and inclination. For simplicity, it is assumed that the variation of λ^2 is associated with the variation of the sag level. For example, $\lambda^2=0$ represents physically the case of a taut cable, and larger λ^2 values correspond to more flexible cables. In practice, stay cables on cable-stayed bridges typically have λ^2 values in the order of 10 or smaller (Johnson et al., 2002). This range will be considered in the current study.
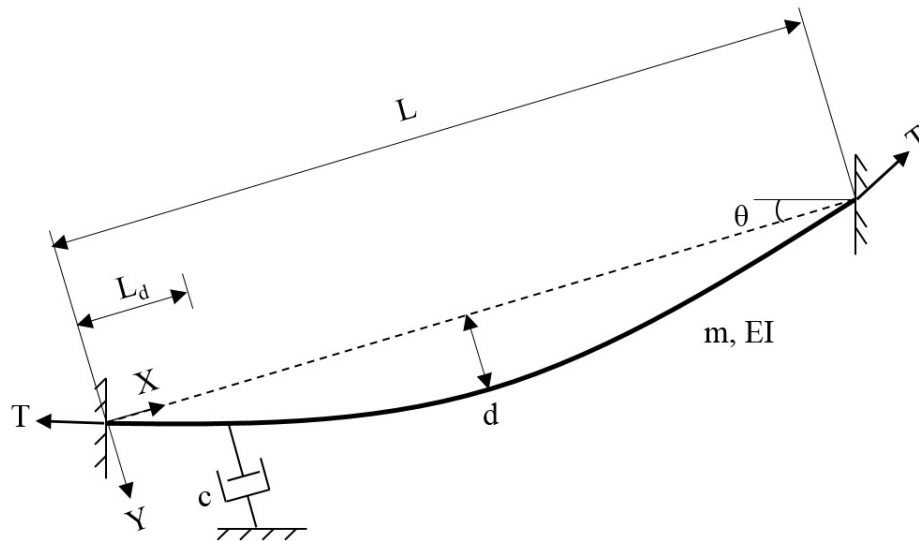
Figure 4.1: A schematic model of an inclined sag cable with a transverse linear viscous damper

For the cable-damper system shown in Figure 4.1, when the damper location is selected, the most influential factors that would affect the efficiency of a viscous damper include the cable tension, *T*, and the damper capacity, *c*. As mentioned earlier, these two system parameters could vary over the life time of a bridge due to change in the ambient conditions such as creep and shrinkage in concrete deck and/or pylon, cable slacking, and

temperature-induced variation in damper fluid properties etc. Further, even at a given time point, the actual cable tension and damper capacity in the system could deviate from their respective nominal values. These facts lead us to consider cable tension and damper capacity as time-dependent random variables in the current study, the uncertainties of which are assumed to come mainly from the above two sources. The former type of uncertainty can be included in the analysis by incorporating the time-varying characteristics of cable tension and damper capacity over the bridge life time, which typically can be collected from field monitoring program; whereas the latter type is counted at a given point of time, by assuming that both the cable tension and the damper capacity follow independent normal distributions, with mean values equal to their respective nominal design values at the specific design point, and the standard deviations defined by the specified coefficient of variations (COVs), as shown in Figure 4.2.
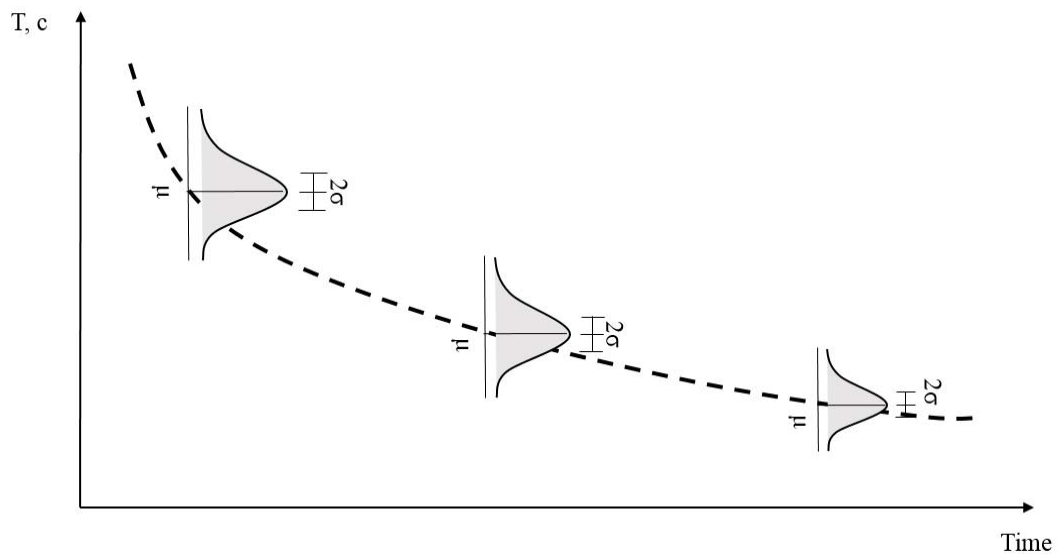
Figure 4.2: Schematic diagram showing uncertainty of cable tension and damper capacity

The representation of the dynamic response of a typical cable-damper system can be simplified by introducing the non-dimensional form of cable-damper system parameters similar to those defined by Mehrabi and Tabatabai (1998). They are defined as follows:

(a) Damper location parameter $\Gamma_d = L_d/L$. Due to the practical limitation on the damper installation position, the maximum damper location parameter is restricted to 6% ($\Gamma_d \leq 0.06$).

(b) Cable bending stiffness parameter $\xi = L\sqrt{H/EI}$, which reflects the flexibility level of the cable. If we assume the flexural rigidity EI of a stay cable remains constant, the cable bending stiffness parameter ξ can then be directly related to the cable tension component, H, along its chord direction. Accordingly, for high ξ values, the cable acts similar to a taut string.

(c) Damping parameter $\psi = (\pi c)/(mL\omega_{1s})$, where $\omega_{1s} = (\pi/L)\sqrt{H/m}$ is the first modal frequency of a taut string equivalent to the cable. Hence, the definition of the damping parameter can be simplified as $\psi = c/\sqrt{mH}$.

In the current study, the practical ranges of the non-dimensional parameters ξ and ψ are selected based on the bridge stay cable database developed by Tabatabai et al. (1998). The non-dimensional bending stiffness parameter ξ is limited to be no greater than 400, whereas the damping parameter ψ is selected between 0 and 60.

4.2.2 Development of time-dependent limit state function (LSF)

If we assume that the vibration suppression effect provided by an external damper to the attached cable can be defined as an equivalent structural damping within the cable, the general form of the LSF for a cable-damper system can be proposed as the difference

between the available structural damping ratio in a cable-damper system, ζ_s, and the damping demand of a damped cable, ζ_r, to avoid large amplitude vibrations. Since the available structural damping ratio ζ_s in a cable-damper system does not only depend on the location and the capacity of the external damper, but also relates to the amplitude of cable vibration, the proposed form of the LSF is thus a function of the cable tension T (in terms of its chord component H) and damper capacity c, or equivalently the non-dimensional parameters ξ and ψ. In the current study, the cable tension and the damper capacity are treated as two independent time-varying random variables; the LSF thus also becomes a time-dependent function, i.e.

$$g(H(t),c(t)) = g(\xi(H(t)),\psi(c(t),H(t))) = \zeta_s(t) - \zeta_r \qquad (4\text{-}3)$$

where $g(\cdot)$ is the time-dependent LSF of the cable-damper system. Because only the structural properties are expected to decay and the stochastic nature of the RWIV is simplified, the time-variant reliability problem associated with Eq. (4-3) can be solved as a series of classical time-independent reliability problems. The underlying assumption is to consider failure events at any time of the bridge lifetime to be independent.

To develop the full expression for $\zeta_s(t)$, we consider the in-plane transverse vibration of the cable-damper system shown in Figure 4.1 at a specific design point (H, c), which can be described by the following partial differential equation (Fujino and Hoang 2008):

$$H\frac{\partial^2\eta(X,t)}{\partial X^2} - m\frac{\partial^2\eta(X,t)}{\partial t^2} + h\frac{d^2Y}{\partial X^2} - EI\frac{\partial^4\eta(X,t)}{\partial X^4} = f_c\,\delta(X-L_d) \qquad (4\text{-}4)$$

where $\eta(X,t)$ is the in-plane transverse displacement of the cable motion in the Y-direction; m is the cable mass per unit length; H is the cable tension component along its chord direction at the given design point; $h(t)$ is the additional tension in the cable due to vibration; EI is the bending stiffness of the cable; $f_c(t)$ is the in-plane damping force of the damper and is a function of damper capacity c, and $\delta(X-L_d)$ is the Dirac delta function. Fujino and Hoang (2008) proposed an asymptotic solution to Eq. (4-4), of which the equivalent n^{th} modal damping ratio, ζ_n, of a damped cable is identified directly from the imaginary part of the complex natural frequency solution:

$$\frac{\zeta_n}{L_d/L} = R_f R_{sn} \frac{\eta_f \eta_{sn} \eta_n}{1 + (\eta_f \eta_{sn} \eta_n)^2} \tag{4-5}$$

where $\eta_n = n\pi(L_d/L)c/\sqrt{Hm}$ is the dimensionless damper coefficient parameter of mode n of a corresponding horizontal non-flexural taut cable-damper system (Krenk, 2000); R_f and R_{sn} are the reduction factors of the maximum modal damping ratio due to respectively cable flexural rigidity and sag as defined by Krenk and Nielsen (2002); and the modification factors for η_n due to the influence of cable flexural rigidity and sag are represented by η_f and η_{sn}, respectively. A simplified form of ζ_n can be obtained when the effects of sag and/or flexural rigidity are neglected. For example, by taking $R_{sn}=\eta_{sn}=R_f=\eta_f=1$, Eq. (4-5) can be reduced to $\zeta_n = \eta_n/(1+\eta_n^2)\cdot(L_d/L)$, which is the equivalent n^{th} modal damping ratio of a horizontal taut non-flexural cable corresponding to a specific design point (H, c). By including the time-varying characteristics of cable tension and damper capacity into formulation, the equivalent n^{th} modal damping ratio of the studied damped cable becomes time dependent, i.e. $\zeta_n(t) = \eta_n(t)/[1+\eta_n^2(t)]\cdot(L_d/L)$. Further, the expression for equivalent

structural modal damping ratio can be applied to a bridge stay cable design case with no damper by assigning the equivalent damper capacity to represent the value of internal damping ratio of a stay cable.

To complete the definition of the limit state function, a damping demand needs to be defined. As reviewed earlier, although the mechanisms associated with RWIV have not been fully understood yet, experimental results (Saito et al., 1994; Yamada, 1997) and field experience (Virlogeux, 1998; Chen et al., 2004; Casasa and Aparicio, 2010) show that the minimum amount of required damping predicted by a Scruton number-based empirical criterion (Irwin, 1997), as given in Eq. (4-1), is sufficient to effectively mitigate RWIV. Considering the fact that this criterion is also recommended by PTI (PTI publication, 2007) when revising the design guideline of bridge stay cables, in the current study, the damping demand for suppressing RWIV will be defined based on this criterion.

Establishing the onset of instability for RWIV as a function of a damping demand by using the Scruton number limit, $S_{c,lim}$, equals to 10, the minimum required structural damping ratio, ζ_r, of a damped cable can thus be expressed as:

$$\zeta_r = \frac{S_{c,lim}\rho D^2}{m} = \frac{10\rho D^2}{m} \tag{4-6}$$

For any specific cable vibration mode n, by substituting Eq. (4-5) for $\zeta_s(t)$ and the minimum amount of required damping defined in Eq. (4-6), the time-dependent LSF in Eq. (4-3) can be written in the form:

$$g(H(t),c(t)) = \left(R_f R_{sn} \frac{\eta_f \eta_{sn} \eta_n(t)}{1+(\eta_f \eta_{sn} \eta_n(t))^2} \cdot \frac{L_d}{L} \right) - \left(\frac{10\rho D^2}{m} \right) \tag{4-7}$$

The failure domain is defined by the region $g(H(t), c(t)) < 0$. Failure in this case refers mainly to the loss of system aerodynamic stability exhibited through large amplitude cable vibrations.

4.3 STRUCTURAL RELIABILITY ANALYSIS METHODS

A number of reliability analysis methods, including the Monte Carlo simulation (MCS), the first-order-second-moment (FOSM), and the second-order-second-moment (SOSM) methods are available to evaluate the reliability of structures. Since the Monte Carlo simulation is perhaps the most common technique for propagating the uncertainty in the various aspects of a system to the predicted performance, it is an acceptable type of simulation that explicitly and quantitatively represents system uncertainties. Thus, results from this approach will be considered as a reference to evaluate the accuracy of the other reliability methods (Zielke, 2005; Frangopol et al., 2007). To reduce the computational cost, the first and the second-order reliability methods (FORM/SORM) are preferred to assess the probabilistic response and safety of structures by approximating the limit state function (Choi et al., 2007). These methods require a search for the most probable point of failure (MPP) on the failure surface in the standard normalized space. FORM employs a linear approximation for the limit state function at the MPP, whereas SORM features an improved accuracy by using a second order approximation. Below, the analysis process of these reliability methods for the defined cable-damper model will be developed.

4.3.1 Monte Carlo simulation (MCS)

Generation of random variables

When the damper location is selected, the cable pretension and the damper coefficient are the two key parameters that would affect the damping property of the system. It is assumed that these parameters have normal (Gaussian) distribution at a design point. The normal distributions of cable tension T and damper property c are assumed to be defined by a mean of μ_T and μ_c and a standard deviation σ_T and σ_c, respectively. The mean point for each parameter in the Monte Carlo simulation is normally selected based on the optimal design points which were obtained from the deterministic analysis in Chapter 3.

The data analysis random number generator Risk-AMP, which is an add-on computer program designed for Microsoft Excel, is used to generate random samples each for T and c within the sample space of each parameter. The studied ranges of these parameters are selected by setting μ-3σ as the lower bound and μ+3σ as the upper bound. This will provide us with an extended range of data covered by a cumulative probability equal to 99.73% to include comprehensive part of the continuous random variable. Samples of T and c can be randomly combined to simulate the simultaneous variation of these two parameters during the life time of a cable-damper system. Considering the independency of the selected random variables T and c, the cable tension samples and damper coefficient samples are combined randomly by the software.

Solution of the deterministic problem for a large number of realizations

In this part, the large number of deterministic realizations in the Monte Carlo simulation has been processed. The equivalent first modal damping ratio of the randomly generated sample space will be evaluated using Eq. (4-5). Subsequently, the value of the limit state function is calculated from Eq. (4-7).

Statistical analysis of MCS results

The last step for completing MCS is to conduct a statistical analysis of the structural response obtained from a large number of deterministic realizations. The probability of failure for the cable-damper system will be obtained by analyzing the outputs of the simulations. A statistical measure that defines a probability distribution of the equivalent damping ratio in a cable-damper system is denoted as f[g(ζ)]. It is important to know that if f[g(ζ)] is the probability density function of a random variable g(ζ), then f[g(ζ)] times dg(ζ) (a small positive quantity) is approximately the probability that g(ζ) falls in the interval of [g(ζ), g(ζ)+dg(ζ)]. So the integral of f[g(ζ)] over an interval [g(ζ)=a, g(ζ)=b] is the probability of a<g(ζ)<b. When the probability density function f[g(ζ)] is graphically portrayed with respect to g(ζ), the area enclosed by the f[g(ζ)]-g(ζ) curve, the horizontal axis, and the two vertical lines of g(ζ)=*a* and g(ζ)=*b* represent the probability of the variable g(ζ) having a magnitude between *a* and *b*.

4.3.2 First and second order reliability methods

In the current study, the Two-point Adaptive Nonlinear Approximation (TANA) method is selected among various FORMs due to its established superiority compared to other methods. The method is based on the definition of an improved linear approximation of LSF, $\tilde{g}(\mathbf{X})$, by including a nonlinear index, r, in the iteration process, i.e.

$$\tilde{g}(\mathbf{X}) = g(\mathbf{X}_k) + \frac{1}{r} \sum_{i=1}^{n} x_{i,k}^{1-r} \frac{\partial g(\mathbf{X}_k)}{\partial x_i} \left(x_i^r - x_{i,k}^r \right) \tag{4-8}$$

where $\mathbf{X} = \{x_1, x_2, ..., x_n\}^T$ is the vector of the system design variables $x_1, x_2, ..., x_n$, $\mathbf{X}_k = \{x_{1,k}, x_{2,k}, ..., x_{n,k}\}^T$ is the vector $\mathbf{X}$ at the kth iteration, g($\mathbf{X}_k$) is the value of the nonlinear

LSF at $\mathbf{X}_k$, $x_{i,k}$ is the ith element of $\mathbf{X}$ in the kth iteration, and n is the total number of system random variables. In the current formulation, $\mathbf{X} = \{x_1 = H, x_2 = c\}^T$ and $n=2$.

The solution uses an iterative process to minimize the discrepancy between the exact nonlinear LSF and the approximate linearized LSF. The nonlinear index, r, can be determined through a process called intervention method by using the values of LSF and its gradients associated with the current and the last iterations as:

$$g(\mathbf{X}_{k-1}) - \left\{ g(\mathbf{X}_k) + \frac{1}{r} \sum_{i=1}^{n} x_{i,k}^{1-r} \frac{\partial g(\mathbf{X}_k)}{\partial x_i} \left(x_{i,k-1}^r - x_{i,k}^r \right) \right\} = 0 \tag{4-9}$$

However, the truncation error from the first-order Taylor series approximation used in this method might be large. In particular, in the case of highly nonlinear LSFs associated with large curvature failure surfaces, this approximation would reduce the accuracy of the reliability assessment considerably. In addition, TANA method can only predict one MPP in each iteration process. Hence, it is not capable of handling problems with multi-design points in the LSF.

To overcome these limitations, second-order reliability methods (SORMs) are selected. In these methods, when approximating the limit state function at MPP, the original limit state surface is replaced by a second-order approximate one with the addition of a second-order derivative term to the Taylor series expansion:

$$\tilde{g}(\mathbf{U}) \approx g(\mathbf{U}^*) + \nabla g(\mathbf{U}^*)^T (\mathbf{U} - \mathbf{U}^*) + \frac{1}{2} (\mathbf{U} - \mathbf{U}^*)^T \nabla^2 g(\mathbf{U}^*)(\mathbf{U} - \mathbf{U}^*) \tag{4-10}$$

where the system variables are presented in a standard normalized U-space, $\mathbf{U}^*$ is the coordinate of the MPP, $\tilde{g}(\mathbf{U})$ is the approximate LSF, $g(\mathbf{U}^*)$ is the LSF value at the MPP,

$\nabla g(\mathbf{U}^{*})$ is the gradient of the LSF at the MPP, and $\nabla^{2} g(\mathbf{U}^{*})$ represents the second-order derivatives of the LSF at the MPP.

Wang and Grandhi (1995) simplified the calculations of the failure probability P_f by proposing an adaptive approximation method for the SORM. In this method, the nonlinear approximate LSF, $\tilde{g}(\mathbf{X})$, developed in the TANA method is used to calculate the second order derivatives of the LSF at the MPP, which considerably reduces the computation time. In addition, it improves the accuracy of failure probability calculations compared to the first-order reliability methods. The failure probability P_f can be computed by either the Breitung's formulation or the Tvdet's formulation (Choi et al., 2007). The SORM with adaptive approximations method is applied to the studied cable-damper system in the current work due to its formulation simplicity.

4.4 RELIABILITY-BASED ASSESSMENT OF A CABLE-DAMPER SYSTEM

4.4.1 Selection of reliability analysis method

In this section, the reliability methods including MCS, FORM, and SORM are applied to a damped bridge stay cable to assess its time specific capacity in resisting rain-wind-induced vibrations. Results from the Monte Carlo simulation are used as a benchmark to compare the efficiency of these numerical methods in predicting the safe performance of the system. Besides, how uncertain deviation of cable tension and damper size from their respective nominal design values at a specific design point would affect the safe performance of a damped cable will be investigated.

A typical bridge stay cable attached with an external linear viscous damper is considered. The properties of the cable are assumed to be: length L = 150 m, unit mass m = 72 kg/m, cable diameter D=0.2 m and bending stiffness EI = 5420 kN·m² (including grout and cover pipe). The damper is located at 6%L from the lower cable anchorage. At any design point, the cable chord tension, H, and the damper damping coefficient, c, are assumed to be random variables having independent normal distributions, with mean values being their respective nominal design values. If the design point considered here corresponds to a nominal cable chord tension H= 3700 kN and a nominal damper damping coefficient c=50kN·s/m, we propose to evaluate the time specific performance of the system under rain-wind-induced vibrations at this design point by assuming the coefficient of variation for H and c being 10% and 5%, respectively.

The non-dimensional parameters of the studied cable-damper system at the given design point are as follow: the cable bending stiffness parameter, ξ=123.94; the damping parameter, ψ=3.06; the damper location parameter, Γ_d=0.06; and the sag parameter, λ^2=0.485.

The equivalent first modal damping ratio of the system, ζ_s, is calculated according to Eq. (4-5). The non-dimensional damper coefficient parameter for the first mode of a corresponding horizontal non-flexural taut cable-damper system is found to be η_1=0.577. By considering the effects of cable sag and flexural rigidity, the reduction factors and modification factors in Eq. (4-5) are respectively η_{sn}= 1.020, R_{sn}= 0.948, η_f= 0.798, and R_f= 0.938. Hence, the equivalent first modal damping ratio of the system is ζ_s=ζ_1=2.055%. On the other hand, if the air density is taken as ρ=1.29 kg/m³, based on Eq. (4-6), the minimum required structural damping ratio for such a cable-damper system to prevent rain-wind-

induced vibrations is $\zeta_r=0.717\%$. The value of the LSF of the current cable-damper system is determined according to Eq. (4-7) as:

$$g(\mathbf{X}) = g(x_1 = H = 3700 \, kN, \; x_2 = c = 50 \, kN \cdot s / m) = 1.339 \; \%$$

The TANA method is applied first to compute the reliability index of the studied damped cable, with the iteration results summarized in Table 4-1. The convergence tolerance for reliability index calculation is set to be 0.001. As can be seen from the table, the reliability index converges after four iterations at point H_4=4410.8kN, c_4= 171.3kN·s/m. This point is the MPP with corresponding reliability-index equals to β_4 = 11.79, and the associated probability of failure equals to $P_f = 5.6 \times 10^{-16}$.

Table 4.1: Summary of reliability analysis results by TANA

Iteration No.	1	2	3	4
H (kN)	3700.0	5230.8	4730.2	4410.8
c (kN·s/m)	50.0	111.8	182.4	171.3
$g(X_k)$	0.00134	0.0188	0.0081	0.00013
$(\partial g / \partial H)\big|_{\mu_H}$	-2.12×10^{-7}	-9.52×10^{-8}	-1.32×10^{-7}	-6.18×10^{-7}
$(\partial g / \partial c)\big|_{\mu_c}$	2.62×10^{-5}	8.32×10^{-6}	4.11×10^{-5}	7.17×10^{-5}
β	10.83	11.47	11.77	11.79
ε	-	0.1099	0.0260	0.0009

It is worth mentioning that although by including a non-linear index r in the formulation and updating the approximate linear LSF during iterations, the TANA method has the advantage over other FOSM approaches in evaluating the reliability of nonlinear systems, the r value depends on the selected design point. For a cable-damper system, if the performance is assessed at different design points, i.e. different cable tension and

damper capacity within the scope of the current study, the corresponding LSF would have different curvatures. Thus, the associated nonlinear indices would be different. For example, in the current example, the design point is $H=3700$ kN and $c=50$ kN·s/m, and the corresponding nonlinearity index is $r=1.015$. This suggests that a linear approximation function would be able to describe the degree of nonlinearity for the LSF at this point. While on the contrary, if the damper coefficient for the design point changes to $c=200$ kN·s/m, the computation of the nonlinear index would yield $r = 12.241$, which indicates a highly nonlinear LSF. Thus, if the linear approximation approach is used to describe the LSF, the reliability assessment results could be inaccurate and misleading. In addition, the selection of the initial trial point for the iteration will also affect the convergence rate especially for a design point associated with large curvature LSF. This is due to the fact that the nonlinear index r would remain the same for the rest of the iteration process, which would affect the efficiency of calculations.

The accuracy of the TANA method can be improved by using the SORM with adaptive approximations. The reliability assessment of the current cable-damper system is continued by transforming the problem to a normalized space using an orthogonalization of the following matrix:

$$\begin{bmatrix} -\dfrac{\partial g(\mathbf{U}^*)/\partial H}{\left|\nabla g(\mathbf{U}^*)\right|} & -\dfrac{\partial g(\mathbf{U}^*)/\partial c}{\left|\nabla g(\mathbf{U}^*)\right|} \\ 0 & 1 \end{bmatrix}$$

where $\partial g(\mathbf{U}^*)/\partial H$ and $\partial g(\mathbf{U}^*)/\partial c$ are the gradients of the limit state function $g(\cdot)$ evaluated at the MPP defined by H and c, and $\left|\nabla g(\mathbf{U}^*)\right|$ is the magnitude of the gradient function. The curvature corresponding to parameters H and c when the orthogonal Y-space has been used

is calculated for the approximate LSF, $\widetilde{g}(\mathbf{X})$, at the MPP using the method proposed by Wang and Grandhi (1995), which resulted in a reliability-index of $\beta = 11.79$ and the corresponding probability of failure of $P_f = 9.1 \times 10^{-16}$.

To perform MCS, a set of 10^8 one-dimensional inputs are generated randomly for each parameter and then the two variables H and c are combined together to generate a total of 10^{16} runs. For each run, Eq. (4-5) is used to evaluate the equivalent first modal damping ratio of the cable-damper system. The reliability-index is determined from the ratio between the mean and the standard deviation of the limit state function, which is $\beta = 12.04$. The corresponding probability of failure is $P_f = 1.1 \times 10^{-15}$. A comparison of the reliability analysis results in terms of the probability of failure, P_f, shows that the SORM with adaptive approximations method would yield more accurate reliability evaluation results of the given cable-damper system than the TANA method. This is mainly due to its capability of handling nonlinear LSF. In addition, it is computationally more efficient than the MCS. Therefore, the SORM with adaptive approximations method will be used in the rest of the paper to predict the performance of cable-damper systems.

4.4.2 Impact of structural parameter uncertainty at a given design point

In this section, the proposed time-dependent reliability-based framework model will be applied to the described cable-damper system in the previous section to assess the impact of the structural parameter uncertainty at a given design point on the damper performance. As mentioned earlier, in the current study it is assumed that cable tension and damper size follow independent normal distributions at any design point, with the mean being their respective nominal design value, and the standard deviation defined by the coefficient of variation (COV). The design point considered here corresponds to a cable

chord tension H=3700kN and a damper capacity c=50 kN·s/m. To isolate the respective

uncertainty effect of H and c, in the analysis, the response of the damped cable is evaluated

by varying COV of one variable while keeping that of the other at a constant level. A set

of sample results are presented in Figure 4.3. The solid line in the figure describes the

variation of system reliability index β when the damper size uncertainty, COV-c, increases

from 1% to 25% and COV-H remains at 10%. The dashed line portrays the relation between

β and cable chord tension uncertainty COV-H within the range of 1% and 25% while COV-

c is 10%.

As can be seen from the figure, in both cases, the reliability index decreases

monotonically with increased level of uncertainty in cable tension and damper size. The

two curves intersect at a point representing the case of COV-H and COV-c both equal to
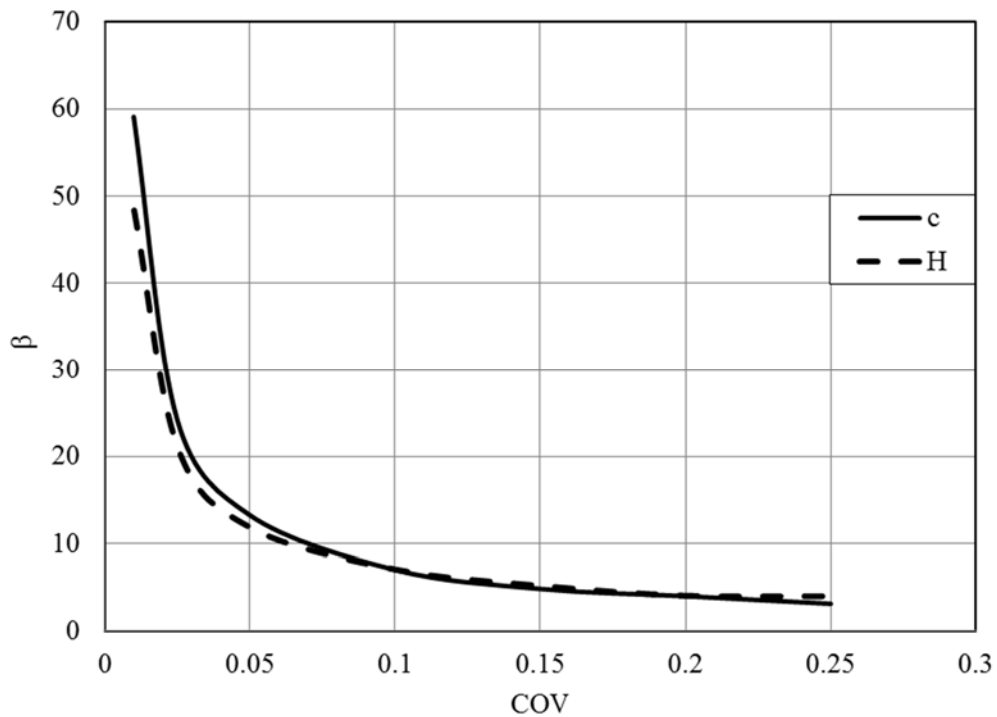
**Figure 4.3: Effect of uncertainty level of cable tension and damper size on the reliability
response of a cable-damper system (Design point, H= 3700 kN, c=50 kN·s/m)**

94

10%. The reliability index associated with this intersection point is $\beta = 7.003$. It is worth mentioning that the deterministic scenario, which corresponds to COV-H and COV-c both being zero, would theoretically lead to a reliability index of infinity. In other words, the presence of uncertainty in the structural parameters would have a sizable impact on the safe performance of a cable-damper system and should not be ignored in the design. Further, a comparison between the two curves in Figure 4.3 indicates that the system performance safety is more sensitive to the uncertainty associated with the damper size. For instance, by increasing the COV of the damper size from 0.01 to 0.1, the reliability index of the system would drop from 59.4 to 7.0 by roughly 8.5 times, whereas the same increase of uncertainty in the cable tension would decrease the reliability index by 7 times from 48.7 to 7.0.

4.5 APPLICATION OF TIME-VARIANT RELIABILITY-BASED FRAMEWORK MODEL

The proposed time-variant reliability-based framework model of a cable-damper system can be applied to refine the current deterministic-based damper design practice by taking into account the possible deviation of structural parameters from their respective nominal design values at a given design point and the impact of such uncertainty on the design outcome. In addition, if the time-dependent variation of system properties are available from site measurement, the influence of these uncertainties on the system performance can be incorporated to assess the life-long performance of a damper and can be used as a base for developing system maintenance strategies. These potential applications will be illustrated in the current section through three numerical examples.

4.5.1 Reliability-based damper design curves

It has been observed in prior section that the presence of uncertainty in system properties at a design point would considerably affect the reliable performance of an external damper. Therefore, the deterministic-based design approach might lead to too optimistic damper design. To refine the current design approach, reliability-based damper design curves can be developed using the proposed framework model. By setting different uncertainty levels for system structural parameters, the relation between damper size and system reliability index can be derived for a range of non-dimensional parameters representing actual cable and damper properties on site collected from over 1400 bridge stay cables by Tabatabai et al. (1998).

Without losing generality, it is reasonable to assume that the random variables H and c, are statistically independent. Since ξ and ψ are functions of cable chord tension H and damper capacity c, they are also random variables. Although the non-dimensional damping parameter is defined as $\psi = c/\sqrt{mH}$, for a specific value of non-dimensional bending stiffness parameter ξ, ψ is a function of damper capacity c solely. Therefore, when assessing the performance of a cable-damper system for a particular level of ξ, it is legitimate to uncouple the reliability analysis. Figure 4.4 shows a sample set of reliability-based damper design curves at five different damper locations of $\Gamma_d =0.02, 0.04, 0.06, 0.10$ and 0.15. In this figure, variability of the reliability-index with the damping parameter ψ is plotted for different levels of non-dimensional bending stiffness parameter ξ. A range of 0 to 60 is considered for the non-dimensional damping parameter ψ. The cable bending stiffness parameter ξ varies between 50 and 400. The damper location parameter Γ_d is limited to a maximum of 0.15 due to practical installation limitation. The sag parameter is

considered to be less than 10, representing typical level of sag for stay cables on cable-stayed bridges. The uncertainty level of cable tension and damper size, represented by COV-H and COV-c, are both assumed to be 10% in this set of sample curves. Should the coefficients of variation of cable tension and damper capacity be different from 0.1, the associated reliability-based damper design curves can be developed similarly using the same procedures as those for Figure 4.4.

It is noteworthy that mathematically, the reliability index β indicates how often the standard deviation of the LSF, σ_g, may be placed between zero and its mean value, μ_g. Therefore, the reliability index β computed at each design point depends on the level of uncertainty of the system random variables. Referring to Figure 4.3, we can observe that the β value would increase with smaller coefficients of variation of H and c, but decrease if σ_H and σ_c become large.

Figure 4.4 shows that in general, the reliability index β increases with the non-dimensional damping parameter ψ up to a maximum level, and then decreases. Comparing the five subplots in Figure 4.4, it can be seen that at the same damper capacity ψ, the further the damper is away from the cable end (larger Γ_d), the higher the reliability index β for the cable-damper system would be, indicating that if achievable in practice, the damper should be installed closer to the cable mid-span, which agrees with the existing experience. The peak points in these curves represent the damper size $\psi_{r,max}$ associated with the maximum achievable reliability level at the studied damper position. This finding suggests that for a specific damper location, there always exists a damper size, $\psi_{r,max}$, which would yield the most reliable performance of a damped cable. This phenomenon is consistent with earlier findings of which an optimum damper size, ψ_{opt}, has been observed for a given damper

location to achieve the maximum damping ratio of a damped cable (e.g. Kovacs, 1982;

Pacheco et al., 1993; Krenk, 2000; and Cheng et al., 2010).

(a) $\Gamma_d = 0.02$

(b) $\Gamma_d = 0.04$

(c) $\Gamma_d = 0.06$
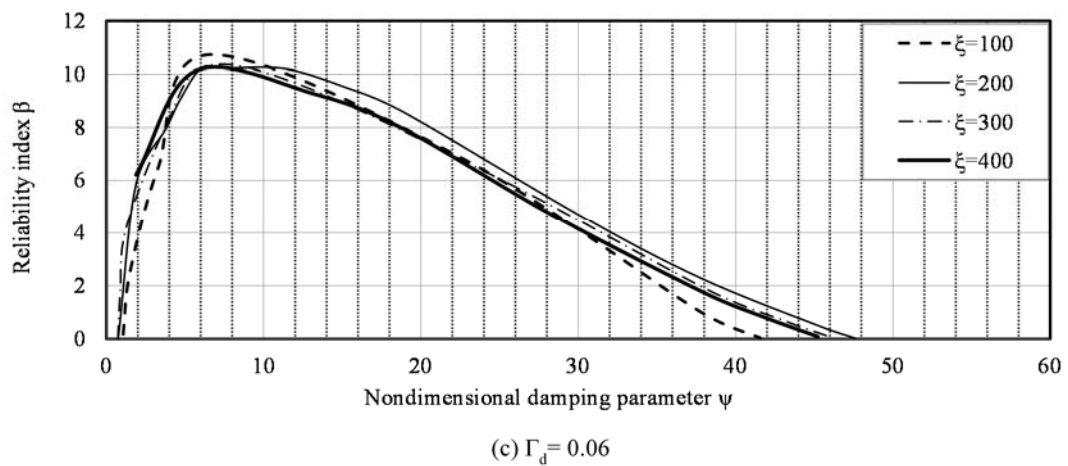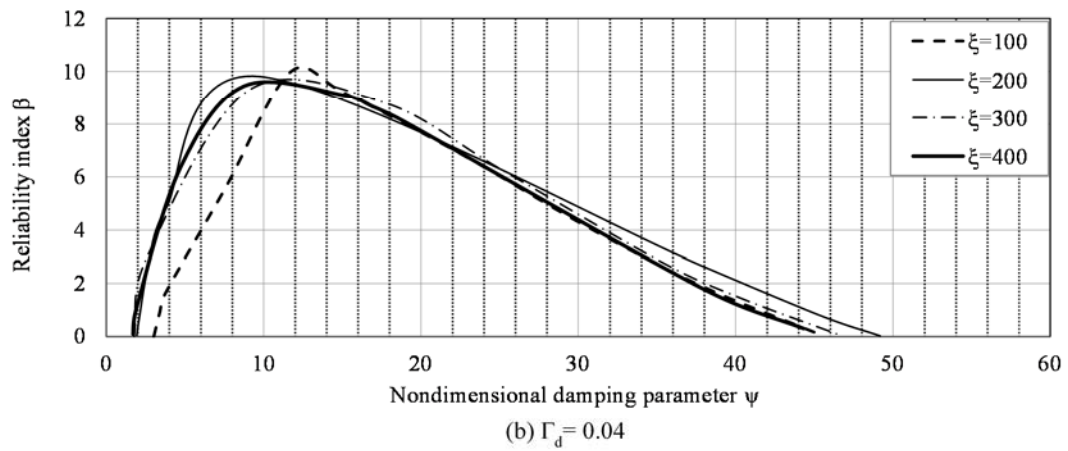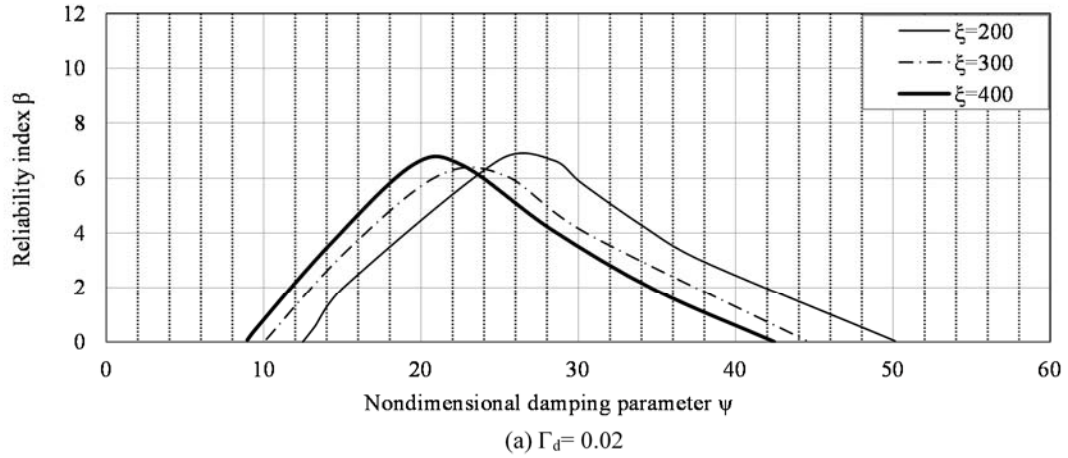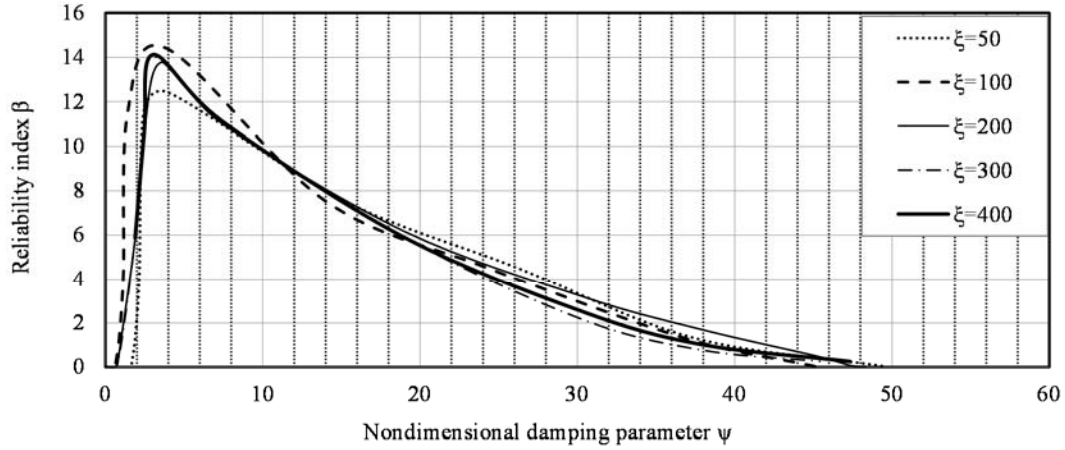
(d) $\Gamma_d = 0.10$
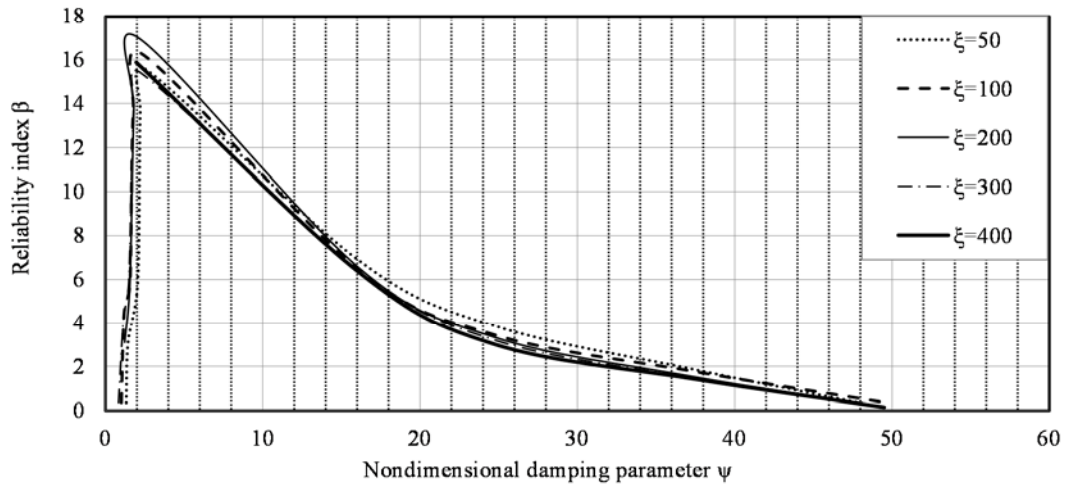
(e) $\Gamma_d = 0.15$

Figure 4.4: Reliability-based damper design curves by assuming normally distributed system parameters with $\sigma_c = 0.1\mu_c$ and $\sigma_H = 0.1\mu_H$ at each design point

In addition, the damper size $\psi_{r,max}$, which corresponds to the most reliable system performance identified in the current study, is found to agree well with the optimum damper size ψ_{opt} reported in the literature. Therefore, in the design of an external damper to suppress cable vibrations, upon the determination of damper location, the objective is then to select a damper size which would produce the optimum vibration control effect

with the most reliable performance. For instance, for a stay cable with a damper located at 0.06L (Figure 4.4(c)), if ξ=200, the optimum damper size which gives the maximum achievable damping ratio of 3.11% would be ψ_{opt} =6.0 (Cheng et al. 2010), whereas that would yield the most reliable performance of the damped cable is $\psi_{r,max}$=6.05, with the associated reliability-index equals to β=10.2.

It should be pointed out that in the case of cable-supported structures such as cable-stayed bridges and suspension bridges, cables (cables and hangers for suspension bridges) play an important role in resisting loads and transferring them from bridge deck to tower and foundation. Therefore, they are designed with larger safety factor as compared to other structural elements. A reliability-based performance assessment of a suspension bridge in Japan (Imai and Frangopol, 2001) reported that the reliability-indices of main cables, hanger ropes, and stiffening girders are very different in their values. The β values of the main cables are around 15, whereas those of the stiffening girders are within the range of 3 to 6. Similarly, a reliability-based optimum design analysis of glulam cable-stayed footbridges performed by Simões and Negrão (2005) showed necessity of having reliability-index of the studied cable-stayed system within the range of 15 to 20 to resist excessive cable deflection.

In addition, it is worth noting that the proposed reliability-based damper design curves can be used to identify the practical range of damper size ψ to satisfy the required reliability-index β for a particular cable with a bending stiffness parameter ξ. Due to the dependence of the formulated limit state function in Eq. (4-3) on the structural damping ζ_s, a practical range of damping parameter ψ should be determined to ensure a safe design. The limit level of the damping parameter ψ_{min} for a safe design is the locus of the points

where $g(H, c)=0$. In the case of $\Gamma_d=0.02$, when a very stiff cable is selected, i.e. $\xi=100$, the obtained structural damping ζ_s for the range of selected damper size ($\psi \leq 60$) is not adequate to resist rain-wind-induced vibrations. Furthermore, a comparison of the β-ψ curves in Figure 4.4 suggests that the impact of cable bending stiffness on the damper size decreases when the damper moves further towards the cable center.

The reliability-based damper design curves proposed in Figure 4.4(a)-(e) suggest that the reliability index depends on the structural parameters. A general formula for the reliability index can be expressed by defining the target expression as:

$$\beta = f(\Gamma_d, \psi, \xi, COV_c, COV_H) \tag{4-11}$$

where Γ_d is the nondimensional damper location parameter ($\Gamma_d= 0.02, 0.04, 0.06, 0.10, 0.15$), ψ is the nondimensional damper size parameter $(0, 60)$, ξ is the nondimensional bending stiffness parameter ($\xi=50, 100, 150, 200, 250, 300, 350, 400$), COV_c is the coefficient of variation associated with the damper size, and the COV_H is the coefficient of variation associated with the cable tension. In this part of analysis, COVs associated with the aforementioned structural parameters are chosen to vary between 0.01 and 0.25. Seven different levels of COVs are considered in the reliability assessment (COV= 0.01, 0.025, 0.05, 0.10, 0.15, 0.20, 0.25). Noting that although in most of the engineering design practices the allowable range of COVs associated with structural parameters are within 0.05 to 0.15, this study aims at further investigating the probabilistic response of bridge stay cables using an extended range of possible structural uncertainties range.

The numerical software, EUREQA, is used to perform the regression analysis of the reliability indices. This software is implemented due to its convenience in conducting the regression analysis by defining the preferred form of output regression function. In this

study, it is intended to propose a simple algebraic form with low mathematical complexity for the reliability index expression using basic operators including division/multiplication and/or power modules. Assume a minimum coefficient of determination as 0.95, the general form of the target expression for the reliability index yields:

$$\beta = \frac{2.83 \times \Gamma_d^{0.367} \times 0.0239^{0.00439\,\Gamma_d\,\psi^2}}{COV_\psi} \tag{4-12}$$

while the optimum nondimensional damper parameter is:

$$\psi_{opt} = 0.283\Gamma_d^{-1.141} \tag{4-13}$$

Despite the fact that the regression analysis is conducted by defining a general function for the reliability index expression, the form of Eq. (4-12) suggests that the impact of cable bending stiffness parameter is insignificant. In contrary, the structural parameters related to the damper (i.e. Γ_d, ψ, and COV_ψ) play an important role in the reliability response of a damped bridge stay cable. In parallel, Eq. (4-13) suggests that the contribution of the bending stiffness parameter in determining the size of optimum damper is negligible. Eqs. (4-12) and (4-13) can be used as empirical formulas toward convenient reliability-based assessment of damped bridge stay cables exposed to RWIVs.

Example 1

For the same cable discussed earlier, which has $L = 150$ m, $m = 72$ kg/m, $D=0.2$ m, $EI = 5420$ kN·m^2, and $H= 3700$ kN, an external damper is restricted to be installed at $\Gamma_d=$ 0.04. We propose to use the reliability-based damper design curves given in Figure 4.4 to determine the minimum required damper size in order to prevent rain-wind-induced

vibration with a reliability index $\beta \geq 4.7$, and calculate the corresponding equivalent first modal damping ratio of the damped cable.

Based on the given cable properties, the non-dimensional cable bending stiffness parameter is $\xi=123.9$. From Figure 4.4(b), when $\beta=4.7$, the damping parameters correspond to $\xi=100$ and 200 are $\psi=6.6$ and 3.7, respectively. Thus, that corresponds to $\xi=123.9$ can be obtained using linear interpolation, which gives $\psi=5.9$. The damper size is then determined as $c=\psi\sqrt{Hm}=5.9\times\sqrt{3700\times10^{3}\times72}=96.3$ kN·s/m.

The equivalent structural damping ratio, ζ_s, for the first mode can be computed according to Eq. (4-5). The non-dimensional damper coefficient parameter for the first mode of a corresponding horizontal non-flexural taut cable-damper system is found to be:

$$\eta_n = \eta_1 = n\pi(L_d/L)c/\sqrt{Hm}=1\times\pi\times0.04\times96.3\times10^{3}/\sqrt{3700\times10^{3}\times72}=0.741$$

The reduction and modification factors are obtained from the numerical solution of the formulation proposed by Fujino and Hoang (2008). They are $R_{s1}=0.946$, $R_f=0.913$, $\eta_{s1}=1.020$, and $\eta_f=0.700$. Hence, the equivalent first modal damping ratio of the system is $\zeta_s=\zeta_1=1.429\%$. On the other hand, the required damping ζ_r for such a cable-damper system to prevent rain-wind-induced vibration is determined to be 0.717%.

Alternatively, by using the results of the regression analysis in Eq. (4-12), to ensure a reliability index of $\beta \geq 4.7$, the nondimensional damping parameter is calculated to $\psi=6.42$.

Example 2

If the non-dimensional bending stiffness parameter of a stay cable is $\xi=250$, and the possible damper location is $\Gamma_d=0.028$, we propose to determine the minimum required

103

damping parameter to satisfy the reliability index of the cable-damper system for resisting rain-wind-induced vibration to be $\beta \geq 6.0$.

Using Figure 4.4(a), along with linear interpolation for bending stiffness parameter $\xi=200$ and 300, the non-dimensional damping parameter corresponding to $\xi=250$ at Γ_d =0.02 is 22.0. Similarly, $\psi=4.6$ for $\xi=250$ and $\Gamma_d=0.04$ can be obtained from Figure 4.4(b). Therefore, by assuming a linear interpolation between results of Γ_d =0.02 and 0.04, for a cable with $\xi=250$, if a damper is attached to it at $\Gamma_d=0.028$, to ensure $\beta \geq 6.0$, the minimum required damping parameter would be $\psi_{min}=15.4$.

Alternatively, the regression analysis expression can be used to simplify the calculation process. Assign Γ_d =0.028 and $\beta=6.0$ in Eq. (4-12), it is yielded $\psi_{min}=15.7$. The results of minimum nondimensional damping parameter calculated by both regression analysis and interpolation are in good agreement with an approximate error less than 2%.

4.5.2 Reliability-based maintenance plan

For a typical stay cable, creep and/or shrinkage in concrete deck and/or pylon as well as slacking in steel cable would cause change in cable tension and thus its bending stiffness. Hence, it is beneficial to investigate the impact of cable bending stiffness variation on the reliability index of a cable-damper system. Figure 4.5 shows the reliability index of a cable-damper system as a function of cable bending stiffness parameter ξ for three different levels of damping parameter, $\psi=0.8$, 6.6 and 41.4, at damper location of 0.06L. Referring to Figure 4.4(c), these three damping parameter levels correspond respectively to $\beta=0$, the maximum achievable β, and the upper limit of the studied damper size to maintain $\beta >0$. It is intended to determine the required bending stiffness parameter corresponding to each damper size to achieve a desired safety level. For example, in the

case of a stay cable with damping parameter ψ=6.6, the required cable bending stiffness parameter satisfying a reliability index of $\beta \geq 3$ is $\xi \geq 44.7$. It can be observed from Figure 4.5 that at higher ξ values ($\xi \geq 250$), the β-ξ curves would reach an asymptotic limit to a certain reliability index level. In other words, for a cable that acts similar to a taut string, a slight reduction in cable tension force would not have an appreciable impact on its reliability response.
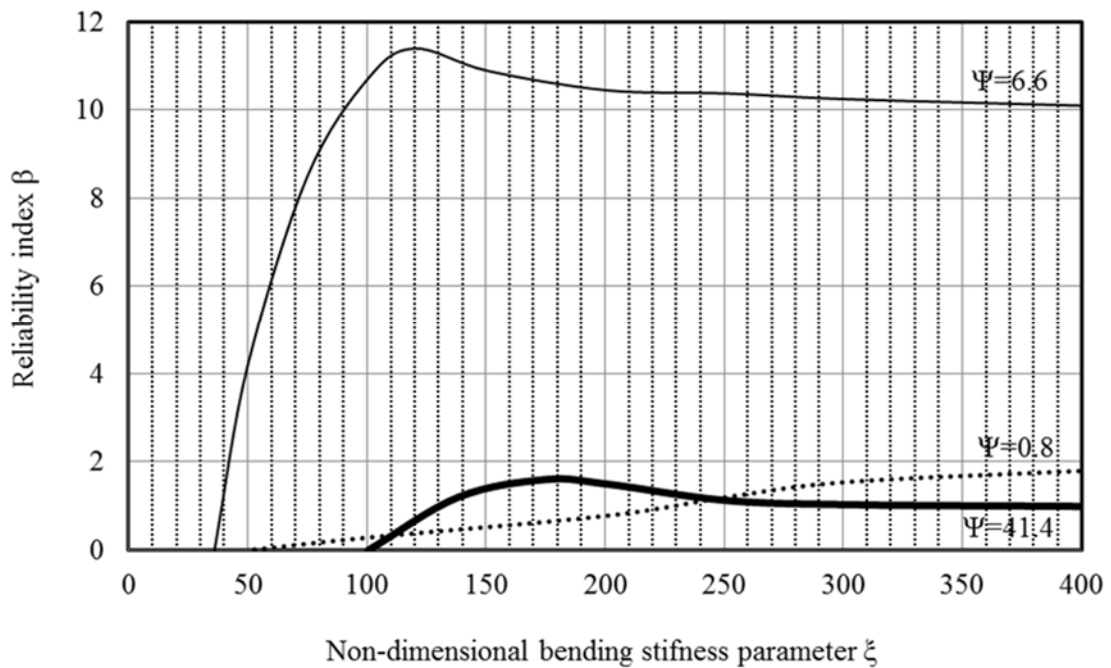
Figure 4.5: Variation of reliability-index with bending stiffness parameter for three different damper sizes at Γ_d=0.06

Nevertheless, referring to Figure 4.4(a), when the damper is closer to cable ends (i.e. at damper location of $0.02L$), the effect of bending stiffness parameter on the reliable response of a damped bridge stay cable would become prominent. To further investigate the impact of cable bending stiffness, variation of the reliability-index with the bending stiffness parameter for a damper design case in terms of the most reliable performance, i.e.

$\psi_{r,max}$= 26.4, is shown in Figure 4.6. For comparison, two other design cases with the same damper size while damper is attached at Γ_d=0.04 and 0.06 are also considered. The reliability results show that:
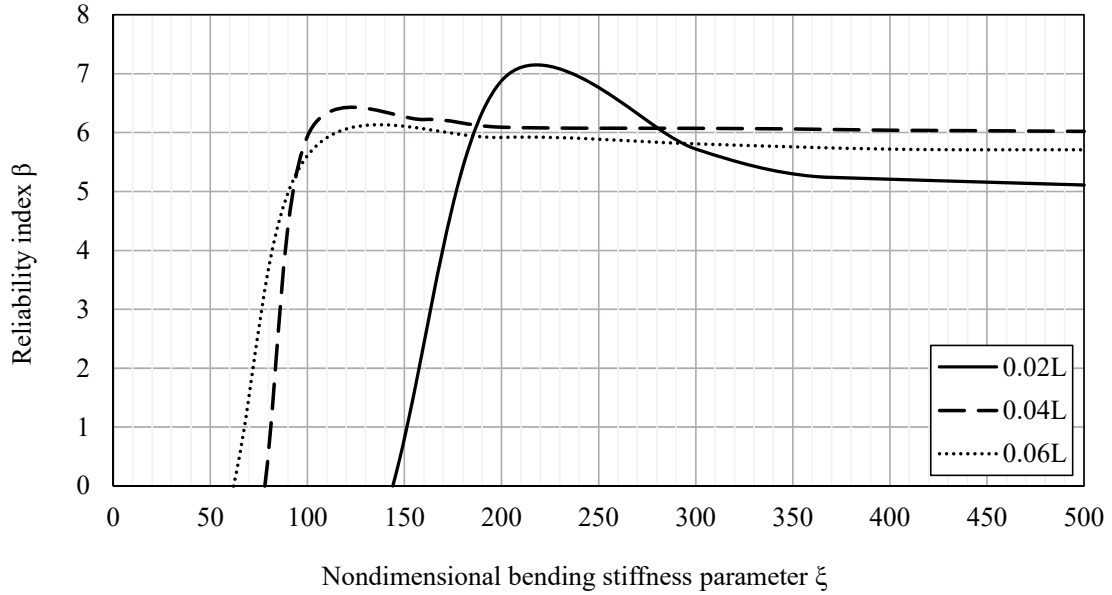
Figure 4.6: Variation of reliability-index with bending stiffness parameter at ψ=26.4

(1) At higher ξ values, each curve asymptotes to a horizontal line. Thus, at each design case when the cable tension reaches a certain level, the reliability response no longer depends on the variation of cable tension. This implies that at higher ξ values (higher cable tension), the cable acts similar to a taut string when the effect of cable sag is ignored.

(2) In view of the minimum required cable tension (or bending stiffness parameter), to ensure reliability of a damped stay cable system, it is noticeable that when the damper location parameter is smaller (Γ_d=0.02), a higher amount of cable tension is necessary.

(3) When the damper moves toward the cable center, the deviation of reliability-index due change in cable tension would be smaller. Besides, in the design case with a damper attached at 0.06L, the reliability index asymptotes at lower cable bending stiffness, which means placing a damper closer to mid-span would help to enhance the reliability response of a damped bridge stay cable.

To ensure the performance of an external damper would sustain at the desired safety level, maintenance should be performed during the bridge service stage to minimize the impact of cable tension and damper capacity variation on the response of a damped cable.

Example 3

In this example, we consider a damped cable on a concrete cable-stayed bridge, of which the cable tension and damper property vary with time. The time-dependent effects on the reliability of this cable-damper system is evaluated using the proposed time-variant reliability analysis framework model. The properties of the cable used in this example are taken from a study by Tabatabai and Mehrabi (2000): L=93 m, D=0.225 m, EI = 3049 kN·m^2, and m=114.09 kg/m. The initial specified cable tension along its chord direction is H=5017 kN (ξ=119.3). To suppress rain-wind-induced cable vibrations, a linear viscous damper is attached 3.72 m from the cable lower end (Γ_d= 0.04). In this example, two different damper design cases are considered. Case 1 represents an optimum damper design case with a c_{opt}=271.1 kN·s/m (ψ_{opt}=11.3), whereas Case 2 assumes a design case using a smaller damper size, c=90.4kN·s/m (ψ=3.8). The cable tension loss is estimated based on the field monitoring data of a cable-stayed bridge over a period of 300 days (Au and Si, 2012), whereas a linear degradation from its original design is assumed for the damper capacity. In addition, it is assumed that the cable chord tension and the damper capacity

are random variables with independent normal distributions, and the time variation of their respective mean values over a period of 300 days are shown in Figure 4.7. We are interested in developing a maintenance plan for the studied cable-damper system over a period of 300 days to ensure its performance remain at a desired safety level during this time period.

Let's define the reliability level of the cable-damper system corresponding to its initial design point as the desired safety level over its lifetime and denote it as β_0. In Case 1, with the initial damper design point being $c_0 = c_{opt} = 271.1$ kN·s/m and $H_0 = 5017$ kN, β_0 equals to 9.50; whereas for Case 2 ($c_0 = 90.4$ kN·s/m, $H_0 = 5017$ kN), the reliability index is reduced to $\beta_0 = 2.24$. This supports that a higher level of system reliability can be achieved when a damper with a size closer to its optimum value is attached to the cable.

The reliability response of the damped cable over this time period is portrayed in Figure 4.8 as the time history of the relative reliability-index $\beta(t)/\beta_0$ for cases 1 and 2. It can be seen that as expected, the reliability index $\beta(t)$ decreases with time, which suggests a higher probability of failure associated with the loss in the cable tension and damper capacity during the lifetime of the cable-damper system. Further, a higher reduction of β value occurs within the first 50 days due to a rapid loss of cable tension over this time period. As can be seen from Figure 4.7(a), within the first 50 days, the loss in cable chord tension is 7.4%, whereas over the entire 300 days, the total loss in cable chord tension is 12.2%. Based on Figure 4.8, the impact of cable tension and damper capacity variation on the reliability of the system performance at any time within the 300 days can be obtained. Hence, the time-dependent reliability index, $\beta(t)$, can be expressed as a function of the damper coefficient and the cable chord tension, i.e., $\beta(c(t), H(t))$.
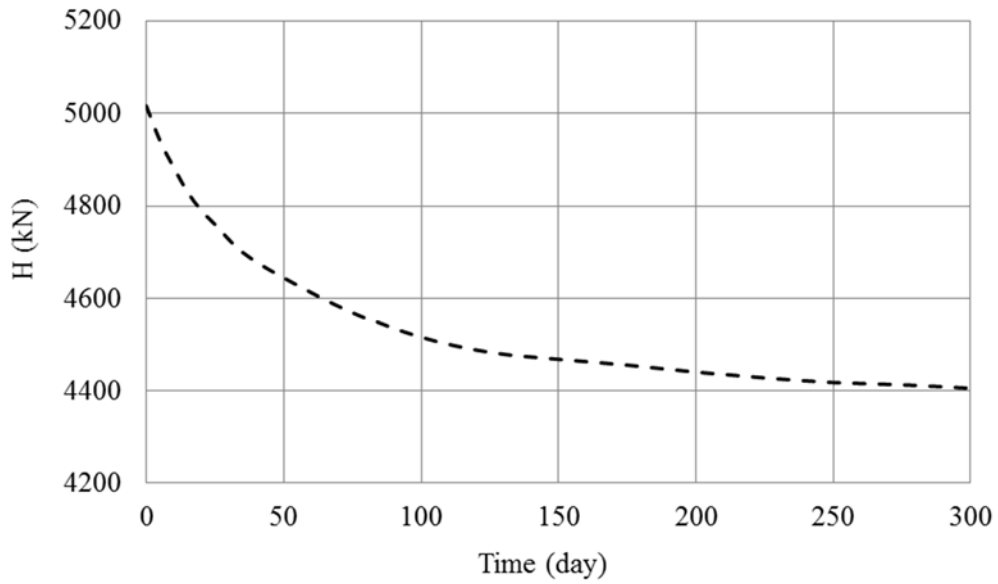
(a) Cable tension along the chord
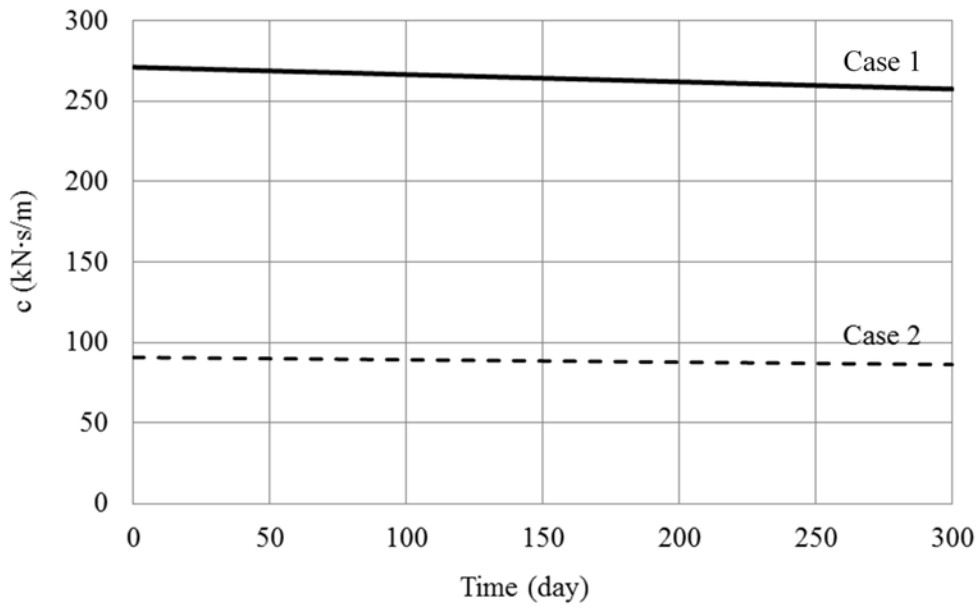
(b) Damping coefficient of damper

Figure 4.7: Time variation of cable tension and damper capacity over a period of 300 days (Case 1: $c_0=c_{opt}=271.1$kN·s/m, Case 2: $c_0=90.4$kN·s/m) (a) Cable tension along the chord; (b) Damping coefficient of damper
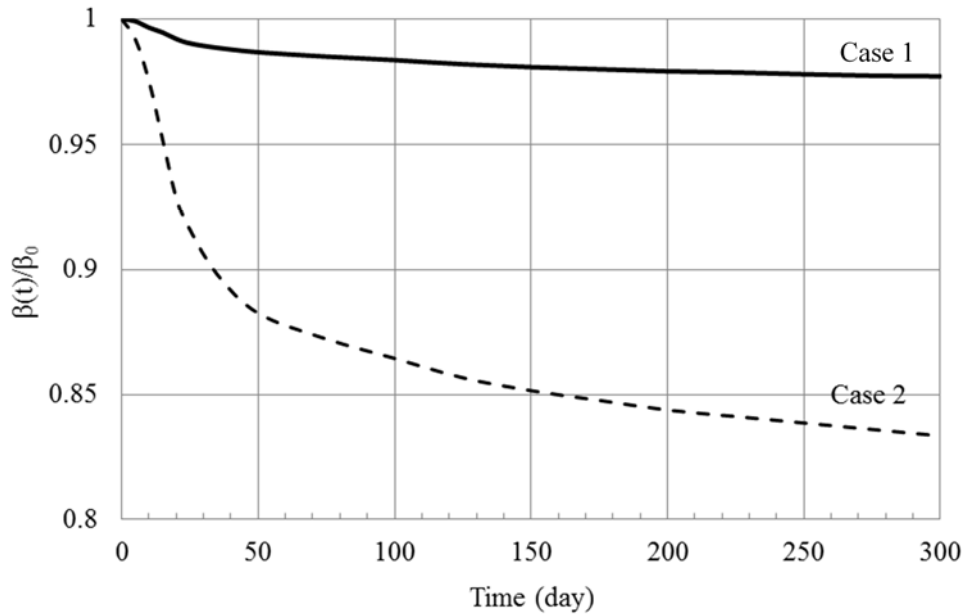
Figure 4.8: Time variation of relative reliability index (Case 1: $c_0 = c_{opt} = 271.1$ kN·s/m, $\beta_0 =$ 9.50; Case 2: $c_0 = 90.4$ kN·s/m, $\beta_0 = 2.24$)

For a more convenient identification of the effect of cable tension loss and damper capacity degradation on the system reliability, this set of results are also plotted in Figure 4. 9 in terms of the relative reliability-index $\beta(t)/\beta_0$ versus the percentage loss of cable chord tension (Figure 4.9(a)) and damper capacity (Figure 4.9(b)).

Though the presentation of Figure 4.9 isolates the dependence of the reliability index reduction on the loss in cable chord tension and damper capacity, it should be pointed out that in the analysis, the variation of H and c are considered simultaneously according to the patterns shown in Figure 4.7. For example, at day 180, when the cable chord tension and the damper capacity are reduced by 11.3% and 3%, respectively, the corresponding relative reliability-index in Case 1 is $\beta(t=180$ day$)/\beta_0 = 0.980$, i.e. the reliability-index drops 2% from its initial value.

110
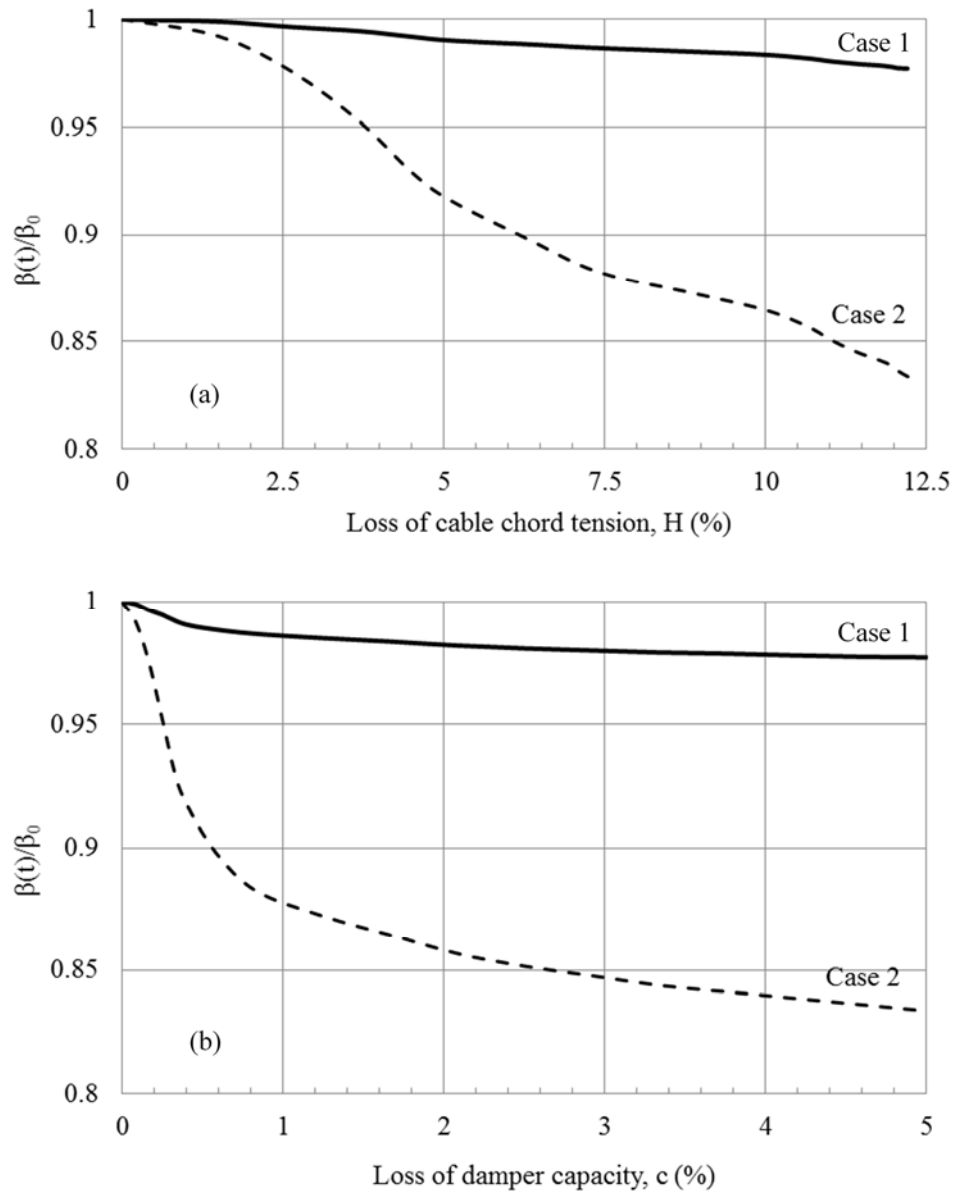
Figure 4.9: Relative reliability-index estimation due to loss of (a) cable chord tension, and (b) damper capacity

Comparing the relative reliability index results of Case 1 and Case 2, it can be seen that Case 2 is more critical. This implies that when the damper capacity c is different from the optimum value, the system performance would be more sensitive and have greater degradation due to uncertainty in system parameters. This can also be verified by

comparing the slope of each reliability curve at different damping parameters in Figure 4.4(b). The slope is less steep when ψ is closer to $\psi_{r,max}$.

The integration of reliability analysis into the lifetime maintenance strategy for the studied cable-damper system can be achieved by considering the time variation of the system performance associated with the loss in cable chord tension and damper capacity. To keep the cable-damper system operating at its designated performance, the lifetime variation of the system reliability-index should remain zero, which means

$$\frac{\partial \beta(c(t), H(t))}{\partial t} = \frac{\partial \beta}{\partial c} \cdot \frac{\partial c}{\partial t} + \frac{\partial \beta}{\partial H} \frac{\partial H}{\partial t} = 0 \tag{4-14}$$

where the lifetime variation of the damper capacity and the cable chord tension are represented by $\partial c/\partial t$ and $\partial H/\partial t$, respectively. If we assume that the maintenance of the studied cable-damper system can be achieved by adjusting cable chord tension to ensure that the performance remains at the designed safety level, Eq. (4-14) can be rewritten as:

$$\frac{\partial H}{\partial t} = -\frac{\partial \beta / \partial c}{\partial \beta / \partial H} \cdot \frac{\partial c}{\partial t} \tag{4-15}$$

Thus, the required adjustment of cable tension at any time of interest can be obtained from the tangents of the reliability index curves with respect to c and H, i.e.:

$$\frac{\partial \beta(c(t), H(t))}{\partial c} = \frac{\partial \left(\dfrac{\beta(t)}{\beta_0} \right) \cdot \beta_0}{\partial \left(\dfrac{c_0 - c(t)}{c_0} \right) \cdot (-c_0)} = -\frac{\beta_0}{c_0} \cdot \frac{\partial \left(\dfrac{\beta(t)}{\beta_0} \right)}{\partial \left(\dfrac{c_0 - c(t)}{c_0} \right)} \tag{4-16}$$

$$\frac{\partial \beta(c(t), H(t))}{\partial H} = \frac{\partial \left(\dfrac{\beta(t)}{\beta_0} \right) \cdot \beta_0}{\partial \left(\dfrac{H_0 - H(t)}{H_0} \right) \cdot (-H_0)} = -\frac{\beta_0}{H_0} \cdot \frac{\partial \left(\dfrac{\beta(t)}{\beta_0} \right)}{\partial \left(\dfrac{H_0 - H(t)}{H_0} \right)} \tag{4-17}$$

112

where the lifetime variation of the relative reliability index $\beta(t)/\beta_0$ versus the percentage loss in cable chord tension and damper capacity can be computed from the results in Figure 4.9.

In the current example, the initial design point in Case 1 is H_0=5017kN, c_0=271.1kN·s/m and the initial reliability index equals to β_0=9.50. For instance, at day 180, it can be deduced from Eqs. (4-16), (4-17), and Figure 4.9 that $\partial\beta/\partial c$=3.7×10^{-5} and $\partial\beta/\partial H$=3.1×10^{-7}. Hence, to ensure β_{180}=β_0= 9.50, the adjustment rate of the cable tension, in terms of its chord component, can be obtained from Eq. (4-15) as $(\partial H/\partial t)|_{\text{Day180}}$= -(3.7×10^{-5})/(3.1×10^{-7})×(-0.056)= 6.73 kN/day, where the lifetime variation of damper capacity at day 180 can be obtained from Figure 4.7, which is $\partial c/\partial t$=-0.056kN·s/m per day.

By repeating the calculations for cable chord tension adjustment rate, $\partial H/\partial t$, at different time instants, a maintenance plan can be defined over the lifetime of the studied cable-damper system. The required additional force after a certain time period can be obtained by integrating the adjustment rates over the maintenance period, i.e.

$$H_m = \int_0^t \frac{\partial H}{\partial t} dt \qquad (4\text{-}18)$$

where H_m is the amount of cable chord tension adjustment required at day t. Figure 4.10 shows the required H_m at different time to maintain the desired performance of the studied cable-damper system.The results show that to keep the system perform at a level corresponding to the designed reliability index β_0=9.50, the required additional amount of cable tension increases monotonically during the lifetime of the cable, which, at the end of the studied 300-day period is 188.1kN. This equals to 3.7% of the initial design value.
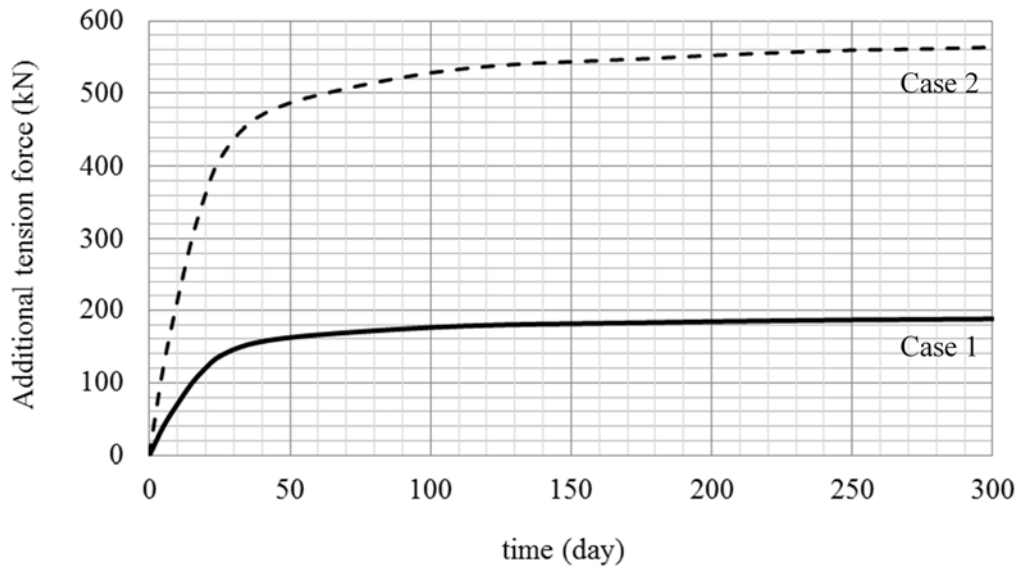
Figure 4.10: Additional tension adjustment to maintain system reliable performance over the period of 300 Days

If conducting the same action for Case 2, the required additional tension force over the 300-day period would be 11.2% of the initial design value. Comparison of the two curves shown in Figure 4.10 indicates that more adjustment in cable tension is needed if the selected damper size is different from the optimum one. Therefore, when an external damper is applied to control cable vibrations, it is very important to select the optimum size or a size as closer as possible to the optimum one. This is not only for a more effective vibration control, but also to ensure a higher reliability of the system.

4.6 SUMMARY

External dampers are commonly used on cable-stayed bridges to control various types of large amplitude cable oscillations. In the case of rain-wind-induced vibrations, due to lack of thorough understanding of its excitation mechanism, current prediction of the required damping, to effectively suppress it, is mainly depending on a Scruton number-

based empirical criterion, and the damper is designed using tools derived by deterministic-based analysis approaches. Therefore, the latent stochastic nature of the problem, including the uncertainty of cable and damper properties with respect to their nominal design values and their potential time variations over the service life of a bridge, is generally excluded in the formulation. Nevertheless, these uncertainties would render the actual system properties deviate from their assumed nominal design value and could have a considerable impact on the performance of a damped cable. The current chapter aims at developing a time-variant reliability-based framework model to evaluate how these uncertainties of the structural parameters of a cable-damper system would affect the performance of an external damper designed according to the current practice.

The problem has been formulated as a limit state up-crossing scenario to determine the time specific system reliability due to rain-wind-induced cable vibrations. The time-variant reliability analysis is conducted by combing the existing time-invariant reliability methods with the time-varying system parameters. The general form of the time-dependent LSF was proposed as the difference between the available time-varying equivalent structural damping ratio in a cable-damper system and the minimum required structural damping ratio of a damped cable to avoid rain-wind-induced vibrations. Results showed that compared to the first-order reliability method, the SORM with adaptive approximations method could improve the accuracy of failure probability prediction while retaining simplicity in the problem formulation and efficiency in computation. Various applications of the proposed time-variant reliability-based framework model, including the development of reliability-based damper design curves and long-term structural maintenance plan, have been demonstrated through numerical examples. It has been found

that the presence of uncertainty in the structural properties of a cable-damper system at a given design point could have a sizable effect on its reliability response and thus should be considered in design. In particular, the performance of a cable-damper system was observed to be more sensitive to the uncertainty associated with damper size. Further, at a specific damper location, the existence of a damper size which would result in the most reliable performance of a damped cable has been identified. Results showed that it agreed well with the optimum damper size reported in literature which can attain the maximum damping ratio at the same damper location. By applying regression analysis, an empirical formula were determined which related the reliability response of damped bridge stay cables to their structural design inputs by proposing general expressions of the reliability index and the optimum nondimensional damper parameter.

CHAPTER 5

RELIABILITY-BASED DESIGN ASSESSMENT OF DAMPED STAY CABLE EXPOSED TO WIND UNDER NO PRECIPITATION CONDITION

This chapter extends the application of the proposed reliability-based design tool in Chapter 4 to the assessment of cable-damper systems performance prone to dry inclined cable galloping conditions. The limit state function is improved by adding uncertainties associated with the wind in the formulations. The wind parameters are derived by applying the statistical analysis methods to the recorded wind speed at a given bridge site. Some design cases show the application of the proposed time-variant reliability-based framework model in predicting aerodynamic stability of a damped stay cable when preliminary design or life time maintenance is needed.

5.1 INTRODUCTION

5.1.1 Background

Inclined stay cables on cable-stayed bridges are prone to wind-induced vibrations due to their long flexible nature and low structural damping. They are often exposed to wind with skew angles, leading to flow patterns with strong three-dimensional characteristics. Thus, besides conventional wind-induced excitation phenomena, such as Kármán-vortex excitation, they also experience possible wind induced-excitation specifically related to their inclined orientation. Severe types of stay cable vibrations under either the combined effect of rain and wind or wind only have been observed in field and wind tunnel tests (e.g. Hikami and Shiraishi, 1988; Main and Jones, 2001; Cheng et al.,

117

2003; Matsumoto et al., 2007). It is learned from literatures that some types of these cable vibrations are more probable and/or critical than the others (Kumarasena et al., 2007):

a) Rain-wind-induced cable vibration (RWIV) is the excitation of cables under combined effect of rain and wind, noting that the majority of large amplitude cable vibration incidents observed on site or wind tunnel tests (e.g. Hikami and Shiraishi, 1988; Yamaguchi, 1990; Flamand, 1995; Cosentino et al., 2003) were associated with this type of vibration.

b) Dry-inclined cable galloping is the excitation solely induced by wind, i.e. without the presence of precipitation. It is a type of unstable bridge stay cable response identified in a number of wind tunnel studies (e.g. Miyata et al., 1994; Saito et al., 1994; Cheng et al., 2003; Nikitas et al., 2009). Experimental results from these studies suggested that the onset conditions of this violent motion are possible to be satisfied on site. Though at present, no field case has been formally confirmed as dry inclined cable galloping, the possibility of its occurrence on real bridges should not be disregarded. This excitation has been recognized as the most critical wind-induced cable vibration phenomenon for bridge stay cables due to its catastrophic consequences.

The vulnerability of stay cables to these excitations has raised great concern in the bridge engineering community (due to increased fatigue stress ranges) and has been a cause of deep anxiety for the observing public. Therefore it is imperative to take into account these issues in bridge design.

Accordingly, the present study is conducted to investigate the impact of the two aforementioned possible vibrations on the reliable performance of a cable-damper system.

As shown in Chapter 4, a reliability-based analysis tool was proposed for the assessment of a damped bridge stay cable under RWIV. The focus of the current chapter is to extend the application of the proposed reliability tool to the assessment of a cable-damper system performance prone to dry inclined cable galloping condition(s). This will be further examined in details as follows.

Divergent response of an oscillating body in wind is accompanied by the occurrence of negative aerodynamic damping. If the induced aerodynamic damping is negative and significant enough to overcome the positive structural damping, it will result in negative effective damping of the body. The response amplitude of the oscillating body will thus be drastically increased, leading to a divergent motion. Therefore, the aerodynamic stability of cables when exposed to various wind conditions can be assessed by evaluating the induced aerodynamic damping/forces.

The conventional approach of deriving aerodynamic damping of an oscillating body in wind is to apply the Den Hartog Criterion. The criterion was derived based on the assumption of cross-flow response. Recent study of Cheng et al. (2008b) showed that such an application led to the same critical physical conditions of negative aerodynamic damping as the experimentally observed galloping type of response. Macdonald and Larose (2006; 2008a; and 2008b) extended this classical approach and made it applicable to a cylindrical body of any arbitrary cross-sectional shape vibrating along any arbitrary direction normal to its axis. Further, Raeesi et al. (2013) presented a more realistic aerodynamic analysis model of a stay cable by introducing the unsteady/turbulent characteristics of the natural wind. The effects of turbulence intensity and the role of each turbulence component in triggering aerodynamic instability of an inclined and/or yawed

cable in unsteady flow condition have been investigated. Results show that while the emergence of critical Reynolds number regime is necessary for the occurrence of negative aerodynamic damping on a cable, the existence of flow unsteadiness in the natural wind would increase the risk of a stay cable to experience galloping type of response. The higher potential of instability occurrence is caused by the enhanced instability strength and expanded physical range of critical conditions due to the presence and increase of flow turbulence.

In contrary, limiting wind-induced cable vibrations is one of the most important safe design requirement for cable-stayed bridges. Adding damping device to increase cable structural damping or modifying cable surface condition have been so far used to control cable vibrations (Matsumoto et al., 1989; Saito et al., 1994; Miyata and Yamada, 1994; Flamand, 1995; Xu et al., 1999; Sun et al., 2003; Bosch and Park, 2005; Matsumoto et al., 2007). For example, cables are lapped by polyethylene with helical fin on cable surface, cross-ties between stay cables and damping devices attached to the cables (FHWA/HNTB, 2005).

To the best knowledge of the author, though the effect of inherent structural damping on the aerodynamic response of a stay cable has been considered in the aforementioned literatures, the effectiveness of external dampers as possible solution to restrain the occurrence of dry inclined cable galloping has not been examined specifically in aerodynamic context. More importantly, existing studies are limited to deterministic-based analysis in which the uncertainties of structural parameters (such as cable tension and damper capacity) and wind parameters (such as speed, direction, etc.) over the service life of a bridge are totally neglected. Thus, to provide complete information regarding the

aerodynamic response of a cable due to dry inclined galloping, the problem should be more rationally studied from a probabilistic-based sense. The advantage is to determine the probability of stay cable failure associated with dry inclined cable galloping when uncertainties of structural and/or wind parameters are considered, rather than stating a single aerodynamic damping ratio.

5.1.2 Organization of the chapter

The remaining of this chapter is organized as follows: In Section 5.2, an analytical model of a cable-damper system under wind excitation is developed. First, the dynamic equation of motion of a cable-damper system subjected to wind load is illustrated. Then, the probabilistic-based analysis of dry inclined cable galloping is presented by defining the limit state function (LSF) based on the effective damping of a damped stay cable under wind load. This LSF contains structural and aerodynamic damping terms, which are identified as the resistant and the loading terms, respectively. The expression of equivalent structural damping ratio of a damped cable is given by Fujino et al. (2008), as described in Chapter 4. On the other hand, a general expression for the quasi-steady aerodynamic damping ratio of an inclined and/or yawed cable oscillating along an arbitrary direction normal to its axis when exposed to wind is adapted from the study of Raeesi et al. (2013). Noteworthy, the uncertainty of structural and wind parameters are reflected in the LSF. The most influential structural factors that would affect the efficiency of a viscous damper (including the cable tension and the damper capacity) are treated as two independent time-varying random variables. Also, the uncertain characteristic of wind loading is expressed by statistical wind-related parameters such as the scale, the shape and the location parameters. They will be calculated through fitting the most pertinent statistical distribution

to the historical wind speed data at a bridge site. The details of applying statistical analysis methods to wind speed data are shown in Appendix B. Later, the second-order-second-moment reliability method (SORM) which is adapted by a tail approximation technique will be applied to solve this probabilistic-based aerodynamic problem. Resultantly, the reliable performance of the studied cable-damper system under wind-induced excitation (in particular, dry inclined cable galloping) will be evaluated in terms of the reliability index. The expected outcomes of the application of the proposed reliability method will be discussed in Section 5.3, in the form of a lifetime reliability-based response diagram of a cable-damper system after N years of service life. In Section 5.4, application of the proposed time-variant reliability-based framework model in predicting aerodynamic stability of a damped stay cable will be demonstrated through numerical examples. First, the applicability of the proposed reliability method in identifying the potential occurrence of dry inclined cable galloping will be verified using data from an existing wind tunnel experiment. Next, a design case will be studied, of which the variation of cable tension (based on field data collected from real stay cables by Au and Su (2012), and the damper capacity degradation over service time (which is recommended by a manufacturer, Reif et al. (2010) is considered. Besides, the uncertainty of wind is evaluated for a set of historical wind data for a selected bridge site. The aerodynamic performance of a damped stay cable will be thoroughly evaluated within a practical range of structural and wind parameters over the service life of the structure. The relation between the critical wind speed condition(s) for galloping and the extreme wind speed on site corresponding to a certain return period will be investigated through a sensitivity-based aerodynamic assessment analysis. In addition, the potential application of the proposed time-variant reliability-based

framework model and results to the development of maintenance strategy over lifetime of a cable-damper system will be demonstrated.

5.2 FORMULATION OF RELIABILITY-BASED PERFORMANCE ASSESSMENT METHOD

5.2.1 Description of a bridge stay cable model under wind excitation

Assuming that the wind blows horizontally and the stay cables are arranged in the vertical plane (i.e. plane perpendicular to the bridge deck), the orientation of a typical stay cable on a cable-stayed bridge with respect to the mean wind direction is shown schematically in Figure 5.1. A global coordinate system $X_gY_gZ_g$ is defined in such a way that the X_gZ_g-plane represents the vertical stay cable plane OAB, with the Z_g-axis along the bridge tower shaft, the X_g-axis along the horizontal projection of the cable. The Y_g-axis is located in the bridge deck plane and is perpendicular to the X_g-axis. The cable is inclined at an angle γ to the horizontal bridge deck plane. It has a length L, a mass per unit length m, a finite flexural rigidity EI, and carries a tension T along the cable chord. A damper with a damping coefficient, c, is attached transversely to the cable at a distance L_d from the lower end support (i.e. point A). It is installed in the vertical stay cable plane, i.e. the X_gZ_g-plane.

The cable is subjected to oncoming wind with a mean velocity U_m. The direction of wind is skewed at an angle θ against the horizontal projection of the cable and measured clockwise from the vertical plane of the cable. The angel θ is known as the yaw angle. A local coordinate system xyz is defined for the cable with the z-axis along the cable chord. The xz-plane collapses onto the plane containing the cable and the mean wind vector, and would be called the cable-wind plane. The y-axis is normal to the xz-plane. The relative angle between the cable axis and the wind direction in the cable-wind plane is shown by φ.

The following angle relationship can be established for the cable-wind angle (Cheng et al., 2003a)

$$\cos\varphi = \cos\gamma\,\cos\theta \qquad (5\text{-}1)$$
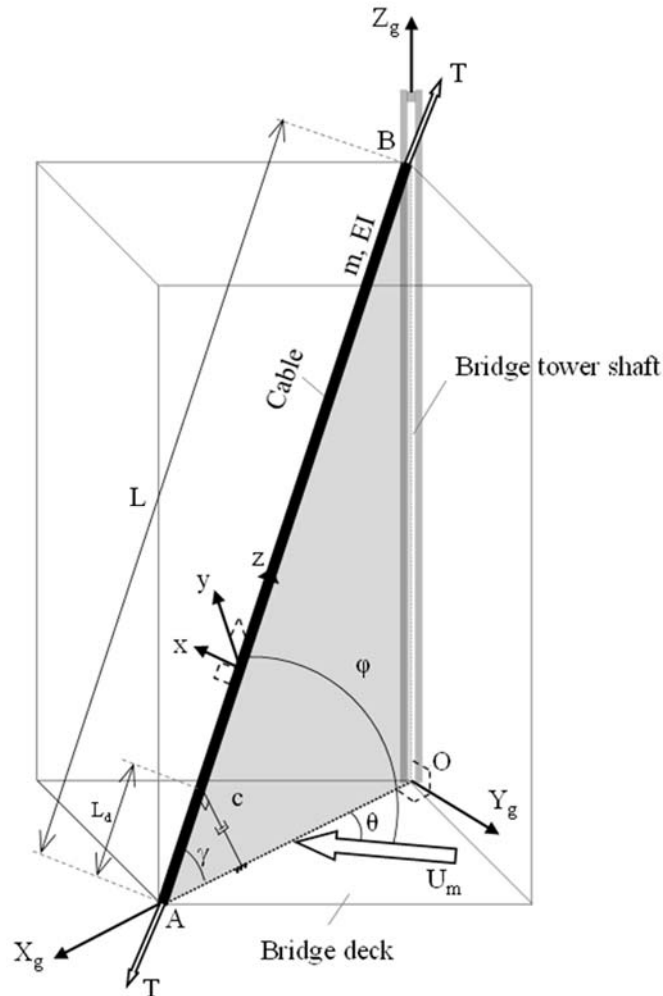
Figure 5.1: Orientation of a typical stay cable and definition of angles with respect to the mean wind speed

Figure 5.2(a) shows the velocity components in the cable-wind plane, where the component of the wind speed normal to the cable axis is calculated by $U_N = U_m \cdot \sin\varphi$ and is along the x-axis.

124

Consider a cross section of the cable in the xy-plane, the cable motion is defined by a vector η as displayed in Figure 5.3(a). Thus, the cable has a velocity of $\dot{\eta}$ in the plane normal to the z-axis and an angle α to the cable-wind plane (xz-plane) due to wind load. For example, it was shown that over the critical Reynolds number range, if wind blows along the cable (i.e. $\theta = 0°$), the cable vibrates in the cable-wind plane with $\alpha = 0°$, which specifies the in-plane cable motion state (Macdonald and Larose, 2006). In contrary, for across-wind vibrations (i.e. $\theta = 90°$), the cable motion direction occurs at $\alpha = 90°$. The dominant motion direction of the cable is determined by (Cheng et al., 2003a)

$$\tan \alpha = \tan\theta / \sin \gamma \tag{5-2}$$

(a) Absolute velocities   (b) Velocities relative to cable
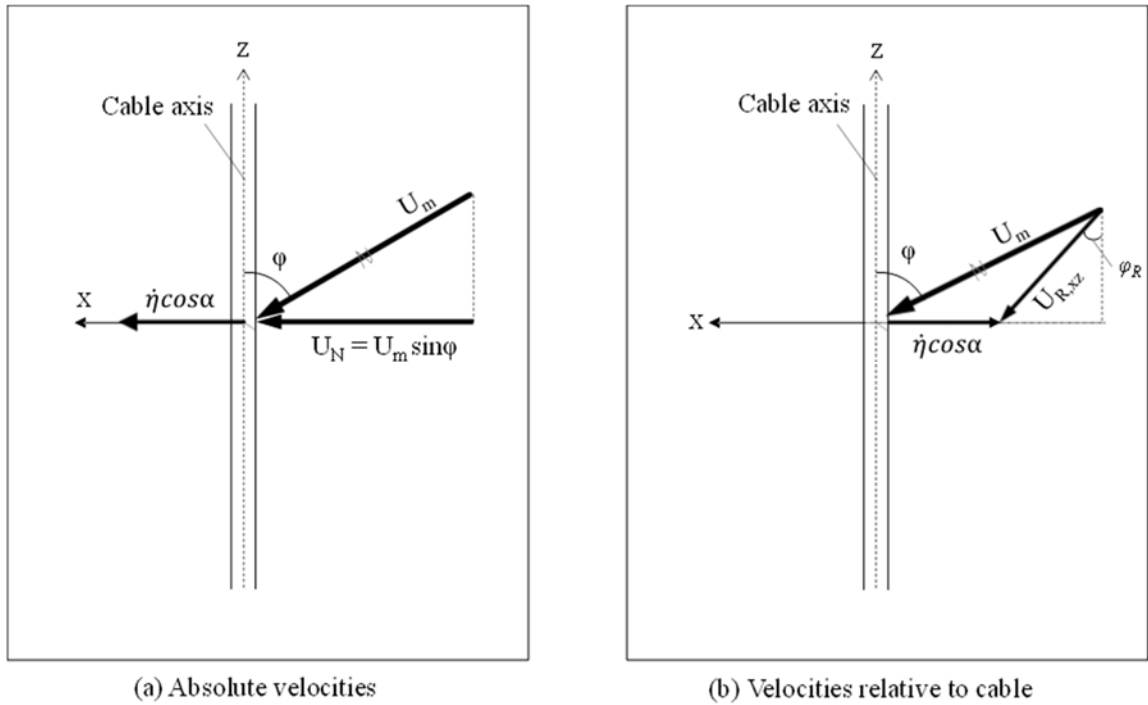
Figure 5.2: Velocity components in the cable-wind plane (xz-plane)

Using Eq. (5-1), the relationship between the cable-wind relative angle φ and the wind yaw angle θ can be obtained for the given cable inclination angle, γ. Also, from Eq.

(5-2) the relationship between the wind yaw angle θ and the dominant cable-motion direction angle α is of interest. Hence, for every orientation of the stay cable (i.e. for every φ), a corresponding α can be determined. Subsequently, the component of the cable motion velocity in the direction of the normal component of the actual flow velocity $\vec{U}_N$ can be calculated by $\dot{\eta}\cos\alpha$, as shown in Figure 5.2(b).

(a) Velocities   (b) Forces
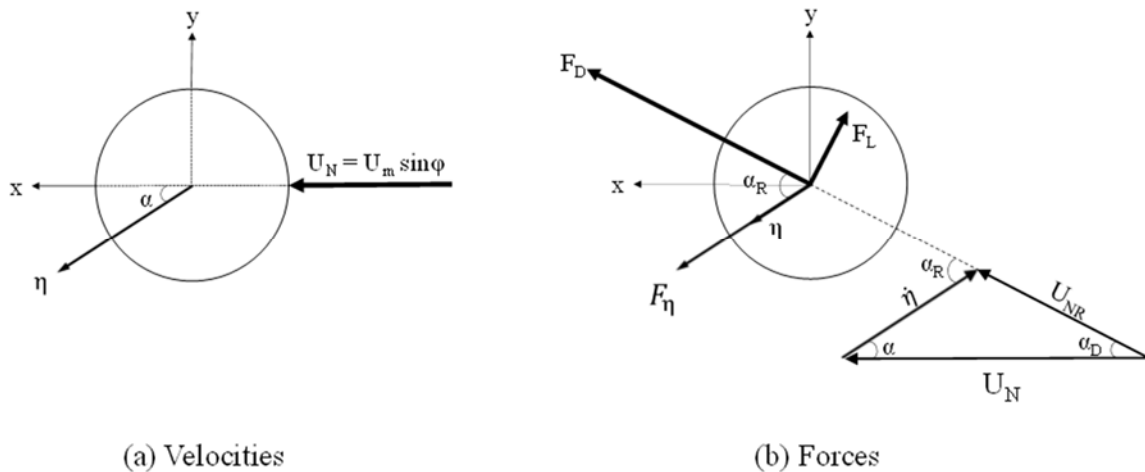
Figure 5.3: Velocities and forces in the plane normal to the cable axis;
(a) Velocities; (b) Forces

Prediction of aerodynamic response of the described system shown in Figure 5.1 is associated with a number of uncertainties in the structural and the loading properties. They are as follow:

1- The intrinsic uncertainties exist in the structural parameters, with the cable tension force T and the external damper capacity c being the most influential parameters on the performance of the system. It is likely that the structural properties might not only deviate from their respective nominal design values at a given design point, but also fluctuate over the lifetime due to changes in the ambient conditions. Hence, the structural

126

characteristic of a cable-damper system can be represented ideally as a function of time. The details of uncertainties in structural parameters were explained in Chapter 4.

2- The uncertainties stem from the random nature and inborn variability of wind load. The establishment of appropriate design wind load is a critical first step towards the reliability-based assessment of structures exposed to wind, as it could enable the associated random variables such as wind speed, wind direction to be modelled mathematically. Since these variables are time-varying random process, the probabilistic analysis of recorded historical wind data is required. Then, the best-fitted distribution of directional wind speeds should be evaluated to follow certain probability distribution. Further, it is also important to define the maximum attainable wind speed (i.e. extreme wind speed), U_{ext} (R), corresponding to the desired return period R for a studied bridge site. In this regard, Appendix B is devoted to provide a review of the probability distribution approaches relevant to wind engineering, by focusing on the statistical analysis of historical wind data and also estimation of extreme wind speed at a bridge site corresponding to the desired return period.

It is also noteworthy that the determination of the correlation between different random system parameters is a challenging task. In fact, some of them are totally independent such as the cable tension, T, and the damper capacity, c, variables as treated in the current study. Similarly, the wind properties such as the wind speed and the direction are also independent of the structural parameters. Therefore, uncertainties of the involved structural and load parameters can be treated separately in the rest of the study.

In this study, when analyzing the aerodynamic response of a damped cable under certain wind condition, the potential deviation of structural parameters, i.e. the cable

tension (T) and the damper capacity (c), from their nominal design values over the lifetime of a cable-stayed bridge will be considered. In addition, the uncertain nature of loading associated with wind conditions (i.e. from the recorded wind speed data set) will be incorporated in defining the LSF.

5.2.2 Development of LSF

In this section, the equation of motion (EOM) for the studied cable-damper system under wind load is presented first. Afterwards, the conditions under which the dry inclined cable galloping was observed in existing wind tunnel studies are considered for the current model. The LSF is established accordingly for the reliability-based design assessment of damped stay cables exposed to wind under no precipitation condition.

The EOM for the described model in Figure 5.1 can be expressed in the matrix form as:

$$\mathbf{M\ddot{Q}}+\mathbf{C\dot{Q}}+\mathbf{KQ}=\mathbf{F_w}+\mathbf{F_d} \qquad (5\text{-}3)$$

where

$$\mathbf{M}=\begin{bmatrix} m & 0 \\ 0 & m \end{bmatrix}, \quad \mathbf{K}=\begin{bmatrix} m\omega_x^2 & 0 \\ 0 & m\omega_y^2 \end{bmatrix}, \quad \mathbf{Q}=\begin{bmatrix} x \\ y \end{bmatrix}$$

Here $\mathbf{M}$ is the mass matrix with m defined as the cable mass per unit length; $\mathbf{K}$ is the stiffness matrix in which the undamped circular frequencies are represented by ω_x and ω_y, respectively; $\mathbf{Q}$ is a vector consisting cable displacement components along the x and the y directions (based on the local coordinate system, xyz). It can be expressed by considering the cable motion along the in-plane and out-of-plane directions; $\mathbf{F_w}$ is the matrix of the external dynamic loading due to wind per unit length; $\mathbf{F_d}$ is the force exerted

by the damper at location of L_d; It is assumed that the axial cable vibration (i.e. vibration along the z direction) is neglected in the formulation.

The damping matrix, $\mathbf{C}$, in Eq. (5-3) is defined as the sum of the structural damping matrix, $\mathbf{C_s}$, and the aerodynamic damping matrix, $\mathbf{C_a}$, i.e. $\mathbf{C}=\mathbf{C_s}+\mathbf{C_a}$. It consists of contributory terms associated with the structural and the aerodynamic damping in the x and y directions (Macdonald and Larose, 2008a):

$$\mathbf{C} = \begin{bmatrix} C_{xx} & C_{xy} \\ C_{yx} & C_{yy} \end{bmatrix} \tag{5-4}$$

The structural damping matrix is defined by

$$\mathbf{C_s} = \begin{bmatrix} C_{s,xx} & C_{s,xy} \\ C_{s,yx} & C_{s,yy} \end{bmatrix} = \begin{bmatrix} 2m\omega_x\zeta_{s,x} & 0 \\ 0 & 2m\omega_y\zeta_{s,y} \end{bmatrix} \tag{5-5}$$

Here $C_{s,xx}$ and $C_{s,yy}$ are the components of the structural damping coefficient along x and y directions; $\zeta_{s,x}$ and $\zeta_{s,y}$ represent respectively the structural damping ratio of the cable in the x-and y-directions. Knowing that the external damper is attached transversely to the stay cable within the vertical stay cable plane (OAB), the supplemental damping provided by the damper should be reflected in the structural damping matrix, $\mathbf{C_S}$.

The structural damping provided by a damper having a damping coefficient of c can be decomposed into the X_g, Y_g and Z_g directions in the global coordinate system by:

$$\mathbf{C_s} = \begin{bmatrix} C_{s,X_g} \\ C_{s,Y_g} \\ C_{s,Z_g} \end{bmatrix} = \begin{bmatrix} c\cdot\cos(\pi/2-\gamma) \\ 0 \\ c\cdot\sin(\pi/2-\gamma) \end{bmatrix} \tag{5-6}$$

Besides, a transformation matrix $[R]$ which relates the global coordinate system $X_gY_gZ_g$ with the local coordinate system xyz is needed in order to express the structural damping term in the local coordinate system. This transformation matrix has the form of

$$[R] = \begin{bmatrix} \cos\theta\cos[-(\pi/2-\gamma)] & \cos(\pi/2-\theta)\cos[-(\pi/2-\gamma)] & -\cos\gamma \\ -\cos(\pi/2-\theta)\cos[-(\pi/2-\gamma)] & -\cos(-\theta)\cos[-(\pi/2-\gamma)] & 0 \\ \cos(-\gamma) & 0 & \cos(\pi/2-\gamma) \end{bmatrix}$$

By applying the transformation matrix $[R]$ to the global damping matrix $[C_s]$ in Eq. (5-6), the effect of external damper on the cable motion could be expressed in the local coordinate system as

$$\mathbf{C_s} = \begin{bmatrix} C_{s,x} \\ C_{s,y} \end{bmatrix} = c \cdot \begin{bmatrix} \cos\theta(\cos(\pi/2-\gamma))^2 - \cos\gamma\,\cos(\pi/2-\gamma) \\ \cos(\pi/2-\theta)(\cos(\pi/2-\gamma))^2 \end{bmatrix} \tag{5-7}$$

where $C_{s,x}$ and $C_{s,y}$ are respectively the structural damping coefficient components along the x and the y directions.

On the other hand, the wind load, $\mathbf{F_w}$, in Eq. (5-3) can be expressed as:

$$\mathbf{F_w} = \begin{bmatrix} F_x \\ F_y \end{bmatrix} = \begin{bmatrix} F_D\cos\alpha_D - F_L\sin\alpha_D \\ F_D\sin\alpha_D + F_L\cos\alpha_D \end{bmatrix} = \frac{1}{2}\rho U_R^2 D \begin{bmatrix} C_D\cos\alpha_D - C_L\sin\alpha_D \\ C_D\sin\alpha_D + C_L\cos\alpha_D \end{bmatrix} \tag{5-8}$$

where F_x and F_y are the components of the wind-induced force per unit length, along the x and y directions, respectively. They are calculated by taking the contribution of the drag force, F_D, and the lift force, F_L, along the x and y directions (Figure 5.3(b)); U_{NR} is the projection of the relative velocity, $\vec{U}_R$, in the plane normal to the cable axis (i.e. xy-plane); $\vec{U}_R$ is obtained by summing up the mean wind speed and the cable motion in a vector system, i.e. $\vec{U}_R = \vec{U}_m + \dot{\vec{\eta}}$; ρ is the air density; D is the cable diameter; C_D and C_L are the

130

drag and lift coefficients; α_D is the angle between U_N and U_{NR}; U_N is the normal component of the oncoming flow velocity (Figure 5.2).

Macdonald and Larose (2006) showed that the wind-induced aerodynamic force on a stay cable is a function of the cable velocity, $\dot{\eta}$. Therefore, it would provide a non-linear damping term in the EOM of the cable. For small amplitude vibrations in a given n^{th} mode (i.e. at the onset of vibrations), the equivalent linear aerodynamic damping ratio is then given by:

$$\zeta_a = \frac{-1}{2m\omega_n} \frac{dF_\eta}{d\dot{\eta}}\bigg|_{\dot{\eta}=0} \tag{5-9}$$

Thus, the aerodynamic damping coefficient components along the x and the y axes are as follow:

$$\mathbf{C_a} = \begin{bmatrix} c_{a,xx} & c_{a,xy} \\ c_{a,yx} & c_{a,yy} \end{bmatrix} = -\begin{bmatrix} \dfrac{\partial F_x}{\partial \dot{x}} & \dfrac{\partial F_x}{\partial \dot{y}} \\ \dfrac{\partial F_y}{\partial \dot{x}} & \dfrac{\partial F_y}{\partial \dot{y}} \end{bmatrix}_{\dot{x}=\dot{y}=0} \tag{5-10}$$

For instance, the equivalent linear aerodynamic damping coefficient in a given n^{th} mode along the y-direction is given by:

$$\zeta_{a,yy} = \frac{-1}{2m\omega_n} c_{a,yy} = \frac{-1}{2m\omega_n} \frac{dF_y}{d\dot{y}}\bigg|_{\dot{y}=0}$$

The characteristics of dry inclined/yawed cable galloping phenomenon and its associated mechanism has been investigated in a few wind tunnel studies. Notable is the work by Cheng et al. (2003a) of which the divergent type of cable motion was observed. The experimental setup of the studied model was equivalent to a real bridge cable inclined

and yawed both at 45° to the mean wind direction. It was shown that once the wind speed reached 32 m/s (corresponding to a Reynolds number of 3.40×10^5), the amplitude of the cable motion increased dramatically within a short period of time. It was observed that the predominant cable motion occurred along the in-plane direction, and the model motion followed a shallow elliptical path. In a more recent wind tunnel test by Jakobsen et al. (2009b), the same divergent motion of dry inclined cable was observed. It was also reported that the in-plane motion component dominated the cable response.

Even though the defined problem of an inclined damped stay cable under wind excitation possesses a three-dimensional characteristic, referring to the results of the aforementioned wind tunnel experiments, the predominant cable motion along the in-plane direction is of interest. Thus, by focusing on the direction along which the predominant cable motion would occur, the problem can be simplified into an aerodynamic analysis of a one-degree-of-freedom cable-damper system along the in-plane cable motion direction. In the remaining of this section, the components of the structural and the aerodynamic damping ratios in the y-direction (i.e. the predominant cable motion direction) are of interest. To keep the notation simple, the sub-index y will be omitted in the development of LSF.

The aerodynamic stability of cables when exposed to various wind conditions can be assessed by evaluating the induced aerodynamic damping/forces. The divergent response of an oscillating cable in wind is accompanied by the occurrence of negative aerodynamic damping. If the induced aerodynamic damping is negative and significant enough to overcome the positive structural damping, it will result in negative effective damping of the cable. The response amplitude of the oscillating body will thus be

drastically increased, leading to a destructive divergent motion. Therefore, the general form of the LSF for evaluating the susceptibility of an inclined damped cable to dry inclined cable galloping can be proposed as the sum of the available structural damping ratio, ζ_s, in a cable-damper system, i.e. the resistant damping and the aerodynamic damping, ζ_a, due to wind excitation condition, or the damping demand. It can be expressed as

$$g(\zeta) = \zeta_s + \zeta_a \tag{5-11}$$

where $g(\zeta)$ is the LSF of the cable-damper system which represents the effective damping, ζ, of the damped cable under wind excitation. Thus, the failure domain is defined by the region where $g(\zeta) \leq 0$.

Knowing that the structural parameters (c and T) are treated as time-varying random variables, the time-dependent stability criterion is represented for LSF in Eq. (5-11) by

$$g(\zeta) = \zeta_s(t) + \zeta_a(U_m, t) = g[H(t), c(t), U_m] \geq 0 \tag{5-12}$$

where $H(t)$ and $c(t)$ represent, respectively, the time varying functions of the cable tension and the damper capacity. Hence the available structural damping ratio, $\zeta_s(t)$, is represented as a time-variant function over the service life of a cable-stayed bridge. On the other hand, the damping demand (aerodynamic damping) depends on wind speed condition over the lifetime of the cable-damper system.

Based on Eq. (5-12), if $g(\zeta) \geq 0$, the cable-damper system is considered stable and safe to resist dry inclined cable galloping. Otherwise, it would become unstable and large amplitude cable vibrations would occur.

The full expression of the nonlinear time-varying n^{th} structural modal damping ratio of a damped cable, $\zeta_{s,n}(t)$, was derived by Fujino et al. (2008) in the form of

$$\zeta_{s,n}(t) = R_f R_{sn} \frac{\eta_f \eta_{sn} \eta_n(t)}{1+(\eta_f \eta_{sn} \eta_n(t))^2} \cdot \frac{L_d}{L} \tag{5-13}$$

The details of the above equation have been explained in Chapter 4.

To further explain the LSF in Eq. (5-12), the expression of the aerodynamic damping ratio, ζ_a, is required. This term is a function of the wind condition (U_m or Re), the cable properties (cable-wind relative angle φ, cable natural frequency ω, cable mass per unit length m, cable diameter D), drag coefficient C_D, lift coefficient C_L, and the direction of cable motion α, noting that the cable motion direction α is an independent variable. The full expression of aerodynamic damping is adapted from the study of Raeesi et al. (2013), which is given by:

$$
\begin{aligned}
\zeta_a = \frac{\mu Re}{4 m \omega_n} \cos\alpha \Bigg\{ & \cos\alpha \left[C_D \left(2 \sin\varphi + \frac{\tan^2 \alpha}{\sin\varphi} \right) + \frac{\partial C_D}{\partial Re} Re \sin\varphi + \frac{\partial C_D}{\partial \varphi} \cos\varphi \right] \\
& \pm \sin\alpha \left[C_L \left(2 \sin\varphi - \frac{1}{\sin\varphi} \right) + \frac{\partial C_L}{\partial Re} Re \sin\varphi + \frac{\partial C_L}{\partial \varphi} \cos\varphi \right]
\end{aligned}
\tag{5-14}
$$

The lift terms in the second part of the above equation have a factor of $\pm \sin\alpha$, which represents the direction of lift and depends on the condition at which side of the cable the laminar separation bubble forms. Based on this, there are two distinct solutions for the aerodynamic damping ratio. However, it is assumed in this analysis that when flow passes, a single separation bubble could persist on the cylinder surface for a narrow range of Reynolds number within the critical regime (Schewe, 1983). This gives an asymmetric flow, and hence generates a mean lift force. Physically, it can be interpreted as that, if the first laminar separation bubble formed on one side of the cylinder, and the induced lift force is defined to be positive, then for the case where the laminar bubble is formed on the other side of the cable surface, the resulted lift force has a negative sign.

Thereof, the damping demand can be calculated based on the wind speed condition at time instant t, by simply substituting $Re = \rho D U_m / \mu$, into Eq. (5-14):

$$\zeta_a(U_m,t) = \frac{\rho D U_m}{4 m \omega_n(t)} \cos\alpha \left\{ \cos\alpha \left[C_D \left(2\sin\varphi + \frac{\tan^2\alpha}{\sin\varphi} \right) + \frac{\partial C_D}{\partial U_m} \cdot U_m \cdot \sin\varphi + \frac{\partial C_D}{\partial \varphi} \cos\varphi \right] \right.$$
$$\left. \pm \sin\alpha \left[C_L \left(2\sin\varphi - \frac{1}{\sin\varphi} \right) + \frac{\partial C_L}{\partial U_m} \cdot U_m \cdot \sin\varphi + \frac{\partial C_L}{\partial \varphi} \cos\varphi \right] \right.$$

$$(5\text{-}15)$$

where the partial derivatives of drag and lift coefficients with respect to wind speed are replaced in the above equation by using the following chain rule

$$\frac{\partial C_D}{\partial Re} = \frac{\partial C_D}{\partial U_m} \cdot \frac{dU_m}{d Re} = \frac{\partial C_D}{\partial U_m} \cdot \frac{\mu}{\rho D}$$
$$\frac{\partial C_L}{\partial Re} = \frac{\partial C_L}{\partial U_m} \cdot \frac{dU_m}{d Re} = \frac{\partial C_L}{\partial U_m} \cdot \frac{\mu}{\rho D}$$

$$(5\text{-}16)$$

The details of calculation of force coefficients and their partial derivatives with respect to Re and φ in Eqs. (5-15) and (5-16) are presented in Appendix A.

Moreover, variation in the cable tension would affect the cable vibration frequency $(\omega_n(t) = 2\pi \cdot n / 2L \cdot \sqrt{H/m})$ in the aerodynamic damping equation, Eq. (5-15). This simply implies that the aerodynamic damping ratio depends on both the structural and the loading parameters over the cable service time. As a result, the aerodynamic damping ratio can be expressed in terms of the mean wind speed and the service time in the form of $\zeta_a (U_m, t)$.

Finally, the full expression of the nonlinear LSF for the aerodynamic stability analysis of such a damped cable is obtained by substituting Eqs. (5-13) and (5-15) into Eq. (5-12), as

$$g(\zeta) = g\left[H(t), c(t), U_m\right] =$$

$$R_f R_{sn} \frac{\eta_f \eta_{sn} \eta_n(t)}{1 + (\eta_f \eta_{sn} \eta_n(t))^2} \cdot \frac{L_d}{L} + \frac{\rho D U_m}{4 m \omega_n(t)} \cos\alpha \left\{ \cos\alpha \left[C_D \left(2 \sin\varphi + \frac{\tan^2\alpha}{\sin\varphi} \right) + \frac{\partial C_D}{\partial U_m} \cdot U_m \cdot \sin\varphi + \frac{\partial C_D}{\partial\varphi} \cos\varphi \right] \right.$$

$$\pm \sin\alpha \left[C_L \left(2 \sin\varphi - \frac{1}{\sin\varphi} \right) + \frac{\partial C_L}{\partial U_{mt}} \cdot U_m \cdot \sin\varphi + \frac{\partial C_L}{\partial\varphi} \cos\varphi \right]$$

$$(5\text{-}17)$$

Consequently, the safety margin M (i.e. aerodynamic stability region) can be represented as a function of basic variables using a defined vector, $\zeta = (t, c, H, U_m)$, as $M = g(\zeta) \geq 0$.

5.2.3 Structural reliability analysis method

In this section, a structural reliability analysis method will be applied to evaluate the reliability index of a wind-excited damped cable under the risk of dry inclined cable galloping. The probability of failure is quantifiable for the proposed LSF by

$$P_f = P\{M \leq 0\} = \int_{M \leq 0} g(\zeta) d\zeta \qquad (5\text{-}18)$$

where $g(\zeta)$ is the joint probability density function of the effective damping due to uncertainty of the structural and the aerodynamic damping variables. Based on the idea of the tail-approximation approach (Rackwitz, 1997), the distribution of $g(\zeta)$ is replaced by an equivalent normal distribution at the design point. Such an equivalent normal distribution at the design point ζ_i^* simultaneously fulfils $f_i^N(\zeta_i^*) = f_i(\zeta_i)$ and $F_i^N(\zeta_i^*) = F_i(\zeta_i)$, where f and F represent PDF and CDF functions, respectively (Schneider 2006).

The mean and the standard deviation of M are then calculated and denoted by μ_M and σ_M, respectively. Accordingly, the reliability index β can be defined for the normalized LSF by $\beta = \mu_M / \sigma_M$, which mathematically represents the inverse function of the probability of failure as follows

$$\beta = -\Phi^{-1}(P_f) \tag{5-19}$$

where $\Phi(\cdot)$ is the statistical function which would yield the standard normalized cumulative distribution value at each design point (Elishakoff 1999).

The probability of failure will be calculated by applying the second-order reliability method (SORM) using adaptive approximation approach. This reliability method is selected among the other methods due to its formulation simplicity in handling high-nonlinearity of the LSF in Eq. (5-17). The accuracy of SORM in predicting the reliability results is verified in Chapter 4 for the case of RWIV of a sample cable-damper system. In addition, the reliability method will be extended by means of a tail numerical technique. Based on this extension, a non-Gaussian random variable can be considered in the reliability analysis. For instance, if the wind speed distribution follows the Weibull distribution, it should be first replaced by the corresponding normal distribution known as the equivalent normal distribution. Hence, the tail approximation technique is applied in which $f_i^N(U_{m,i}) = f_i^W(U_{m,i})$ and $F_i^N(U_{m,i}) = F_i^W(U_{m,i})$, where $U_{m,i}$ is the mean wind speed at design point i, $f_i^N(U_{m,i})$ and $f_i^W(U_{m,i})$ are the PDFs of the equivalent normal and the Weibull distributions, respectively. Similarly, $F_i^N(U_{m,i})$ and $F_i^W(U_{m,i})$ are the CDFs of the corresponding assigned distributions. As the tail of the distribution, which is to be replaced by a normal distribution, is of concern here, this approximation is called tail approximation. Thus, the implemented reliability method (i.e. SORM with adaptive approximation) is now ready to be applied to the case of which wind speeds follow Weibull distribution.

Subsequently, the time-dependent probabilistic analysis response for the defined LSF in Eq. (5-17) is computable. Wherein, the vibration control efficiency of an external

damper in resisting the occurrence of dry inclined cable galloping instability is evaluated in a probabilistic sense.

5.3 ESTABLISHMENT OF A LIFETIME RELIABILITY-BASED RESPONSE DIAGRAM

The probability of occurrence of dry inclined cable galloping of a stay cable during the service life of a cable-stayed bridge can be assessed by considering the structural and/or wind uncertainties over lifetime with the application of the reliability method. Besides, the sensitivity of influential parameters over the lifetime of a stay cable in triggering galloping would be predictable. Consequently, the results yielded from the proposed reliability-based framework model could be utilized to achieve a probabilistic-based damper design/maintenance guide for a cable-damper system to ensure its aerodynamic stability.

Figure 5.4 shows a schematic view of the reliability-based analysis results of a cable-damper system after N years of service life due to uncertain structural and/or wind condition(s). According to this figure, the system performance is shown by the reliability index $\beta(t)$ at different operational time instants. It is attained by including the lifetime variations of structural parameters, i.e. cable tension $H(t)$ and damper capacity $c(t)$ for the studied bridge stay cable. Also, the loading parameters (i.e. wind speed and direction) are characterized by a distribution function. The assigned PDF/CDF reflects the uncertain nature of the wind defined over the possible range of wind speed up to an extreme value (i.e. the extreme wind speed condition associated with a selected return period of R years, $U_{ext}(R)$).
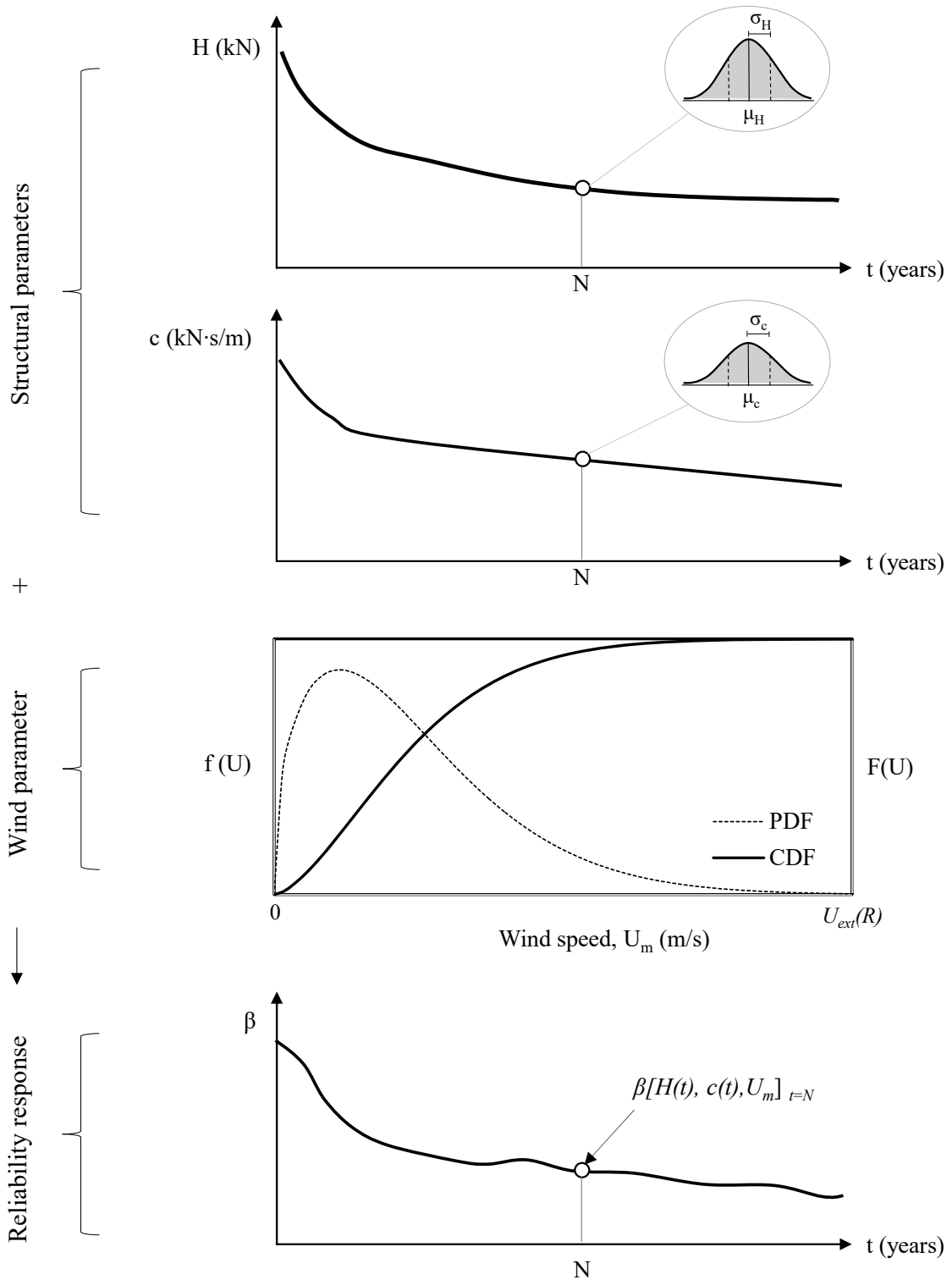
Figure 5.4: A schematic view of the reliability-based analysis results of a cable-damper system after N years of service life due to uncertain structural and/or wind condition(s)

For example, if we assume the structural parameters follow a normal distribution and the wind speed follows a Weibull distribution, the reliability index at the time instant of service year N is shown in the figure by $\beta[H(t), c(t), U_m]_{t=N}$. Conducting the probabilistic-based analysis at different time instants, the results would be expandable to develop a reliability diagram for a damped-stay cable performance over a continued service life.

5.4 CASE STUDY EXAMPLES

5.4.1 Case study No.1: Reliability-based aerodynamic performance assessment of a stay cable in an existing study

In an earlier wind tunnel experiment by Cheng et al. (2003), wind-induced response of stay cables was studied in a dynamic test. The investigated cable had a length L= 6.7 m, a unit mass m = 72 kg/m, and a cable diameter D=0.16 m. It was made of a steel pipe covered by smooth polyethylene sheet from an actual cable-stayed bridge construction site. The results showed that divergent type of cable response occurred at a wind speed of 32 m/s with the corresponding $Re = 3.40 \times 10^5$, when the cable was inclined and yawed both at 45° against the oncoming wind direction, which was equivalent to a wind-cable relative angle of φ=60°.

In this example, it is of interest to first verify the applicability of the proposed reliability method in recognizing the potential occurrence of dry inclined cable galloping for the discussed cable model. Next, by adding an external damper to the studied cable at a location of 4% cable length to the cable-deck anchorage point, the performance of the damped stay cable will be assessed at different structural damping levels. Further, how uncertain deviation of structural parameters, i.e. cable tension and damper size, from their

respective nominal design values at a specific design point would affect the safe performance of a damped stay cable will also be investigated.

Calculation of aerodynamic damping ratios

The mean force coefficients C_D and C_L are taken from the wind tunnel static model testing results by Cheng et al. (2008a), as shown in Figure 5.5. Accordingly, the derivative terms (i.e. $\partial C_D/\partial Re$, $\partial C_D/\partial \varphi$, $\partial C_L/\partial Re$, $\partial C_L/\partial \varphi$) are calculated over the ranges of Re and φ. The details of these calculations are described in Appendix A. Thus, the values of aerodynamic damping ratio can be determined using Eq. (5-15) for any given vibration direction angle α. The results of the calculated aerodynamic damping ratio, ζ_a, for the studied stay cable are shown in Figure 5.6. Knowing that the sign of the lift force on a circular cylinder is arbitrary, thus under the same set of condition, there are two solutions for the predicted aerodynamic damping ratios, ζ_a.

The changes in the relative velocity, U_R (or Reynolds number, Re), over the vibration cycle cause corresponding changes in the aerodynamic forces/damping. Results show positive aerodynamic damping values (i.e. $\zeta_a \geq 0$) within low Re range (i.e. approximately $Re = 2.50 \times 10^5$ or less). In contrary, within the critical Re range, the variations of U_R can be unfavorable due to rapid changes in drag and lift coefficients. This can lead to a negative aerodynamic damping ratio, which, when significant enough to overcome the positive structural damping, would lead to a galloping-type instability.

It is noticeable in Figure 5.6(a) that when we consider positive sign for the lift terms, results show an instability zone of $55° < \varphi < 64°$ in the critical regime of $2.85 \times 10^5 < Re < 3.54 \times 10^5$. The predicted instability region agrees with the onset condition observed in the dynamic model test by Cheng et al. (2003). In addition, there is a region of greater instability
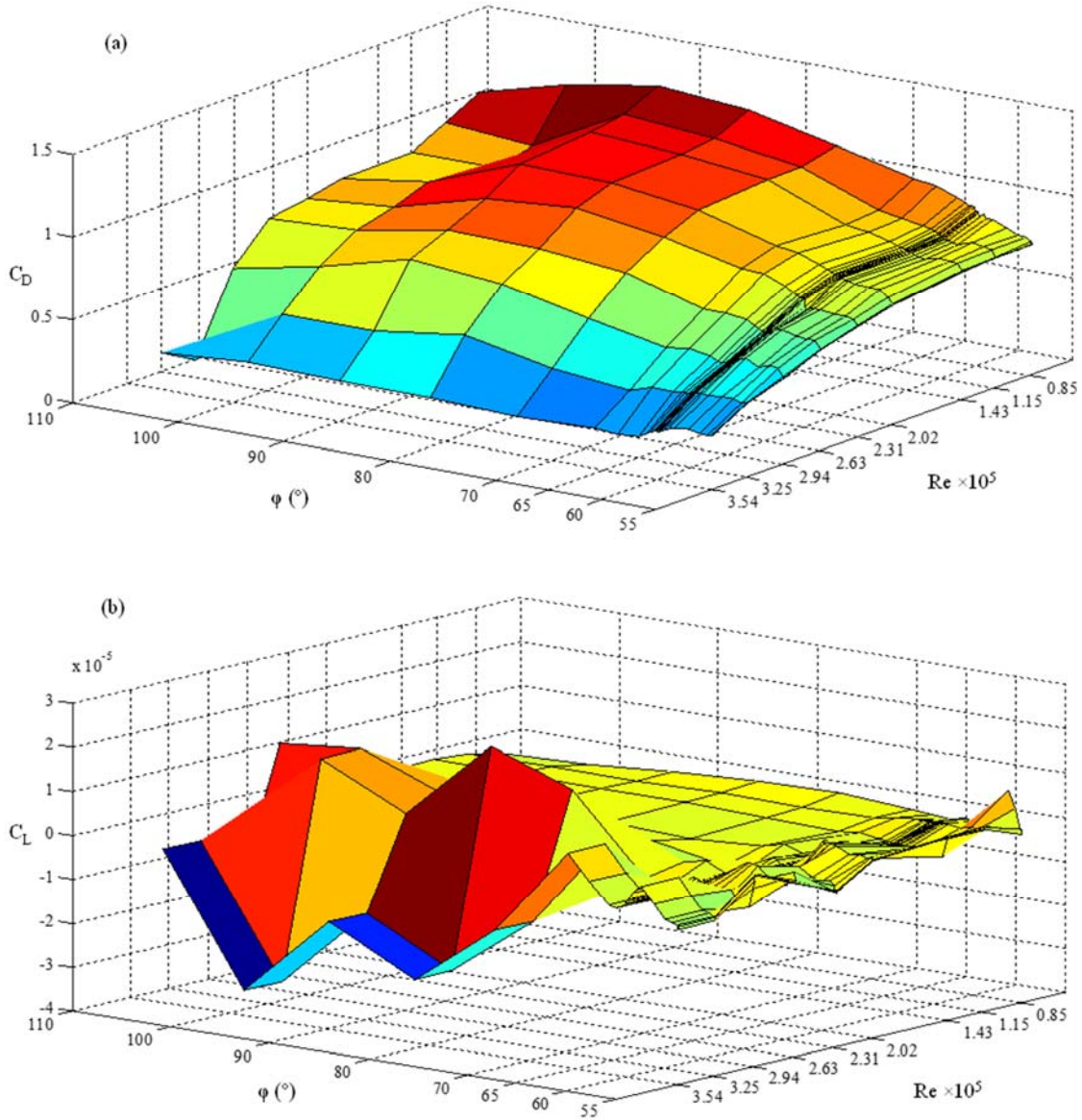
Figure 5.5: Aerodynamic force coefficients from study of Cheng et al. (2008a), (a) C_D, (b) C_L

predicted for $68° < \varphi < 88°$ when $3.15 \times 10^5 < Re < 3.54 \times 10^5$. Similarly, by considering a negative sign for the lift force term (i.e. $-\sin\alpha$) in Eq. (5-15), two instability zones can be observed from Figure 5.6(b). The first aerodynamic instability zone is identified in the region of $55° < \varphi < 69°$ and $3 \times 10^5 < Re < 3.54 \times 10^5$, with a wider range of cable-wind
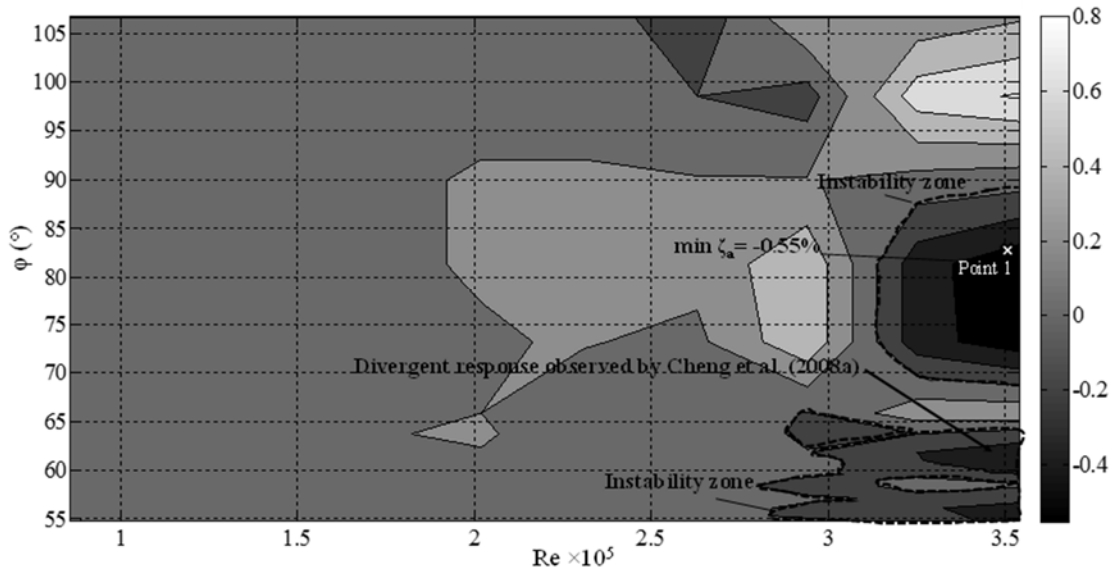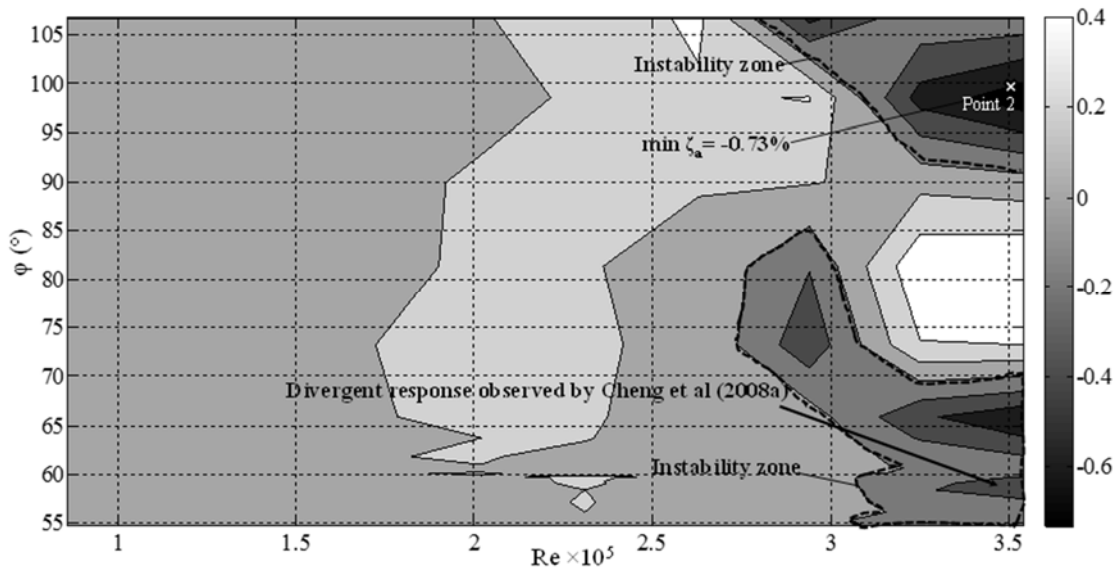
Figure 5.6: Aerodynamic damping ratio ζ_a; (a) with positive sign for lift (+sinα), (b) with negative sign for lift (-sinα)

orientation angle in comparison to Figure 5.6(a). It even shows negative values over a wider range of cable-wind relative angle up to $\varphi=83.5°$ for the range of $2.7\times10^5 < Re <$

2.95×10^5. The second instability region occurs in $92° < \varphi < 105°$ with $2.8 \times 10^5 < Re < 3.54 \times 10^5$. The calculated aerodynamic damping ratios and the identified instability regions predicted in the current study agrees well with the previous findings of Raeesi et al. (2013). The advantage of the current calculations is that the aerodynamic results in this study are presented by extending the cable-wind relative angle range from $\varphi = 55°\text{-}90°$ in the former study to $\varphi \approx 55°\text{-}106.77°$ in the current piece of work.

It is also of interest to determine the minimum aerodynamic damping ratio, for designing against the worst scenario. In Figure 5.6(a), the minimum value of $\zeta_a = -0.55\%$ occurs when $Re = 3.54 \times 10^5$ and $\varphi = 81.36°$, which is marked by Point 1. Figure 5.6(b) contains a more critical design case due to a lower value of $\zeta_a = -0.73\%$ at $Re = 3.54 \times 10^5$ and $\varphi = 98.56°$, as shown by Point 2. For these two minimum design points, the individual contributions to the total aerodynamic damping of each of the six governing factors in Eq. (5-15) are listed in Table 5.1. The contribution from the C_D term is always positive, i.e. beneficial to the aerodynamic performance of the stay cable. The term, $\partial C_D / \partial Re$, gives a negative contribution in both cases due to the drag crisis effect. The $\partial C_D / \partial \varphi$ has little effect on the overall behaviour. Summing up the first three terms (induced by C_D, $\partial C_D / \partial Re$, $\partial C_D / \partial \varphi$), the total contribution of the drag force to the aerodynamic damping ratio of the stay cable for Points 1 and 2 are limited to $\zeta_{a,Drag} = 0.027\%$ and 0.049%, respectively.

Comparing the drag-induced aerodynamic damping ratio, $\zeta_{a,Drag}$, with the total aerodynamic damping induced by drag and lift forces (either $\zeta_{a,+\sin\alpha}$ or $\zeta_{a,-\sin\alpha}$), it shows that drag has a trivial effect on the aerodynamic response of the current two design points. On the other hand, the terms relating to the lift coefficients may have a larger effect. In particular, the $\partial C_L / \partial Re$ term has large value and can be recognized as the dominant term in

Table 5.1: Contribution to aerodynamic damping ratio ζ_a of each of the six terms in Eq. (5-16) for Point 1 and Point 2

Design point		Point 1	Point 2
Reynolds number (Re)		3.54×10^5	3.54×10^5
Cable-wind angle (φ)		81.36°	98.56°
Cable-motion orientation angle (α)		77.61°	102.29°
Drag contribution	(1) C_D	7.91×10^{-4}	8.48×10^{-4}
	(2) $C_D/\partial Re$	-2.61×10^{-4}	-3.58×10^{-4}
	(3) $\partial C_D/\partial\varphi$	1.09×10^{-8}	1.01×10^{-7}
	$\zeta_{a,Drag}$ (%)	0.027 (%)	0.049 (%)
Lift contribution	(4) C_L	4.40×10^{-5}	2.00×10^{-5}
	(5) $\partial C_L/\partial Re$	-5.82×10^{-3}	7.73×10^{-3}
	(6) $\partial C_L/\partial\varphi$	-9.81×10^{-8}	-2.64×10^{-7}
	$\zeta_{a,Lift}$ (%)	-0.578 (%)	0.775 (%)
Total	$\zeta_{a\,+\sin\alpha}$	-0.578 (%)	0.825 (%)
	$\zeta_{a,-\sin\alpha}$	0.605 (%)	-0.726 (%)

causing instability for both design points. As it can be seen from Table 5.1, the positive or negative sign of the lift on the total aerodynamic damping ratio of the stay cable could be either beneficial or detrimental, depending on the first laminar separation bubble happens to form on which side of the cable. Thus, there always exist two arbitrary solutions at each design point. Take Point 2 as an example, the lift with negative sign would cause instability state with $\zeta_{a,-\sin\alpha}$= -0.726%, whereas the positive lift would have a beneficial effect on the total aerodynamic ratio, i.e. $\zeta_{a,+\sin\alpha}$ = 0.825%. Noteworthy, to ensure a safe structural design, the lift condition corresponding to the lower value of the aerodynamic damping ratio, i.e. ζ_a = -0.726% should be considered.

Reliability response at different structural damping levels

In this part of the analysis, the effect of structural damping on the aerodynamic performance of the stay cable is investigated. First, four levels of equivalent structural damping ratio of the damped cable that are the same as those used in the wind tunnel test

conducted by Cheng et al. (2003) are considered. In the experimental study, these four levels of damping were obtained by applying rubber bands and pneumatic dampers to the cable model suspension system, which yielded respectively ζ_s= 0.03%, 0.06%, 0.24% and 0.60%. To better understand the effect of structural damping, two additional design cases are defined in the current study with the equivalent damping ratio of the damped cable being ζ_s= 1.00% and 2.00%. It is assumed that the damping in these two cases is acquired by attaching an external damper to the stay cable at 4% cable length from the cable-deck anchorage point.

The SORM with adaptive approximation method is applied to compute the reliability index of these design cases. It is assumed in the analysis that the cable tension and the damper capacity follow independent normal distributions at any design point, with the mean being their respective nominal design value, and the standard deviation is defined by the coefficient of variation (COV) of 0.10. The obtained results of reliability responses are presented in Figure 5.7(a)-(f). It can be seen that:

(1) The reliability index increases monotonically with the increasing level of structural damping. Consider a special design case of φ=60° and Re=3.4×10^5, of which the onset conditions of wind-induced divergent type of motion of a dry stay cable was observed by Cheng et al. (2003), the results show that in the design cases (a)-(c), the calculated reliability indices are zero which simply represents the occurrence of aerodynamic instability. Based on the presented results, when φ=60° and Re=3.4×10^5, the required structural damping to assure no dry-state galloping occurs between ζ_s = 0.24% and ζ_s = 0.6%. Applying a linear interpolation within the range of ζ_s = 0.24% and ζ_s = 0.6%, the minimum required structural damping ratio to prevent galloping at the studied design point
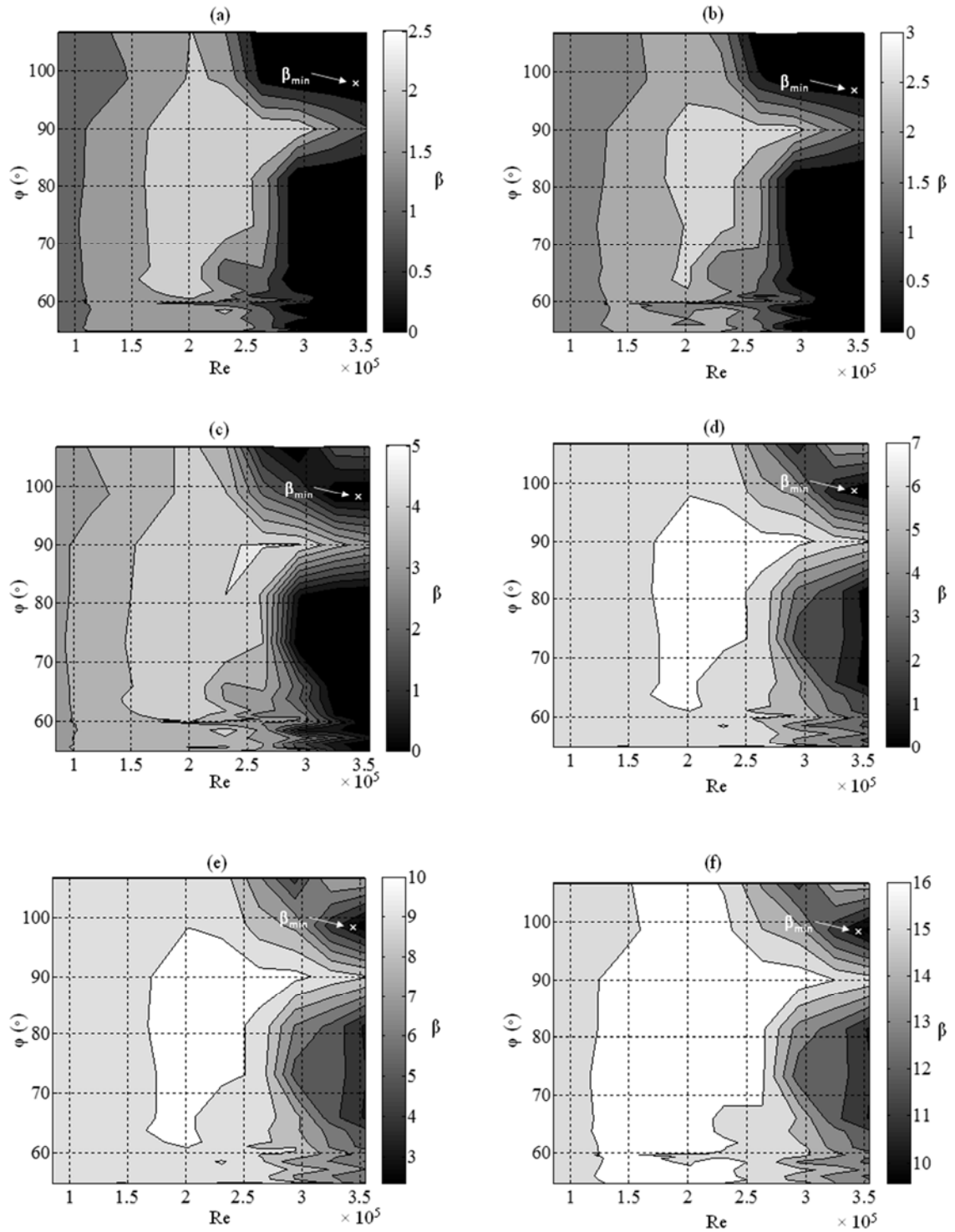
Figure 5.7: Effect of structural damping on the dry-state cable galloping reliability response; (a) ζ_s=0.03%, (b) ζ_s=0.06%, (c) ζ_s=0.24%, (d) ζ_s=0.60%, (e) ζ_s=1.00%, (f) ζ_s=2.00%

equals to $\zeta_{s,min}$=0.31%. Thereof, having an equivalent structural damping $\zeta_s \geq \zeta_{s,min}$, the reliability index of the damped stay cable under the risk of galloping would increase rapidly which implies a greater aerodynamic stability condition. For example, in the design cases (d)-(f) where the structural damping ratios are ζ_s= 0.6%, 1.0%, and 2%, the reliability indices increase to 2.21, 6.94 and 13.66, respectively. Thus, increasing structural damping to overcome the negative aerodynamic damping would be an effective method in mitigating stay cable vibrations.

(2) When damping level is low, i.e. 0.03% of critical (Case a), the reliability index is predicted to be zero within the critical Reynolds range ($2.90 \times 10^5 < Re < 3.54 \times 10^5$) over approximately the entire cable-wind relative angles except for $82° < \varphi < 96°$. The failure region in Figure 5.7(a), wherein the reliability index equals zero, is in good agreement with the identified instability zones shown in Figure 5.6. This consistency implies direct influence of the aerodynamic damping ratio on the LSF calculations. A particular design point in this figure is the one of which the dry inclined cable galloping has been observed in the wind tunnel experiment of Cheng et al. (2003), i.e. at φ=60° and Re=3.4×10⁵. Refer to Figure 5.7(a), with ζ_s=0.03%, the calculated reliability index at this design point is β=0. This physically implies that cable under this design condition would experience a dry inclined cable galloping.

(3) Low reliability indices in all structural damping levels are observed to occur in the critical Re region. This is expected by knowing that the changes in force coefficients, C_D and C_L, in the critical Re region ($3 \times 10^5 < Re < 3.54 \times 10^5$) has an important contribution to the aerodynamic damping ratio, particularly within the range of $59° < \varphi < 79°$. Lower values of reliability indices are associated with the effect of drag crisis and/or non-zero lift

resulted from asymmetric pressure distribution due to formation of a single laminar separation bubble on one side of the cylinder surface over a narrow range of Re.

(4) The design condition corresponding to the calculated minimum reliability index in each design case is shown by a cross sign in each sub-figure. It possess an identical design condition for all six structural damping levels, with $Re=3.54\times10^5$ and $\varphi=98.56°$. This point is identified as the most critical design condition as a result of a greater negative effect of aerodynamic damping.

As an application of the reliability analysis results presented in Figure 5.7 for the aforementioned design cases, if a structural damping level is specified, then the acceptable/unacceptable range of Reynolds number (or wind speed) and cable-wind relative angle within which the stay cable exhibits an aerodynamic stable/unstable behavior would be assessable.

Figure 5.8 displays the reliability index results for the dynamic cable model setup of $\varphi=60°$ and $Re=3.4\times10^5$, under which the divergent type of cable response has been observed (Cheng et al., 2008a). The reliability results are presented by varying the structural damping ratio up to the optimum damping level achievable at the damper location of 4%L from the cable anchorage point, i.e. $\zeta_{s,opt}=2.31\%$. The vertical dashed lines specifies the design points corresponding to the cases (d), (e), and (f) in Figure 5.7 with $\zeta_s=$ 0.6%, 1%, and 2%, respectively. If a required safety level to prevent dry-state cable galloping is specified in terms of the reliability index, then by using the results shown in Figure 5.8, the minimum required structural damping can be determined. For example, knowing that the aerodynamic stability criterion can be defined by $\beta\geq0$, thus the minimum required structural damping ratio to assure no dry inclined cable galloping would be

$\zeta_{s,min} \approx 0.31\%$. Thus, the design cases (a), (b), and (c) are prone to galloping excitation. Nevertheless, in view of the engineering design, it is necessary to ensure a higher level of reliability due to uncertainty associated with the system parameters. For instance, define a reliability index level of $\beta \geq 6$ to avoid the occurrence of dry inclined cable galloping, the minimum amount of required structural damping is $\zeta_s \approx 0.89\%$.
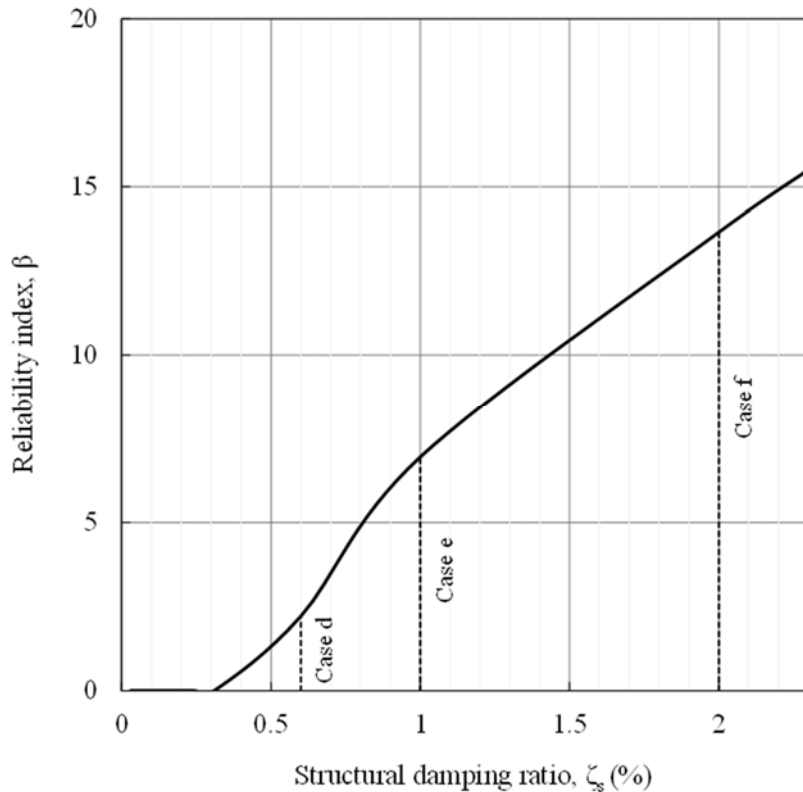
Figure 5.8: Reliability index of the studied dynamic stay cable model at a design point $\varphi = 60°$, Re=3. 4×10⁵, by varying the structural damping ratio up to the optimum damping level

Table 5.2 summarizes the reliability analysis results at the six studied structural damping levels shown in Figure 5.7. The minimum and the maximum values of the LSF and the calculated reliability index at each structural damping level are listed. From the safety point of view, when the value of LSF is negative or zero, instability of cable would occur, as obtained in cases (a)-(d).

Table 5.2: Summary of reliability analysis results

Case	Structural damping, ζ_s (%)	LSF, g(ζ) (%)		Reliability index, β	
		min	max	min	max
a	0.03	-0.70	0.85	0	2.94
b	0.06	-0.67	0.88	0	3.24
c	0.24	-0.49	1.04	0	5.04
d	0.60	-0.13	1.42	0	7.78
e	1.00	0.27	1.82	2.33	10.75
f	2.00	1.27	2.82	9.55	16.98

The data presented in the table implies that the aerodynamic performance of a stay cable improves significantly when increasing the structural damping level by equipping the stay cable with an external damper. This simply reveals the efficiency of an external damper in mitigating galloping response of a stay cable.

The boundary to attain the onset of instability can be defined by a limit of the calculated reliability index which is below the allowable reliability level. Even though the calculated non-zero reliability indices in the design cases (e) and (f) imply that the structural damping provided by damper is significant enough to overcome the aerodynamic instability over the studied Re and φ range, it should be pointed out that due to important structural role of stay cables on cable-stayed bridges in resisting loads and transferring them from bridge deck to tower, a higher safety level should be designated. Keeping the safety level in an order of $\beta \geq 10$ as suggested by Imai and Frangopol (2001), the acceptable design condition is achievable once $\zeta_s \geq 0.0202$ (i.e. $\zeta_s \approx 2\%$). This approximately corresponds to design Case (f). It is noteworthy that although design Case (e) possess a maximum reliability index of $\beta=10.75$, it does not satisfy the acceptable safety level of $\beta \geq 10$, within the entire studied Re range. Therefore, the structural design condition in Case (e), would not satisfy an aerodynamic safe performance from an engineering design

perspective, even though mathematically shows an aerodynamic stable condition (i.e. $g(\zeta) \geq 0$).

Effect of uncertainty level of structural parameters on the reliability response

In this section, the proposed reliability-based analysis approach will be applied to the same damped cable at a given design point to assess the impact of uncertainty level of structural parameters on the cable aerodynamic response. The analysis is performed for a design case with a cable equivalent structural damping ratio of ζ_s =1%. Three different coefficients of variation are assigned to the structural parameters. They are selected to be 0.05, 0.10, and 0.15, respectively. It is assumed that the COV values are assigned to each parameter once at a time. The COV of the other parameter is kept at a constant value of 0.10, noting that this amount, represents a common uncertainty level for the structural engineering application (Choi et al., 2007). Besides, by varying the uncertainty level of the studied parameters separately in the reliability analysis, the system response would be presented in a sensitivity-based manner.

Figure 5.9 shows the results of three different reliability analysis cases when the impact of uncertainty in H is studied at three different levels with COV-H=0.05, 0.10, and 0.15 while COV-c remains at 0.10. On the other hand, Figure 5.10 illustrates the reliability analysis results when the variation of c is under study and COV-H remains at 0.10. Case (b) in both figures represents the same uncertainty in c and H, i.e. COV-c=COV-H=0.10. In the presented figures, contours of reliability index β are shown to describe different safety levels at intervals of 1. Darker shading indicates lower reliability index values (or more susceptible to galloping).

Results show that the reliability indices at all three studied uncertainty levels have lower values in two regions, i.e. within $3\times10^5 < Re < 3.54\times10^5$ and $63° < \varphi < 82°$ or $94° < \varphi < 98°$. These regions are situated nearly identical to the aerodynamic instability regions shown earlier in Figure 5.7(e). This implies that even though the uncertainty level of the structural parameters play an important role on the reliability response of the aerodynamically excited cable, the negative aerodynamic damping effect (as the loading term) in the aforementioned regions is still the governing factor.

The comparison of the three cases in Figure 5.9 or Figure 5.10 shows that the reliability index decreases monotonically by increasing the level of uncertainty of the structural parameters. Thus, the presence of uncertainty associated with cable pretention and/or damper size would have a sizeable impact on the safe performance of a cable-damper system and should not be ignored in the design. This again supports the needs to conduct probabilistic-based analysis in assessing wind-induced response of a bridge stay cable.

Even though structural uncertainty level plays an important role on the magnitude of the reliability index, it does not have a sizeable impact on the variation pattern of the reliability response contours. Focusing on the critical Re range within which the instability regions are identified, the reliability analysis results are found to have a similar trend. In all the cases, the minimum reliability design point occurs at $Re \approx 3.5\times10^5$ and $\varphi \approx 98.5°$. This point represents a design point with the most critical aerodynamic loading condition.
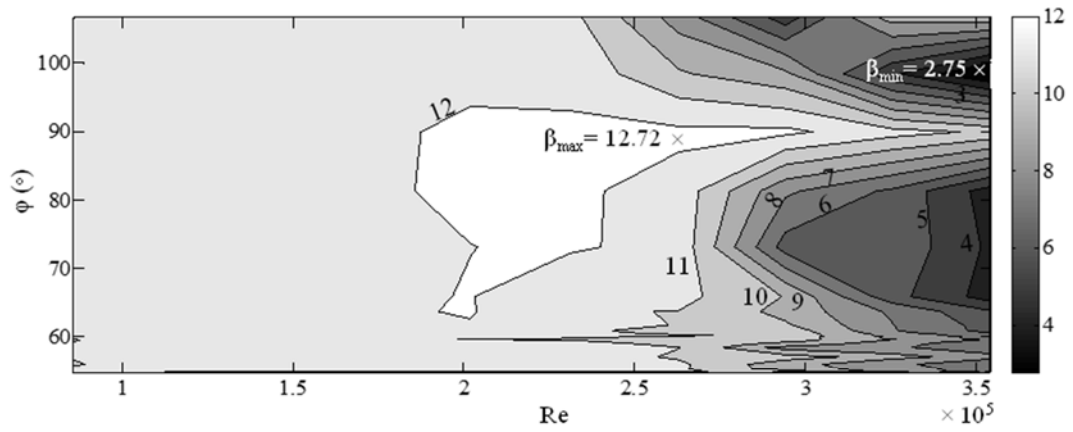
(a) COV-H=0.05
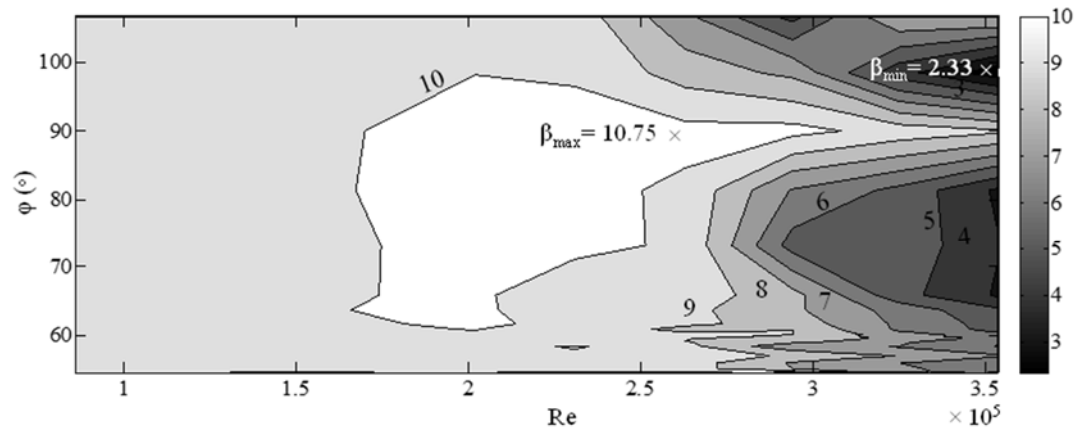
(b) COV-H=0.10
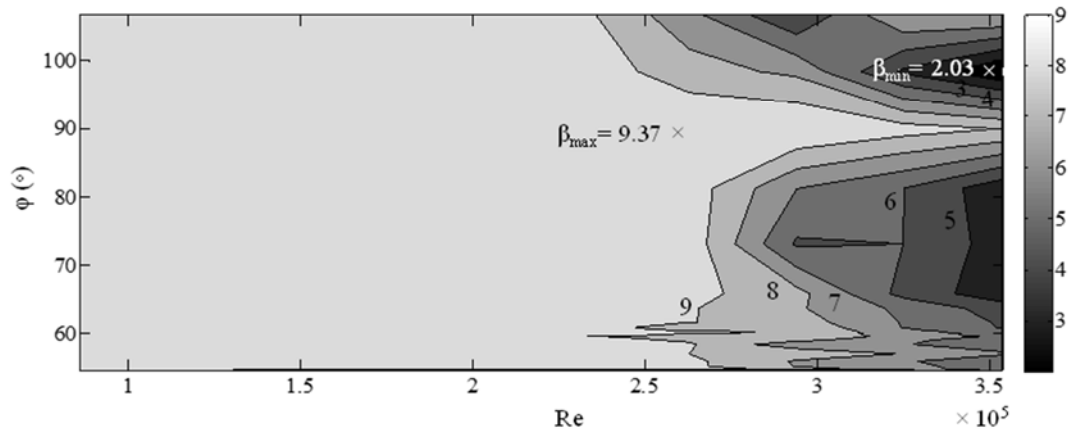
(c) COV-H=0.15

Figure 5.9: Effect of uncertainty level of the cable tension on the reliability response, when COV-c=0.10: (a) COV-H=0.05, (b) COV-H=0.10, (c) COV-H=0.15

154
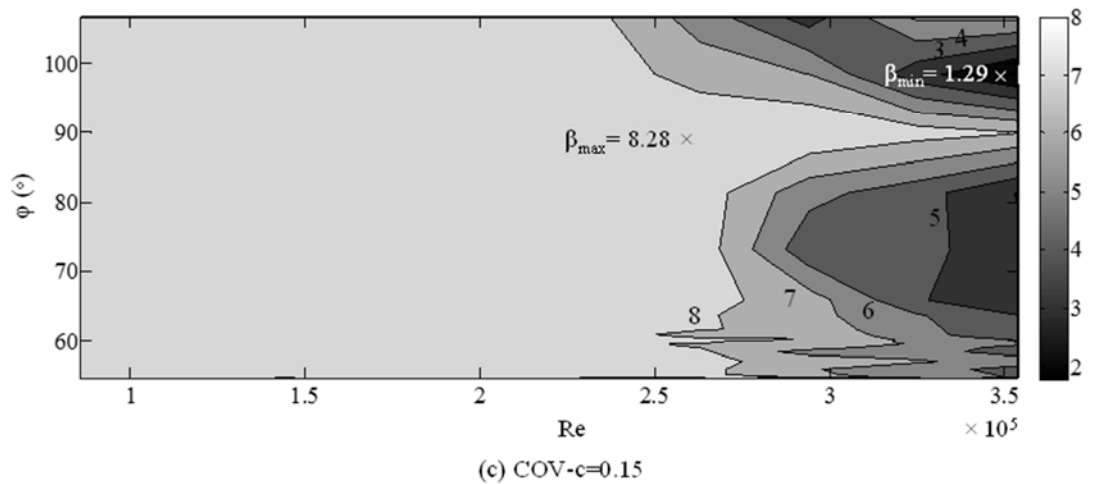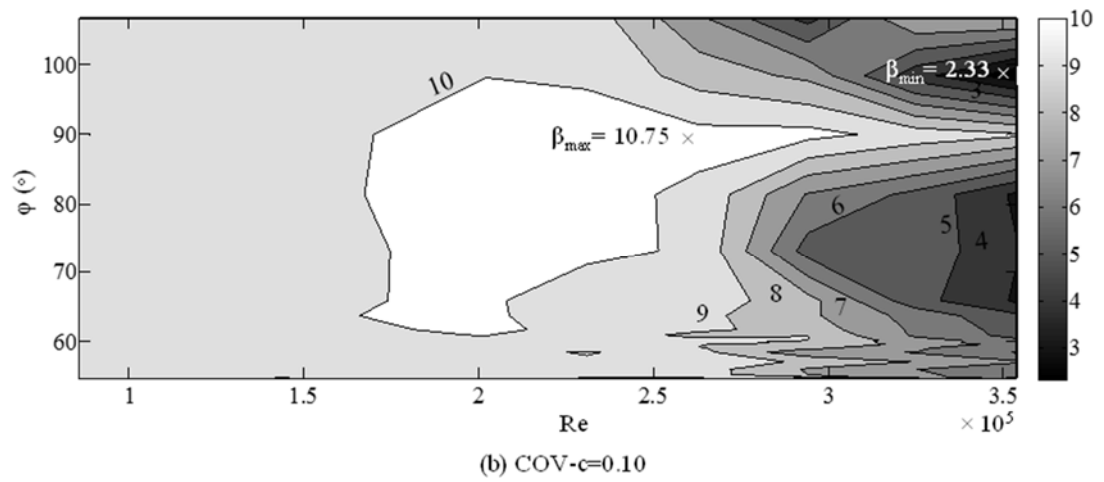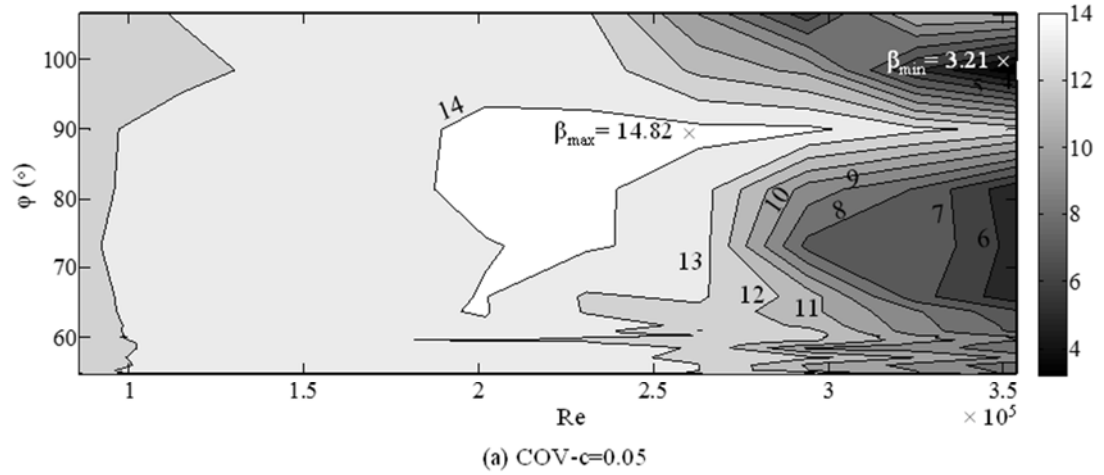
Figure 5.10: Effect of uncertainty level of the damper capacity on the reliability response, when COV-H=0.10: (a) COV-c=0.05, (b) COV-c=0.10, (c) COV-c=0.15

The analysis results can be employed to assess the aerodynamic response of the defined damped stay cable when uncertainty of structural parameters are considered. Accordingly, the range of wind speed and cable-wind relative angle within which dry inclined cable galloping would occur can be identified. It should be pointed out that these failure regions are obtained by neglecting the inherent uncertainty in the wind load conditions. Noting that in reality, the wind speed and direction acting on a stay cable are also stochastic, the consideration of uncertain nature of wind for a more realistic assessment is necessary.

5.4.2 Case study No. 2: Reliability-based service life assessment of a damped bridge stay cable

In this example, a case study is presented to demonstrate the application of the proposed reliability method in estimating the lifetime aerodynamic stability of a damped stay cable at a selected bridge site. The problem is described by introducing properties of the structural and the wind parameters, of which the uncertain characteristics of the cable tension, the damper capacity, the wind speed and the wind direction over the bridge service time at the specified design site are illustrated. The aerodynamic performance of the damped stay cable under the defined wind conditions is evaluated. The critical wind speed range for galloping and its relationship with the extreme wind speed at the bridge site is discussed. Afterwards, a sensitivity-based reliability analysis is conducted to investigate the effect of uncertainty associated with wind speed and direction. Finally, the service-life reliability responses due to probable dry-state cable galloping excitation are estimated. The results would be useful for planning the effective long-term cable-stayed bridge maintenance strategy.

Properties of structural and wind parameters

- *Structural parameters*

The properties of the stay cable used in this example are defined to represent a typical bridge stay cable as given in Table 5.3. The natural frequency of the cable first mode is 2.37 Hz. The stay cable by itself possess an inherent structural damping ratio of 0.1%. To further increase the structural damping level, an oil damper with a capacity of $c=$ 146.8 kN·s/m is attached 6 m from the cable lower end ($\Gamma_d=$ 4%).

Table 5.3: Cable-damper system properties

Cable		Damper	
Length [L]	150.0 m	Size [c]	146.8 kN·s/m
Inclination angle [γ]	37°	Location [L_d/L]	0.04
Mass [m]	72 kg/m	Equivalent structural damping ratio [ζ_s]	1.69%
Diameter [D]	0.15 m		
Cable chord tension [H]	3700 kN		
Bending stiffness [EI]	5420 kN·m²		
Fundamental freq. [f]	2.37 Hz		
Inherent cable damping	0.1%		

The damping property of the damped cable is determined by using the formulations which has been proposed in the study of Fujino and Hoang (2008). Thereof, the equivalent structural damping ratio, ζ_s, for the first mode is computed according to Eq. (5-13), where the non-dimensional damper coefficient parameter for the first mode of a corresponding horizontal non-flexural taut cable-damper system is calculated by

$$\eta_n = \eta_1 = n\pi(L_d/L)c/\sqrt{Hm} = 1\times\pi\times0.04\times1468\times10^3/\sqrt{3700\times10^3\times72} = 1.130$$

The reduction and modification damping factors are calculated, they are R_{s1}=0.946, R_f=0.913, η_{s1}=1.020, and η_f=0.700. This would yield the equivalent first modal damping ratio of $\zeta_s=\zeta_1$=1.687%.

The variation of the tension force due to relaxation of cable is modeled based on field data taken from a real cable-stayed bridge over a period of 300 days (Au and Su, 2012). It is assumed that the reduction in the tension force over the bridge service life would continue with the same trend to reach 80% of its initial design amount after 50 years of stay cable operation. For simplicity, it is assumed that no tension adjustment will be applied during the investigated 50 years period. To derive the time-degradation pattern of the cable tension in terms of the loss of cable chord pretension H over the time, a nonlinear regression analysis is performed, which yields

$$H(t) = H_0(1 - 0.002\,t - 0.00004t^2) \qquad (5\text{-}20)$$

where H_0 is the initial design value of cable chord pretension in Table 5.3, and t represents the bridge service time in year.

Similarly, damper capacity reduction because of oil leakage is modeled based on the assumption of a linear reduction over damper lifetime as taken from the study of Mohammadi et al. (2011). Hence, the time-dependent damper capacity formula can be expressed in terms of the initial design value of damper capacity, c_0, and service time t by

$$c(t) = c_0(1 - 0.0094\,t) \qquad (5\text{-}21)$$

Besides the lifetime uncertainty of structural parameters, the actual cable tension and the damper capacity in the system could deviate from their respective nominal design

values at each time instant. It is assumed that both of structural parameters (i.e. cable chord tension and damper capacity) follow independent normal distributions, with mean values equal to their respective nominal design values at a specific design point. The standard deviations are considered based on the assumption of COV-c=COV-H=0.1.

- **Wind parameters**

    The aerodynamic response of a stay cable exposed to wind directly depends on the properties of the wind. In this case study, a statistical analysis will be applied to the recorded historical wind speed data set at a given bridge site. The obtained results in terms of the uncertain characteristics of wind as well as the design wind speed corresponding to desired return period at the studied bridge site are used in the reliability analysis. It is assumed that the bridge is located in the Toronto region.

    Subsequently, as shown in Appendix B, the wind speed data are collected from the Environmental Canada Meteorological website (Retrieved from World Wide Web http://climate.weatheroffice.gc.ca) for Toronto Lester B. Pearson International Airport, Ontario, covering years 1957 to 2012 (56 years). They are available in the form of average hourly mean wind speed including their direction at each time step. Apply the parent probability distribution analysis method to the existing wind speed data set, the PDF of wind speed data set was explicated in the form of the most relevant wind probability distributions including the Rayleigh, the Weibull and the Gamma distributions. The results in Appendix B show that the Weibull distribution is the best fitted distribution to represent the uncertain characteristic of wind speed in this data set. The PDF of the fitted Weibull distribution model *Weibull*(c=1.564, k=9.309) to the non-directional wind speed data set can be expressed by:

$$f(U_m) = \left(\frac{U_m}{9.309}\right)^{0.564} \exp\left[-\left(\frac{U_m}{9.309}\right)^{1.546}\right]$$

Similarly, by distinguishing the directional effect at different wind yaw angles, the results of the wind speed Weibull distribution fitting for 36 different directional sectors are taken from Table B.7. Each row contains the Weibull parameters (i.e. shape parameter $k(\theta)$ and scale parameter $c(\theta)$) and the percentage of occurrence, $A(\theta)$, for a certain directional sector.

The next step of wind speed data analysis is to estimate the extreme wind speed corresponding to the selected return period at the studied bridge site. It physically represents the maximum attainable wind speed at the bridge site associated with the desired return period. Assuming the return period is R years, the corresponding extreme wind speed is denoted by $U_{ext}(R)$. The magnitude of extreme wind speed is obtained in Appendix B by applying an inverse analysis of the cumulative density function of the fitted Weibull distribution model. The results of the extreme wind speed corresponding to different return periods for directional and non-directional-based analysis are given by Tables B-11 and B-12, respectively.

Calculation of aerodynamic damping ratios

The aerodynamic damping ratio of the studied stay cable model is presented in Figure 5.11 by choosing the minimum value between the two yielded from Eq. (5-15) for the positive and negative lift sign at each design point. The results are shown over the ranges of Re and φ covered in the wind tunnel test performed by Cheng et al. (2003). For every orientation of the stay cable model (i.e. for every φ), in this figure a corresponding α which represents the major direction of cable oscillation is determined from Eq. (5-2).

A boundary line separating the regions of positive and negative aerodynamic damping ratios is shown by a dashed line in the Figure 5.11, characterizing the aerodynamic damping ratio equal to zero (ζ_a=0). Among the exhibited negative ζ_a regions, the ones located in the critical Reynolds range are more important because of having greater negative aerodynamic damping values which gives higher chance of aerodynamic instability. As a comparison, the lowest aerodynamic damping ratio is occurred in the critical Re range with a magnitude of ζ_a= -0.29%, while in the low Re range (i.e. $Re \leq 1.2 \times 10^5$ wherein $\zeta_a \leq 0$), the aerodynamic damping ratio is limited to ζ_a= -0.07%.
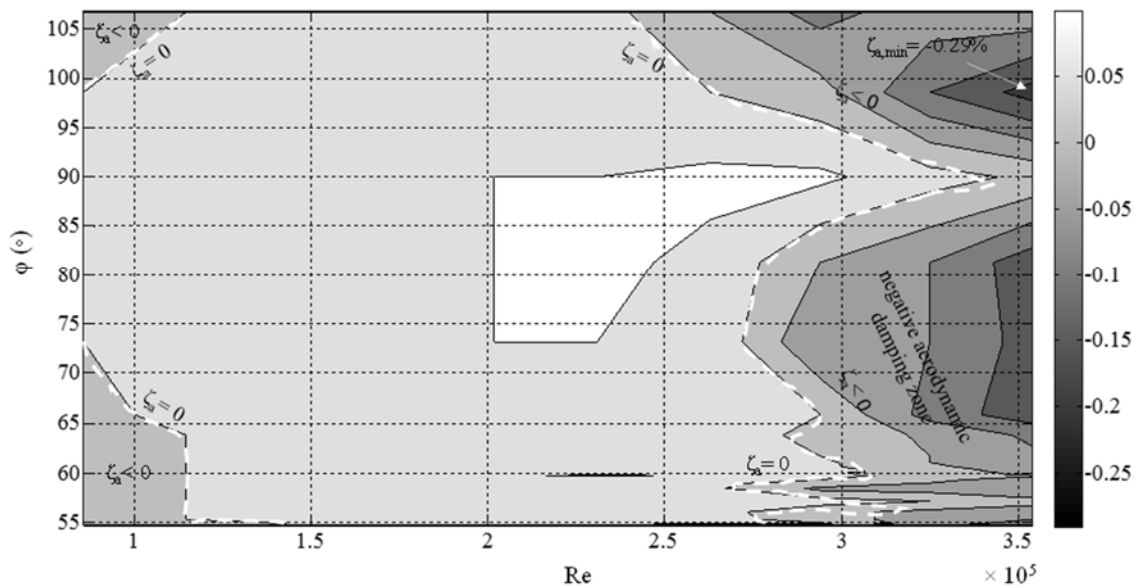
Figure 5.11: Minimum aerodynamic damping ratio ζ_a

Taking ζ_s= 0.1% from Table 5.3, the studied stay cable will be susceptible to galloping excitation when the effect of wind load (i.e. the induced aerodynamic damping) overpass the structural damping in the regions when 58°< φ <82° and $3.20 \times 10^5 < Re < 3.54 \times 10^5$ or 92°< φ <104° and $3.1 \times 10^5 < Re < 3.54 \times 10^5$. These regions define the

aerodynamic instability conditions of which dry inclined cable galloping is possibly excited. Of particular interest is the design point with the lowest aerodynamic damping ratio ζ_a= -0.29% at $Re \approx 3.54 \times 10^5$ and $\varphi \approx 98.6°$, as denoted in the Figure 5.11 by $\zeta_{a,min}$.

Figure 5.12 displays the calculated aerodynamic damping ratio versus the mean wind speed (i.e. ζ_a-U_m) for the direction set up where the lowest aerodynamic damping ratio, $\zeta_{a,min}$, is achieved. It is equivalent to section through Figure 5.11 at φ=98.6°, plotted for the vibration direction α=96.5° with Re converted to the corresponding wind speed U_m. It can be seen that at low wind speeds the aerodynamic damping is positive. Above wind speed $U_1 \approx 22.4$ m/s, corresponding to the start of the critical Re range, significant reduction
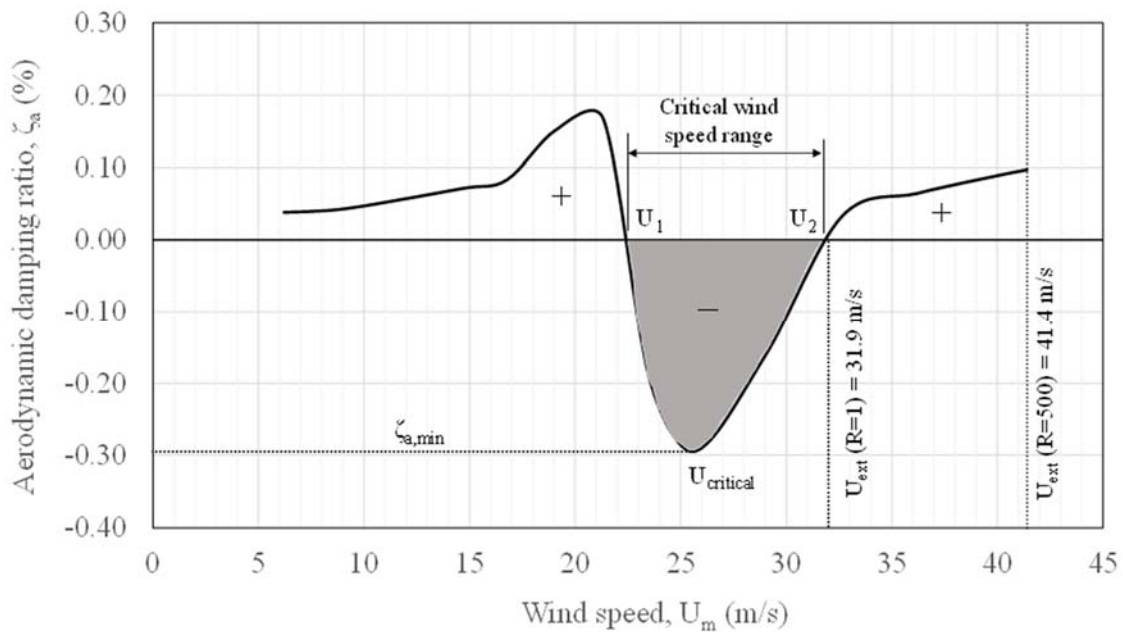
Figure 5.12: Calculated aerodynamic damping ratios ζ_a of stay cable model for φ = 98.6° by varying wind speed, U_m. Vertical dotted lines indicate extreme wind speeds corresponding to return periods of 1 and 500 years

of the aerodynamic damping occurs. The magnitude of the aerodynamic damping ratio remains negative over the critical wind speed range up to U_2=31.8 m/s. Notable is the

minimum aerodynamic damping design point, $\zeta_{a,min}$, which occurs at $U_{critical}$=25.6 m/s. This design point is associated with the most unfavorable aerodynamic loading condition of the studied stay cable.

The remaining of the aerodynamic damping ratio curve is plotted over the super critical range, i.e. for $U_m \geq U_2$, by continuing the calculations up to the predicted extreme wind speed corresponding to a return period of 500 years, i.e. $U_{ext}(R=500) = 41.4$ m/s. Apply the formulations in Table A-2 to the drag force coefficients, their corresponding partial derivatives are calculated. Due to the fact that the asymmetry in the flow condition would not be significant any longer beyond the critical Reynolds number range, the aerodynamic contribution induced by the lift force could be eliminated from Eq. (5-15) and calculation of ζ_a can be simplified by solely evaluating the drag force contribution.

Results show that the aerodynamic damping ratios possess positive values over the super critical range. It is important to mention that even though $U_{ext}(R)$ represents the maximum wind speed that could possibly occur at the studied bridge site corresponding to a return period of R years, it does not necessarily correspond to the worst loading condition for dry inclined cable galloping. This is due to the fact that the governing factor in the excitation mechanism is the drastic change of lift and drag force coefficients within the critical Re range. Beyond this region, the force coefficients have nearly constant values, so the mechanism is not activated. Therefore, if the extreme wind speed is higher than the critical wind speed range (which is the case in the current example), it does not impose an adverse effect on the aerodynamic stability of the system. This suggests that to ensure a safe aerodynamic design for a bridge stay cable, identifying the critical wind speed range is essential, rather than simply evaluating the aerodynamic response at a certain predicted

extreme wind speed. Nevertheless, recognizing the relationship between the predicted extreme wind speed and the critical wind speed range for galloping is still an essential step in the design.

Reliability-based aerodynamic analysis results

Assuming the inherent structural damping ratio of the stay cable is 0.1%, the results in Figure 5.12 suggest that the negative aerodynamic damping would be dominant within $U_m \approx$ 22.9-30.2 m/s. Accordingly, the limit state function would yield negative values, i.e. $\zeta_a + \zeta_s \leq 0$, and the physical behavior would emerge as an aerodynamic instability in the form of dry inclined cable galloping excitation.

As a solution to control cable vibrations, an external damper is added to the studied stay cable at 4% of the cable length from its anchorage point at the bridge deck. Resultantly, the equivalent structural damping ratio of the cable-damper model increases up to ζ_s =1.69%. Now, it is of interest to assess the aerodynamic performance of the same stay cable by applying the proposed probabilistic-based method.

In the analysis, the uncertainty of structural parameters is modelled by assuming COV=0.1 for the cable tension and the damper capacity. The wind speed distribution follows Weibull distribution *Weibull*(c=1.564, k=9.309) as fitted to the non-directional wind speed data set. Figure 5.13 shows the reliability-based aerodynamic analysis results of the cable with and without the installation of damper. It can be seen that:

(1) The reliability index curves for both cases (with and without damper) have similar pattern as that of the aerodynamic damping curve in Figure 5.12. The reliability indices have lower values within the critical wind speed range due to negative aerodynamic damping effect. In particular, the design point with the minimum

reliability index, β_{min}, occurs at $U_{critical}$, represents the available safety level of the system.

(2) A comparison between the two reliability index curves shows that the reliability level of cable performance increases considerably by adding external damper to the stay cable model. The stay cable with no damper has reliability index equal to zero over the critical wind speed range. In contrary, by adding a damper, the reliability index of the cable performance increases to β_{min}=8.92 at $U_{critical}$. Thus, the aerodynamically violent response can be controlled by equipping it with an external damper with adequate capacity.
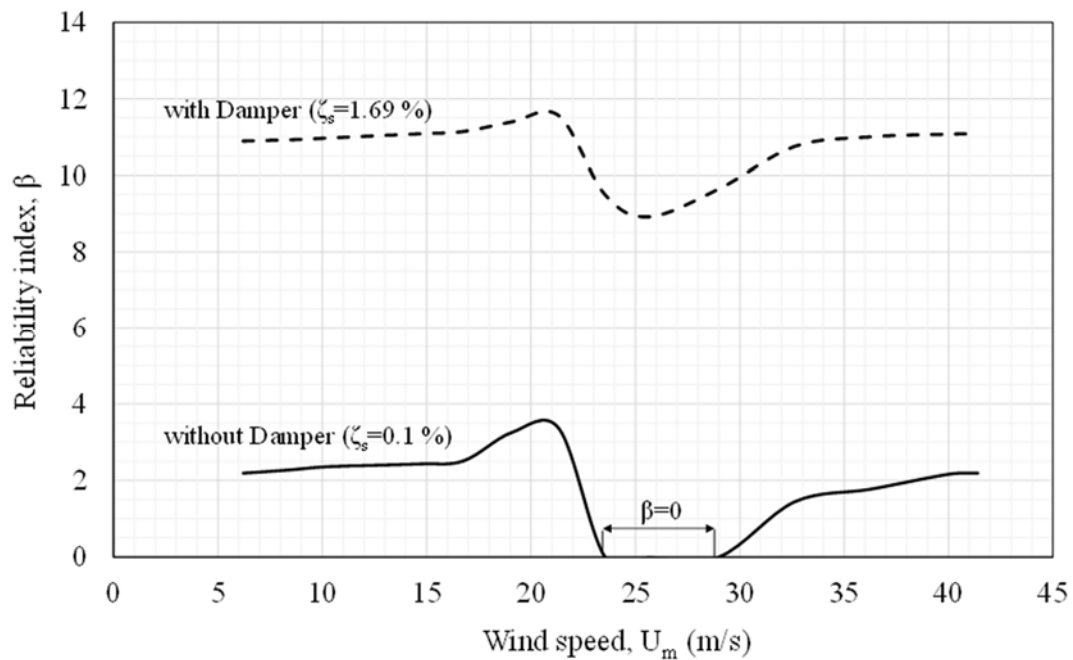
Figure 5.13: Reliability-based aerodynamic analysis results of the stay cable model with and without damper by using non-directional wind speed Weibull distribution

It should be pointed out that due to important structural role of stay cables in resisting loads, it is required to provide a design with a higher safety factor (or equivalently

a higher reliability index than other structural elements). A reliability-based performance assessment of a suspension bridge in Japan by Imai and Frangopol (2001) reported that the reliability indices of main cables are within the range of 15 or more, whereas those of other structural elements such as stiffening girders and hanger ropes are within the range of 3 to 6. Similarly, a reliability-based optimum design analysis of Glulam cable-stayed footbridges that is performed by Simões and Negrão (2005) showed the necessity of having high value of reliability-index for the studied cable-stayed system within the range of 15 to 20 to resist excessive cable deflection.

Therefore, though $\beta>0$ can be considered as an indicator for reliability response, it does not necessarily satisfy the acceptable level of structural safety. If assume $\beta=10$ as an acceptable reliability level for the current design example, it can be seen from Figure 5.13 that the extra structural damping supplied by the damper is not sufficient over the wind speed range of 23.1-30.0 m/s. In other words, the structural design does not meet the safety level obligation even though it assures no occurrence of dry inclined cable galloping occurrence. To resolve the problem, a higher capacity of external damper or possibly applying another techniques on structural damping amplification are required.

Sensitivity-based reliability analysis of wind parameters

- ***Impact of uncertainty in wind speed***

To study the impact of uncertain characteristic of wind speed on the aerodynamic performance of a cable-damper system, two cases are analyzed. In the first case, it is assumed that the wind speed distribution follows the *Weibull*(c=1.564, k=9.309). This case represents the best fitted distribution to the existing wind speed data set at the bridge site. Another case is defined by considering a uniform wind speed distribution (i.e.

Uniform(0.02)). This set can be treated as a deterministic-based analysis case of which the uncertain characteristic of wind speed is neglected. The corresponding PDF curves are plotted in Figure 5.14(a).

The variation of the reliability index versus the wind speed for both cases are shown for the stay cable without and with damper in Figure 5.14(b) and (c), respectively. The results show similar response pattern as reported in Figure 5.12. However, it is noticeable that there is a distinguishable difference of cable performance between the two wind loading conditions, especially for the undamped design case.

The dependence of reliability analysis results on the wind speed distribution can be explained by integrating the wind probability density functions in an aerodynamic-based context. Refering to Figure 5.12, it can be seen that the aerodynamic damping has a detrimental effect on the stay cable response if the wind speed is located within the critical wind speed range. Further, comparison of the two types of wind speed distributions in Figure 5.14(a) shows that the uniform wind speed distribution has higher values of PDF within this range, i.e. $f_i^U(U_{m,i}) > f_i^W(U_{m,i})$; where $U_{m,i}$ is the mean wind speed at design point i, $f_i^U(U_{m,i})$ and $f_i^W(U_{m,i})$ are the PDFs of the uniform and Weibull distributions, respectively. Therefore, it is expected to obtain lower reliability indices for the uniform distribution over the critical wind speed range. The results in Figure 5.14(c) show dependability of the reliability response to the uncertainty of wind load within the critical wind speed range. For example, at critical wind speed, $U_{critical}$=25.6 m/s, the reliability index decreases from 8.92 for Weibull distribution to 8.67 for uniform distribution. On the contrary, over the
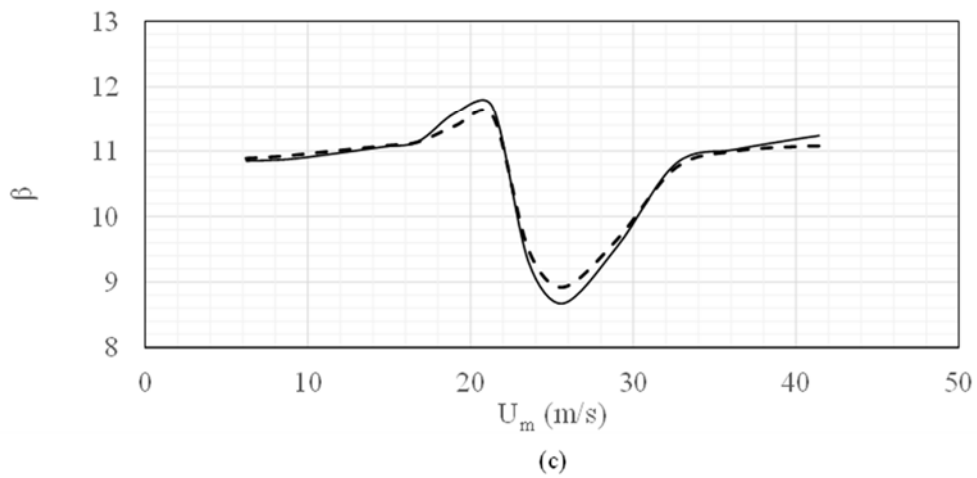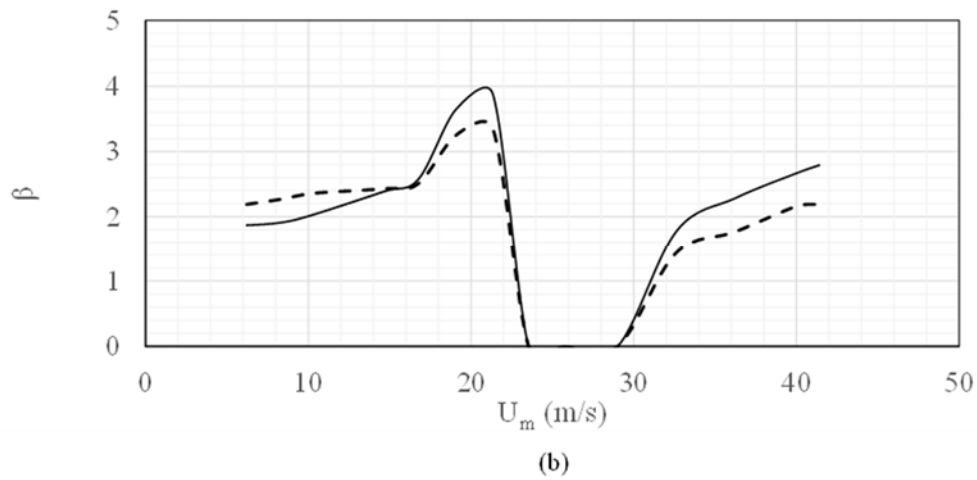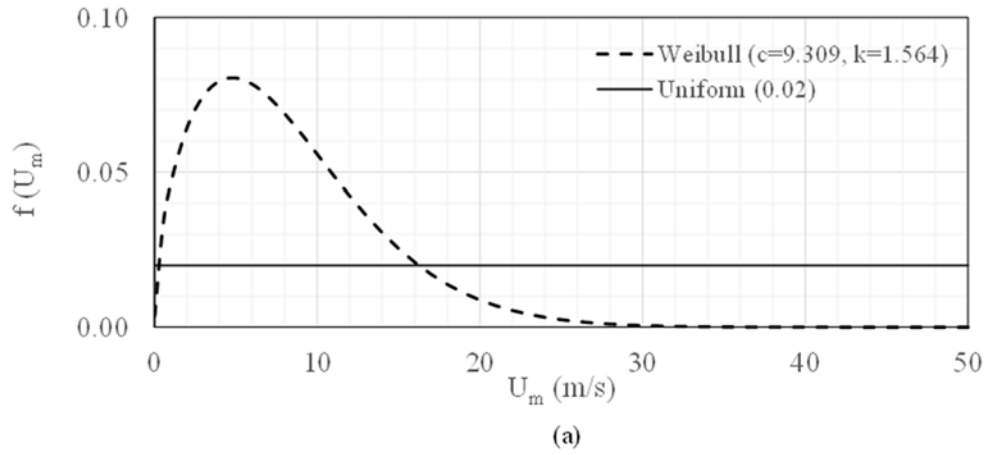
Figure 5.14: Sensitivity of reliability index to the uncertainty in the wind speed (non-directional); (a) wind speed distribution; (b) No damper, ζ_s=0.1%; (c) with damper, ζ_s=1.69%

wind speed range(s) with positive aerodynamic effect ($\zeta_a \geq 0$), the Weibull distribution, has higher reliability indices.

It is also of concern to ensure reliable performance of a stay cable under different wind load conditions. Figure 5.14(c) clearly explains that by adding a damper to the stay cable, not only the reliability index can be increased, but also the variation of structural response due to different wind speed distributions can be reduced.

- ***Impact of uncertainty in wind direction***

Referring to the collected wind database, the wind direction was recorded in degree showing the direction of the wind speed vector at each hour relative to the North geographical direction (Base Azimuth). Each sector covers an angle range of 10°. Thus, the recordings can be classified by dividing the wind rose into 36 different sectors, assuming that the base azimuth is located in Sector #1. Accordingly, each wind direction is assigned to a relevant sector. For instance, in Sector #8, the wind yaw angle θ varies between 70° and 79.9°.

In this section, the entire sample space of wind speed data, corresponding to wind Sectors #1 to #36 are investigated. The wind speed distribution at each directional sector is considered by fitting a Weibull distribution to the recorded wind speed data set. Table 5.4 summarizes the results of the statistical-based wind speed analysis from Appendix B by showing the scale, the shape and the frequency parameters of Weibull distribution function in each directional sector. Next, the aerodynamic calculation is performed for each case. The results for the minimum aerodynamic damping ratio, $\zeta_{a,min}$, and its corresponding wind yaw angle, $\theta_{critical}$, are also shown in Columns 4 and 5 of the table.

Assuming the structural damping ratio of ζ_s =0.1%, aerodynamic stability of the studied cable under wind excitation within different directional sectors are evaluated. Two terms are used in the table to express the stay cable behavior. The term "Safe" denotes aerodynamic stability condition, whereas "Failure" designates that the negative aerodynamic damping overpasses the structural damping and resulted in unstable galloping response.

The aerodynamic stability assessment includes the wind speed variation over the practical wind speed range. Thereof, the value of extreme wind speed needs to be calculated at different wind sectors. The amount of $U_{ext}(R)$ is considered as an upper bound value for the wind speed in the reliability analysis. Four different extreme wind speed values correspond respectively to a return period of R=1, 50, 100, 500 years are presented in the table.

Afterwards, the reliability-based assessment of aerodynamic response of the studied stay cable is conducted for each directional sector. The critical wind speed range, i.e. $[U_1,U_2]$ and the wind speed value corresponding to the lowest aerodynamic damping ratio, i.e. $U_{critical}$, in the directional sectors where unstable cable response could occur is listed. The reliability indices in these sectors are zero, which suggests the onset of instability. The directional Sectors #5, 6, 7, 8, 23, 31, and 32 in which the cable exhibits unstable aerodynamic response are highlighted in the table.

Despite the fact that the overall behavior of the stay cable shows instability within the aforementioned sectors, in the other sectors, the cable retains an aerodynamic stable behavior. For instance, calculation of the reliability index in Sector #19 yields β_{min}=4.65. Knowing that the wind excitation is indeterminate, this proofs the necessity of having a

comprehensive aerodynamic analysis, of which the uncertainty of wind speed at each directional sector is included in a probabilistic context.

Table 5.4: Reliability-based analysis results of the aerodynamically-excited damped stay cable at different wind directional sectors

Sector #	θ (°)	W(k,c,A)			$\zeta_{a,min}$ (%)	$\theta_{critical}$ (°)	Status	U_{ext} (R)				$U_{critical}$ (m/s)				β_{min}
		k(θ)	c(θ)	A(θ)				1	50	100	500	U_1	U_2	$U_{critical}$		
1	0-9.9	1.665	9.553	0.016	0.15	0	SAFE	30.4	39.8	41.4	44.8					5.81
2	10-19.9	1.699	10.460	0.018	0.11	18	SAFE	32.5	42.4	44.0	47.5					4.45
3	20-29.9	1.590	9.597	0.009	0.02	29	SAFE	32.2	42.8	44.5	48.4					2.52
4	30-39.9	1.645	9.573	0.019	-0.03	39	SAFE	30.9	40.6	42.2	45.7					1.66
5	40-49.9	1.699	10.604	0.007	-0.15	49	Failure	33.0	43.0	44.6	48.2	26.5	29.1	27.4	Case 1	0
6	50-59.9	1.436	9.228	0.008	-0.20	53	Failure	35.3	48.3	50.5	55.3	23.2	32.2	26.4	Case 1	0
7	60-69.9	1.222	6.650	0.011	-0.29	65	Failure	32.2	46.5	49.0	54.5	21.6	34.1	31.9	Case 2	0
8	70-79.9	1.387	8.061	0.009	-0.13	71	Failure	32.3	44.8	46.8	51.5	24.5	30.8	27.4	Case 1	0
9	80-89.9	1.754	10.210	0.018	-0.03	83	SAFE	30.6	39.6	41.0	44.2					1.61
10	90-99.9	1.428	8.094	0.016	0.02	90	SAFE	31.2	42.8	44.7	49.0					2.91
11	100-109.9	1.657	9.498	0.017	0.07	100	SAFE	30.4	39.9	41.4	44.8					3.88
12	110-119.9	1.521	8.841	0.019	0.04	118	SAFE	31.4	42.2	44.0	47.9					3.02
13	120-129.9	1.326	7.382	0.014	0.02	129	SAFE	31.6	44.3	46.5	51.3					3.5
14	130-139.9	1.580	9.267	0.023	0.02	139	SAFE	31.4	41.7	43.4	47.2					2.25
15	140-149.9	1.710	9.897	0.028	-0.03	149	SAFE	30.5	39.8	41.2	44.5					1.24
16	150-159.9	1.272	6.975	0.020	0.01	151	SAFE	31.7	45.2	47.5	52.7					2.45
17	160-169.9	1.332	7.136	0.016	0.03	161	SAFE	30.3	42.5	44.6	49.2					2.91
18	170-179.9	1.495	8.629	0.021	0.09	171	SAFE	31.3	42.3	44.1	48.2					4.25
19	180-189.9	1.486	9.007	0.025	0.09	184	SAFE	32.9	44.6	46.5	50.8					4.65
20	190-199.9	1.400	7.950	0.022	0.03	198	SAFE	31.5	43.4	45.4	49.9					2.9
21	200-209.9	1.594	9.494	0.029	-0.02	209	SAFE	31.8	42.2	43.9	47.6					1.66
22	210-219.9	1.745	10.138	0.044	-0.05	218	SAFE	30.6	39.6	41.0	44.2					0.92
23	220-229.9	1.707	10.227	0.046	-0.11	229	Failure	31.6	41.2	42.7	46.1	24.6	28.8	26.9	Case 1	0
24	230-239.9	1.592	9.452	0.048	-0.07	234	SAFE	31.7	42.1	43.8	47.5					0.34
25	240-249.9	1.626	9.617	0.043	-0.02	241	SAFE	31.5	41.5	43.1	46.8					0.92
26	250-259.9	1.519	8.968	0.038	0.04	251	SAFE	31.9	42.9	44.7	48.7					1.98
27	260-269.9	1.412	8.192	0.043	0.02	266	SAFE	32.1	44.1	46.1	50.6					1.75
28	270-279.9	1.498	8.628	0.032	0.01	277	SAFE	31.2	42.2	44.0	48.0					1.9
29	280-289.9	1.476	8.960	0.031	-0.02	289	SAFE	33.1	44.9	46.8	51.2					2.11
30	290-299.9	1.329	7.931	0.025	-0.05	298	SAFE	33.8	47.5	49.7	54.9					0.72
31	300-309.9	1.494	9.116	0.039	-0.23	309	Failure	33.1	44.8	46.7	51.0	21.9	33.4	28.0	Case 2	0
32	310-319.9	1.613	9.761	0.041	-0.15	318	Failure	32.2	42.6	44.3	48.1	23.4	31.6	27.3	Case 1	0
33	320-329.9	1.645	9.917	0.045	-0.07	327	SAFE	32.0	42.1	43.7	47.3					0.34
34	330-339.9	1.628	9.371	0.038	0.02	332	SAFE	30.6	40.4	41.9	45.5					1.76
35	340-349.9	1.841	10.978	0.072	0.09	340	SAFE	31.3	39.9	41.3	44.4					2.98
36	350-359.9	1.526	9.150	0.046	0.13	351	SAFE	32.3	43.5	45.3	49.3					3.9

Table 5.4 shows that the relationship between the predicted extreme wind speed, $U_{ext}(R)$, and the critical wind speed, $U_{critical}$, in the directional sectors where a cable

instability could occur is different. If the calculated $U_{ext}(R)$ is beyond the critical wind speed range, i.e. $U_{ext}(R){\geq}U_2$, this defines Case 1 of which the extreme wind speed is higher than the critical wind speed range. This condition occurs for directional Sectors #5, 6, 8, 23, and 32. Another design case (Case 2) occurs if the extreme wind speed is within the critical wind speed range. This happens for Sectors #7 and #8. The third possible design case could be if $U_{ext}(R){\leq}U_1$. This case represents an optimistic design case of which there will be no risk for the cable to suffer from dry inclined cable galloping since the extreme wind speed, i.e. $U_{ext}(R)$, does not reach the critical wind speed range. However, this case does not happen in the current design example. These design cases simply clarify that although the extreme wind speed represents the maximum possible attainable wind speed that could occur at a bridge site, it does not necessarily relate to the worst aerodynamic loading condition for dry inclined cable galloping. Thus, it should be emphasized that the structural safety of a stay cable should be cautiously evaluated over the entire wind speed range rather than solely picking the extreme wind speed. This simply denotes the importance of performing a probabilistic-based wind speed analysis over a broad range of wind speed to assure the most critical aerodynamic loading condition due to the uncertain nature of wind can be captured.

Service life reliability response of the damped stay cable

Knowing that the loss of cable tension and damper capacity during cable-stayed bridge service life results in reduction of structural damping, it is of interest to determine how the uncertainty of these structural characteristic might affect the reliability of a stay cable under wind. Figure 5.15 shows the lifetime variation of the reliability index of the studied cable-damper system if no structural maintenance (enhancement) is provided. The

reliability index. β_0, represents the safety level at the initial design point. The result shows that due to structural degradation over the service life of 50 years, the reliability index reduces to 83.4% of its primary value. Subsequently, the required adjustment of cable tension at any time of interest is shown in Figure 5.16. The cable tension at each time instant represents the required amount of cable tension adjustment to sustain a reliability level of β_0.
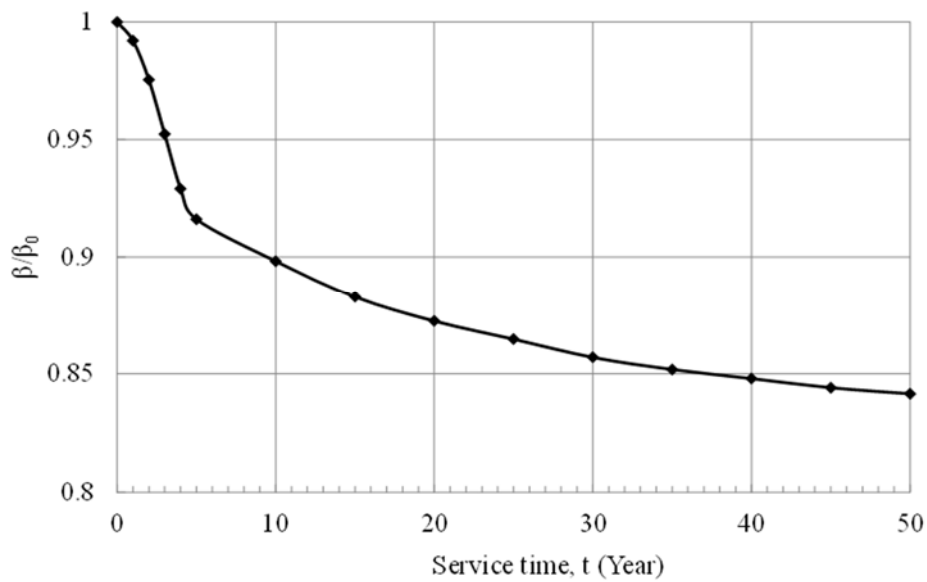
Figure 5.15: Time variation of relative reliability index (β_0=8.92) over the operation period of 50 years
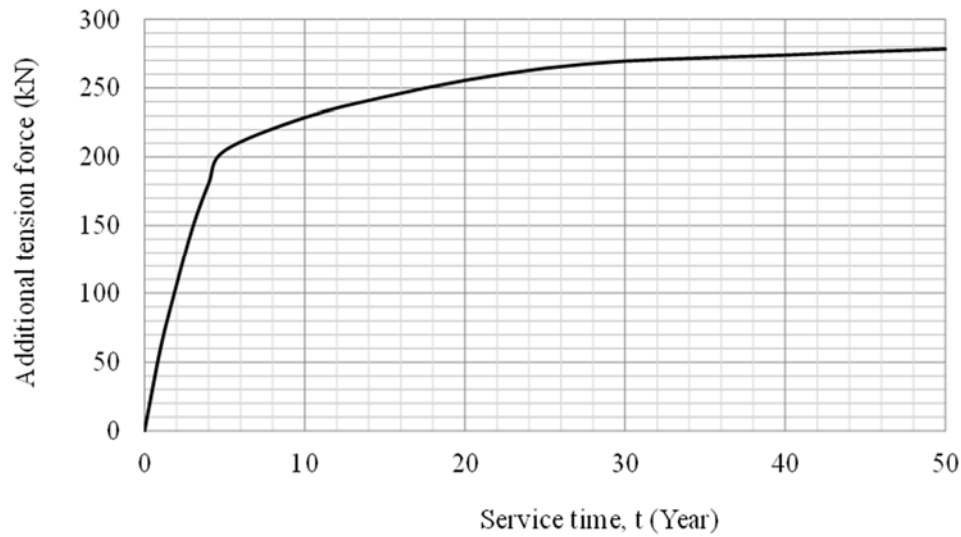
**Figure 5.16: Cable tension adjustment as system maintenance over the lifetime
of the studied damped stay cable**

5.5 SUMMARY

Wind-induced response of a dry inclined cable has been studied in a probabilistic-based context. It was shown that the aerodynamic stability of a cable can be related to the effective damping of the system. Accordingly, the general form of the LSF was proposed as the effective damping level of the system which can be obtained by summing up the equivalent structural damping and the aerodynamic damping of the studied cable-damper system under wind excitation, knowing that the uncertainties of structural and wind parameters were included in the analysis. Thus, the problem has been formulated as a limit state up-crossing scenario to determine the time specific system reliability due to dry inclined cable galloping. The structural reliability analysis method from Chapter 4, i.e. SORM with adaptive approximation, has been modified by a tail approximation technique and then applied to the proposed LSF. The intended result has been suggested in the form

174

of a lifetime reliability-based response diagram for a cable-damper system after N years of service life due to uncertain inherent and/or time-dependent structural and/or wind condition(s).

Two numerical examples have been presented to show the various applications of the proposed reliability-based framework model. The first example was analyzed to comprehend the reliability-based performance assessment of a stay cable in an existing wind tunnel experiment. It has been shown that the proposed reliability-based model is capable of predicting the instability regions within which the dry inclined cable galloping could occur as captured in the existing wind tunnel tests. The effect of structural damping level on the reliability response of an aerodynamically excited stay cable have been investigated. Also, it has been found that the presence of uncertainty in the structural properties of a cable-damper system at a given design point could have a sizable impact on its reliability response and thus should be considered in design.

In the second example, the reliability response of a typical bridge stay cable under practical wind speed conditions at a given bridge site over its service life has been evaluated. The time variation of cable tension was modeled based on field monitoring data. In addition, the damper capacity variation over the service time was modeled in accordance to a guideline which has been suggested by a manufacturer. The design wind speed at the given bridge site has been determined by applying statistical analysis method to the historical wind speed data. The sensitivity-based reliability analysis of wind parameters has been performed by considering the impact of the uncertainty of the wind speed and the wind direction on the reliability response. In addition, the stability of cable-damper system subjected to wind has been assessed over a practical wind speed range up to a calculated

extreme wind speed value corresponding to the selected return period. Consequently, the critical wind speed range within which the reliable response could not be satisfied has been determined. Finally, the reliability-based design assessment results have been presented for the stay cable over its service lifetime.

Due to inherent uncertainties in cable, damper, and wind properties, variabilities in structural responses are unavoidable. To ensure reliable performance of stay cables, these uncertainties or variabilities must be considered in design. Accordingly, this study can be categorized as an effort to integrate the reliability techniques with the state-of-the-art relevant to wind-induced cable vibrations. To the best knowledge of the author, effect of adding external damper as a common technique to mitigate stay cable vibrations due to wind load has not been investigated in a probabilistic-based context before. Therefore, the proposed reliability-based framework model can be implemented as a preliminary tool to evaluate performance of new/existing damped stay cables under wind conditions.

The current study is developed for reliability-based performance assessment of a stay cable with an attached linear viscous damper exposed to wind load. Nevertheless, it is feasible to apply the proposed reliability-based framework to assess performance of different types of dampers like nonlinear viscous dampers, magneto-rheological (MR) dampers, etc., by simply adjusting the resistant damping term, i.e. the equivalent structural damping ratio, in the LSF expression.

CHAPTER 6

CONCLUSION AND FUTURE RECOMMENDATIONS

The current study is an effort to perform reliability-based design assessment of damped bridge stay cables exposed to wind load conditions. This chapter summarizes the research work completed under the scope of the thesis and highlights outcomes of the study. Based on the insights gained from the proposed reliability-based model, some recommendations are made for future research on this topic.

6.1 SUMMARY OF RESEARCH WORK

Due to their low intrinsic damping and flexible nature, cables on cable-stayed bridges are often sensitive to dynamic excitations by various sources. With the increased popularity of cable-stayed bridge in the medium to long-span ranges and more matured field monitoring programs, many unfavourable cable vibration incidences were observed and reported from bridge sites or wind tunnel experiments in recent years, most of which are related to wind excitation or a combination of wind and rain. To suppress these vibrations, fluid dampers are often attached to the stay cables near the anchorages. In order to facilitate effective and economical design of dampers for stay cable vibration mitigation, thorough understanding of both the vibration characteristics and the dynamics of the cable-damper system is necessary. Nevertheless, existing studies are limited to deterministic-based analysis of which the uncertainties of structural parameters (such as cable tension and damper capacity) and wind parameters (such as speed, direction, etc.) over the service life of a bridge are totally neglected. Thus, to provide complete information regarding the aerodynamic response of a damped cable, the problem should be more rationally studied

from a probabilistic-based sense. In the current study, a reliability-based analysis model of a typical damped bridge stay cable subjected to wind load with and without the presence of precipitation has been proposed.

In Chapter 2, literature review was conducted by covering the essential components required to carry out reliability-based assessment on the performance of external dampers in controlling wind-induced bridge stay cable vibrations. Chapter 3 was aimed at providing ample understanding from the existing literatures on the performance of bridge stay cables equipped with external dampers using a deterministic-based framework. First, a basic model of a horizontal taut cable with an externally attached damper was introduced. The equation of motion of the studied cable-damper system was derived. Subsequently, solution to this complex eigenvalue problem was presented in the form of an attainable structural modal damping ratio for a given damper location. The influence of the cable inclination, the cable sag, and the cable bending stiffness on the structural modal damping ratio, as discussed in previous studies, was added in the formulation. In addition, the kinetic energy decay ratio method integrated with a finite element based model was implemented to evaluate the equivalent structural modal damping ratio of cable-damper systems. The presented information in Chapter 3 paved the road for the work in the subsequent chapters of which the uncertainties associated with structural and load parameters were considered in the problem formulation from a probabilistic-based sense.

Two types of cable vibrations that are more probable, i.e. rain-wind-induced cable vibrations, and/or critical, i.e. dry-inclined cable galloping, than the others were investigated by proposing a time-variant reliability-based framework model of a damped stay cable subjected to wind load conditions. Accordingly, in Chapter 4, reliability-based

design assessment on the performance of external dampers in controlling rain-wind induced bridge stay cable vibration has been presented. Subsequently, Chapter 5 continued the reliability based assessment of such a damped stay cable system when it is exposed to wind conditions under no precipitation susceptible to dry-inclined cable galloping.

The following components have been completed in these chapters, to develop a methodology on the reliability-based design assessment of damped bridge stay cables.

- Defining the probabilistic-based model of a cable-damper system subjected to wind load conditions

  A probabilistic-based model for studying wind-induced vibration of a typical cable-damper system has been developed. The established model was operated as a time-variant reliability-based framework to assess how uncertainties in the structural and the wind parameters would influence the time specific reliability performance of an external damper designed according to the current deterministic-based practice.

- Development of time-dependent limit state function

  The limit state function has been established by defining the stability criterion in terms of the effective damping. It has been proposed in terms of the difference between the available structural damping in a cable-damper system and the damping demand of a damped cable to avoid large amplitude vibrations due to RWIV and dry inclined cable galloping.

- Applying structural reliability analysis methods

  A set of structural reliability-based analysis methods, including the first-order-reliability methods (FORMs) and the second-order-reliability methods (SORMs),

have been applied to evaluate the behavior of a cable-damper system under wind and rain-wind-induced vibrations.

- Applying MCS to identify the most admissible structural reliability analysis method

  The Monte Carlo simulation (MCS) has been used as a reference reliability analysis method to compare the analysis outputs (i.e. reliability index/probability of failure) from different reliability methods. As a result, the most admissible structural reliability method in the reliability-based analysis of the studied cable-damper system has been identified.

- Collecting the reliability-based analysis results

  In Chapter 4, the reliability-based analysis results have been presented in the form of damper design estimation curves over the typical practical range of system parameters using a non-dimensional form. Besides, the reliability-based aerodynamic analysis results of the damped stay cable model have considered the uncertainty of wind speed.

- Demonstrating the applicability of the proposed reliability model

  The application of the proposed reliability-based design tool to the assessment of cable-damper system performance prone to RWIV/dry inclined cable galloping conditions has been demonstrated through case studies.

6.2 RESEARCH FINDINGS

The current study pointed out that for a rational assessment of the life-long performance of a cable-damper system, it is crucial to carry out a time-dependent probabilistic analysis, which considers impact of the system parameter uncertainties on the vibration control efficiency of an external damper designed according to the current

practice. The main contribution of the research work is that a reliability-based framework on the performance assessment of external dampers in controlling wind-induced bridge stay cable vibrations has been proposed. To the knowledge of the author, this is the first time that a non-deterministic design approach is developed for damped bridge stay cables under wind load conditions. The research outcomes are categorized below in terms of the structural design and the maintenance of damped bridge stay cables by applying the proposed reliability-based analysis tool.

6.2.1 Ensure reliability of design

The outcomes presented in this study would facilitate the reliability-based design of external dampers for bridge stay cables. They are collectively discussed as follows:

The most admissible reliability analysis method

A comparison of the reliability analysis results, in terms of the probability of failure, P_f, obtained by applying different reliability methods showed that the SORM with adaptive approximations method yielded the most accurate reliability evaluation results of the studied cable-damper systems. This was mainly due to its capability of handling nonlinear LSF. In addition, it was shown that this method is computationally more efficient than the MCS. Therefore, SORM with adaptive approximation can be considered as the most admissible reliability method in the analysis of aerodynamic response of cable-damper systems.

Reliability-based damper design curves

The procedure of designing external dampers for stay cables in bridges has been simplified by deriving a set of reliability-based damper design curves. These curves are presented in a non-dimensional form of the associated system parameters. This would

provide structural/bridge engineers with a convenient design tool to assess a damped bridge stay cable performance, especially in the preliminary stage. The results were presented over a typical range of structural and wind parameters.

Impact of uncertainty of cable and damper properties as well as wind parameters

The current practice of external damper design for controlling bridge stay cable vibrations has been improved by taking into account the uncertainties existed in the structural (cable and damper) and the load (wind) parameters of the system. It was suggested in this study that uncertainty should reflect both the inherent and the time-varying uncertain characteristics of a studied parameter. Also, the wind stochastic nature should be reflected by conducting statistical-based analysis on wind speed data. Results showed that the presence of uncertainty in the structural/wind parameters would have a sizable impact on the safe performance of a cable-damper system and should not be ignored in the design. The reliability analysis outcomes suggested a quantitative-based tool of which the trend of reliability index versus time-varying wind and structural parameters have been reflected for a wide range of structural coefficient of variations (COV= 0.01-0.25).

A comparison between the reliability results indicated that the cable-damper system performance is more sensitive to the uncertainty associated with the damper size. For instance, by increasing the COV of the damper size from 0.01 to 0.1, the reliability index of the system would drop from 59.4 to 7.0 by roughly 8.5 times, whereas the same increase of uncertainty in the cable tension would decrease the reliability index by 7 times from 48.7 to 7.0. Further, it was concluded that even though the uncertainty level of the structural parameters play an important role on the reliability response of the aerodynamically excited

cable, the negative aerodynamic damping effect (as the wind loading term) in the critical Reynolds regions is still the governing factor.

6.2.2 Enhance maintainability

One of the most important considerations in structural performance assessment is to ensure serviceability. Serviceability is defined as the ability of the structure to maintain its targeted/expected performance when is under operation (Frangopol and Maute, 2003). The findings of this study presented some useful insights for improving bridge stay cables maintainability during the operational stage.

Service life reliability response diagram

A service life reliability response diagram for an existing damped-stay cable has been presented, of which the performance of a cable-damper system under design wind speed condition is related to the lifetime variation of system parameters (including the cable tension, the damper capacity and the wind). A curve would provide engineers with an estimation of the reliability response of the external damper design due to design wind speed after N years of system operation. The results would facilitate the reliability-based procedure of a bridge maintenance life cycle assessment.

Preventive optimized maintenance

Findings of the current study would recommended an optimized strategy for the maintenance of a cable-damper system over the service life of the bridge within expected operational period. Noteworthy, combining the sensitivity-based reliability analysis results would help to ensure the most efficient maintenance strategy.

6.3 FUTURE RECOMMENDATIONS

Some recommendations are made below to be considered for future research on this topic:

Extending the problem scope

In this study, the fundamental mode is selected as the target mode for damper optimization. Because of the range of different cable lengths, the collection of stay cables on a cable-stayed has a practical continuum of fundamental and higher-mode frequencies. Thus, any excitation mechanism with any arbitrary frequency is likely to find one or more cable with either a fundamental or higher-mode frequency sympathetic to the excitation. Therefore, it is recommended to extend the study by carrying out multiple modes optimization to better investigate effect of higher structural modes on the reliability response of a typical damped bridge stay cable subjected to wind excitation.

Even though the current study was developed for the assessment of stay cable with an attached linear viscous oil damper, it is feasible to apply the proposed reliability-based tool to different types of damper, such as the nonlinear viscous dampers, magneto-rheological (MR) dampers, etc.

By modifying the structural damping ratio term (Resistant damping) in the defined LSF, the proposed reliability-based tool can be adapted to investigate other types of cable vibration mitigation techniques such as the cable surface treatment, the cross-ties, and also the hybrid systems.

The generality of the reliability-based method allows more wind-induced cable scenarios such as galloping of cables with ice accumulations, cable motions due to

buffeting with wind turbulence, etc. to be examined. The LSF should be adopted in each analysis case to reflect the entity of investigated excitation.

Reliability-based design guidelines

There are no specific guidelines and procedures to incorporate the design/maintenance requirements of a bridge stay cables equipped with external dampers in a probabilistic context. The reliability analysis would be implied to develop a set of consistent design guidelines for the mitigation of excessive cable vibration on cable-stayed bridges.

Impact of uncertainty of structural parameters

It would be beneficial to incorporate the uncertainties associated with structural parameters in the reliability assessment by incorporating the structural health monitoring data on real cable-stayed bridges.

REFERENCES

Abbas, K., & Tang, Y. (2013). Estimation of parameters for Frechet distribution based on Type-II censored samples. *Caspian Journal of Applied Sciences Research, 2*(7), 36-43.

Ahmed, S. A., & Mahammed, H. O. (2012, April). A statistical analysis of wind power density based on the Weibull and Ralyeigh models of "Penjwen Region" Sulaimani/ Iraq. *Jordan Journal of Mechanical and Industrial Engineering, 6*(2), 135-140.

Akpinar, E., & Akpinar, S. (2004). Statistical analysis of wind energy potentials on the basis of Weibull and Rayleigh distributions for Agin-Elazig, Turkey. *Journal of Power and Energy, 218*, 557-565.

Argentini, T., Pagani, A., Rocchi, D., & Zasso, A. (2014). Monte Carlo analysis of total damping and flutter speed of a long span bridge: Effects of structural and aerodynamic uncertainties. *Journal of Wind Engineering and Industrial Aerodynamics, 128*, 90–104.

Arora, J. S. (2004). *Introduction to optimum design.* London, UK: Elsevier Academic Press.

Au, F. T., & Si, X. T. (2012). Time-dependent effects on dynamic properties of cable-stayed bridges. *Structural Engineering and Mechanics, 41*(1), 139-155.

Benjamin, J. R. (1970). *Probability, Statistics, and Decision for Civil Engineers.* New York: McGraw-Hill.

Bosch, H. R., & Pagenkopf, J. R. (2014). *Dynamic properties of stay cables on the Penobscot Narrows Bridge.* Hampton, VA: FHWA-HRT-14-067.

Bosch, H. R., & Park, S. W. (September 2005). Effectivness of external dampers and crossties in mitigation of stay cable vibrations. *Sixth International Symposium on Cable Dynamics.* Charleston, SC.

Bourinet, J. M., Mattrand, C., & Dubourg, V. (2010). A Review of recent features and improvements added to FERUM software. *Safety, Reliability and Risk of Structures, Infrastructures and Engineering Systems*, 1564-1571.

Breitung, K. (1984). Asymptotic approximations for multinormal Integrals. *Journal of the Engineering Mechanics Division, 110*(3), 357-366.

Chen, Z. Q., Wang, X. Y., Ko, J. M., Ni, Y. Q., Yang, G., and Hu, J. H. (2004). MR damping system for mitigating wind-rain induced vibration on Dongting Lake cable-stayed bridge. *Wind and Structures*, 7(5), 293-304.

Cheng, J., & Li, Q. S. (2009). Reliability analysis of a long span steel arch bridge against wind-induced stability failure during construction. *J. of constructional Steel Research, 65*, 552-58.

Cheng, J., & Li, Q. S. (2009). Reliability analysis of long span steel arch bridges against wind-induced stability failure. *Journal of Wind Engineering and Industrial Aerodynamics, 97*, 132-139.

Cheng, J., & Xiao, R.-c. (2005). Probabilistic free vibration and flutter analyses of suspension bridges. *Engineering Structures, 27*(10), 1509–1518.

Cheng, S., & Tanaka, H. (2005). Correlation of aerodynamic forces on an inclined circular cylinder. *Wind and Structures, An International Journal, 8*(2), 135–146.

Cheng, S., Darivandi, N., & Ghrib, F. (2010). The design of an optimal viscous damper for a bridge stay cable using energy-based approach. *Journal of Sound and Vibration, 329*(22), 4689-4704.

Cheng, S., Larose, G. L., Savage, M. G., Tanaka, H., & Irwin, P. A. (2008a). Experimental study on the wind-induced vibration of a dry inclined cable—Part I: Phenomena. *Journal of Wind Engineering and Industrial Aerodynamics, 96*, 2231-2253.

Cheng, S., Larose, G. L., Savage, M. G., Tanaka, H., & Irwin, P. A. (2008b). Experimental study on the wind-induced vibration of a dry inclined cable—Part II: Proposed mechanisms. *Journal of Wind Engineering and Industrial Aerodynamics, 96*, 2254–2272.

Cheng, S., Tanaka, H., Larose, G. L., & Savage, M. G. (2003). Aerodynamic behavior of an inclined circular cylinder. *Wind and Structures, An International Journal, 6*(3), 197-208.

Chiralaksanakul, A., & Mahadevan, S. (2005). First-order approximation methods in reliability-based design optimization. *Journal of Mechanical Design, 127*(5), 851-857.

Choi, S. K., Grandhi, R. V., & Canfield, R. A. (2007). *Reliability-based structural design.* London: Springer.

Christenson, R. E., Spencer, B. J., & Johns, E. A. (2006). Experimental verification of smart cable damping. *Journal of engineering mechanics, 132*(3), 268-278.

Costa Rocha , P. A., De Sousa , R. C., De Andrade , C. F., & Da Silva, M. V. (2012). Comparison of seven numerical methods for determining Weibull parameters for wind energy generation in the northeast region of Brazil. *Appl. Energy, 89*, 395–400.

Der Kiureghian, A., Lin, H. Z., & Hwang, S. J. (1987). Second order reliability approximations. *Journal of engineering mechanics, 113*, 1208-1225.

Dragonette, J. (2000). *Long Term Life Cycle Evaluation of Taylor Devices Products.* N. Tonawanda, NY: Taylor Devices Inc.

Duy, H. V., Katsuchi, H., Yamada, H., & Nishio, M. (2014, March). Experimental study on dry-state galloping with various wind relative angles and its countermeasures. *Journal of Structural Engineering, 60A*, 428-435.

Elishakoff, I. (1999). *Probabilistic theory of structures* (2nd ed.). Mineola, New York: Dover publications, Inc.

Ellingwood, B. (1980). *Development of a probability based load criterion for American National Standard A58: Building code requirements for minimum design loads in buildings and other structures* (Vol. 577). US Department of Commerce, National Bureau of Standar.

Enevoldsena, I. (2011). Practical implementation of probability based assessment methods for bridges. *Structure and Infrastructure Engineering: Maintenance, Management, Life-Cycle Design and Performance, 7*(7-8), 535-549.

ESDU, 8. (1986). *Mean forces, pressures and flow field velocities for circular cylindrical structures: Single cylinder with two-dimensional flow.* London: ESDU Int. Ltd.

Eureqa, "http://creativemachines.cornell.edu/Eureqa."

Fisher, R. A., & Tippett, L. C. (1928). Limiting forms of the frequency distribution of the largest and smallest member of a sample. *Proc. Cambridge Phil. Soc.*, *24*, pp. 180–190.

Flamand, O. (1995). Rain-wind-induced vibration of cables. *J. Wind Eng. Ind. Aerodyn., 57*(2-3), 353–362.

Flamand, O., Peube , J., & Papanikolas, P. (2001). An explanation of the rain-wind induced vibration of inclined stays. *Proceedings of the 4th International Symposium on Cable Dynamics*, Montreal, Canada, May 28-30, 69-76.

Fournier, J. A., & Cheng, S. (2014). Impact of damper stiffness and damper support stiffness on the efficiency of a linear viscous damper in controlling stay sable vibrations. *Journal of Bridge Engineering, 19*(4), p. 04013022.

Frangopol, D. M., & Maute, K. (2003). Life-cycle reliability-based optimization of civil and aerospace structures. *Journal of Computers and Structures, 81*, 397–410.

Frangopol, D. M., & Moses, F. (1994). Chapter 13 in Advances in design optimization. In H. Adeli, *Reliability based structural optimization* (pp. 492-570). London: Chapman and Hall.

Frangopol, D. M., Maute, K., & Liu, M. (2007). Optimization of structural and mechanical systems. In J. S. Arora, & J. S. Arora (Ed.), *Design optimization with uncertainty,*

life-cycle performance and cost considerations (pp. 291-329). London, England: World Scientific Publishing.

Fujino, Y. (2002). Vibration, control and monitoring of long-span bridges: Recent research development and practice in Japan. *Journal of Constructional Steel Research, 58*, 71-97.

Fujino, Y., & Hoang, N. (2008). Design formulas for damping of a stay cable with a damper. *Journal of Structural Engineering, 134*(2), 269–278.

Fujino, Y., Kimura, K., & Tanaka, H. (2014). *Wind resistant design of bridges in Japan: Developments and practices.* Japan: Springer.

Ge, Y. J., Xiang, H. F., & Tanaka, H. (2000). Application of a reliability analysis model to bridge flutter under extreme winds. *Journal of Wind Engineering and Industrial Aerodynamics, 86*, 155-167.

Georgakis, C. T., & Taylor, C. A. (2005). Nonlinear dynamics of cable stays. Part 1: sinusoidal cable support excitation. *Journal of Sound and Vibration, 281*, 537-564.

Guerts, C., & Van Staalduinen, P. C. (1999). Estimations of the effect of rain-wind-induced vibration in the design stage of inclined stay cables. *Proc. of 10th Int. Conf. on Wind Eng.*, *6*, pp. 885-892. Copenhagen, Denmark.

Geurts, C., Vrouwenvelder, T., Staalduinen, P. and Reusink, J. (1998). Numerical modelling of rain-wind-induced vibration: Erasmus Bridge, Rotterdam. *Structural Engineering International*, SEI, 8(2), 129-135.

Gu, M., & Lu, Q. (2001). Theoretical analysis of wind–rain induced vibration of cables of cable-stayed bridges. *J. Wind Eng., 89*, 125–128.

Gu, M., Du, X. Q., & Li, S. Y. (2009). Experimental and theoretical simulations on wind-rain-induced vibration of 3-D rigid stay cables. *Journal of Sound and Vibration, 320*(1-2), 184-200.

Gumbel, E. J. (1954). Statistics theory of extreme values and some practical applications. *Applied math series, 33*.

Gringorten, I. I. (1963). A plotting rule for extreme probability. *Journal of Geophysical, 68*, 813–14.

Hasofer, A. M., & Lind, N. (1974). An exact and invariant first-order reliability. *Journal of Engineering Mechanics, 100*(1), 111-121.

Haukaas, T., & Der Kiureghian, A. (2005). Parameter sensitivity and Importance measures in nonlinear finite element reliability analysis. *Engineering Mechanics, 131*(10), 1013–1026.

Haukaas, T., & Der Kiureghian, A. (2007). Methods and object-oriented software for FE reliability and sensitivity analysis with application to a bridge structure. *Journal of Computing in Civil Engineering, 21*(3), 151–163.

Harlow, D. G. (2002). Applications of the Frechet distribution function. *International Journal of Material and Product Technology, 5*(17), 482-495.

Hennesessey, J. (1977). Some aspects of wind power statistics. *Journal of Applied Meteorology, 16*, 119-128.

Hikami, Y., & Shiraishi, N. (1988). Rain-wind induced vibration of cables in cable-stayed bridges. *Journal of Wind Engineering and Industrial Aerodynamics, 29*, 409-418.

Hohenbichler, M., & Rackwitz, R. (1981, Dec.). Non-normal dependent vectors in structural safety. *Journal of the Engineering Mechanics Division, 107*(EM6), 1227-1238.

Holmes, J. D. (2002). Fatigue life under along-wind loading- closed-form solutions. *Journal of engineering structures*, 109-114.

Holmes, J. D. (2007). Wind loading of structures. London: Taylor and Francis.

Honga, H. P., Beadlea, S., & Escobarb, J. A. (2001). Probabilistic assessment of wind-sensitive structures with uncertain parameters. *Journal of Wind Engineering and Industrial Aerodynamics, 89*, 893–910.

Huang, L. (2011). *Experimental study on bridge stay cable vibration mitigation using external viscous damper.* Windsor, ON, Canada: M.S. thesis, Univ. of Windsor.

Imai, K., & Frangopol, D. M. (2001). Reliability-based assessment of suspension bridges: application to the Innoshima bridge. *Journal of Bridge Engineering, 6*(6), 398-411.

Irvine, H. M., & Caughey, T. K. (1974). The linear theory of free vibrations of a suspended cable. *Proceedings of the Royal Society of London, Series A341*, 299-315.

Irvine, M. (1981). *Cable structures.* New York: Dover Publications Inc.

Irwin, P.A. (1997). Wind vibrations of cables on cable-stayed bridges. *Building To Last: Proceedings of Structural Congress XV*, Portland, Oregon, April 13-16, 383-387.

Jakobsen , J. B., & Tanaka, H. (2003). Modelling uncertainties in prediction of aeroelastic bridge behaviour. *Journal of Wind Engineering and Industrial Aerodynamics, 91*, 1485–1498.

Jenkinson, A. (1955). The frequency distribution of the annual maximum (or minimum) values of meteorological elements. *Quarterly Journal of the Royal Meteorological Society, 81*, 158–71.

Jiang, J., Li, G.-Q., & Lu, Y. (2013). Vibration control of cables with damped flexible and restraint: Theoretical model and experimental verification. *Journal of sound and vibration, 332*(15), 3626-3645.

Johnson, E. A., Christenson, R. E., & Spencer, J. B. (2002b). *Flat-sag cables with semiactive damping.* Dept. of Civil and Env. Engrg. Los Angeles: University of Southern California.

Kim, I.-H., Hyung-Jo, J., & Jeong-Hoi, K. (2010). Experimental evaluation of a self-powered smart damping system in reducing vibrations of a full-scale stay cable. *Smart Mater. Struct., 19*, 1-10.

Ko. (2002). Implementation of magneto-rheological dampers to Dongting Lake Bridge for cable vibration mitigation. *Proceedings of the Third World Conference on Structural Control. 3*, pp. 777-786. Como, Italy: John Wiley & Sons, Chichester .

Kovacs, I. (1982). Zur frage der seilschwingungen und der seildämpfung. *Bautechnik*, 325-332.

Koyluoglu, H. U., & Nielsen, S. K. (1994, Apr.). New approximations for SORM integrals. *Structural Safety, 13*(4), 235-246.

Krenk, S. (2000). Vibrations of a taut cable with an external damper. *Journal of Applied Mechanics, 67*(4), 772-776.

Krenk, S., & Nielsen, S. (2002). Vibrations of a shallow cable with a viscous damper. *Proceedings of the Royal Society of London, Series A458*, 339-357.

Kulhawy, F. H., & Phoon, K.-K. (1996). Engineering judgement in the evolution from deterministic to reliability-based foundation design. *Proceedings of Uncertainty '96, Uncertainty in the Geologic Environment - From Theory to Practice* (pp. 29-48). New York: (GSP 58), Eds. C. D. Shackelford, P. P. Nelson & M. J. S. Roth, ASCE, New York,.

Kumarasena, S., Jones, N. P., Irwin, P., & Taylor, P. (2007). *Wind-induced vibration of stay cables.* Boston: FHWA-HRT-05-083.

Kusano, I., Baldomir, A., Jurado, J. Á., & Hernández, S. (2015). Probabilistic optimization of the main cable and bridge deck of long-span suspension bridges under flutter constraint. *Journal of Wind Engineering and Industrial Aerodynamics, 146*, 59–70.

Larose , G. L., & Zan, S. J. (2001). The aerodynamic forces on stay cables of cable-stayed bridges in the critical Reynolds number range. *In: Proceedings of 4th International Symposium on Cable Dynamics*, (pp. 77-84). Montreal, Canada.

León, D. d., Manjarrez , L., & Ang, A. (2015). Structural reliability of the Tampico Bridge under wind loading. *Ciencia Ergo Sum*, 161-166.

Li, J., Chen, J. B., & Fan, W. L. (2007). The equivalent extreme value event and evaluation of the structural system reliability. *Structural Safety, 29*, 112-131.

Li, Y. S., & Lence, B. J. (2007). Numerical approximations of design points in reliability analysis under parametric changes. *Journal of Engineering Mechanics, 133*(11), 1213-1221.

Macdonald, J. G. (2002). Separation of the contributions of aerodynamic and structural damping in vibrations of inclined cables. *Journal of Wind Engineering & Industrial Aerodynamics, 90*, 19–39.

Macdonald, J. G., & Larose, G. L. (2006). A unified approach to aerodynamic damping and lift/drag instabilities and its application to dry inclined cable galloping. *Journal of Fluids and Structures, 22*, 229-252.

Madsen, H. O., & Tvedt, L. (1990). Methods for time-dependent reliability and sensitivity analysis. *J. of Engineering Mechancis, 116*(10), 2118-2135.

Main, J. A., & Jones, N. P. (2002a). Free vibrations of a taut cable with attached damper. I: inear viscous damper. *Journal of Engineering Mechanics, 128*(10), 1062-1071.

Main, J. A., & Jones, N. P. (2002b). Free vibrations of a taut cable with attached damper. II: nonlinear damper. *Journal of Engineering Mechanics, 128*(10), 1072-1081.

Main, J. A., Jone, N. P., & Yamaguchi, H. (2001). Characterization of rain-wind-induced stay-cable vibrations from fullscale. *Proceedings of 4th International Symposium on Cable Aerodynamics from full-scale measurements*, (pp. 235-242). Montreal.

Matsumoto , M., Hikami, Y., & Kitazawa, M. (1989a). Inclined-cable aerodynamics. *Proceesings of Structural Design, Analysis & Testing, Structures Congress '89* (pp. 81-90). ASCE.

Matsumoto, M. (1998). Observed behavior of prototype cable vibration and its generation mechanism, in: Bridge Aerodynamics. *Proceedings of the International Symposium on Advances in Bridge Aerodynamics*, (pp. 189–211).

Matsumoto, M., Shirashi, N., & Shirato, H. (1992). Rain-wind induced vibration of cables of cable-stayed bridges. *Journal of Wind Engineering and Industrial Aerodynamics, 44*, 2011-2022.

Matsumoto, M., Shirato, H., Yagi, T., Jones, N. P., & Hayashi, T. (2001). Field observation system of cable aerodynamics in natural wind. *In: Proceedings of the Fourth International Symposium on Cable Dynamics*, (pp. 219–225). Montreal, Canada.

Matsumoto, M., Shirato, H., Yagi, T., Goto, M., Sakai, S., and Ohya, J. (2003). Field observation of the full-scale wind induced cable vibration. *Journal of Wind Engineering and Industrial Aerodynamics*, 91, 13-26.

Matsumoto, M., Yagi, T., Adachi, Y., & Hatsuda, H. (2007). Cross flow response of circular cylinders influenced by Kárman vortex mitigation. *Proceedings of Seventh International Symposium on Cable Dynamics.* Vienna, Austria.

Matsumoto, M., Yagi, T., Adachi, Y., Hatsuda, H., & Shima, T. (2007). Karman vortex effects on aerodynamic instabilities of inclined stay-cables. *Proceedings of the 12th International Conference on Wind Engineering*, (pp. 175-182). Cairns, Australia.

Matsumoto, M., Yagi, T., Hatsuda, H., Shima, T., Tanaka, M., & Naito, H. (2010). Dry galloping characteristics and its mechanism of inclined/yawed cables. *Journal of Wind Engineering and Industrial Aerodynamics, 98*, 317–327.

Mehrabi, A., & Tabatabai, H. (1998). Unified finite difference formulation for free vibration of cables. *Journal of Structural Engineering, 124*(11), 1313-1322.

Melchers, R. E. (1987). *Structural reliability analysis and prediction.* UK: Ellis Horwood Limited.

Melchers, R. E., & Ahammed, M. (2004). A fast approximate method for parameter sensitivity estimation in Monte Carlo structural reliability. *Journal of Computer and Structures, 82*, 55-61.

Michael P Enright, D. M. (1998). Probabilistic analysis of resistance degradation of reinforced concrete bridge beams under corrosion. *Engineering structures, 20*(11), 960-971.

Miyata, T., Yamada, H., & Hojo, T. (1994). Aerodynamic response of PE stay cables with pattern-indented surface. *In: Proceedings of International Conference on Cable-Stayed and Suspension Bridges (AFPC)*, (pp. 515-522). Deauville, France.

Mohammadi, S., Cheng, S., & Ghrib, F. (2011). Reliability assessment for damped bridge stay cables under dynamic excitation. *Proceding of the 8th International Conference on Structural Dynamics* (pp. 2993-2999). Leuven, Belgium: Eurodyn.

Mohammadi, S., Cheng, S., & Ghrib, F. (2013). *Assessment of dynamic behavior of an inclined sag cable with a transverse linear viscous damper using reliability-based approaches.* Montreal, Canada: Canadian Society of Civil Engineering.

Mohammadi, S., Cheng, S., & Ghrib, F. (2014). A reliability-based framework to assess damper performance in controlling cable vibrations. *Structural Engineering and Mechanics*, in press.

Montgomery, D. C., & Runger, G. C. (2003). *Applied statistics and probability for engineers* (3rd ed.). New York, NY: John Wiley & Sons, Inc.

Mori, Y., & Ellingwood, B. R. (1993). Reliability-based service life assessment of aging concrete structures. *Journal of Structural Engineering, 119*(5), 1600-21.

Nadarajah, S., & Kotz, S. (2008). Sociological models based on Frechet random variables. *Quality and Quantity, 42*, 89-95.

Nakamura, Y., & Hirata, K. (1994). The aerodynamic mechanism of galloping. *Transaction of the Japan Society for Aeronautical and Space Science, 36*(114), 257-269.

Namini, A., Albrecht, P., & Bosch, H. (1992). Finite element-based flutter analysis of cable-suspended bridges. *Journal of structural engineering, 118*, 1509-1526.

Nikitas, N., Macdonald, J. G., Andersen, T. L., Jakobsen, J. B., Savage, M. G., & McAuliffe, B. R. (2009). Wind tunnel testing of an inclined aeroelastic cable model-pressure and motion characteristics, Part I. *EACWE 5* . Florence, Italy.

Ohunakin, O. (2011). Wind characteristics and wind energy assessment in Uyo, Nigeria. *Journal of Engineering and Applied Sciences, 6*(2), 141-146.

Olaofe, Z. O., & Folly, K. A. (2012). Statistical analysis of the wind resources at Darling for energy production. *INTERNATIONAL JOURNAL of RENEWABLE ENERGY RESEARCH, 2*(2), 250-261.

Pacheco, B. M., Fujino, Y., & Sulekh, A. (1993). Estimation curve for modal damping in stay cables with viscous damper. *Journal of Structural Engineering, 119*(6), 1961-1979.

Pagnini, L. (2010). Reliability analysis of wind-excited structures. *Journal of Wind Engineering and Industrial Aerodynamics, 98*, 1-9.

Palutikof, J. P., Brabson, B. B., Lister, D. H., & Adcock, S. T. (1999). A review of methods to calculate extreme wind speeds. *Meteorol. Appl., 6*, 119-132.

Petrini, F., & Bontempi, F. (2011). Estimation of fatigue life for long span suspension bridge hangers under wind action and train transit. *Structure and Infrastructure Engineering, 7*(7-8), 491-507.

Pourzeynali, S., & Datta, T. K. (2005). Reliability analysis of suspension bridges against fatigue failure from the gusting of wind. *Journal of bridge engineering, 3*, 262-271.

Publication, P. (2001). *Recommendations for stay-cable design, testing and installation, fourth ed.* Post-Tensioning Institute.

Rackwitz, R. (1977). First order reliability theories and stochastic models. *ICOSSAR'77 Tu Munchen.*

Raeesi, A., Cheng, S., & Ting, D. S.-K. (2013). Aerodynamic damping of an inclined circular in unsteady flow and its application to the prediction of dry inclined cable galloping. *Journal of Wind Engineering and Industrial Aerodynamics, 113*, 12-28.

Saito, T., Matsumoto, M., & Kitazawa, M. (1994). Rain-wind excitation of cables on cable-stayed Higashi-Kobe Bridge and cable vibration control. *Proceedings of the*

International Conference on Cable-Stayed and Suspension Bridges (AFPC), 2, pp. 507–514. Deauville, France.

Saleh , H., Abou El-Azm, A., & Abdel-Hady, S. (2012). Assessment of different methods used to estimate Weibull distribution parameters for wind speed in Zafarana wind farm, Suez Gulf, Egypt. *Energy, 44*, 710-719.

Schewe, G. (1983). On the force fluctuations acting on a circular cylinder in cross-flow sub-critical up to transcritical Reynolds numbers. *J. of Fluid Mechanics, 133*, 265-285.

Schneider, J. (2006). *Introduction to safety and reliability of structures.* Zürich, Switzerland: IABSE-AIPC-IVBH.

Seguro, J., & Lambert, T. (2000). Modern estimation of the parameters of the Weibull wind speed distribution for wind energy analysis. *J. Wind Eng. Indust. Aerodyn., 85*, 75-84.

Simiu, E., & Scanlan, R. (1996). *Wind effect of structur* (3rd ed. ed.). New York: Wiley-Interscience.

Simões, L. C., & Negrão, J. H. (2005). Reliability-based optimum design of Glulam cable-stayed footbridges. *Journal of Bridge Engineering, 10*(1), 39-44.

Spencer, B. F., & Nagarajaiah, S. (2003). State of the art of structurlal control. *Journal of Structural Engineering, 159*(7), 845-856.

Su, C., Luo, X., & Yun, T. (2010). Aerostatic reliability analysis of long-span bridges. *Journal of Bridge Engineering, 15*(3), 260–268.

Sun, B., Wang, Z., Ko, J. M., & Ni, Y. Q. (2003). Parametrically excited oscillation of stay cable and its control in cable-stayed bridges. *Journal of Zhejiang University Science, 4*(1), 13-20.

Symes, J. A., & Macdonald, J. H. (2006). Quasi-steady "dry-galloping" analysis of inclined cables in turbulent flow. *Proceedings of 7th UK Conferences on Wind Engineering*, (pp. 121-124).

Symes, J. A., Macdonald, J. H., & Stoyanoff, S. (2007). Combined buffeting and dry-galloping analysis of inclined stay cables. *Proceedings of the 7th International Symposium on Cable Dynamics* (pp. 201-208). Vienna, Austria: University of Bristol.

Tabatabai, H., & Mehrabi, A. (2000). Design of mechanical viscous dampers for stay cables. *Journal of Bridge Engineering, 5*(2), 114–123.

Tabatabai, H., Mehrabi, A. B., Morgan, B. J., & Lotfi, H. R. (1998). *Non-destructive bridge evaluation technology: bridge stay cable condition assessment.* Report Prepared for Federal Highway Admin. Skokie, III: Construction Technology Laboratories.

Torres , G., Prieto, J., & Francisco, E. (1998). Fitting wind speed distribution: A case study. *Solar Energy, 62*(2), 139-144.

Torres, J. L., Garcia, A., Prieto, E., & Francisco, A. d. (1999). Characterization of wind speed data according to wind direction. *Solar Energy , 66*(1), 57-64.

Triantafyllou, M. S., & Grinfogel, L. (1986). Natural frequencies and modes of inclined cables. *Journal of structural engineering, 112*(1), 139-148.

Tvedt, L. (1984). *Two second-order approximations to the failure probability.* Hovik: A/S Vertas Research.

Tvedt, L. (1990). Distribution of quadratic forms in normal space applications to structural reliability. *Journal of the Engineering Mechanics Division, 116*, 1183-1197.

Uno, K., Kitagawa, S., Tsutsumi, H., Inoue, A., & Nakaya, S. (1991). A simple method of designing cable vibration dampers of cable-stayed bridges. *Journal of Structural Engineering, Japan Society of Civil Engineers, 6*(1), 167-178.

Verwiebe, C., & Ruscheweyh, H. (1998). Bridge stay cable vibration: Phenomena, criteria and damper technology. *Proceedings of the 3rd International Symposium on Cable Dynamics*, (pp. 163–170). Troudheim.

Virlogeux, M. (1998). Cable vibrations in cable-stayed bridges. *In: Proceedings of International Symposium on Advances in Bridge Aerodynamics*, (pp. 213–233). Copenhagen, Denmark.

Waewsak, J., Chancham, C., Landry, M., & Gagnon, Y. (2011). An analysis of wind speed distribution at Thasala, Nakhon Si Thammarat, Thailand. *Journal of Sustainable Energy & Environment, 2*, 51-55.

Wang, L. P., & Grandhi, R. V. (1995). Improved two-point function approximation for design optimzation. *AIAA Journal, 32*(9), 1720-1727.

Wang, L. P., Grandhi, R. V., & Hopkins, D. A. (1995). Structural reliability optimization using an efficient safety index calculation procedure. *International Journal for Numerical Methods in Engineering, 38*, 1721-1738.

Watson, S. C., & Stafford, D. (1988). Cables in Trouble. *Civil Engineering, ASCE, 58*(4), 38–41.

Xiao, Y. Q., Li, Q. S., Li, Z. N., & Chow, Y. W. (2006). Probability distributions of extreme wind speed and its occurrence interval. *Journal of Engineering Structures, 28*, 1173-1181.

Xu, Y., Chen, J., Ng, C. & Zhou, H. (2008). Occurrence probability of wind-rain-induced stay cable vibration. *Advances in Structural Engineerig. 11*(1), 53-69.

Xu, Y. L., Zhan, S., Ko, J. M., & Yu, Z. (1999). Experimental study of vibration of bridge stay cables. *Journal of Structural Engineering, 125*(9), 977-986.

Y.Q. Nia, X. W. (2007). Field observations of rain-wind-induced cable vibration in cable-stayed Dongting Lake Bridge. *Journal of Wind Engineering and Industrial Aerodynamics, 95*(5), 303–328.

Yamada, H. (1997). Control of wind-induced cable vibrations from a viewpoint of the wind resistance design of cable-stayed bridges. *Proceedings of the 2nd International Seminar on Cable Dynamics*, Tokyo, 129-138.

Yamaguchi, H. (1990). Analytical study on growth mechanism of rain vibration of cables. *J. Wind Eng. Ind. Aerodyn., 33*, 73–80.

Yamaguchi, H. (1995). *Control of cable vibrations with secondary cables.* Liege: A.I.M.

Yamaguchi, H., & Fujino, Y. (1998). Stayed cable dynamics and its vibration control. In A. L. eds. (Ed.). Balkema, Rotterdam, The Netherlands.

Yan, D., & Chang, C. C. (2009). Vulnerability Assessment of Cable-Stayed Bridges in Probabilistic Domain. *Journal of Bridge Engineering, 14*(4), 270-278.

Yoneda, M., & Maeda, K. (1989). A study on practical estimation method for structural damping of stay cable with damper. *Proceeding of Canada-Japan Workshop on Bridge Aerodynamics*, (pp. 119-128). Ottawa, Canada.

Zhang, W., Cai, C. S., & Pan, F. (2013). Fatigue reliability assessment for long-span bridges under combined dynamic loads from winds and vehicles. *J. of Bridge Engineering, 18*(8), 735-747.

Zuo, D. J. (2010). Interpretation of field observations of wind-and rain-wind-induced stay cable vibrations. *Journal of Wind Engineering and Industrial Aerodynamics, 98*(2), 73–87.

APPENDIX A

AERODYNAMIC FORCE COEFFICIENTS AND THEIR PARTIAL DERIVATIVES WITH RESPECT TO REYNOLDS NUMBER AND CABLE-WIND RELATIVE ANGLE

A.1 INTRODUCTION

The flow pattern around a circular cylinder and the resulting force coefficients are primarily determined by the position of the separation points at which the upstream boundary layer leaves the cylinder surface to form the wake region. The location of the separation points is primarily determined by the Reynolds number, turbulence characteristics of the approaching flow, and by the roughness of the cylinder surface. Hence, in practice, the force coefficients of a circular cylinder should be correlated with the flow and surface roughness conditions (ESDU, 1986). To compute the aerodynamic damping ratio from Eq. (5-14), the magnitude of the aerodynamic mean force coefficients (C_D, C_L) and their partial derivatives in respect to Re and cable-wind relative angle φ (i.e. $\partial C_D/\partial Re$, $\partial C_D/\partial \varphi$, $\partial C_L/\partial Re$, $\partial C_L/\partial \varphi$) are required.

A.2 AERODYNAMIC FORCE COEFFICIENTS

The mean force coefficients are collected from the results of the previous wind tunnel experiments. First, the wind tunnel tests data and adjunct formulations reported in Engineering Science Data Unit (ESDU), Item No. 80025, will be utilized. The ESDU data set has the advantage because it is prepared for an extensive range of flow regime including subcritical, critical and supercritical flow conditions up to $Re_e \approx 3\times10^7$. It is also capable

of considering effects of flow turbulence and surface roughness in the estimation of mean force coefficients. Hence, the mean drag force coefficient (C_D) for two-dimensional circular cylinder can be computed at each aerodynamic design point in terms of the Reynolds number Re, cable-wind relative φ angle, and cable roughness for the specified flow turbulence condition.

Though the ESDU data set is quietly flexible for the calculations of mean drag force coefficients, it does not provide information about cable lift coefficient. While, the aerodynamic damping ratio expression in Eq. (5-14) suggests that lift force would also contribute to excite the cable when the asymmetry in flow field around the cylinder surface exists and thus non-zero lift occurs. The limitation is noticeable especially over the critical range of Re when the formation and existence of single separation bubble (i.e. adverse effect of lift force due to strong negative effect of $\partial C_L/\partial Re$, and $\partial C_L/\partial \varphi$) plays an important role (Macdonald and Larose, 2006). In another expression, if the imposed aerodynamic loading condition is mainly contributed by the lift force rather than the typical drag crisis condition (i.e. adverse effect of drag force due to negative values of $\partial C_D/\partial Re$ and $\partial C_D/\partial \varphi$), then drag force by itself does not certainly represent the actual loading effect. Thus, to overcome this issue, it is necessary to include effect of the lift force as well as the drag force in the analysis. As a solution, the calculated aerodynamic force coefficients from another wind tunnel test can be alternatively used. In this regard, the lift and drag coefficients of a rigid static circular cylinder model measured by Cheng et al. (2008a) in a wind tunnel test conducted at National Research Council Canada (NRC) are selected. Here, the mean force coefficients are calculated based on the surface pressure of a stationary cylinder model measured over a range of Reynolds number up to the critical regime. The

data set is available for a certain range of flow conditions i.e. $Re \leq 3.54 \times 10^5$, and $54.7° \leq \varphi \leq 106.8°$. This set of data is referred to as NRC data. Figure A.1 shows the drag and lift coefficients from the NRC data set over the tested range of Reynolds number and cable-wind relative angle.
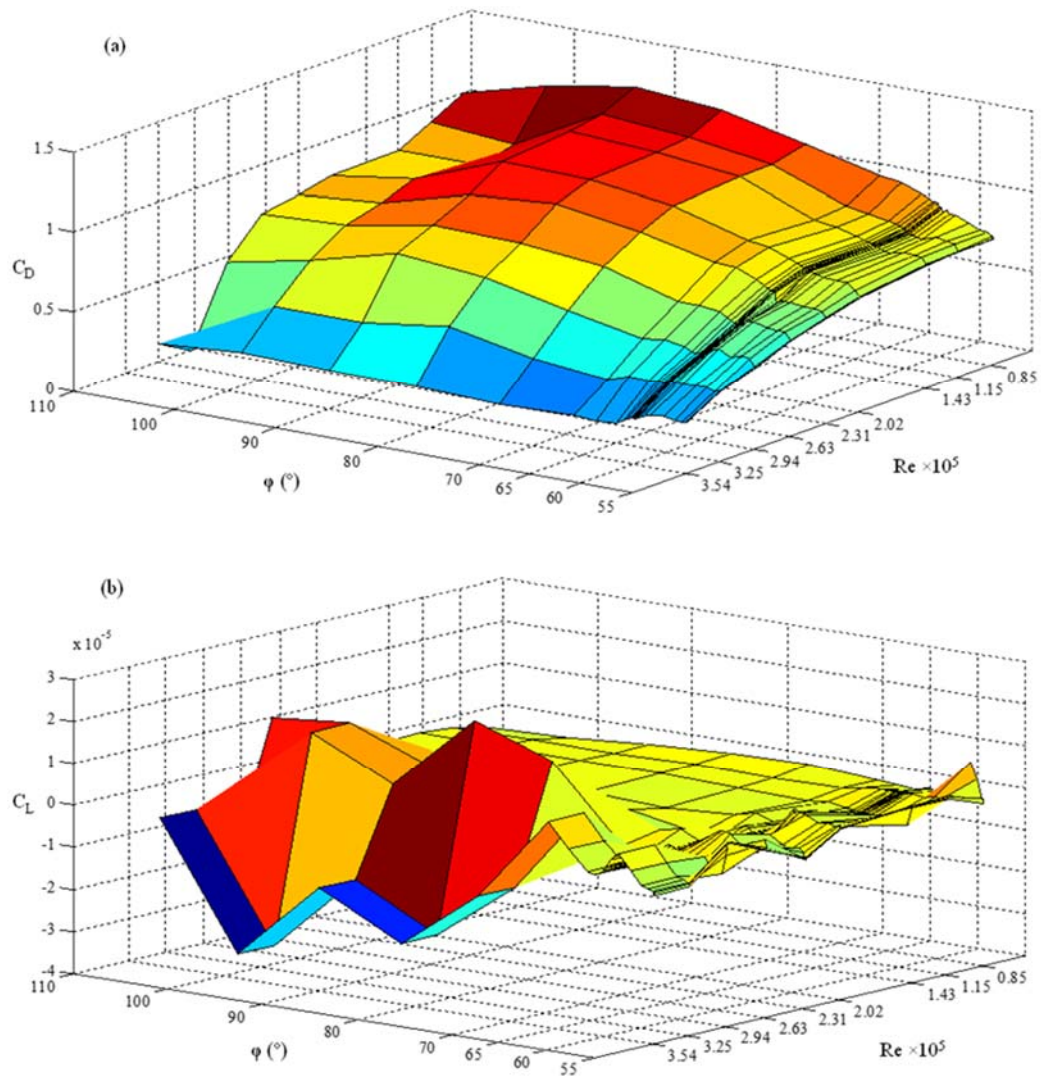
Figure A.1: Aerodynamic force coefficients from study of Cheng et al. (2008a),
(a) C_D, (b) C_L

It should be pointed out that the NRC data set is capable of predicting the aerodynamic response of the stay cable (i.e. the divergent motion due to cable galloping) within the critical Re range (Cheng et al., 2008a; Raeesi et al., 2013). However, to investigate the effect of load and/or physical parameters, such as the excitation wind speed U_m and direction (wind-yaw angle θ in terms of cable-wind relative angle φ), beyond the studied range, or a cable surface condition other than the model used in the NRC test, the application of the ESDU wind tunnel test data set is alternatively required.

Below, calculations of the mean force coefficients and their corresponding partial derivatives with respect to Re and φ in accordance to the recommended procedure in ESDU 80025 wind tunnel data set are illustrated. Table A.1 shows a summary of the required steps to evaluate the mean drag force coefficient C_D of a two-dimensional circular cylinder. The suggested method for estimation of the drag coefficient (C_D) of an inclined cylinder depends on whether the flow is in the subcritical ($Re_e < Re_{Crit} = 3 \times 10^5$) or supercritical ($Re_e > Re_{Crit} = 3 \times 10^5$) regime. Noting that the effective Reynolds number $Re_e = \lambda_T \lambda_R Re$ is a modified Reynolds number incorporating the factor λ_T, dependent on the turbulence characteristics of the approaching flow, and λ_R, dependent on the surface roughness parameter ε/D.

Subsequently, the derived formulations of the partial derivatives, $\partial C_D/\partial Re$, and $\partial C_D/\partial \varphi$, from derivations in Appendix A are listed in Table A.2 and Table A.3. As can be seen, the effective term, $\partial [C_{D0}/(1+2\varepsilon/D)]/\partial Re_e$, appears in all the equations, which basically denotes the importance of considering drag coefficient variation with respect to the effective Reynolds number, Re_e, especially within the critical Reynolds range.

Table A.1: Calculations of mean drag coefficient for two-dimensional circular cylinder (prepared from Calculation Sheet 1, ESDU 80025)

INPUT DATA

1	U_m: Wind speed (m/s)	
2	D : Cable diameter (m)	
3	φ (°) : [φ=90°- φ; φ: Cable-wind relative angle (°)]	
4	ε : Effective roughness height (m) *	
5	$\varepsilon/D \times 10^3$	
6	I_u : Turbulence intensity *	
7	rL_u : Lateral scale of turbulence (m) *	
8	$I_u(D/rL_u)^{1/5}$	

CALCULATION OF Re_e

9	λ_R : Roughness factor *	
10	$Re = U_m D \sec\phi/\nu$	
11	If $Re > 2 \times 10^6$, $\lambda_T \approx 1.0$; go to step 17	
12	λ_{Tcrit} *	
13	$Re_{crit} = 4.5 \times 10^5/((9)\times(12))$	
14	$Re/Re_{crit} = (10)/(13)$	
15	$(\lambda_T\text{-}1)/(\lambda_{Tcrit}\text{-}1)$ *	
16	$\lambda_T=(15) \times ((12)\text{-}1)+1$	
17	$Re_e=(9) \times (16) \times (10)$	

PLAIN CYLINDER NORMAL TO FLOW

18	$C_{D0}/(1+2\ \varepsilon/D)$ *	
19	C_{D0}	
20	Effect of aspect ratio, shear flow	

CYLINDER INCLINED TO FLOW

21	Re_e (steps 1 to 17)	
22	C_{D0} (step 19)	
23	if $Re_e \leq 3 \times 10^5$ go to step 25	
24	if $Re_e > 3 \times 10^5$ go to step 26	
25	C_D ($C_D = C_{D0}\times\cos^2\phi$)	
26	f_φ *	
27	C_D ($C_D = C_{D0}\times f_\phi$)	
28	If C_D (step 27) > 1.2 $\cos^2\phi$ take C_D= 1.2 $\cos^2\phi$	

* Refer to ESDU 80025 (1986) for these terms: ε {Table 10.1}; I_u {Table 10.2}; ^rL_u {Table 10.2}; λ_R {Fig.2}; λ_{Tcrit} {Fig. 3a}; $(\lambda_T\text{-}1)/(\lambda_{Tcrit}\text{-}1)$ {Fig. 3b}; $C_{D0}/(1+2\ \varepsilon/D)$ {Fig. 1}; f_φ factor giving normal force coefficient for inclined cables at supercritical Reynolds numbers {Fig. 4}

Table A.2: Derivation of partial derivative of drag force coefficient with respect to Reynolds number (Re)

$Re_e \leq 3 \times 10^5$	$C_D = C_{D0} \sin^2 \varphi$
	$\dfrac{\partial C_D}{\partial \text{Re}} = \dfrac{\partial (C_{D0} \sin^2 \varphi)}{\partial \text{Re}} = \dfrac{\partial C_{D0}}{\partial \text{Re}} \cdot \sin^2 \varphi$
	$\text{Re} = \dfrac{1}{\lambda_T \lambda_R} \text{Re}_e$
	$\partial \text{Re} = \dfrac{1}{\lambda_T \lambda_R} \partial \text{Re}_e$
	$\dfrac{\partial C_D}{\partial \text{Re}} = \lambda_T \lambda_R \dfrac{\partial C_{D0}}{\partial \text{Re}_e}$
	$\dfrac{\partial C_D}{\partial \text{Re}} = \lambda_T \lambda_R (1 + 2\dfrac{\varepsilon}{D}) \left[\dfrac{\partial (C_{D0} /(1+2\varepsilon / D))}{\partial \text{Re}_e} \right] \cdot \sin^2 \varphi$
$Re_e > 3 \times 10^5$	$C_D = C_{D0} f_\phi$
	$\dfrac{\partial C_D}{\partial \text{Re}} = \dfrac{\partial (C_{D0} f_\phi)}{\partial \text{Re}} = \dfrac{\partial C_{D0}}{\partial \text{Re}} \cdot f_\phi$
	$\dfrac{\partial C_D}{\partial \text{Re}} = \lambda_T \lambda_R (1 + 2\dfrac{\varepsilon}{D}) \left[\dfrac{\partial (C_{D0} /(1+2\varepsilon / D))}{\partial \text{Re}_e} \right] \cdot f_\phi$

*Similar formulations are applied to calculate $\partial C_D / \partial \varphi$

As an example, assume a new smooth steel stay cable with cable diameter of $D=$ 0.15 m and a roughness ratio parameter of $\varepsilon / D \times 10^3 = 0.33$. This would yield $Re_{eA} = 5.04 \times 10^5$, and $Re_{eB} = 6.26 \times 10^5$, respectively. Thus, the expected effective range of Reynolds number lies between 3×10^5 and 6.26×10^5. The results of the drag coefficient and its partial derivative in respect to the Reynolds number are presented for this cable in Figure A.2. As can be seen, the drag coefficient in the subcritical range ($Re_e \leq 3.0 \times 10^5$ or equally $Re \leq 2.46 \times 10^5$) has a constant value of $\partial C_D / \partial Re = 1.20$. After critical point ($Re_e \geq 3.0 \times 10^5$), it starts decreasing noticeably over the critical Reynolds range until reaching a minimum value of $C_D = 0.41$ at $Re = 4.71 \times 10^5$. Then, at higher Reynolds numbers, the C_D value increase slightly to $C_D = 0.43$ and finally remain constant. In addition, the variation of the

drag force coefficient in respect to Reynolds number ($\partial C_D/\partial Re$) is plotted by using a dashed line. Notable, is the significant change in the magnitude of the calculated partial derivatives over the critical Reynolds range with the minimum value of $\partial C_D/\partial Re=-8.77\times10^{-6}$ at $Re=3.90\times10^5$. The obtained curve consists of three consecutive stages: (i) nearly constant amount for C_D (in this example equals to 1.20) in the subcritical Re range up to the start of critical Reynolds number, $Re_e=3.0\times10^5$; (ii) reduction in the C_D values associated with the negative slope of $\partial C_D/\partial Re$ within the critical range ($3.0\times10^5 \le Re_e \le Re_{eB}$); and (iii) slight increase of C_D values in the supercritical Re range which finally reaches an upper limit (in this example, $C_D = 0.43$).

Table A.3: Partial derivatives of drag force coefficient with respect to Reynolds number (Re) and cable-wind relative angle (φ)

$Re_e \le 3\times10^5$	$\dfrac{\partial C_D}{\partial \mathrm{Re}} = \lambda_T \lambda_R (1+2\varepsilon/D)\left[\dfrac{\partial(C_{D0}/(1+2\varepsilon/D))}{\partial \mathrm{Re}_e}\right]\cdot \sin^2\varphi$
	$\dfrac{\partial C_D}{\partial \varphi} = \sin\varphi\cos\varphi\left[2C_{D0}-(1+2\varepsilon/D)\cdot\dfrac{\partial(C_{D0}/(1+2\varepsilon/D))}{\partial \mathrm{Re}_e}\cdot \mathrm{Re}_e\right]$
$Re_e > 3\times10^5$	$\dfrac{\partial C_D}{\partial \mathrm{Re}} = \lambda_T \lambda_R (1+2\varepsilon/D)\left[\dfrac{\partial(C_{D0}/(1+2\varepsilon/D))}{\partial \mathrm{Re}_e}\right]\cdot f_\varphi$
	$\dfrac{\partial C_D}{\partial \varphi} = -\left[\dfrac{\partial f_\varphi}{\partial \varphi}\cdot C_{D0}+f_\varphi\cdot\mathrm{Re}_e\cdot\tan\varphi\cdot(1+2\varepsilon/D)\cdot\dfrac{\partial(C_{D0}/(1+2\varepsilon/D))}{\partial \mathrm{Re}_e}\right]$

In general, experimental data by ESDU show that in the subcritical range ($Re_e < 3\times10^5$), the drag coefficients are dependent on the component of free-stream velocity normal to the cylinder axis, i.e. $U_N=U_m \sin\varphi$, and on the stream wise component of Reynolds number. Thus, the drag coefficient with respect to the normal component of flow
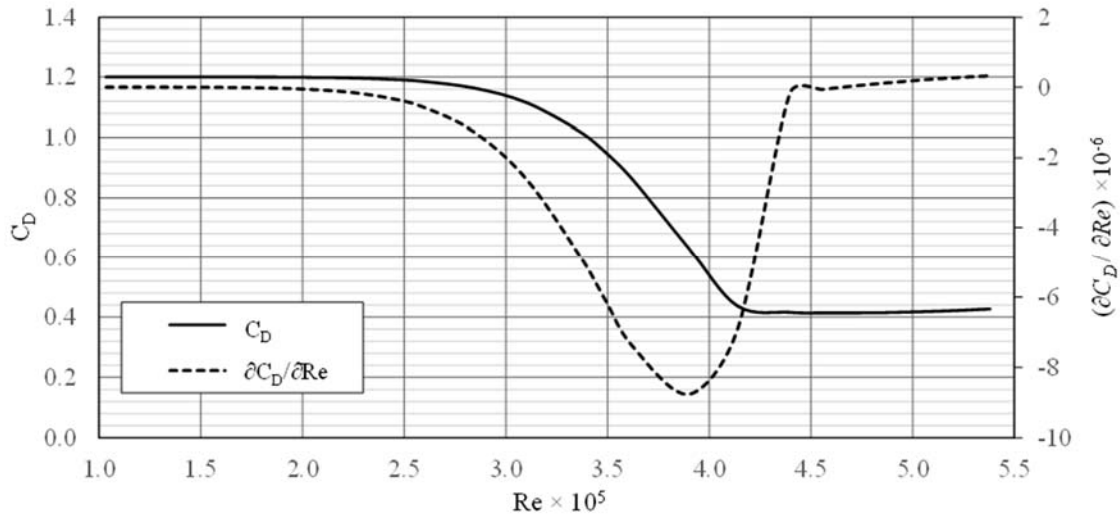
Figure A.2: Aerodynamic force coefficients of a stay cable (D=0.15 m, φ=60°) by using ESDU data set

velocity (C_{DN}) may be taken as a constant. Conversely, in supercritical flow regime when transition to turbulent flow in the boundary layer has occurred ($Re > Re_{Crit}$), separation of the boundary layer is adversely affected by the three dimensional nature of the turbulent wake flow. This would significantly influence the pressure distribution and increase the flow-induced forces. Thus, the magnitude of force coefficients in super critical regime are different in comparison to the flow-induced forces which has been predicted relying on single cross-flow theory in the subcritical range (Macdonald and Larose, 2006).

Similar variation pattern is noticeable in the NRC data set for the drag coefficients. It shows the reduction with increasing *Re*, characteristic of the critical *Re* region. Conversely, the mean lift coefficient is close to zero in the subcritical *Re* range, but in the critical range ($Re \approx 3 \times 10^5$) it has large magnitudes, particularly for *φ* close to 90°, due to the formation of single laminar separation bubble. This implies that to determine the aerodynamic damping in this region, effect of lift should not be neglected. Hence, the

measured values of the force coefficients from the NRC wind tunnel experiment are applied consequently, especially within the critical Reynolds range.

APPENDIX B

STATISTICAL METHODS ON WIND SPEED ANALYSIS

B.1 INTRODUCTION

In order to assess the reliable performance of a damped stay cable when subjected to wind load, effect of uncertainty associated with wind should be considered in a way which can be handled in a probabilistic approach. Knowing that the wind variables including the wind speed and the wind direction possess random nature, i.e. they have time-varying characteristics, thus the statistical analysis of historical data on recorded wind speed is required. The conventional statistical-based methods for identification of wind properties and prediction of extreme wind speed are divided into those based on the parent distribution analysis methods, and those based on the extreme value wind distribution analysis methods (Holmes, 2007).

In the parent probability distribution analysis method, the frequency distribution of population of recorded wind speed data at a design site will be fitted with some of the most common wind engineering probability distributions including the Weibull, the Rayleigh and the Gamma probability distributions. Then, the best-fitted probability distribution will be selected by means of a numerical technique such as Root Mean Square Error (RMSE) or Correlation Coefficient (R). The adapted distribution could be applied to estimate the probability of occurrence of a certain wind speed or to predict the extreme wind speed corresponding to a selected design return period.

Alternatively, the generalized extreme value (GEV) distribution analysis method is available. In this method, the magnitudes of annual extreme wind speeds at the design site

over the studied time period are collected and accordingly the cumulative density function (CDF) is calculated. It has been shown that the adapted CDF tends to converge to certain limiting forms of the asymptotic extreme-value distributions including the Gumbel (Type I), the Frechet (Type II), and the Weibull (Type III) (Fisher and Tippette, 1928). Then, the goodness-of-fit of the distribution models will be compared, which depends on the form of the tail of the underlying parent distribution. Finally, by performing an inverse analysis of the results of the corresponding cumulative distribution function, the value of extreme wind speed can be calculated for the expected structural design return period at the studied site.

This Appendix is organized as follows: In Section B.2, the basic concepts of parent probability distribution analysis are reviewed. The probability distributions relevant to wind engineering, including the Weibull, the Rayleigh, and the Gamma distributions are summarized with pertinent details presented in each section. In Section B.3, the theory of the generalized extreme value distribution models is described. The three extreme value distributions, i.e. Gumbel (Type I), Frechet (Type II), and Weibull (Type III) probability distribution models are reviewed and available approaches on fitting the extreme wind speeds including the plotting position method (i.e. Gumbel fitting regression technique) and the Probability Weighted Moments (PWM) method are explained. The comparison tool on evaluating the goodness-of-fit of the distribution models to wind speed data set by using Kolmogorov test is discussed. Subsequently, the calculations on prediction of extreme wind speed corresponding to a desired design return period are shown. In conclusion, Section B.5 summarizes the contents of this chapter.

B.2 PARENT PROBABILITY DISTRIBUTION ANALYSIS

The wind speed variation at a given site is usually described by using the probability distribution functions. The parent probability distribution analysis aims at simplifying the behavior of wind velocity at a given site by fitting the real wind speed data into a definite form of a probability distribution function. Accordingly, the selected distribution model will be chosen to provide a mathematical expression as an approximate probability density function (PDF) of the available database. This is attainable by simply determining associated parameters of the selected PDF using a mathematical fitting technique.

Over the past few decades, a number of studies have been conducted on the use of probability density functions for modeling of the wind speed around the world (e.g. Hennesessey, 1977; Torres et al., 1998; Waewsak et al., 2011). Some of these density functions include the Weibull, Rayleigh, Gamma, Lognormal, Exponential, and Gaussian etc. Among these methods, the Rayleigh and the Weibull functions are the widely accepted and extensively used statistical models for wind speed and energy applications. The following section presents the basics of these parent probability distribution functions with particular application to wind velocity.

B.2.1 Rayleigh distribution

This distribution is suitable to describe wind speed U independent of wind direction (Olaofe and Folly, 2012). A continuous wind speed variable U is said to have a Rayleigh distribution if its probability density function (PDF) is given by

$$f(U) = \frac{U}{\alpha^2} \exp(\frac{-U^2}{2\alpha^2}) \tag{B-1}$$

where U is the wind speed variable, and α is the scale parameter which can be deduced from the given wind speed datB. Accordingly, the cumulative density function (CDF) of the Rayleigh distribution can be obtained by integrating the $f(U)$ over the specified velocity range $U \leq U_i$, which is

$$F(U) = 1 - \exp(\frac{-U^2}{2\alpha^2}) \qquad \text{(B-2)}$$

Replacing $U=U_i$ in the above equation would yield the value of CDF at wind speed U_i. The scale parameter α in the Rayleigh distribution can be approximately evaluated for a set of N data points of wind speed, U_i. Figure B.1 shows the Rayleigh CDF curves for different scale parameters. Since the Rayleigh scale parameter, α, is proportional to the mean wind speed, its spatial variation shows a pattern similar to the mean wind speed in the existing wind speed database.
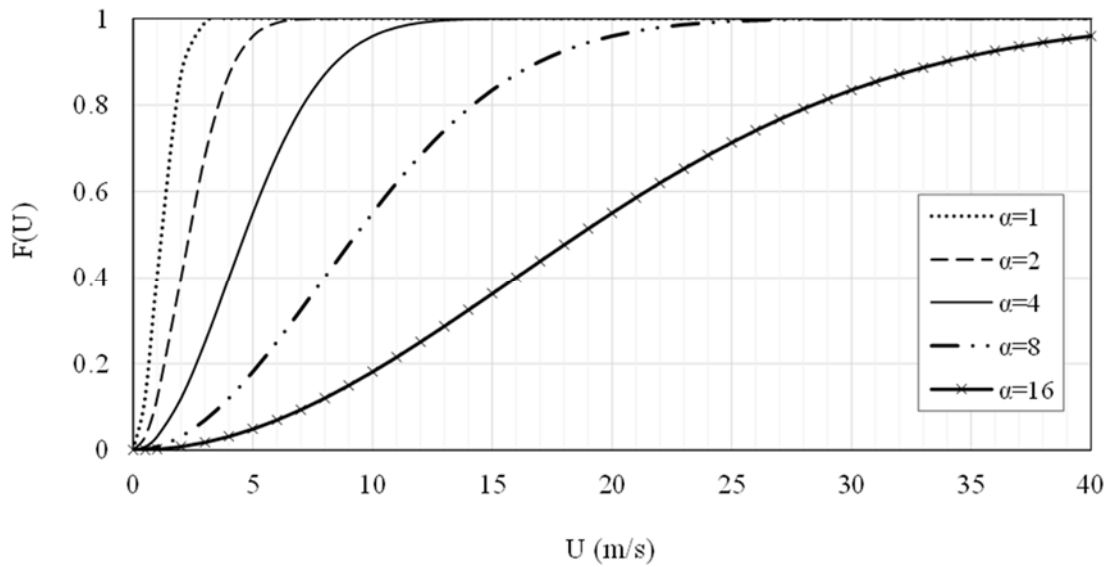
Figure B.1: Rayleigh CDF curves (α=1, 2, 4, 8, 16)

Mathematically, when experimental data are used to determine parameters in probability distributions, the computed result is called an estimate of the true parameter (Elishakoff, 1999). Here in the case of a Rayleigh distribution, we use the symbol $\hat{\alpha}$ to indicate that the equation below gives us an estimate of the true distribution parameter, α.

$$\hat{\alpha} = \sqrt{\frac{1}{2N} \sum_{i=1}^{N} U_i^2} \qquad \text{(B-3)}$$

Table B.1: Properties of the Rayleigh distribution

Scale parameter	$\alpha > 0$
Support	$U \in [0,+\infty]$
PDF	$\dfrac{U}{\alpha^2} \exp(\dfrac{-U^2}{2\alpha^2})$
CDF	$1 - \exp(\dfrac{-U^2}{2\alpha^2})$
Mean	$\alpha\sqrt{\dfrac{\pi}{2}}$
Median	$\alpha\sqrt{\ln(4)}$
Mode	α
Variance	$\dfrac{4-\pi}{2}\alpha^2$

To determine the goodness of fit (i.e. how well the data fits the distribution) for the assigned Rayleigh distribution, it is required to determine the mean and standard deviation of the experimental wind speed data.

The minimum-least-squares-error (MLE) estimate of the mean of the wind speed distribution is the arithmetic mean (the sum of all values divided by the number of values, N), i.e.

$$\overline{U} = \frac{1}{N} \sum_{i=1}^{N} U_i \qquad \text{(B-4)}$$

The formula for the MLE estimate of the variance, s^2, is also defined by (Elishakoff 1999)

$$s^2 = \frac{1}{N-1} \sum_{i=1}^{N} \left(U_i - \overline{U} \right)^2 \qquad \text{(B-5)}$$

The discrepancy between the obtained value of the true variance s^2 for the experimental data in Eq. (B-5) and the variance $\sigma^2 = (4-\pi)/2 \cdot \alpha^2$ of a Rayleigh distribution with scale parameter α, determines the goodness of fit for the calculated Rayleigh distribution. A summary of the statistical properties of the Rayleigh distribution is listed in Table B.1.

B.2.2 Weibull distribution

The Weibull function is the most widely used function among the several distribution functions for modeling wind speed at a given site due to its simplicity and ability to closely mirror the distribution of observed wind speeds (Akpinar and Akpinar, 2004; Ohunakin, 2011). The Weibull distribution can only be used for random variables that are always positive. It is often used as the parent distribution to represent nature of the wind (variability or stability of the wind). The two-parameter Weibull probability distribution function for the wind speed database with the wind speed U and the directional angle γ is given by

$$f(U,\gamma) = \frac{k(\gamma)}{c(\gamma)} \cdot \left(\frac{U}{c(\gamma)}\right)^{k(\gamma)-1} \exp\left[-\left(\frac{U}{c(\gamma)}\right)^{k(\gamma)}\right] \qquad \text{(B-6)}$$

where $c(\gamma)>0$ is the scale parameter, and $k(\gamma)>0$ is the shape parameter. The simple form of the PDF of a Weibull model by disregarding effect of wind direction angle can be simply written as (Montgomery and Runger, 2003)

$$f(U) = \frac{k}{c} \cdot \left(\frac{U}{c}\right)^{k-1} \exp\left[-\left(\frac{U}{c}\right)^{k}\right] \qquad \text{(B-7)}$$

If U has a Weibull distribution with parameters c and k, then the cumulative distribution function (CDF) of U is

$$F(U) = 1 - \exp\left[-\left(\frac{U}{c}\right)^{k}\right] \qquad \text{(B-8)}$$

The above equation can be used to determine the possibility of the occurrence of an observed wind speed, equals or below U.

As shown in Figure B.2, the shape of the PDF for the Weibull distribution is quite sensitive to the value of the shape parameter, k. If k increases for a given value of c, the maximum in the PDF will increase. Because of this, k is called the shape parameter; noting that it is dimensionless. As the value of c increases for a given value of k, the shape of the distribution gets wider based on Eq. (B-7). Because of this, c is called the scale parameter; it has dimension of velocity, U. For most fair wind site, the value of the shape parameter k ranges between 1.5 and 2.5. The Weibull distribution with $k=2$ is a special case known as the Rayleigh distribution. Smaller values of $k \leq 1.5$ correspond to highly variable or gust

wind, whereas $k=2$ corresponds to moderate wind speed and $k \geq 3$, indicates regular, steady wind (Olaofe and Folly 2012).
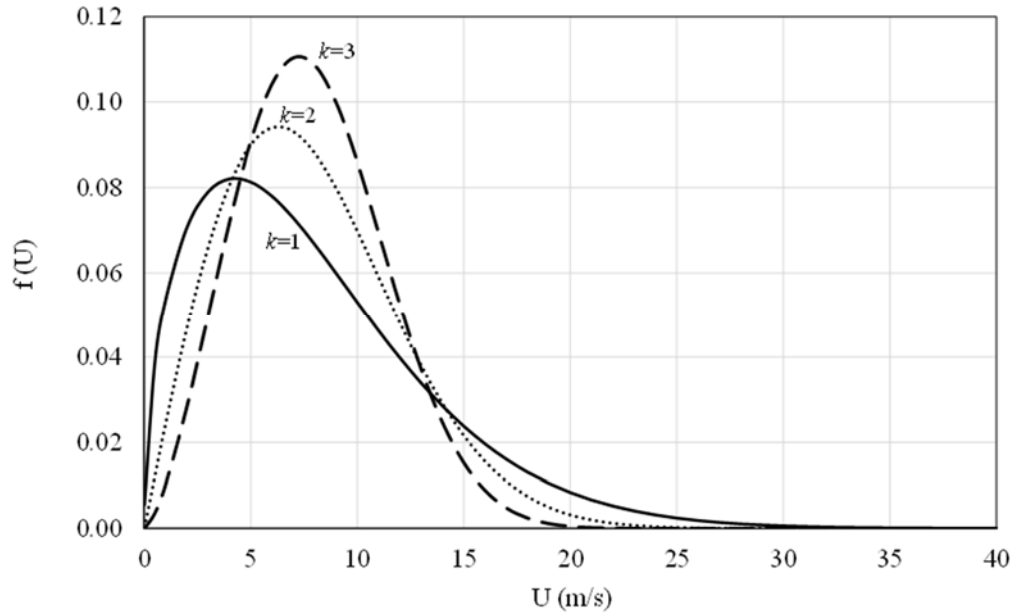
Figure B.2: Probability density function (PDF) for Weibull

A number of methods have been developed to estimate the Weibull parameters (Seguro and Lambert, 2000; Costa Rocha et al., 2012; Saleh et al., 2012). The maximum likelihood, graphic, moment, Chi-square, and regression methods are commonly used in fitting wind speed frequency distribution using the Weibull function.

To fit the Weibull distribution for the wind speed database by using the regression method, the following steps are required (Palutikoff, 1999):

1- Calculate the probability of occurrence of wind speed $U > u$ by applying the following formulations to the cumulative density function of the wind speed database extracted from the field:

$$P(> u) = \exp\left[-\left(\frac{u}{c}\right)^k\right] \qquad \text{(B-9)}$$

$$\ln[P(> u)] = -\left[\left(\frac{u}{c}\right)^k\right] \qquad \text{(B-10)}$$

$$\ln\{-\ln[P(> u)]\} = k\{\ln(u) - \ln(c)\} \qquad \text{(B-11)}$$

2- Plot the Weibull CDF curve corresponding to wind speed database in which the vertical axis is $\ln\{-\ln[P(>u)]\}$ and the horizontal axis equals to $\ln(u)$.

3- Apply a linear regression to the plotted curve. Slope of the fitted line is the value of the shape parameter k, and the horizontal eccentricity of the fitted line is $\ln(c)$.

Figure B.3 shows a schematic view of the Weibull distribution fitting procedure and determination of the Weibull parameters, c and k. Table B.2 summarizes the properties of the Weibull distribution.
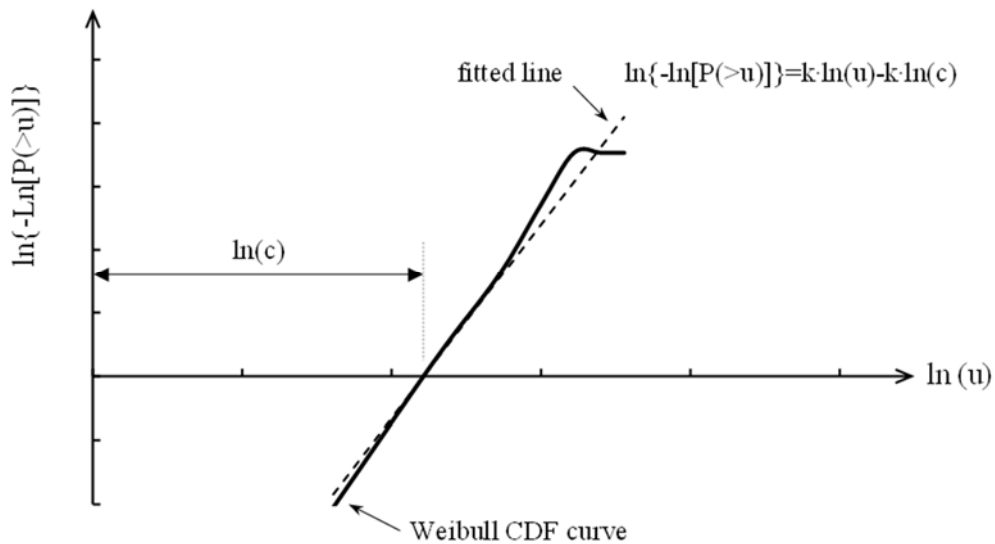
Figure B.3: Weibull distribution fitting

Table B.2: Properties of the Weibull distribution

Parameters	Scale parameter $c > 0$
	Shape parameter $k > 0$
Support	$U \in [0,+\infty]$
PDF	$\dfrac{k}{c}(\dfrac{U}{c})^{k-1} e^{(\frac{-U}{c})^k}$
CDF	$1 - e^{-(\frac{U}{c})^k}$
Mean	$c\,\Gamma(1+\dfrac{1}{k})$
Median	$c(\ln(2))^{1/k}$
Mode	$c(\dfrac{k-1}{k})^{1/k}$
Variance	$c^2[\Gamma(1+\dfrac{2}{k}) - (\Gamma(1+\dfrac{1}{k}))^2]$

$\Gamma(\cdot)$ is the Gamma function

B.2.3 Gamma distribution

The probability density function of a Gamma distribution is defined by (Montgomery and Runger, 2003)

$$f(U) = \frac{U^{k-1}}{c^k \Gamma(k)} \exp\left[-\left(\frac{U}{c}\right)\right] \tag{B-12}$$

where c and k are the shape and the scale parameters, respectively, and $\Gamma(\cdot)$ is the Gamma

function defined by $\Gamma(k) = \int\limits_{o}^{\infty} U^{k-1} e^{-U} dU$. Accordingly, the cumulative distribution

function is given by

$$F(U) = \frac{1}{c^k \Gamma(k)} \int_o^U U^{k-1} \exp\left[-\left(\frac{U}{c}\right)\right] dU \qquad \text{(B-13)}$$

The moment estimators of the Gamma distribution are defined by the following equations

$$\hat{k} = \left(\frac{\overline{U}}{s}\right)^2 \qquad \text{(B-14)}$$

$$\hat{c} = \frac{s^2}{\overline{U}} \qquad \text{(B-15)}$$

where $\overline{U}$ and s are the sample mean and standard deviation, respectively. The Gamma distribution function is found applicable to the modeling of low wind speed data and modeling errors in multi-level Poisson regression models. A summary of the properties of Gamma distribution is presented in Table B.3.

Table B.3: Properties of the Gamma distribution

Parameters	Scale parameter $c > 0$
	Shape parameter $k > 0$
Support	$U \in [0, +\infty]$
PDF	$f(U) = \frac{U^{k-1}}{c^k \Gamma(k)} \exp\left[-\left(\frac{U}{c}\right)\right]$
CDF	$F(U) = \frac{1}{c^k \Gamma(k)} \int_o^U U^{k-1} \exp\left[-\left(\frac{U}{c}\right)\right] dU$
Mean	k
Mode	k-1 $k \geq 1$
Variance	$\sqrt{k}$
Skewness	$2/\sqrt{k}$
COV	$1/\sqrt{k}$

B.2.4 Goodness of fit

The probability density function of an actual distribution (field database), f_a, for wind speed variable U with the mean $\overline{U}$ and standard deviation s is defined as:

$$f_a = \frac{1}{s\sqrt{2\pi}} \exp\left[-\frac{(U-\overline{U})}{2s^2}\right] \tag{B-16}$$

Use the maximum likelihood estimator (MLE), which is also called the biased estimator, the standard deviation in terms of the sampled wind speed data U_i with population size N, and the mean wind speed $\overline{U}$ can be defined as:

$$s = \sqrt{\frac{1}{N}\sum_{i=1}^{N}(U_i - \overline{U})^2} \tag{B-17}$$

There are several tests used for validating the accuracy of the predicted wind distribution obtained from various statistical functions. The wind speed distributions obtained from these functions indicate whether there is an accurate modeling of the wind speed, or that the functions fail to accurately model the wind speed at a given site.

Root Mean Square Error (RMSE)

The RMSE has been used for comparison of the actual deviation between the predicted and the actual (measured) values. The root mean square error value is defined by:

$$RMSE = \left[\frac{\sum_{i=1}^{N}(y_i - U_i)^2}{N}\right]^{\frac{1}{2}} \tag{B-18}$$

where U_i is the ith wind speed value from the actual distribution, y_i is the ith predicted wind speed from the fitted distribution (i.e. Weibull, Rayleigh, Gamma functions, etc.), and N is the number of the wind speed samples in the data set. Here, the actual wind speed distribution can be obtained from Eq. (B-16) and the predicted wind distributions are also obtained from the Weibull, Rayleigh and Gamma functions.

Correlation Coefficient (R)

The correlation coefficient is a statistical technique that is used to determine the linear relationship between two data sets. The mathematical equation for R is defined as

$$R = \frac{\sum_{i=1}^{N}(U_i - \overline{U})(y_i - \overline{y})}{\sqrt{\sum_{i=1}^{N}(U_i - \overline{U})^2 \sum_{i=1}^{n}(y_i - \overline{y})^2}} \tag{B-19}$$

where $\overline{U}$ and $\overline{y}$ are the mean of the actual and the assigned wind speed distribution models, respectively. The value of R always lies between -1 and 1, and is greater than the value of R^2.

B.3 THE GENERALIZED EXTREME VALUE DISTRIBUTION (GEV) ANALYSIS

It has been shown by Fisher and Tippett (1928) that if a sample of n cases is chosen from a parent distribution, and the maximum of each sample is selected, then the distribution of the maxima approaches one of the three limiting forms, including Gumbel (Type I), Frechet (Type II), and Weibull (Type III) distribution models, as the size of the samples increases. Thus, the Fisher-Tippett distributions could be fitted to the set of annual

maxima of wind speed database. In practice, there will be a finite number in a wind speed population, but in order to make predictions, the asymptotic extreme value distributions are used as empirical fits to the annual extreme wind speed data. Which one of the three is theoretically "correct" depends on the form of the tail of the underlying parent distribution. This is the basis of the classical extreme value theory. The aim is to define the form of the limiting distribution and estimate the parameters, so that values of extreme wind speed can be calculated.

Later, the generalized extreme value distribution was introduced by Jenkinson (1955) by combining three extreme value distributions into a single mathematical form which has been widely applied in wind engineering as follows:

$$F(U) = \exp\left\{-\left[1 - k\frac{(U-u)}{\alpha}\right]^{\frac{1}{k}}\right\}$$
(B-20)

where $F(U)$ is the cumulative probability distribution function of random wind speed variable U. The parameters α, u and k are the scale factor, the location factor and the shape factor, respectively. In the case of $k = 0$, $k > 0$, and $k < 0$, this equation will become the Type I extreme value distribution (Gumbel distribution), the Type II extreme value distribution (Frechet distribution), and the Type III extreme value distribution (Weibull distribution), respectively. The GEV with different shape factors (k=-0.2, 0, 0.2) are plotted in Figure B.4, assuming scale factor a=1.0 and location factor u=0. It is noteworthy to mention that Type I and Type II predict unlimited values for the extreme wind speeds. They are therefore suitable distributions for variables that are unbounded. Since we would expect that there is an upper limit to the wind speed that the atmosphere can produce, the Type III distribution may be more appropriate for statistical wind speed analysis.

Accordingly, the Type III extreme distribution methods including the three-parameter Weibull model (Weibull 3P) and the two-parameter Weibull model (Weibull 2P) can be applied to estimate the values of the extreme wind speed. However, the Type I extreme distribution method (Gumbel method) would be applied to wind speed database as a primary method due to its simplicity in formulation among other methods. For the purpose of completeness in statistical comparison, the Frechet distribution (Type II) will also be employed to fit the annual extreme wind speed database. Finally, the Kolmogorov test method as a statistical-error-identifier tool will be introduced to comment on the goodness-of-fit of the assigned distributions.
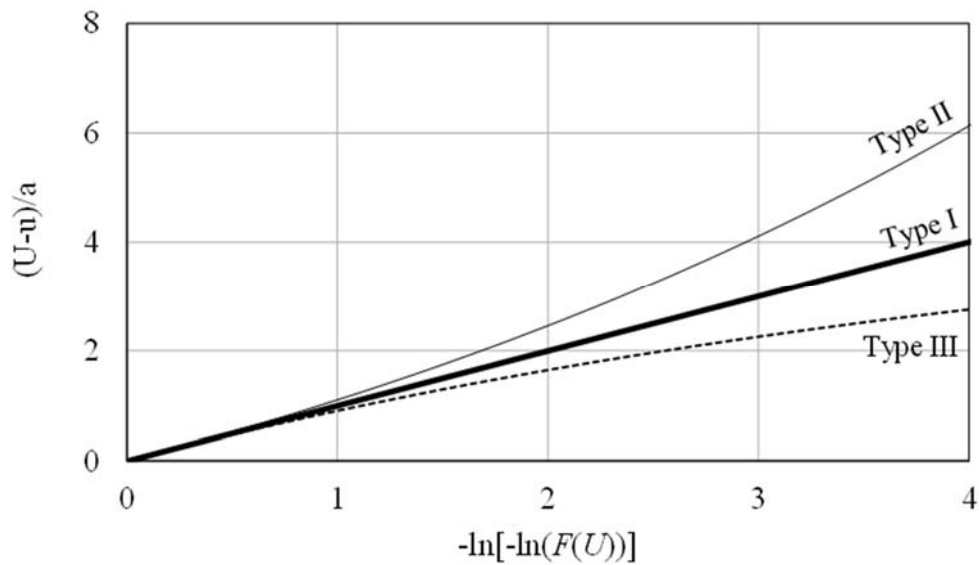

Figure B.4: The GEV distribution curves (a =1.0, u = 0, k = -0.2, 0, 0.2)

B.3.1 Gumbel distribution

The most commonly used distribution of the three generalized extreme value distribution is Type I, which is also known as the Gumbel distribution. It is especially used

to describe the distribution of annual maximum wind speed. The cumulative distribution function, $F(U)$, of Type I distribution can be written in the following form:

$$F(U) = \exp\left\{-\exp\left[-\frac{(U-u)}{\alpha}\right]\right\}$$ (B-21)

The corresponding probability density function (PDF), $f(U)$, is

$$f(U) = \frac{1}{\alpha}\exp\left[-\frac{(U-u)}{\alpha}\right]\exp\left\{-\exp\left[-\frac{(U-u)}{\alpha}\right]\right\}$$ (B-22)

The scale parameter α, and the mode of the distribution u, can be obtained by applying a linear regression analysis to the wind speed database which is known as the "plotting position method". The following procedure has been suggested by Gumbel (1958):

- Determine the number of calendar years considered for the analysis;

- Find the maximum wind speed in each calendar year, i.e. the annual maximum wind speed, and rank them from low to high;

- Assign a probability of non-exceedence, p, to each annual maxima, according to Gringorten (1963) formula, $p \approx (m\text{-}0.44)/(N\text{+}0.12)$; where N is the number of the calendar years considered, and m is the rank number for each wind record;

- Calculate a reduced variate, y, for each annual maximum wind speed as $y = -\ln(-\ln p)$;

- Plot the annual maximum wind speed, U, against the corresponding reduced variate y, and perform linear regression to draw the best-fit line. The slope of this line is

the scale parameter, α, and the shape parameter, u, is the intersection on the annual maxima wind speed axis.

Therefore, the equation for prediction of the annual maximum wind speed can be simply represented in a form of a linear equation as

$$U = ay + u \qquad\qquad (B\text{-}23)$$

B.3.2 Weibull distribution

Another existing model for describing the probability distribution of extreme values is the Weibull distribution model. The method can be applied to the extreme wind speed database using the three-parameter Weibull distribution model (Weibull 3P) and the two-parameter Weibull distribution model (Weibull 2P).

The three-parameter Weibull distribution (Weibull 3P)

If an extreme wind speed variable U obeys a three-parameter Weibull distribution, the cumulative distribution function $F(U)$ and the probability density function $f(U)$ of U are given by (Palutikof, 1999):

$$F(U) = 1 - \exp\left[-\left(\frac{U-\lambda}{\alpha}\right)^{\beta}\right], \quad if\ U \geq \lambda \qquad\qquad (B\text{-}24)$$

$$f(U) = \frac{\beta}{\alpha}\left(\frac{U-\lambda}{\alpha}\right)^{\beta-1}\exp\left[-\left(\frac{U-\lambda}{\alpha}\right)^{\beta}\right], \quad if\ U \geq \lambda \qquad\qquad (B\text{-}25)$$

where the three parameters α, β and λ are the scale parameter, the shape parameter and the location parameter, respectively.

The values of these parameters can be determined by the method of probability weighted moments (PWMs). The Weibull distribution moments are defined as follows:

$$\mu_k = \int_0^\infty [R(U)]^k \, dU = \lambda + (\alpha / k^{1/\beta}) \Gamma(1 + 1/\beta) \tag{B-26}$$

where $R(U) = 1 - F(U)$ and k is the moment estimator index (normally selected to be 1, 2, and 4).

The estimated value of μ_k is:

$$m_k = \sum_{i=0}^{n-1} (1 - i/n)^k (U_{i+1} - U_i) \tag{B-27}$$

For $\mu_k = m_k$, $k = 1$, 2 and 4. The estimated three parameters can be determined by the following three equations:

$$\hat{\beta} = \ln(2) / \ln[(\mu_1 - \mu_2)/(\mu_2 - \mu_4)] \tag{B-28}$$

$$\hat{\lambda} = (\mu_1 \mu_4 - \mu_2^2)/(\mu_1 - 2\mu_2 + \mu_4) \tag{B-29}$$

$$\hat{\alpha} = (\mu_1 - \gamma)/\Gamma(1 + 1/\beta) \tag{B-30}$$

The two-parameter Weibull distribution (Weibull 2P)

If disregard the location parameter λ in the three-parameter Weibull model (i.e. $\lambda = 0$), the model becomes a two-parameter Weibull (Weibull 2P). Hence, the modified expressions of PDF and CDF are as follow:

$$F(U) = 1 - \exp\left[-\left(\frac{U}{\alpha} \right)^\beta \right] \tag{B-31}$$

$$f(U) = \frac{\beta}{\alpha} \left(\frac{U}{\alpha} \right)^{\beta - 1} \exp\left[-\left(\frac{U}{\alpha} \right)^\beta \right] \tag{B-32}$$

The estimation of α and β for the two-parameter Weibull model is relatively simple. By using the least-square method, the values of α and β can be determined. It is noticed that, if the natural logarithm is applied twice to both sides of CDF, then one has

$$\ln[-\ln(1 - F(U))] = -\beta \ln \alpha + \beta \ln U \qquad \text{(B-33)}$$

This leads to a straight line on a double logarithmic plot, i.e.

$$Y = b + \beta z \qquad \text{(B-34)}$$

where

$$Y = \ln[-\ln(1 - F(U)] \qquad \text{(B-35)}$$

$$b = -\beta \ln \alpha \qquad \text{(B-36)}$$

$$z = \ln U \qquad \text{(B-37)}$$

As the transformation $z = \ln U$ can be performed easily, a straight line can readily be obtained, and thus the two parameters α and β are determined.

B.3.3 Frechet distribution

This distribution does not seem to have received enough interest in the statistical wind speed analysis, due to the fact that the atmosphere would produce a limited value for the maxima of wind speed and the Frechet method entails an unbounded value for its higher end. Therefore, it lacks capability to be fitted for the annual extreme wind speed data set. However, it has been used as a useful method for modeling and analyzing several extreme events such as the accelerated life testing, earthquake, flood, rainfall, and sea current probability density function (Harlow, 2002; Nadarajah and Kotz, 2008; Abbas and Tang, 2013).

The CDF for the Frechet distribution is given by

$$F(U) = \exp\left[-\left(\frac{\alpha}{U}\right)^k \right]$$

(B-38)

where α and k are the scale and shape parameters, respectively.

It is worth noting that the Frechet distribution is equivalent to taking the reciprocal of values from a Weibull distribution. Therefore, the probability density function (PDF) of the Frechet distribution is given by:

$$F(U) = \frac{k}{\alpha}\left(\frac{\alpha}{U}\right)^{k+1} \exp\left[-\left(\frac{\alpha}{U}\right)^k \right]$$

(B-39)

The method of maximum likelihood (ML) as the most popular fitting technique can be applied to estimate the parameters of the Frechet distribution (Abbas and Tang, 2013).

B.3.4 Comparison of GEV distribution models using Kolmogorov test

In order to verify the goodness-of-fit of the distribution model to wind speed data (annual extreme wind speed data), the Kolmogorov test should be conducted (Xiao et al., 2006). According to the Kolmogorov test method, the distribution function of the parent set U is called by $F(U)$. The empirical distribution function is also defined by

$$F_N^*(U) = \frac{n}{N} \quad n = 1, 2, ..., N-1$$

(B-40)

where n is the field cumulative frequency and N is the sample size.

Define the statistical term D_N as:

$$D_N = \max_{1 \leq k \leq N} | F_N^*(U) - F(U) |$$

(B-41)

If a confidence level related parameter, q, is given, the critical value of D_q can be found in the critical value table of the Kolmogorov test method according to the sample size N and the confidence level q. As the value of D_N is equal to the maximum value of the difference between the cumulative probability obtained from the observed frequency distribution and that calculated from the distribution model, so the smaller the value of D_N is, the better the distribution fitting will be. If $D_N \leq D_q$, then the distribution fitting is good, otherwise the fitting is not satisfactory. Usually the confidence level is taken to be 90%, and thus $q = 0.1$ (Montgomery and Runger 2003). Accordingly, the statistical term D_N can be used as a quantitative-based confidence parameter to evaluate goodness-of-fit of different GEV distribution models.

B.4 PREDICTION OF EXTREME WIND SPEED CORRESPONDING TO RETURN PERIOD R

It is of interest to predict the value of extreme wind speed because obtained results would be necessary in identifying the maximum attainable wind speed at a design site. Knowing that the return period, R, is directly related to the cumulative distribution function, $F(U)$, of wind speed database at a site, the following equation is established

$$R = \frac{1}{1 - F(U)} \tag{B-42}$$

Substituting for $F(U)$ from the results of the fitted distribution models, the extreme wind speed corresponding to selected return period R can be calculated which is denoted here by $U_{ext}(R)$. Due to stochastic nature of wind, probability of annual extreme wind speed U to be less than or equal to $U_{ext}(R)$ in N-discrete events (i.e. N years) is calculated by

assuming an independent relationship between probability of occurrence of each single wind speed when $U \leq U_{ext}$. This is given by:

$$P(U \leq U_{ext}(R)) = \left[P(U \leq U_{ext}) \right]^N \qquad \text{(B-43)}$$

where $U_{ext}(R)$ is the extreme wind speed corresponding to return period R, and U_{ext} is the estimated annual extreme wind speed. Accordingly, the probability of occurrence of non-exceeding wind speed $U_{ext}(R)$ is obtained by taking the complementary part of Eq. (B-43) as:

$$P(U \leq U_{ext}(R)) = 1 - P(U > U_{ext}(R)) = 1 - \left[P(U > U_{ext}) \right]^N \qquad \text{(B-44)}$$

The extreme wind speed value corresponding to return period R can be obtained by performing an inverse analysis of the results of the cumulative distribution function for the selected distribution model knowing that:

$$F(U_{ext}) = 1 - P(U > U_{ext}(R)) \qquad \text{(B-45)}$$

The above equation can be used by both types of distribution models, including the parent probability distribution and the generalized extreme value (GEV) distribution models, to determine the extreme wind speed corresponding to desired structural return period.

B.4.1 Parent probability distribution analysis

Assume that a Weibull distribution with scale and shape parameters, c and k, is fitted to wind speed database, then the probability of occurrence of wind speed $U > U_{ext}(R)$ can be written as:

$$P(U > U_{ext}(R)) = N \cdot e^{\left[-\frac{U_{ext}(R)}{c} \right]^k} \qquad \text{(B-46)}$$

where N is defined over the period of interest as:

$$N = v \cdot T \qquad \text{(B-47)}$$

Here v is the representative frequency of the events (cycling rate), and T is the period of interest. Substitute N from Eq. (B-47) into Eq. (B-46) and apply Eq. (B-45) to Eq. (B-42), the following equation is obtained:

$$\frac{1}{R} = v \cdot T \cdot e^{[-\frac{U_{ext}(R)}{c}]^k} \qquad \text{(B-48)}$$

where R is the annual risk of exceedence (i.e. return period). Thus, the general equation for extreme wind speed corresponding to return period R can be written as:

$$U_{ext}(R) = c[\ln(R \cdot v \cdot T)]^{\frac{1}{k}} \qquad \text{(B-49)}$$

where $U_{ext}(R)$ is the extreme wind speed corresponding to return period of R. Let's consider $T=1$ year (8766 hrs) and $v=0.11$/hr (typically). Thus, the simplified form of $U_{ext}(R)$ is:

$$U_{ext}(R) = c[\ln(960R)]^{\frac{1}{k}} \qquad \text{(B-50)}$$

in which, the extreme wind speed corresponding to return period R is calculated for the fitted Weibull distribution with scale and shape parameters, c and k, respectively.

B.4.2 GEV distribution

Assume that the cumulative density function of a Gumbel distribution (Type I), Eq. (B-21), is substituted into Eq. (B-42), then the derivation for the extreme wind speed would yield:

$$U_{ext}(R) = u + a\left\{-\ln\left[-\ln\left(1-\frac{1}{R}\right)\right]\right\} \qquad \text{(B-51)}$$

For large values of return period, R, Eq. (B-51) can be reduced to:

$$U_{ext}(R) \cong u + a \ln(R) \qquad \text{(B-52)}$$

The proposed equation for estimation of the extreme wind speed using Gumbel distribution model (Type I) can be criticized due to the fact that Eq. (B-52) predicts unlimited values of $U_{ext}(R)$ as the return period R increases, while on physical grounds, there must be an upper limit to the wind speeds that can be generated in the atmosphere in different types of storms.

B.5 A CASE STUDY

In this section, the application of the two statistical approaches on the analysis of recorded wind speed data at the design site Toronto Lester B. Pearson Int'L A. Ontario, Canada will be shown. The historical wind speed data are collected from the Environmental Canada Meteorological website covering years 1957 to 2012 (56 years). Measurement was taken at the height of 173.4 m above the sea level at the studied station. They are available in the form of an average hourly wind speed including their direction at each time step. Table B.4 shows a sample set of wind data on Aug 15th, 2012. The wind direction is recorded in degree showing the direction of the wind speed vector at each hour relative to the North geographical direction (Base Azimuth). The recording process was classified by dividing the wind rose into 36 different sectors. Each sector covers an angle range of 10°, assuming that the Base Azimuth is located in Sector 1.

First, the parent probability distribution analysis method will be performed by applying the Weibull, Rayleigh and Gamma distribution models to the average hourly wind speed observations. The accuracy of predicted wind distributions will be examined by

applying the RMSE test method. In the next section, the generalized extreme value distribution analysis will be applied to the wind data set. The Gumbel (Type I), Frechet (Type II), and Weibull (Type III) distributions will be fitted to the recorded annual extreme wind speed data. The goodness-of-fit of the GEV distribution models will be examined through a Kolmogorov-based statistical test. Finally, the extreme wind speed corresponding to selected return period will be evaluated at the studied design site by applying an inverse analysis of the cumulative density function of the fitted distribution models.

Table B.4: Average hourly mean wind speed recorded at station Toronto Lester B. Pearson Intl. A. for Aug 15th, 2012

Time	Wind Direction (°)	Wind Speed (m/s)
0:00	340	3.06
1:00	310	2.50
2:00	310	2.50
3:00	310	3.06
4:00	310	3.61
5:00	310	3.61
6:00	320	4.17
7:00	340	6.11
8:00	340	5.28
9:00	360	4.72
10:00	330	5.28
11:00	330	4.72
12:00	350	5.28
13:00	360	5.56
14:00	340	6.11
15:00	340	4.72
16:00	10	3.61
17:00	340	1.94
18:00	20	1.94
19:00	10	5.28
20:00	360	4.72
21:00	360	4.17
22:00	360	4.17
23:00	350	3.61

B.5.1 Parent probability distribution analysis

To perform the parent probability distribution analysis, it is necessary to have information on the distribution of wind speed and direction of the complete population at a site over the studied years. This is done for the current example by collecting the details of the measured wind speed over the years 1957-2012 by simply classifying them into 7 different wind speed levels at the studied directional sectors. The wind speed ranges are considered to represent the wind conditions; knowing that the lower wind speed range (0-5 m/s) describes calm and/or light wind condition and the upper range (30-35 m/s) describes strong storms. Hence, as follows each record of the wind speed is assigned to its corresponding wind speed range and direction. Table B.5 presents a summary of the percentage of observations of the wind speed data set. Here, the probability distribution frequency of average hourly wind speed for each sector is calculated by dividing the number of occurrence of each wind speed to the total number of recorded wind speed over the period of 56 years. By summing up the percentage of observations at each wind speed range (i.e. in each column), the non-directional wind speed frequency and accordingly the cumulative density function (CDF) can be calculated as listed in Table B.6.

Rayleigh distribution analysis

The calculation steps to fit a Rayleigh distribution to the available wind speed data set in Table B.6 are as follow:

1- Calculate the MLE estimate of the mean wind speed and the variance of the experimental wind speed data set. It is resulted in $\overline{U} = 8.35$ m/s and $s^2{=}25.88$ (m/s)^2, respectively.

Table B.5: Percentage of wind speed observations at Toronto Lester B. Pearson Int'l A. Ontario Canada station (1957-2012)

Wind sector		Direction (°)	Wind speed (m/s)						
			0~5	5~10	10~15	15~20	20~25	25~30	30~35
N	1	0	0.361	0.831	0.337	0.093	0.015	0.004	0.000
	2	10	0.387	0.721	0.413	0.143	0.052	0.028	0.009
	3	20	0.213	0.408	0.154	0.045	0.020	0.014	0.003
	4	30	0.457	0.856	0.428	0.141	0.018	0.005	0.000
	5	40	0.167	0.280	0.196	0.049	0.025	0.019	0.006
	6	50	0.287	0.290	0.129	0.055	0.040	0.026	0.010
	7	60	0.492	0.426	0.149	0.024	0.003	0.013	0.000
	8	70	0.330	0.356	0.173	0.036	0.014	0.006	0.000
	9	80	0.374	0.774	0.541	0.121	0.019	0.004	0.002
E	10	90	0.554	0.623	0.339	0.071	0.008	0.006	0.000
	11	100	0.413	0.714	0.501	0.076	0.012	0.004	0.000
	12	110	0.556	0.869	0.387	0.093	0.021	0.010	0.003
	13	120	0.498	0.658	0.136	0.051	0.012	0.007	0.000
	14	130	0.658	0.882	0.623	0.154	0.022	0.008	0.001
	15	140	0.599	1.309	0.701	0.181	0.032	0.003	0.000
	16	150	0.832	0.811	0.260	0.073	0.018	0.002	0.000
	17	160	0.608	0.765	0.232	0.032	0.005	0.005	0.000
	18	170	0.613	0.915	0.421	0.076	0.022	0.009	0.004
S	19	180	0.790	1.026	0.459	0.174	0.060	0.023	0.010
	20	190	0.767	0.876	0.406	0.092	0.015	0.006	0.004
	21	200	0.790	1.058	0.748	0.221	0.051	0.002	0.000
	22	210	0.922	1.872	1.254	0.329	0.031	0.014	0.005
	23	220	1.017	1.861	1.261	0.329	0.096	0.029	0.005
	24	230	1.312	1.852	1.268	0.301	0.051	0.035	0.015
	25	240	1.098	1.734	1.006	0.380	0.048	0.014	0.002
	26	250	1.131	1.654	0.702	0.289	0.058	0.014	0.000
	27	260	1.476	1.839	0.749	0.186	0.082	0.007	0.000
W	28	270	1.096	1.275	0.587	0.186	0.062	0.029	0.009
	29	280	0.984	1.308	0.449	0.287	0.094	0.010	0.000
	30	290	0.996	0.840	0.355	0.198	0.063	0.005	0.000
	31	300	1.242	1.408	0.714	0.397	0.098	0.011	0.005
	32	310	1.009	1.872	0.852	0.219	0.132	0.037	0.010
	33	320	1.172	1.609	1.245	0.421	0.094	0.008	0.000
	34	330	0.972	1.534	1.009	0.245	0.011	0.005	0.012
	35	340	1.377	2.648	1.882	1.239	0.053	0.027	0.004
	36	350	1.387	1.771	0.922	0.421	0.081	0.016	0.000

Table B.6: Summary of non-directional wind speed records in percentage at Toronto Lester B. Pearson Int'l A. Ontario Canada (1957-2012)

Scale	Speed range (m/s)	Frequency (%)	CDF (%)
1	0-5	27.94	27.94
2	5~10	40.53	68.46
3	10~15	21.99	90.45
4	15~20	7.43	97.88
5	20~25	1.54	99.42
6	25~30	0.47	99.88
7	30~35	0.12	100

2- Compute the true distribution parameter $\hat{\alpha}$ by using Eq. (B-3). The obtained value is $\hat{\alpha}$ =14.0.

3- Determine the corresponding value of the variance of the fitted Rayleigh distribution, $\sigma^2 = (4-\pi)/2 \cdot \alpha^2 = (4-\pi)/2 \times 14^2 = 84.13$.
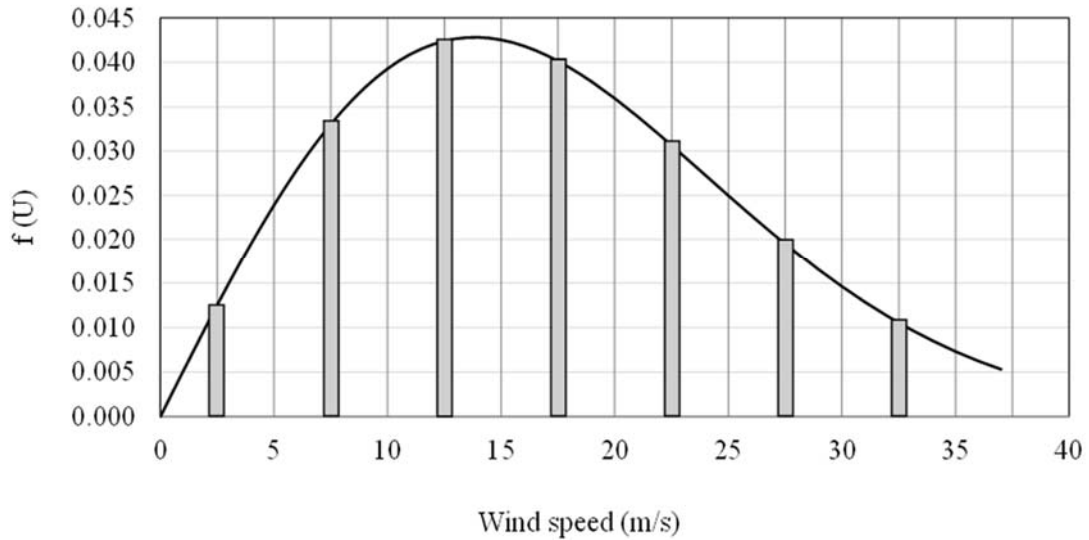

Figure B.5: PDF of the fitted Rayleigh distribution (α=14.0) to the average hourly wind speed database of Toronto (1957-2012)

As can be seen form the above results, $\sigma^2 \neq s^2$. This inconsistency reflects impreciseness of the fitted Rayleigh distribution in predicting the wind speed data set. It

should be pointed out that higher value of σ^2 reveals more deviation of the corresponding equivalent wind speed data obtained by fitting a Rayleigh distribution. Figure B.5 shows the histogram diagram of the occurrence frequency of the existing wind speed data set. The corresponding fitted PDF curve of the Rayleigh distribution, Rayleigh (α=14.0), is displayed.

Weibull distribution analysis

Apply a parent Weibull distribution model to the non-directional wind speed data set in Table B.6, the scale and shape parameters are calculated. For example, if wind speed is U=12.5 m/s (i.e. Scale 3), the results show that $P(U>12.5m/s)=1-0.9045=0.0955$; noting that P(>U) is the probability of exceedence of wind speed larger than U. The corresponding Weibull point is shown in Figure B.6 by (x=2.53, y=0.85). Knowing that the horizontal axis (x) represents the natural logarithm of the wind speed, ln(U), and the vertical axis (y) represents ln(-ln(P(>U))).
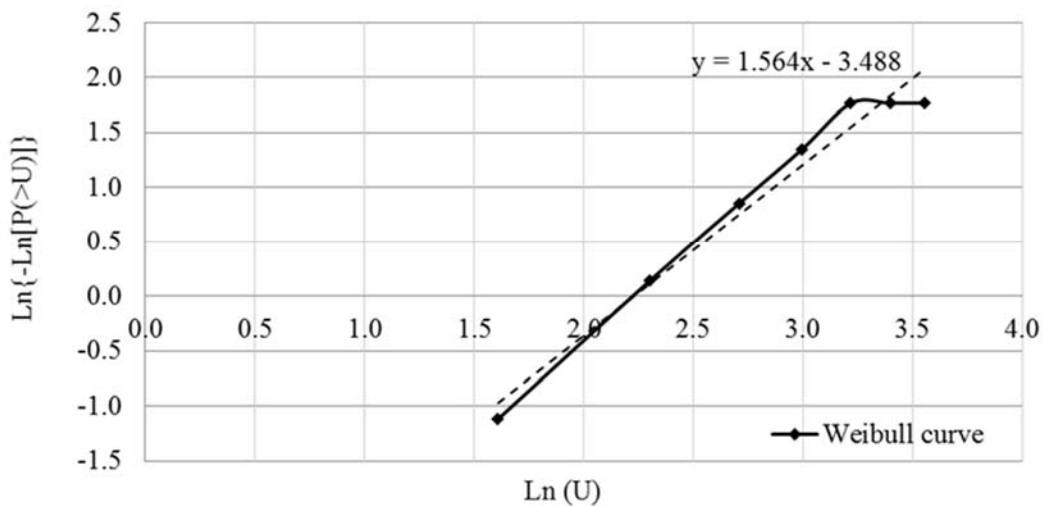

Figure B.6: Weibull distribution fitting for the non-directional wind speed database
(c=1.564, k=9.309)

By repeating the calculations for other wind speed design points, the Weibull curve is plotted as shown by a bold line in Figure B.6. The adopted equation after performing a linear regression on the Weibull curve is $y=1.564x-3.488$. The slope of this line is the value of the shape parameter k and its horizontal eccentricity is $\ln(c)$, knowing that c represents the scale parameter. Therefore, the adopted shape and scale parameters for the non-directional wind speed data set are $c=9.309$ and $k=1.564$, respectively.

Similarly, the results of the directional wind speed analysis after fitting the Weibull probability distribution method to the data set of Table B.5 are listed in Table B.7. The shape and scale parameters are represented in each row of the table by specifying the wind direction angle γ associated with the defined sector. For example, the expression for the PDF of the fitted Weibull probability distribution at Sector 12 is written by applying Eq. (B.6) as:

$$f(U,\gamma) = 0.172 \times \left(\frac{U}{8.841}\right)^{0.521} \exp\left(-\left(\frac{U}{8.841}\right)^{1.521}\right)$$

The above equation is valid within the direction angle range of $\gamma=[110°, 119.9°]$.

Gamma distribution analysis

Assume that the distribution of the wind speed data follows a Gamma distribution, then the shape and scale parameters are calculated using Eqs. (B-14) and (B-15). Figure B.7 shows the CDF curve of the fitted Gamma distribution model Γ ($c=6.0$, $k=2.92$).

Comparison of the parent probability distribution analysis methods

The CDF results of different parent probability distribution analysis methods are plotted in Figure B.8 for the non-directional wind speed data set of the studied site. As can

be seen from the curves, the goodness-of-fit for the assigned Weibull distribution, W

(c=9.309, k=1.564), is better than the remaining distributions. The correlation coefficient

test method is also applied to the CDF results which reveals the lowest value of R^2 =0.004

for the adapted Weibull distribution among the fitted distributions.

Table B.7: Collection of Weibull parameters, k(γ), c(γ) and the force term A(γ), for the directional wind speed data set

| Sector	Direction range (°)	k(γ)	c(γ)	A(γ)
1	0-9.9	1.665	9.553	0.01641
2	10-19.9	1.699	10.460	0.01753
3	20-29.9	1.590	9.597	0.00857
4	30-39.9	1.645	9.573	0.01905
5	40-49.9	1.699	10.604	0.00742
6	50-59.9	1.436	9.228	0.00837
7	60-69.9	1.222	6.650	0.01107
8	70-79.9	1.387	8.061	0.00915
9	80-89.9	1.754	10.210	0.01835
10	90-99.9	1.428	8.094	0.01601
11	100-109.9	1.657	9.498	0.0172
12	110-119.9	1.521	8.841	0.01939
13	120-129.9	1.326	7.382	0.01362
14	130-139.9	1.580	9.267	0.02348
15	140-149.9	1.710	9.897	0.02825
16	150-159.9	1.272	6.975	0.01996
17	160-169.9	1.332	7.136	0.01647
18	170-179.9	1.495	8.629	0.0206
19	180-189.9	1.486	9.007	0.02542
20	190-199.9	1.400	7.950	0.02166
21	200-209.9	1.594	9.494	0.0287
22	210-219.9	1.745	10.138	0.04427
23	220-229.9	1.707	10.227	0.04598
24	230-239.9	1.592	9.452	0.04834
25	240-249.9	1.626	9.617	0.04282
26	250-259.9	1.519	8.968	0.03848
27	260-269.9	1.412	8.192	0.04339
28	270-279.9	1.498	8.628	0.03244
29	280-289.9	1.476	8.960	0.03132
30	290-299.9	1.329	7.931	0.02457
31	300-309.9	1.494	9.116	0.03875
32	310-319.9	1.613	9.761	0.04131
33	320-329.9	1.645	9.917	0.04549
34	330-339.9	1.628	9.371	0.03788
35	340-349.9	1.841	10.978	0.0723
36	350-359.9	1.526	9.150	0.04598
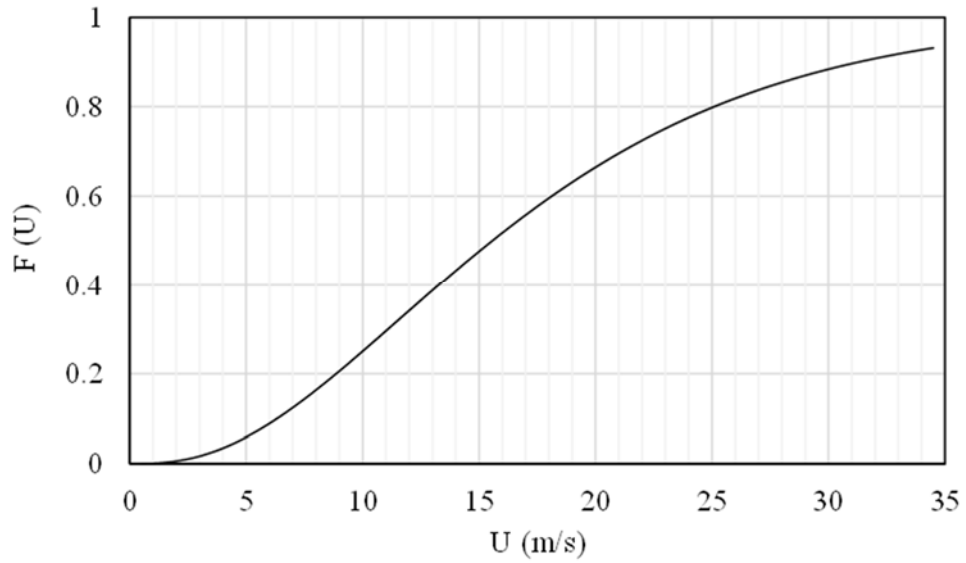
Figure B.7: CDF of Γ(*c*=6.0, *k*=2.92) to the average hourly wind speed database of Toronto (1957-2012)
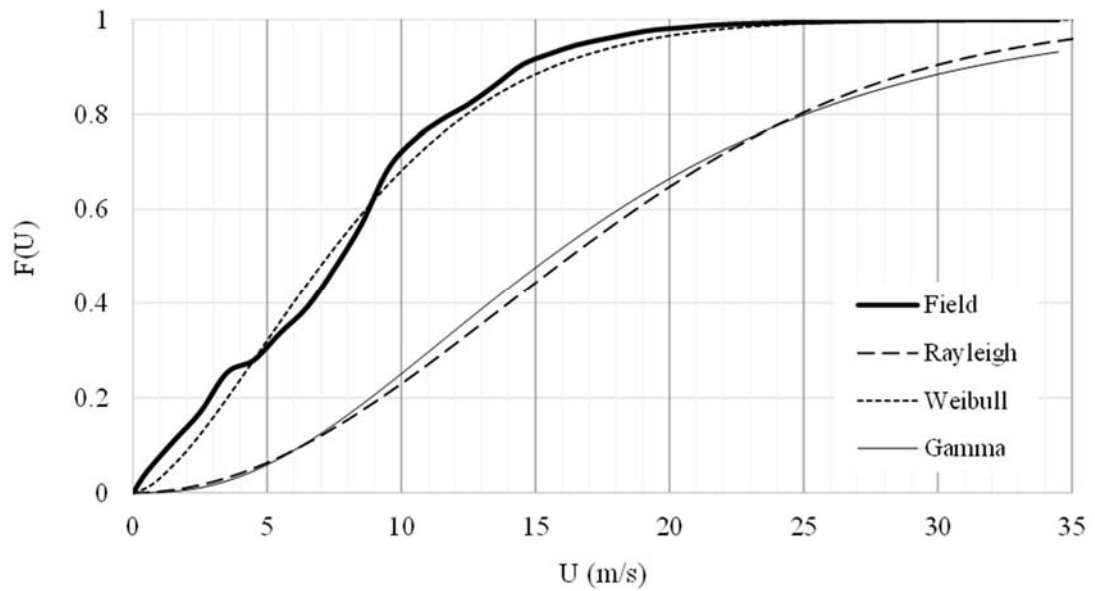

Figure B.8: CDF of the field database (Toronto 1957-2012) and the corresponding fitted probability distributions

It is notable that the fitted Rayleigh and Gamma distributions underestimates the values of CDFs over the studied wind speed range. Since, in the structural reliability analysis underestimation of the risk of occurrence of a certain wind speed is not acceptable, hence the adapted Rayleigh and Gamma distribution will be rejected.

As a result, the fitted Weibull distribution is selected as the best parent probability distribution method among the other fitted distributions due to its capability in handling wind directionality and also its superiority in prediction of the wind speed data set by including a margin of safety for the risk of occurrence of the design wind speed at the studied site.

B.5.2 The generalized extreme value wind speed analysis

In this section, the analysis of the wind gust speed data recorded in Toronto during years 1957-2012 (56 years) is performed by using the GEV distribution models, i.e. Type I, II, and III. Subsequently, the comparison of the distribution fitting models is attained by applying the Kolmogorov test to the fitted distributions.

The wind speed input data are collected from the Environmental Canada website as listed in Table B.8. Each item in this table represents the corresponding yearly maximum wind storm speed, with the peak value of 34.4 m/s as occurred in the calendar year 1964.

Table B.9 shows a summary of the Gumbel processing technique as applied to the annual extreme wind speed data set by using the modified Gringorten formulation for the reduced variate. The fitted Gumbel curve is plotted in Figure B.9, with corresponding scale and shape parameters equal to 2.12, and 25.89. Refer to the definition of the reduce variate, $y = -\ln(-\ln p)$, as a function of the probability of failure $p \approx (m-0.44)/(N+0.12)$, the return

period corresponding to each y, is also shown in the figure by using the return period

equation, i.e. $R=1/(1-p)$, noting that p depends on the wind speed rank in Table B.9.

Table B.8: Annual maximum gust speeds from Toronto Lester B. Pearson Int'L A. Ontario, Canada (1957-2012)

Year	Maximum gust speed (m/s)	Year	Maximum gust speed (m/s)
1957	29.2	1985	26.7
1958	27.2	1986	23.6
1959	33.9	1987	25.8
1960	25.0	1988	24.2
1961	26.9	1989	28.9
1962	25.8	1990	29.7
1963	28.6	1991	27.2
1964	34.4	1992	25.8
1965	25.0	1993	24.7
1966	23.3	1994	25.8
1967	24.7	1995	29.4
1968	24.2	1996	30.3
1969	24.7	1997	26.7
1970	25.0	1998	27.8
1971	25.0	1999	26.4
1972	26.4	2000	23.6
1973	25.8	2001	26.7
1974	27.8	2002	28.3
1975	28.6	2003	25.8
1976	28.1	2004	21.7
1977	27.2	2005	24.7
1978	31.9	2006	27.2
1979	30.8	2007	26.7
1980	28.3	2008	29.7
1981	24.7	2009	31.9
1982	28.9	2010	29.4
1983	30.3	2011	26.7
1984	27.8	2012	22.2

Next, the Frechet distribution model (Type II) is applied to the recorded wind speed

data set in Table B.8. The estimated values of the shape and scale parameters are $k=12.6$,

and $\alpha=25.7$, respectively. Further, two Weibull models, including Weibull 3P and Weibull

2P, are applied to the annual maximum wind speed. The values of the corresponding parameters are calculated using PWMs statistical analysis technique. A summary of the results are shown in Table B.10.

Table B.9: Gumbel processing for Toronto annual maximum wind speed data (1957-2012)

Rank	1	2	3	4	5	6	7	8
Gust speed	21.7	22.2	23.3	23.6	23.6	24.2	24.2	24.7
Reduced variate	-1.528	-1.276	-1.127	-1.014	-0.920	-0.838	-0.764	-0.695
Rank	9	10	11	12	13	14	15	16
Gust speed	24.7	24.7	24.7	24.7	25.0	25.0	25.0	25.0
Reduced variate	-0.631	-0.571	-0.513	-0.457	-0.403	-0.351	-0.300	-0.249
Rank	17	18	19	20	21	22	23	24
Gust speed	25.8	25.8	25.8	25.8	25.8	25.8	26.4	26.4
Reduced variate	-0.199	-0.150	-0.101	-0.053	-0.004	0.044	0.093	0.142
Rank	25	26	27	28	29	30	31	32
Gust speed	26.7	26.7	26.7	26.7	26.7	26.9	27.2	27.2
Reduced variate	0.191	0.240	0.290	0.341	0.392	0.445	0.498	0.552
Rank	33	34	35	36	37	38	39	40
Gust speed	27.2	27.2	27.8	27.8	27.8	28.1	28.3	28.3
Reduced variate	0.608	0.665	0.724	0.785	0.847	0.912	0.980	1.051
Rank	41	42	43	44	45	46	47	48
Gust speed	28.6	28.6	28.9	28.9	29.2	29.4	29.4	29.7
Reduced variate	1.125	1.203	1.285	1.373	1.467	1.568	1.678	1.799
Rank	49	50	51	52	53	54	55	56
Gust speed	29.7	30.3	30.3	30.8	31.9	31.9	33.9	34.4
Reduced variate	1.933	2.085	2.260	2.468	2.725	3.064	3.569	4.602

*Gust speed in m/s and reduced variate, y, is calculated by Gringorten formula

The assessment of the distribution fitting models is accompanied by applying the Kolmogorov test to the fitted distributions. Assuming the confidence level to be 90% ($q = 0.1$), the critical value of D_q can be found from the critical value table of the Kolmogorov test. It is D_q=0.1604 for sample size n=56. By comparing the results in Table B.10, it can be seen that the three-parameter Weibull distribution (Weibull 3P) appears to have the lowest Kolmogorov statistical term, D_n, which implies that it is the best distribution model among the other GEV distributions for the available data set (i.e. ranked 1st).
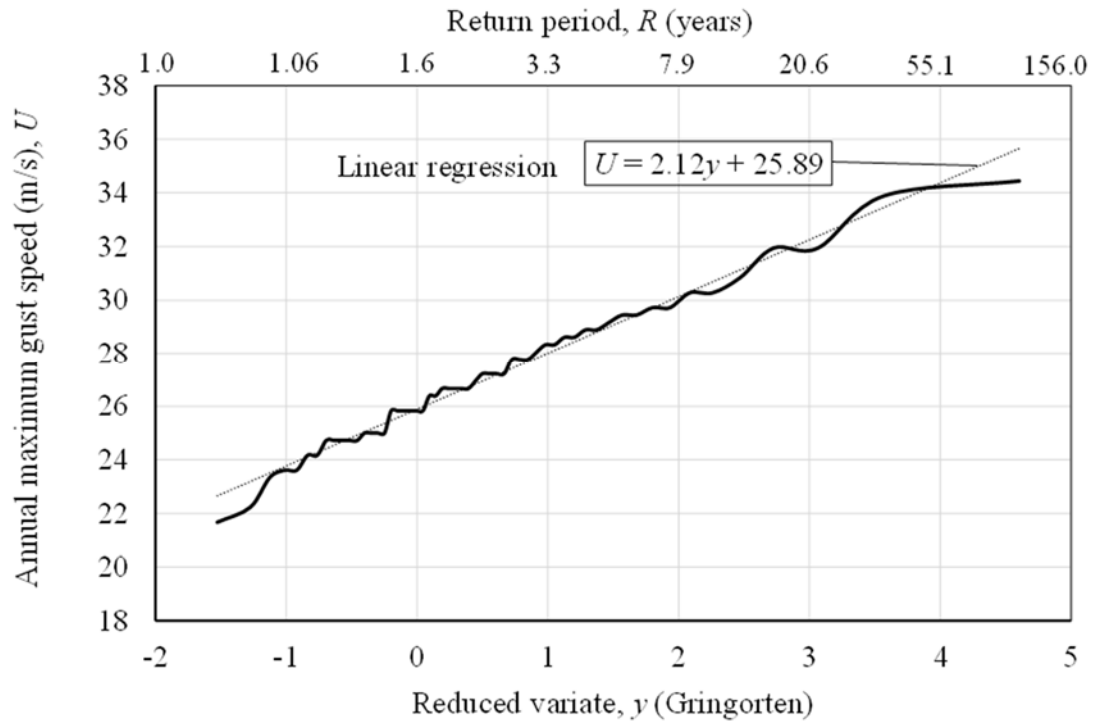
Figure B.9: Gumbel analysis of annual maximum wind gusts for Toronto (1957-2012), using the Gringorten formula

According to statistical outputs obtained by Kolmogorov test, all the GEV distributions models except Frechet distribution (Type II) would satisfy the hypothesis test criteria for fitting of the extreme wind speed records. It is noteworthy that the annual maximum wind speed of the given wind speed database of Toronto can also be well described by the Gumbel distribution model (Type I), which is agreed by D_n=0.1093< D_q. Even though the three-parameter Weibull distribution (Weibull 3P) was found to be the most accurate distribution based on the Kolmogorov test results, but the Gumbel distribution as the most common statistical wind speed analysis method is preferred due to its simplicity in estimation of the wind speed parameters, and also its capability in satisfying the acceptable level of statistical term, D_n.

Table B.10: Values of the estimated parameters and D_n of the GEV distribution models

Distribution models	Scale parameter α	Shape parameter u or γ	Location parameter β	D_n	$D_{n,q}$ (q=0.1, n=56)	Difference ($D_n-D_{n,q}$)	Rank
Gumbel	2.12	25.89	-	0.1093	0.1604	-0.0511	3
Frechet	25.70	12.60	-	0.1810	0.1604	+0.0206	4
Weibull 3P	6.87	21.00	2.43	0.0745	0.1604	-0.0860	1
Weibull 2P	28.06	-	12.42	0.0844	0.1604	-0.0760	2

Figure B.10 shows a comparison of the cumulative distributions of the field (actual) database, empirical distribution, the Type I extreme value (Gumbel) distribution, the Type II (Frechet) distribution, and the Type III (Weibull 3p and 2P) distributions of the annual maximum gust wind speeds for Toronto over calendar years 1957-2012. The CDF curves are plotted in the extreme wind speed range (21.5-35.5 m/s) which is obtained from the recorded annual extreme wind speed database. It can be observed from this figure that comparing the GEV estimation curves, Gumbel and Weibull fits are both within the proximity of the actual (field) database which verifies results of the Kolmogorov test.

B.5.3 Prediction of extreme wind speed

The results of the predicted extreme design wind speeds corresponding to different return periods are calculated by using the best fitted distributions including Weibull parent probability distribution method and GEV distribution Type I (Gumbel). They are listed in Table B.11 and B.12, respectively.
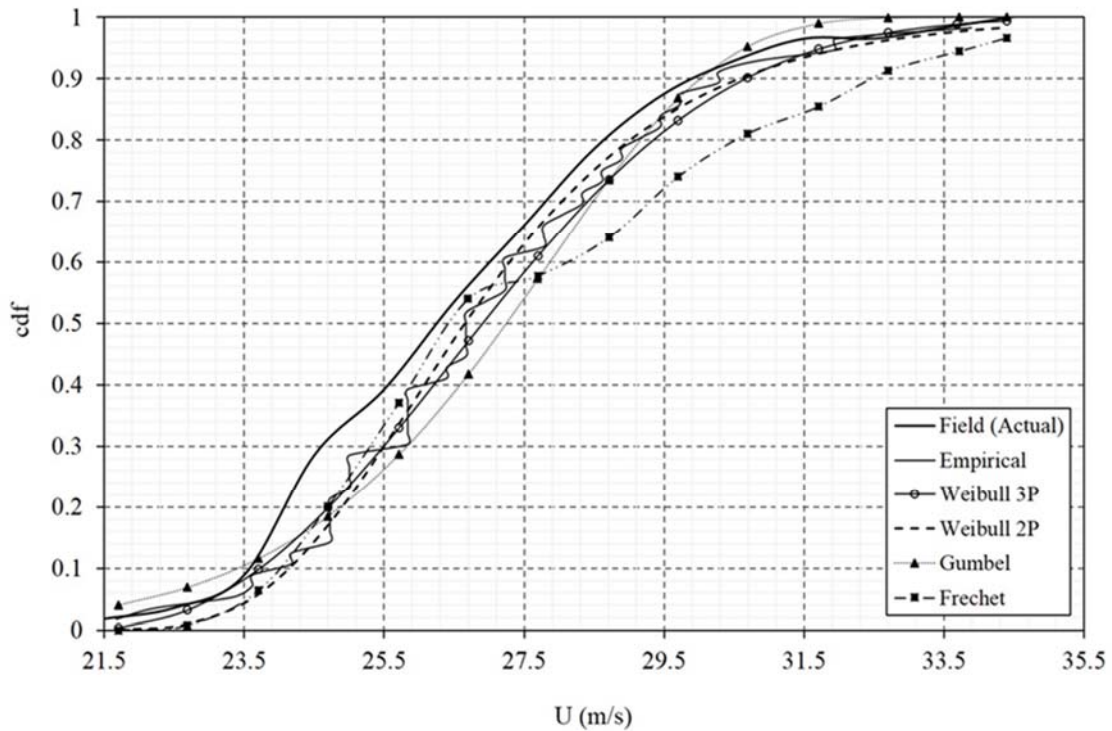
Figure B.10: Comparison of CDF curves of the fitted GEV distributions obtained for the annual maximum wind speed database at Toronto (1957-2012)

B.6 SUMMARY

A review of the probability distributions relevant to wind engineering has been presented in this appendix to predict the extreme wind speed corresponding to desired structural return period. The approaches to probabilistic analysis of wind speed database have been categorized, depending on the availability of wind speed data set. In this regard, the parent probability distribution analysis has been applied on the average-mean wind speeds dataset, whereas GEV distributions have been used to analyze the annual-maximum gust speeds.

The most relevant wind probability distribution analysis methods including Rayleigh, Weibull and Gamma distributions have been applied to the wind speed data set.

The statistical comparison tools such as RMSE and Correlation Coefficient (R) have been presented in detail. This has been beneficial to recognize the best-fitted probability distribution to a wind speed data set at a design site.

Table B.11: Extreme wind speed obtained for different return periods at Pearson Int'l A. design site using Weibull parent probability distribution analysis method

Sector	$U_{ext}(R)$ m/s Return period, R years							
	1	5	10	30	50	100	200	500
1	30.39	34.48	36.15	38.69	39.84	41.36	42.84	44.75
2	32.51	36.80	38.54	41.20	42.39	43.98	45.52	47.51
3	32.24	36.81	38.67	41.52	42.81	44.52	46.20	48.35
4	30.88	35.10	36.82	39.44	40.62	42.19	43.72	45.69
5	32.96	37.31	39.07	41.77	42.98	44.58	46.15	48.16
6	35.30	40.88	43.18	46.72	48.33	50.47	52.57	55.30
7	32.18	38.23	40.77	44.73	46.54	48.97	51.38	54.53
8	32.34	37.64	39.83	43.22	44.76	46.81	48.84	51.46
9	30.63	34.53	36.11	38.52	39.60	41.04	42.43	44.22
10	31.20	36.16	38.20	41.35	42.78	44.69	46.56	48.99
11	30.38	34.50	36.18	38.73	39.88	41.41	42.90	44.83
12	31.38	36.04	37.95	40.88	42.21	43.97	45.70	47.94
13	31.57	37.00	39.26	42.76	44.35	46.48	48.59	51.32
14	31.37	35.84	37.67	40.47	41.73	43.41	45.05	47.17
15	30.54	34.54	36.16	38.64	39.75	41.23	42.67	44.52
16	31.72	37.43	39.82	43.53	45.22	47.49	49.73	52.65
17	30.31	35.51	37.66	41.00	42.53	44.56	46.57	49.18
18	31.31	36.04	37.99	40.98	42.33	44.13	45.90	48.18
19	32.94	37.95	40.01	43.18	44.61	46.52	48.40	50.82
20	31.48	36.59	38.70	41.96	43.44	45.42	47.36	49.89
21	31.80	36.29	38.12	40.93	42.19	43.88	45.52	47.64
22	30.58	34.50	36.09	38.51	39.60	41.04	42.44	44.25
23	31.62	35.77	37.46	40.02	41.18	42.71	44.20	46.12
24	31.71	36.19	38.02	40.82	42.08	43.77	45.41	47.53
25	31.45	35.80	37.57	40.28	41.50	43.12	44.71	46.75
26	31.88	36.62	38.57	41.55	42.90	44.70	46.46	48.73
27	32.06	37.22	39.35	42.63	44.12	46.12	48.07	50.61
28	31.22	35.94	37.87	40.84	42.19	43.98	45.74	48.01
29	33.05	38.12	40.21	43.41	44.86	46.80	48.70	51.15
30	33.80	39.61	42.02	45.75	47.46	49.73	51.98	54.90
31	33.10	38.12	40.17	43.34	44.77	46.67	48.54	50.96
32	32.23	36.72	38.56	41.36	42.62	44.30	45.94	48.06
33	31.99	36.36	38.14	40.86	42.08	43.71	45.29	47.34
34	30.60	34.83	36.55	39.18	40.37	41.94	43.48	45.47
35	31.26	35.05	36.58	38.90	39.94	41.31	42.65	44.37
36	32.34	37.13	39.09	42.10	43.46	45.27	47.04	49.34

Table B.12: Extreme design wind speeds (m/s) predicted by the GEV distribution Type I (Gumbel method)

Return period, R (years)	$U_{ext}(R)$ (m/s)
5	29.5
10	31.0
20	32.6
50	34.7
100	36.2
200	37.8
500	39.8
1000	41.4

Alternatively, the theory of the generalized extreme value analysis on assessment of the wind speed data set has been explained by showing the application of three asymptotic extreme value distributions to the annual extreme wind speed database, including the Gumbel (Type I), the Frechet (Type II), and the Weibull (Type III) distribution models.

An inverse analysis of the corresponding cumulative distribution function of the fitted probability distribution has been adopted to calculate the value of wind speed corresponding to an expected structural design return period at a studied site.

A case study has been presented to show the application of the statistical methods to the measured wind speed data set at a definite design site. The results would provide a probabilistic tool on stipulating uncertainty of wind parameters in reliability assessment of aerodynamically excited structures.

VITA AUCTORIS

NAME: Seyed Ali Mohammadi

PLACE OF BIRTH: Mashhad, IRAN

YEAR OF BIRTH: 1984

EDUCATION: Amirkabir University of Technology, B.Sc.
                  Civil Engineering, Tehran, IRAN
                  2006

                  Amirkabir University of Technology, M.Sc.
                  Earthquake Engineering, Tehran, IRAN
                  2008

                  University of Windsor, Ph.D.
                  Structural Engineering, Windsor, ON, CANADA
                  2016